Distribution Agreement

In presenting this thesis or dissertation as a partial fulfillment of the requirements for an advanced degree from Emory University, I hereby grant to Emory University and its agents the non-exclusive license to archive, make accessible, and display my thesis or dissertation in whole or in part in all forms of media, now or hereafter known, including display on the world wide web. I understand that I may select some access restrictions as part of the online submission of this thesis or dissertation. I retain all ownership rights to the copyright of the thesis or dissertation. I also retain the right to use in future works (such as articles or books) all or part of this thesis or dissertation.

Signature:

_____ _____

Madeline M. Dekarske Date

Synthesis and Biological Investigation of Membrane-targeting Antimicrobials

By

Madeline M. Dekarske

Doctor of Philosophy

Chemistry

_____

William M. Wuest, Ph.D.

Advisor

_____

Simon B. Blakey, Ph.D.

Committee Member

_____

Frank E. McDonald, Ph.D.

Committee Member

Accepted:

_____

Kimberly Jacob Arriola, Ph.D, MPH

Dean of the James T. Laney School of Graduate Studies

_____

Date

Synthesis and Biological Investigation of Membrane-targeting Antimicrobials

By

Madeline M. Dekarske
B.Sc., Agnes Scott College, 2017

Advisor: William M. Wuest, Ph.D.

An abstract of
A dissertation submitted to the Faculty of the
James T. Laney School of Graduate Studies of Emory University
in partial fulfillment of the requirements for the degree of
Doctor of Philosophy
in Chemistry
2022

Abstract

Synthesis and Biological Investigation of Membrane-targeting Antimicrobials
By Madeline M. Dekarske

Experts currently think of antibiotic resistance as a second, “silent” pandemic. The Centers for Disease Control and Prevention released a report in 2019 about their efforts to stymie bacterial resistance to current antibiotics and now detail that the COVID-19 pandemic will likely decrease the progress previously attained. Thus, in this battle of constant bacterial evolution and development of resistance, we require new tools to better combat antibiotic resistance. During my time in the Wuest Lab, I have worked on three projects that center around fighting resistance. One project was a medicinal chemistry collaboration, in which we made nTZDpa derivatives in order to combat not only *Staphylococcus aureus* resistance but also persistence. Another focused on a biology collaboration, in which we investigated how C2 affects planktonic *Streptococcus mutans*, the primary pathogenic agent in the oral microbiome. I also designed a project centered around the ogipeptins, a class of macrocyclic peptides, with selective Gram-negative activity and crafted syntheses and a mechanism of action hypothesis.

Synthesis and Biological Investigation of Membrane-targeting Antimicrobials

By

Madeline M. Dekarske
B.Sc., Agnes Scott College, 2017

Advisor: William M. Wuest, Ph.D.

A dissertation submitted to the Faculty of the
James T. Laney School of Graduate Studies of Emory University
in partial fulfillment of the requirements for the degree of
Doctor of Philosophy
in Chemistry
2022

Acknowledgments

First off, I would like to acknowledge my advisor, committee, lab mates, and subgroup for guiding me as well as pushing me to be a better scientist. I would also like to thank the Emory Chemistry department, particularly Kira Walsh, for creating a supportive environment that receives feedback, fights for students, and aids in our all-around development.

Secondly, I would like to thank my families, both mine and my husband's, for their support throughout this difficult journey called grad school.

I would also like to thank my friends, particularly those I made in the Wuest Lab. You all have given me strength and helped me plod along even when I couldn't see the light at the end of the tunnel but knew it was there. It sounds trite, but I learned the value of friendship from you guys. Furthermore, I want to highlight two groups of people: Midwest Moms and Mémé Bay. I will miss you guys terribly, and while I can't propose quality time of walk-and-talk anymore, I am more than prepared to facetime.

Most importantly, thank you to my husband (and our cat, Vera). Some people have made comments to me in the past about how it's crazy to date another organic chemist. However, I find that we enhance each other's science with the questions that we ask as well as how we approach a problem. We make a great team—not only considering science but also in life. You're my best friend, and I am so grateful to have been given the opportunity to get to know you. I wouldn't have made it without you.

Table of Contents

List of Figures

Chapter 1:

Chapter 2:

Chapter 4:

List of Tables

Chapter 2:

Chapter 4:

Chapter 1: Introduction

1.1 Antibiotic history and use

Antibiotics have revolutionized society. In 1928, Alexander Fleming, a professor of bacteriology, identified on one petri dish (of many infected with *Staphylococcus* strains) a zone of inhibition surrounding a mold (*Penicillin notatum*).[1] People often mark this as the first instance of antibiotics; however before Fleming even noticed the antibacterial-producing mold, antibiotics were already present in society with the ancient example of tetracycline (**Fig. 1.1**).[1,2] Tetracycline was found in skeletal remains dating back to 350-550 CE from Sudanese Nubia.[1] Skeletons from the late Roman period in Dakhleh, Egypt also contained tetracycline.[1] Other ancient antibiotics are more difficult to detect, but tetracycline is a strong chelator that incorporates into bones, hence making it easier to identify.[1] Thus, antibiotics are not new to society, and we have always looked to nature for inspiration.[1]

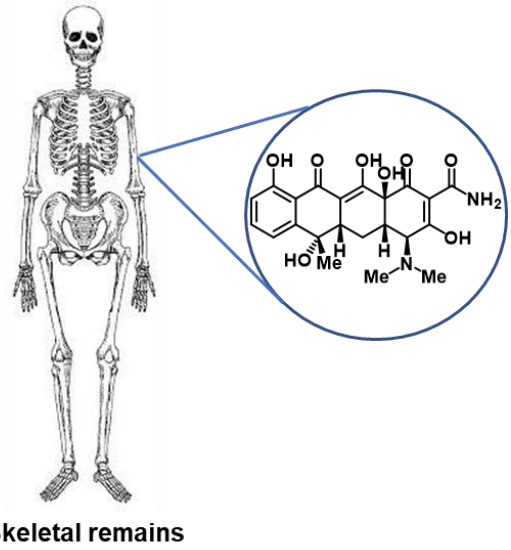

Figure 1.1: Skeletal remains dating back to 350-550 CE in Sudanese Nubia and the late Roman period in Egypt both contained tetracycline, indicating that antibiotics were not a new concept during their discovery in the twentieth century.

During the start of the antibiotic boom, Fleming assigned his assistants, Stuart Craddock and Frederick Ridley, to isolate the “mold juice” obtained from his unusual petri dish; the two found it to be a difficult task as it was unstable and could only obtained crude mixtures.[2] Another

scientist, Harold Raistrick, attempted to purify penicillin but failed.[2] Finally, Howard Florey, Ernst Chain, Norman Heatley, Edward Abraham, and colleagues at Oxford University succeeded in isolating penicillin during World War II.[2] In order to bring penicillin to market, they needed to handle 500 liters of mold filtrate a week to perform animal studies and clinical trials, for which they paid "penicillin girls" £2 a week to grow the cultures (**Fig. 1.2)**.[2] In their studies, Abraham utilized alumina column chromatography to isolate penicillin, which was a newly discovered technique at the time.[2] There were several more hurdles in fermenting enough of the mold filtrate to isolate an adequate amount of penicillin to treat humans and conduct the studies.[2] These hurdles led to the colleagues working with the US Department of Agriculture's Northern Regional Research Laboratory as well as US-based industry collaborators.[2] Eventually, the US War Production Board became involved and utilized 21 pharmaceutical companies to produce enough penicillin for military use in the World War II.[2] While the War Production Board was involved, word spread about the life-saving nature of penicillin and led to its introduction into general society.[2]

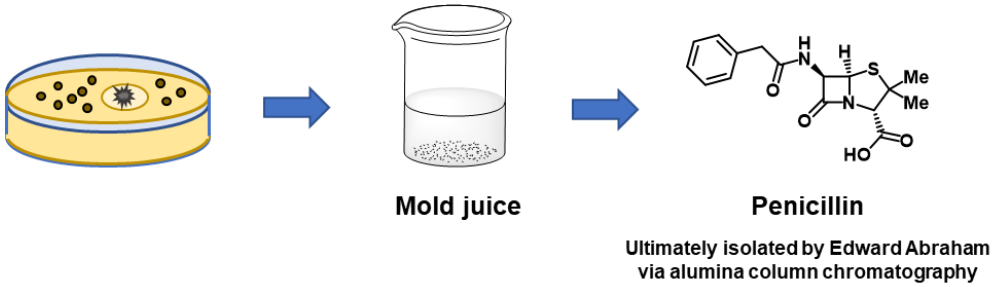

Figure 1.2: Schematic of penicillin's discovery and (difficult) isolation. However, isolation of penicillin still did not produce enough material for continual treatment.

While we commonly credit only Alexander Fleming with the discovery of penicillin and its initial activity, it was a group effort in uncovering the true power of penicillin.[2] Furthermore, the penicillin team was not the only interested in antibiotics. Selman Waksman is known as the "father of antibiotics" due to his contributions to the field (**Fig. 1.3**).[3] Waksman was first introduced to the actinomycetes from his studies at Rutgers University.[3] He then further examined them during his Ph.D. research at University of California, Berkley.[3] After graduating, he returned to Rutgers as faculty to research effects of soil organisms on one another. Rene Dubos, a French biologist who

joined Waksman's lab, discovered a soil organism that could attack *Streptococcus pneumoniae,* through its capsular polysaccharide.[3] Dubos unearthed this revelation in conjunction with Oswald Avery at Rockefeller Hospital.[3] Dubos and Avery's research inspired Waksman to further investigate antibacterial soil organisms.[3] Then, Waksman and H. Boyd Woodruff invented a screening method to test for antibacterial properties via isolating the strain, obtaining single colonies, plating them, examining the growth inhibition zones surrounding the single colonies, and then testing the hits against a number of pathogenic bacteria.[3]

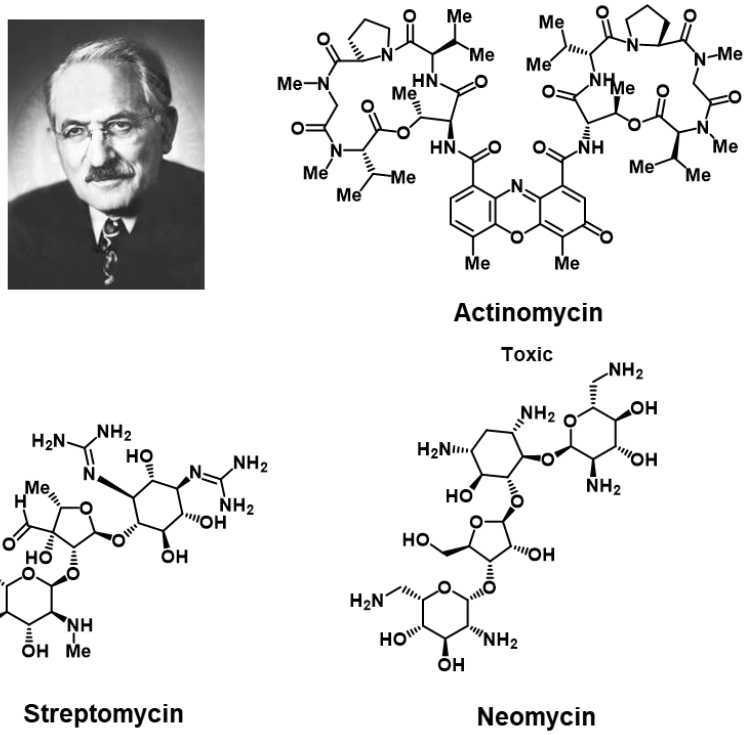

Figure 1.3: Selman Waksman, "the father of antibiotics" and his first antibacterial natural product, actinomycin. Unfortunately, actinomycin is toxic and so could never function as an antibiotic. Waksman also discovered streptomycin and neomycin, among his other eighteen natural product discoveries.

During their studies, Waksman and Woodruff discovered actinomycin, which possessed bacteriostatic and bactericidal properties (**Fig. 1.3**).[3] They were able to separate actinomycin into actinomycin A, an orange-red product with bacteriostatic and bactericidal properties, and actinomycin B, a colorless product with only bactericidal properties.[3] Waksman provided three possible molecular formulas for actinomycin A as well as detailed its quinine-like pigment.[3] He

also noted that while actinomycin A had activity against Gram-positive bacteria, it had little to no activity against Gram-negative bacteria.[3] Furthermore, in cell viability testing, actinomycin was found to be toxic to the animals subjected.[3] Because of the work involved to isolate the toxic actinomycin and its failure, Waksman initiated a screen of actinomycetes for their antibacterial properties in hopes of obtaining a hit.[3] From his screens, he obtained 20 novel antibacterials, two of which are streptomycin and neomycin, currently well-known aminoglycosides.[3] Furthermore, from his screening results, he proposed a new term for the inhibitors with antibacterial activity: antibiotics.[3]

Antibiotics are still a cornerstone in our society, but we are currently past the "Golden Age of Antibiotics."[4,5] Traditionally, doctors prescribe antibiotics to treat bacterial infections.[4,5] However, this is not the only use of antibiotics. Historically, antibiotics have been used to fatten livestock within the agriculture industry.[4] Furthermore, antibacterials make an appearance within the oral healthcare industry with cetylpyridinium chloride (CPC), the active ingredient in most mouthwashes.[6] CPC is a quaternary ammonium compound (QAC) that aids in fighting gingival infections that stem from plaque (**Fig. 1.4**).[6] CPC lowers the connectivity of local and microbiota-

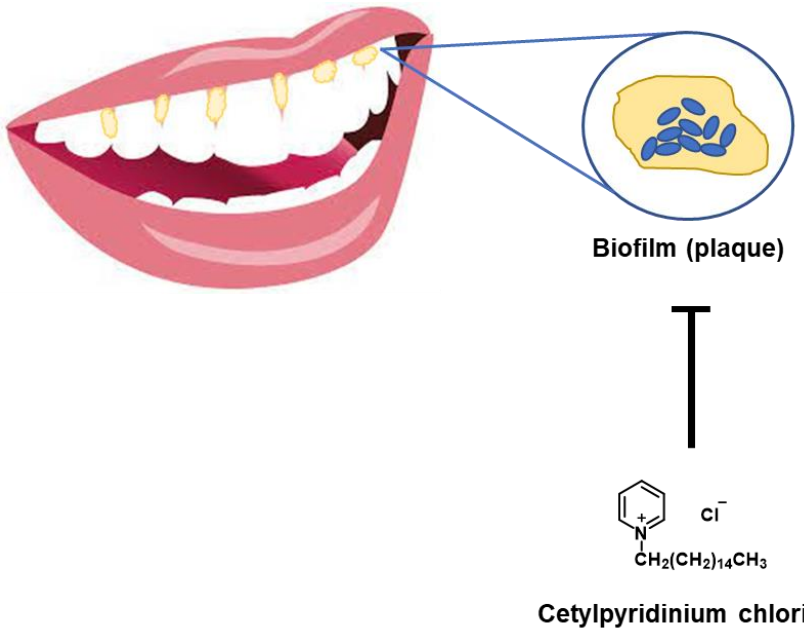

Figure 1.4: Cetylpyridinium chloride (CPC) aids in fighting gingivial infections through inhibiting biofilm connectivity.

wide bacteria, which is key in plaque (a form of biofilm), and plaque can cause gingivitis (a gum disease) via inflaming the gingivae.[6]

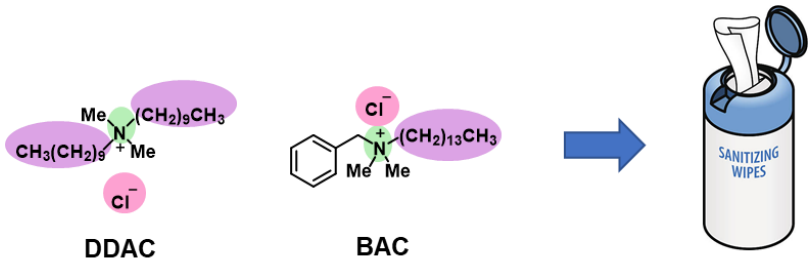

Figure 1.5: DDAC and BAC are two of the most well known QACs and are present in disinfecting wipes.

While CPC is one QAC present in many mouthwashes as the active ingredient, it is not the only QAC present in common household goods.[5] Two of the most popular QACs are benzylalkonium chloride and didecyldimethylammonium chloride (**Fig. 1.5**).[5] Interestingly, QACs are a controversial topic within hygiene and household cleaning. QACs are small molecules that contain at least one positively charged nitrogen, a long hydrophobic side chain(s), and a proportional number of counterions to the positively charged nitrogen.[5] QACs operate via intercalating into the negatively charged phospholipid bacterial membrane, which then disrupts the membrane, causing lysis.[5] While QACs are cheap to manufacture and effective as an antimicrobial (as well as anti-static and surfactant) and thus heavily present in many common household items, there are several drawbacks to their broad-spectrum usage.[7,8] They are considered relatively safe, but Hrubec and coworkers examined the reproductive effects of newer QAC exposure to mice and found decreased fertility.[7] In their studies, they observed longer pregnancy intervals, fewer pregnancies, increased time to first litter, and fewer pups per litter.[7] An important note for the study is that the mice were dosed via their food, which QACs are not intended for internal use and instead only recommended for external use.[6,7] Despite their intended use, QACs have been found in surface water and sediment, even after processing downstream from a waste-water treatment plant.[8] They can also be detected downstream of hospital (laundry) and industrial (food processing) applications.[8] While simple detection may not sound dire, QACs

are high production volume chemicals and thus beyond abundant.[6,8] Furthermore, because of the triclosan ban by the US Food and Drug Administration in hand soaps, QAC usage as an antimicrobial increased, particularly during the Covid-19 pandemic.[8] Thus, QACs have advanced society but do come at a cost.[6-8] Plus, the rise of resistance to QACs exacerbates this "cost" with the current, wide-spread utilization of QAC-containing antimicrobials during the Covid-19 pandemic.[9]

1.2 Resistance

Experts now indicate that we are in a "Post-Golden Era of Antibiotics," due in large part to resistance.[4] While resistance did not occur overnight, the misuse and over-use of antibiotics further drove evolution and resistance development.[4] Resistance to penicillin was observed soon after its discovery in 1928.[4,10]

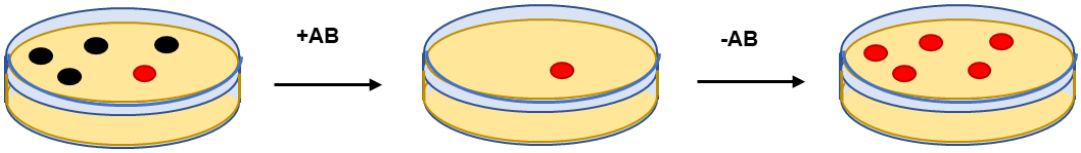

Figure 1.6: Diagram of resistance. Black cells are susceptible cells. Resistant cells are red. When treated with antibiotic (AB), the susceptible cells are killed, leaving behind the resistant cells, which are able to proliferate once antibacterial pressure is removed.

A common misconception when discussing resistance is the idea that the human body is resistant to the antibiotic instead of the bacteria being resistant to the antibiotic.[4] In actuality, bacteria developed resistance either via spontaneous mutation or horizontal gene transfer such that that particular antibiotic can no longer kill that strain.[4,10-12] So, if one treats a bacterial infection, in which there are both susceptible cells and resistant cells, the antimicrobial will only kill the

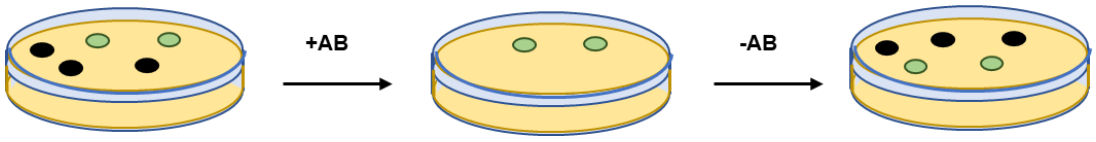

Figure 1.7: Diagram of persistence. Black cells are susceptible cells. Green cells are persistent. Upon treatment with antibiotic (AB), the susceptible cells are killed, leaving behind the "dormant" persister cells. Once the antibacterial pressure is removed, the persister cells can reconstitute the infection.

susceptible cells (**Fig. 1.6**).[10] The resistant cells remain, and when the antibacterial pressure is removed, the resistant cells can proliferate (**Fig. 1.6**).[10]

In studies to further understand resistance and the mechanisms employed by bacteria, another bacterial tactic was identified: persistence (**Fig. 1.7**).[13,14] Persistence is different from resistance in that it is a phenotypic change as opposed to genotypic.[13,14] Furthermore, persister cells can be thought of as dormant cells: they have slowed (or stopped) their cellular functions.[13,14] For example, antibiotics that target cell wall synthesis cannot physically undergo their mechanism of action, because persister cells are not performing cell wall biosynthesis.[10] Therefore, persister cells are part of the reason why chronic infections are incredibly arduous to treat.[14]

1.3 Gram-positive and Gram-negative bacteria

To further understand the implications of the work contained herein, one must understand the differences between Gram-positive and Gram-negative bacteria.[26-30] In 1884, Hans Christian Gram established a staining method, which has subsequently been used to discuss the two types of bacteria.[26] Gram-positive bacteria stain blue in Gram's method, while Gram-negative bacteria do not. This is largely a result of membrane differences.[26]

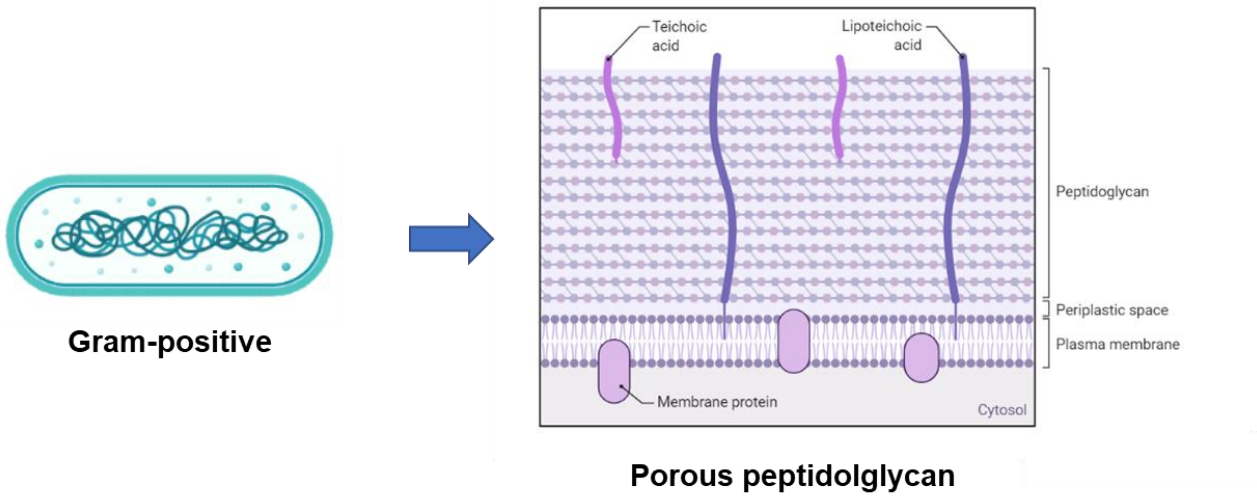

Figure 1.8: General Gram-positive cell membrane. Figure made with BioRender.

Gram-positive bacteria possess a thick (20 to 80 nm) membrane comprised of peptidoglycan, which is cross-linked glycan chains (**Fig. 1.8**).[27] Teichoic acid and polysaccharides also further functionalize the peptidoglycan and add complexity to the cell wall.[27] Gram-positive bacterial cell membranes must be multi-functional: they must be flexible to allow for division and growth, but they also must be rigid enough to disallow abiotic entry into the cell.[27,28] Furthermore, while Gram-positive bacteria share quite a few characteristics across their cell membranes, there are more complexities to their cell walls that are species dependent, such as how peptidoglycan maturation results in a porous structure.[28] In *Staphylococcus aureus*, peptidoglycan maturation results in random pores that form from reorientation during cell division; however, in *Bacillus subtilis*, peptidoglycan maturation results in cylindrical shapes as pores.[28] Pasquina-Lemonche and coworkers account for this divergence through the differences in cell division.[28]

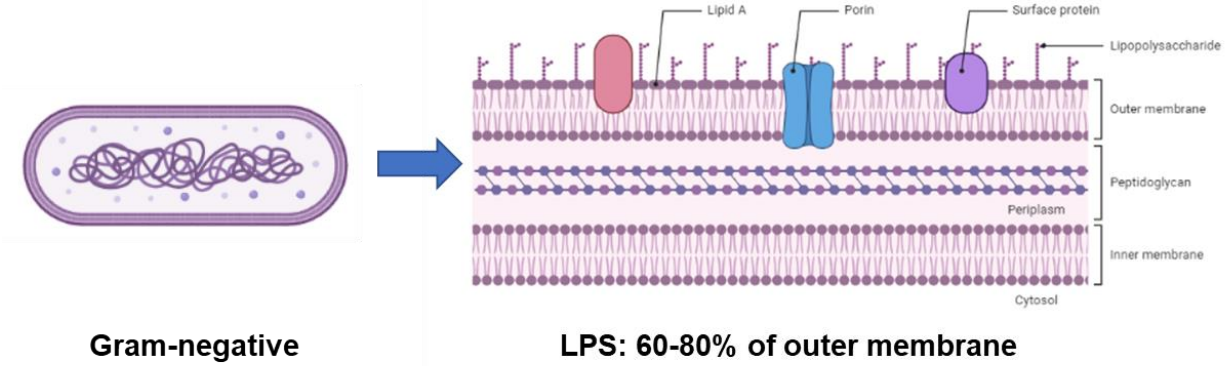

Figure 1.9: Gram-negative bacterial cell membrane. Figure made with BioRender.

Gram-negative bacteria differ from Gram-positive bacteria in quite a few manners.[29,30] First and foremost is the outer membrane (**Fig. 1.9**).[29,30] The outer membrane is an asymmetrical, key protective barrier for Gram-negative bacteria.[29,30] It is a diderm that consists of two sections: an inner and outer leaflet.[29,30] The inner leaflet is comprised mostly of phospholipids, while the outer leaflet is that of glycolipids, like lipopolysaccharide.[29,30] Lipopolysaccharide accounts for most of

the outer membrane (60-80% of the outer membrane) and is largely responsible for prohibiting unwanted small molecule access.[29,30] Lipopolysaccharide consists of three components: Lipid A, sugars, and the O-antigen. [29,30] Lipid A connects the rest of the lipopolysaccharide to the membrane itself. Lipid A is a phosphorylated disaccharide with fatty acyl chains, resulting in a net negative charge. [29,30] Thus, negatively charged lipopolysaccharide can then interact with divalent cations embedded within the outer membrane, such as Ca^{2+}, in order to strengthen the outer membrane. [29,30] Therefore, Lipid A is not only essential for most Gram-negative bacteria but also is responsible for the robust nature of the outer membrane. [29,30] Furthermore, polymyxin E (colistin) operates by displacing the divalent cations, which destabilizes the lipopolysaccharide, ultimately leading to cell death. [30] As a mechanism of resistance, Gram-negative bacteria are able to decrease phosphorylation of Lipid A, leading to less of a negative charge, which attracts less colistin. [29,30] Moreover, only three Gram-negative bacteria are able to survive without Lipid A, and one example is *Acinetobacter baumannii*, one of the six ESKAPE pathogens (*Enterococcus faecium, S. aureus, Klebsiella pneumoniae, A. baumannii, Pseudomonas aeruginosa,* and *Enterobacter spp*.). [29]

1.4 Mechanisms of resistance

In studying how bacteria evolved to resist antibiotics, four prominent mechanisms emerged: drug modification, target modification, efflux, and cell permeability.[4,10]

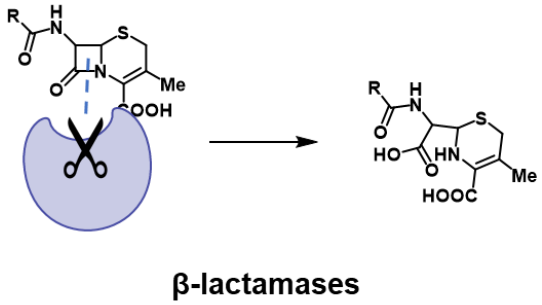

Figure 1.10: β-lactamases hydrolyze antibiotics containing β-lactams via clipping the β-lactam ring, thus destroying the warhead of the molecule.

1.4.1 Drug modification

Regarding drug modification, bacteria are able to change the antibiotic enough to render it inactive.[4,10] β-lactams function by mimicking the substrate of penicillin binding proteins, which assemble peptidoglycan for the cell wall. [4,10] Then, penicillin binding proteins, after recognizing the β-lactam antibiotic as their desired substrate, hydrolyze the β-lactam ring of the antibiotic, which then arrests any cell wall synthesis that particular penicillin binding protein could participate in. [4,10] β-lactamases then inactivate β-lactam antibiotics by hydrolyzing the β-lactam ring (for which the class was named after), similarly to how the class inhibits cell wall biosynthesis (**Fig. 1.10**). [4,10] Thus, β-lactamases exist to deactivate the β-lactam warhead before the penicillin binding protein mistakes it for its substrate. [4,10]

However, this is not the only class to be render ineffective by hydrolysis—tetracyclines are hydroylzed by TetX.[10,15] TetX deactivates tetracyclines by oxidation, which then can form a stable hemiketal upon acidic workup of the enzymatic degradation products. [10,15] Tetracyclines operate via a Mg^{2+} chelation mechanism, which enables them to pass through the cell membrane, to bind to the ribosome inside the bacterial cell. [10,15] However, this oxidation event by TetX disallows this mechanism and disrupts the stability of the tetracyclines, leading to side products. [10,15] TetX is hypothesized to create a reactive hydroxyflavin intermediate via NADPH, which then serves as an electrophilic hydroxyl source for the tetracyclines. [10,15]

While hydrolysis is a popular drug modification mechanism of resistance, it is not the only method employed by bacteria.[10,16] Bacteria also utilize transferases to chemically modify antibiotics and render them ineffective. [10,16] These modifications include (but are not limited to) acetylation, phosphorylation, adenylation, and methylation. [10,16] All four previously mentioned groups have been used to inactivate aminoglycosides. [10,16] Furthermore, adenylation is the preferred transferase method as it is quite popular for antibiotic deactivation based on its use for the following antibiotic classes: chloramphenicol, streptogramins, fluoroquinolones, and aminoglycosides.[10,16]

1.4.2 Target modification

Bacteria may also develop resistance via modifying the intended drug target.[10,17] Regarding β-lactam antibiotics, bacteria change the structure or concentration of penicillin binding proteins, such that β-lactams can no longer bind to the penicillin binding protein or that there is not enough target for the drug to bind to (**Fig. 1.11**).[10,17] The previously mentioned mechanisms are typically employed by Gram-positive bacteria.[10,17] For example, *S. aureus* changes its penicillin binding protein's structure via uptake of the gene, *mecA*.[10,17] Further, methicillin-resistant *S. aureus* is able to resist vancomycin (a glycopeptide which targets cell wall biosynthesis) via modification of the starting materials for peptidoglycan through acquiring the *van* genes.[10,17]

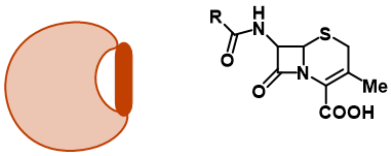

Figure 1.11 Penicillin binding proteins modify the target by closing the active site; thus, β-lactam containing antibiotics cannot access their desired active site.

Another example of bacterial structural modification to resist antibiotics is with daptomycin.[10] This lipopeptide is known to depolarize the membrane (reversing the charge distribution across the cell membrane and making the cell interior more negatively charged, ultimately leading to cell death).[10] However, daptomycin needs calcium ions to facilitate binding to the negatively charged membrane surface, which then allows for the depolarization event.[10] In resisting daptomycin, bacteria create a more positive charge to the cell surface, thus disallowing daptomycin binding and subsequent depolarization.[10]

In regard to non-membrane resistance mechanisms, antibiotics target the ribosome (responsible for protein synthesis), DNA gyrase (nucleic acid synthesis), or metabolic pathways within the bacterial cell.[4,10] Bacteria typically employ methylation of the 30S or 50S ribosomal subunits to circumvent aminoglycoside activity. [4,10] Furthermore, bacteria can modify the DNA gyrase structure thus rendering it incompatible for fluoroquinolone binding. [4,10] Finally, for

metabolic pathways, bacteria are able to undergo enzyme mutations within its active site (such as dihydrofolate reductase) that render trimethoprim ineffective as a competitive binder but still allow for its natural substrate to bind. [4,10]

1.4.3 Efflux

A third mechanism of resistance that bacteria utilize is efflux (**Fig. 1.12**). [4,10] Some efflux pump genes are always "on," while others require an inducement, such as a certain substrate or an environment stimulus. [4,10] Thus, efflux pumps' main function is to expel substrates that are toxic to the cell. [4,10] Efflux pumps sometimes transport a multitude of different classes of compounds, as is the case with multi-drug resistant pumps. [4,10] However, other efflux pumps prefer more specific substrates like how the MexY operon is selective for aminoglycosides. [4,10]

Figure 1.12: Bacteria utilize efflux to shuttle unwanted compounds out of the cell. Figure made with BioRender.

There are five main families of efflux pumps, and bacteria are not limited to only containing one family of pumps, which are typically determined by structure and energy source. [4,10] Four of the five are single component pumps, while the RND pump family is a multi-component system, featured mainly in Gram-negative bacteria.[4,10] Interestingly, while RND is the only multi-component pump, other pumps are able to work in conjunction with another efflux pump, similar to the instance with the ATP-binding cassette pump, MacB, forming a tripartite pump with MacA and TolC to efflux out macrolides. [4,10]

1.4.4 Cell permeability

As previously mentioned, Gram-negative bacteria utilize the outer membrane to stop unwanted small molecule entry into the cell, particularly with the lipopolysaccharide decorating the outermost part of the membrane. [4,10] While Gram-positive bacteria do not possess this same membrane, making them more vulnerable to small molecules, they have developed methods to thicken their cell wall so as to stop undesirable compound entry. [4,10] An example of this phenomenon occurs with *S. aureus*, in which it can make its cell wall denser, thus disallowing the cell-wall targeting antibiotic, vancomycin, access (**Fig. 1.13**). [4,10] Bacteria can also reduce number of porins, which Gram-negative bacteria utilize to transport hydrophilic compounds into the cell. [4,10] Furthermore, Gram-negative bacteria can structurally modify the porins to reverse porin affinity. Another cell permeability resistance mechanism is biofilm. [4,10] Biofilm matrix, comprised of polysaccharides and bacterial DNA and proteins, ensures that an antibiotic cannot easily access and perform its mechanism on that bacterial strain. [4,10] Furthermore, biofilm bacteria often possess a slowed metabolism and are slowly undergoing cell division; thus, biofilm bacteria are impervious to antibiotics that target fast-dividing, growing bacteria. [4,10]

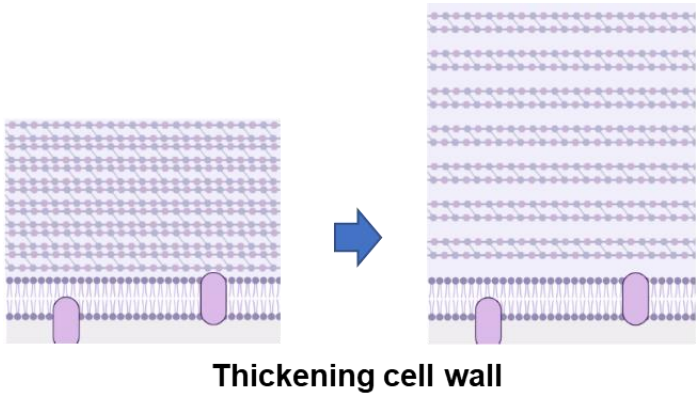

Figure 1.13: Bacteria, particularly Gram-positive bacteria, can change their cell permeability via thickening their cell wall to resist uptaking antibacterials. Figure made with BioRender.

1.5 Methods around mechanisms of resistance

While bacteria evolved and developed resistance to antibacterials, we also evolved in our techniques to bypass antibiotic resistance. These methods are combination therapy, adjuvants, new targets, new mechanisms, and membrane mechanisms.

1.5.1 Combination therapy

Combination therapy rests on the idea that instead of developing new chemical entities, we restore the effectiveness of old antibiotics through utilizing more than one.[4,18] This idea relies on the combination of two antibiotics leading to synergistic effects, which means that the combined effect is greater than each antibacterial alone (**Fig. 1.14**). [4,18] This idea of combination therapy is also not the first example within the medical community as it has been utilized with

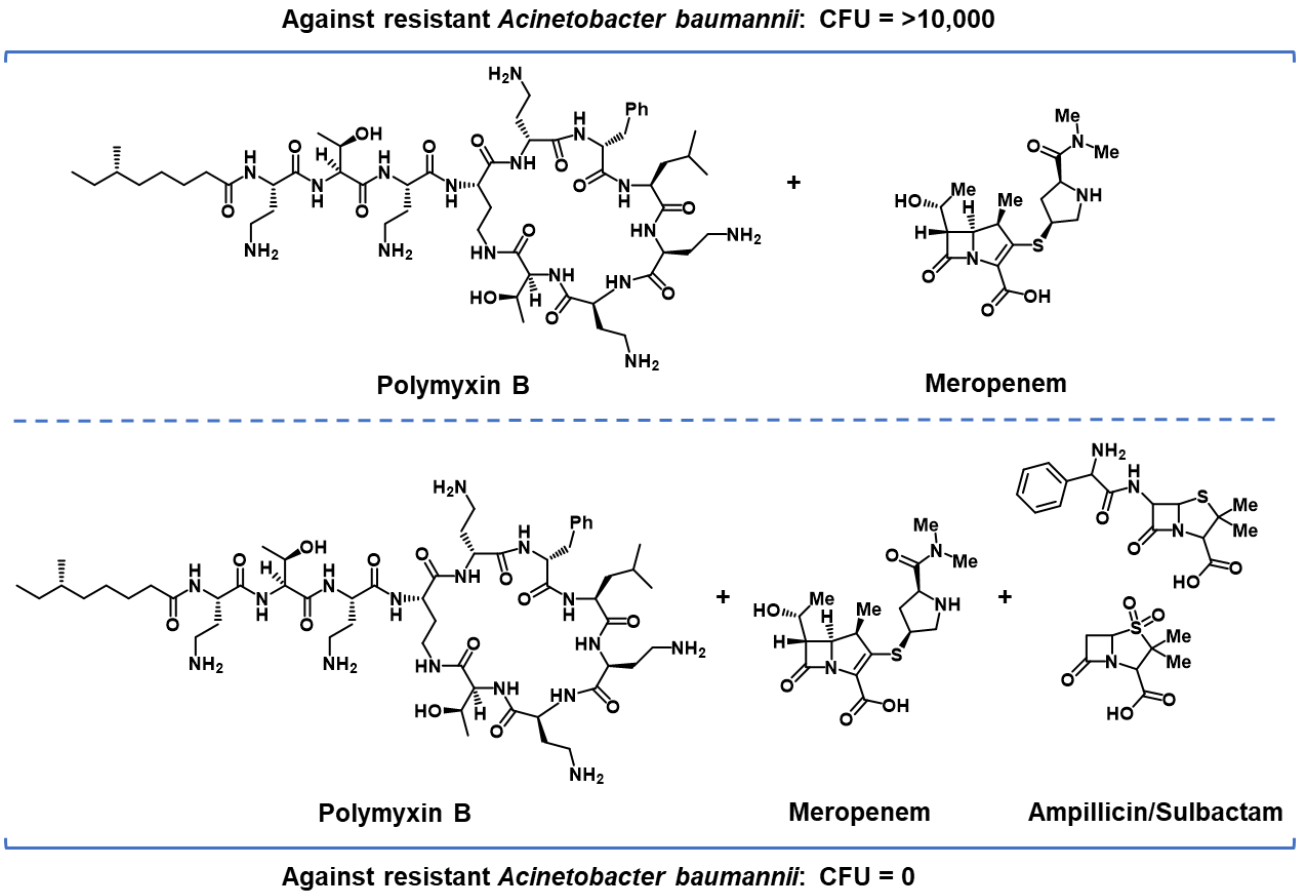

Figure 1.14: An example of combination therapy. Polymyxin B and meropenem together were unable to kill resistant *Acinetobacter baumannii*. However, with the added ampillicin/sulbactam drugs, they were able to eradicate the same resistant strain.

treating tumors and chemotherapy. [4,18] Furthermore, the combination of two antibiotics actually leads to less resistance development, as exemplified in other disease states like tuberculosis, thus displaying the benefits to combination therapy. [4,18] Another beneficial effect to combination therapy is the reduced dosing, which can lead to fewer toxic side effects. [4,18] Combination therapy requires less lead time from drug development to market in the pipeline for pharmaceutical companies because the lead has already been developed and did not fail in clinical trials (this is not to say that the conventional antibiotic could not be improved upon or will become the early development candidate). Less lead time translates to less money spent and more lives saved. Furthermore, the combination and formulation utilized can be patented, which is how pharma recoups its invested cost (currently estimated at $2.6 billion to bring a single drug to market from bench).[19] Thus, combination therapy is a less risky business venture for pharma and is currently being used to treat resistant bacterial infections.

1.5.2 Adjuvants

Adjuvants act in conjunction with an antibiotic to either enhance antibacterial activity or overcome resistance mechanisms.[4,20] While this seems similar to combination therapy, it differs in that adjuvants have little to no antibacterial activity. [4,20] Thus, the purpose of adjuvants is to potentiate the antibiotic activity through either affecting the invading bacterial cell or the host. [4,20]

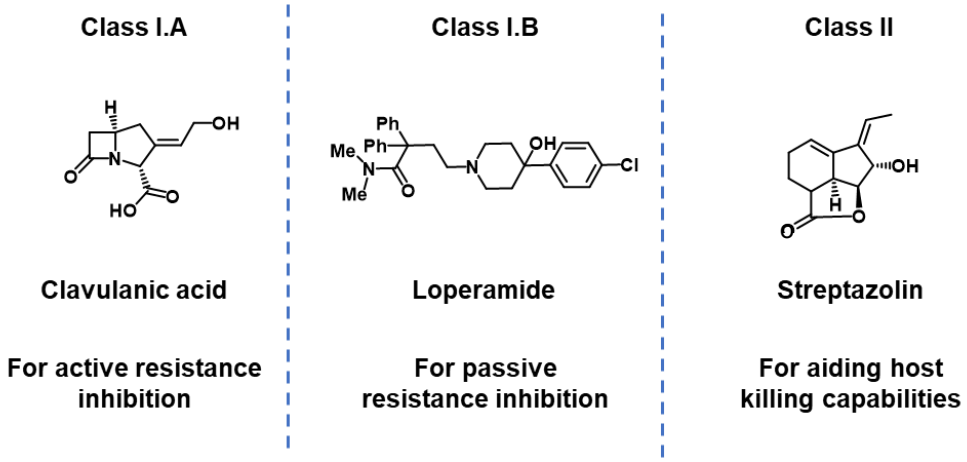

Figure 1.15: The three adjuvant classes with examples.

There are several classes of adjuvants: Class I.A, Class I.B, and Class II (**Fig. 1.15**). Class I adjuvants directly affect the bacterial cell and target either active (Class I.A) or passive (Class I.B) resistance mechanisms. [4,20] An example of a Class I.A adjuvant is clavulanic acid, a β-lactam, that targets TEMβ-lactamase, which destroys β-lactam antibiotics. [4,20] Thus, TEMβ-lactamase is preoccupied with clavulanic acid, thereby allowing the associated β-lactam antibiotic to perform its mechanism of action. [4,20] A Class I.B adjuvant is loperamide. [4,20] Loperamide acts in Gram-negative bacteria and affects the electrical aspect of proton motive force. [4,20] Thus, the bacteria then increase the pH gradient, which in turn, increase tetracycline uptake. [4,20] Finally, Class II adjuvants operate via activating the immune system. [4,20] One such instance is with streptazolin, which activates host macrophages through the phosphoinositide 3-kinase pathway. [4,20] However, the downside to this type of therapy is that it could over-activate the immune system and produce damaging effects. [4,20]

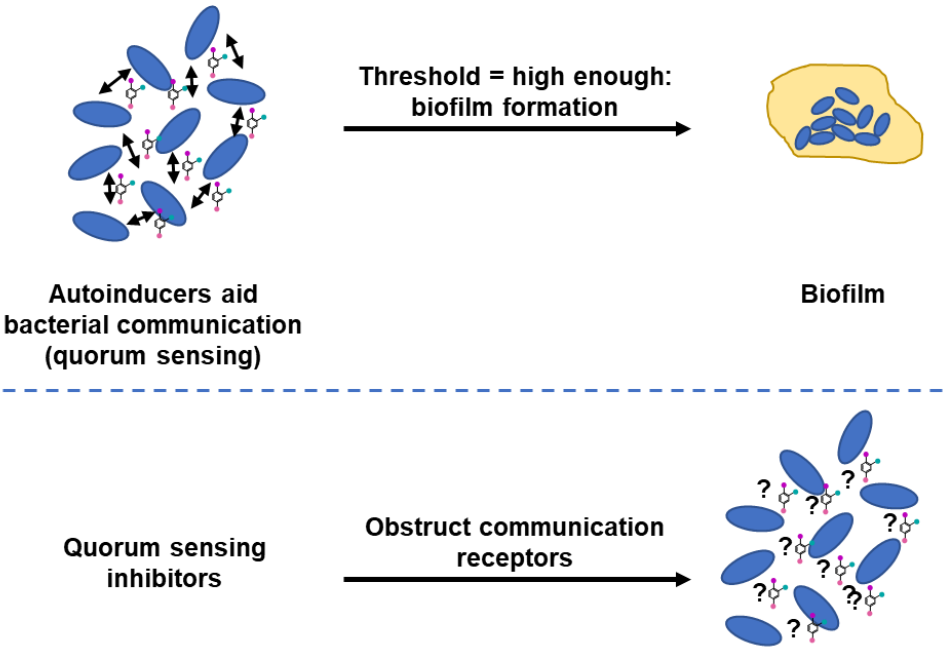

Figure 1.16: Autoinducers aid bacteria in pathogenesis. New mechanisms aim to inhibit quorum sensing, which most likely will not enable resistance, because quorum sensing is not necessary for bacterial survival, thus lessening evolutionary pressure for resistance.

1.5.3 New targets

Several antibiotics possess the same or similar targets, thus conferring resistance if they operate in similar mechanisms.[4,21,22] A method to circumvent this is to explore new targets. [4,21,22] Analysis of the microbial genome indicates that there are other promising targets for antibacterial activity. [4,21] One such strategy is to inhibit virulence factor expression (**Fig. 1.16**). [4,21,22] Virulence factors are typically but not always small molecules produced by the infecting bacterial cell that aid in host infection.[4,21,22] Inhibiting virulence factors would lead to less evolutionary pressure for the bacteria to develop resistance, because inhibiting virulence will not outright kill the bacteria. [4,21,22] Another novel target method is to pursue other cell wall biosynthesis targets, such as Lipid II or Mur enzyme inhibition. [4,21,22] Lipid II being necessary for peptidoglycan synthesis but not necessary for eukaryotic cells, thereby lessening potential toxic effects. [4,21,22] The idea of Mur enzyme inhibition stems from that Mur enzymes catalyze the first step in peptidoglycan synthesis and are necessary to prokaryotic survival. [4,21,22]

1.5.4 New mechanisms

New mechanisms are intertwined with new targets, because often new targets require a new mechanism of action, such as with Lipid II inhibition. [4,21,22] Teixobactin is a natural product that was cultured from the previously "unculturable" *Eleftheria terrae*. [4,21,22] Teixobactin kills *S. aureus* and *Mycobacterium tuberculosis* via sequestering lipid II and lipid III, leading to bacterial cell death. [4,21,22]

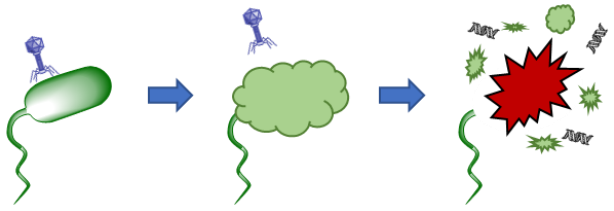

Figure 1.17: Bacteriophages can infect bacteria and then kill them via causing the bacterium to explode, which then releases the viral DNA for infecting other bacteria.

Another new mechanism utilizes bacteriophages (**Fig. 1.17**). [4,21,22] It capitalizes on the viral nature of bacteriophages in infecting other bacterial cells and lysing them. Its main use is for integrating into the human genome and replicating human DNA without lysing the host. [4,21,22] However, bacteriophages can also synthesize antimicrobial peptides *in situ* or carry the genes to the host cell for it to synthesize the antibacterial. [4,21,22]

1.5.5 Membrane mechanisms

Membrane mechanisms are often overlooked as methods to circumvent resistance due to selectivity issues.[23-25] Mechanisms that target the membrane capitalize on that bacterial cell wall structure and organization is species specific and better understood now, which has lead to membrane-targeting antimicrobials, but there are still toxicity issues as exemplified with QACs.[4-8,23-25] There is a slew of membrane mechanisms that target cell wall biosynthesis in Gram-positive bacteria (β-lactams and glycopeptides), and there exist a few antibiotics that target the outer membrane in Gram-negative bacteria (polymyxin B and E, colistin); however, these are not the only membrane mechanisms in existence.[23-25] There also are mechanisms that affect membrane permeabilization or membrane potential (depolarization or hyperpolarization).[23-25] Permeabilization is the result of tiny holes being created in the membrane, which then allows for the contents within the bacterial cell to seep out (**Fig. 1.18**).[23-25] A change in membrane potential

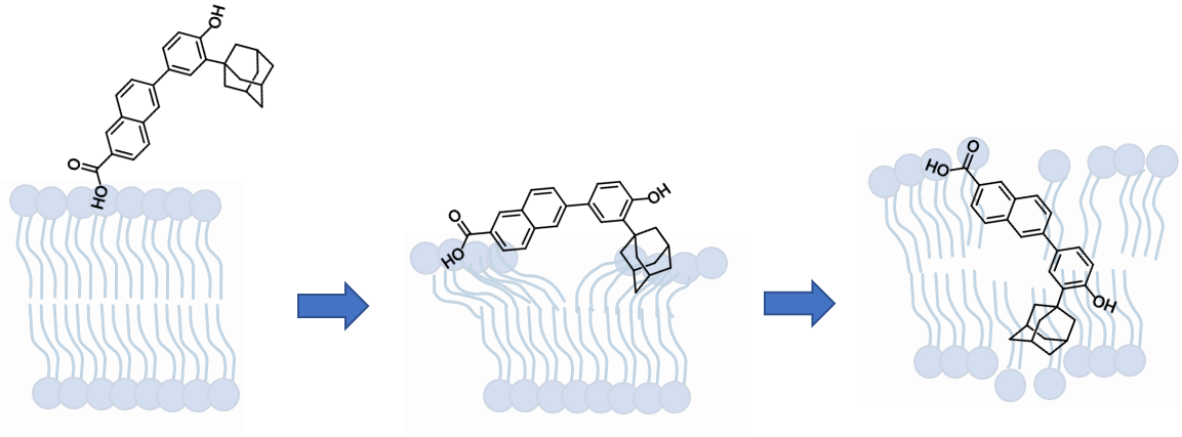

Figure 1.18: CD437 permeabilizes Gram-positive bacterial cell membranes via intercalation.

switches the electrical gradient across the membrane, which can lead to cell death.[23-25] For more detail on permeabilization or membrane potential, please see Chapter 3 as it discusses our explorations into the mechanism of honokiol and how it affects *Streptococcus mutans* planktonic cell membranes.

1.6 My projects

In this dissertation, I will discuss my efforts toward creating new antibacterials through three different projects (**Fig. 1.19**). The first project focuses on the small molecule, **nTZDpa**, and our efforts toward designing a non-toxic derivative. The second project involves the biological investigation of **honokiol** derivatives and elucidating the mechanism of action of **C2**. Chapter 3 focuses on my efforts toward synthesizing the **ogipeptins**, which I hypothesize inhibit LpxC biosynthesis, and is a project I developed for my National Science Foundation Graduate Research Fellowship Program application.

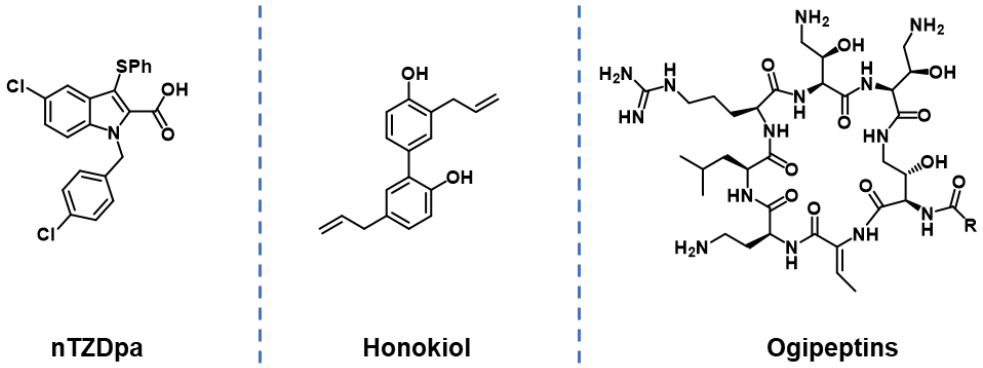

Figure 1.19: My three projects in the Wuest Lab.

Works Cited:

1. Aminov, R.I.; *Frontiers in Microbiol*., **2010**, *1(134)*, 1.
2. Aldrige, S., Parascandola, J.; Sturchio, J.L.; American Chemical Society Inernational Historic Chemical Landmarks. Discovery and Development of Penicillin. http://www.acs.org/content/acs/en/education/whatischemistry/landmarks/flemingpenicillin.html. Accessed 12 March 2022
3. Kresge, N.; Simoni, R.D.; Hill, R.L.; *J. Biol. Chem.*, **2004**, *279(48)*, e7.
4. Rossiter, S.E.; Fletcher, M.H.; Wuest, W.M.; *Chem. Rev.*, **2017**, *117*, 12415.
5. Morrison, K.R.; Allen, R.A.; Minbiole, K.P.C.; Wuest, W.M.; *Tet Lett*, **2019**, *60*, 150935.
6. Teng, F.; He, T.; Huang, S.; Bo, C.-P.; Li, Z.; Chang, J.-L.; Liu, J.-Q.; Charbonneau, D.; Xu, J.; Li, R.; Ling, J.-Q.; *Internat. J. Oral Sci.*, **2016**, *8*, 182.
7. Melin, V.E.; Potineni, H.; Hunt, P.; Griswold, J.; Siems, B.; Werre, S.R.; Hrubec, T.C.; *Reprod. Toxicol.*, **2014**, *50*, 163.
8. Hora, P.I.; Pati, S.G.; McNamara, P.J.; Arnold, W.A.; *Environ. Sci. Technol. Lett.*, **2020**, *7*¸ 622.
9. Centers for Disease Control and Prevention. “COVID-19 & Antibiotic Resistance.” **2021**. Accessed 17 Jan 2022.
10. Reygaert, W.C. *AIMS Microbiol.* **2018**, *4*, 482.
11. Centers for Disease Control & Prevention, “Antibiotic Resistance Threats in the United States 2019” **2019**, 1.
12. Centers for Disease Control and Prevention. “About Antibiotic Resistance.” **2021**. Accessed 9 Feb 2022.
13. Fisher, R.A.; Gollan, B.; Helaine, S.; *Nat. Rev.: Microbio*, **2017**, *15*, 453.
14. Brauner, A.; Fridman, O.; Gefen, O.; Balaban, N.Q.; *Nat. Rev. Microbiol.*, **2016**, *14*, 320.
15. Markley, J.L.; Wencewicz, T.A.; *Frontiers in Microbiol.*, **2018**, *9*, 1058.

16. Zhong, S.-F.; Yang, B.; Xiong, Q.; Cai, W.-W.; Lan, Z.-G.; Ying, G.-G.; *Ecotox. Environment. Safety*, **2022**, *229*, 113063.
17. Worthington, R.J.; Melander C.; *J. Org. Chem.*, **2013**, *78*, 4207.
18. Coates, A.R.M.; Hu, Y.; Holt, J.; Yeh, P.; *Expert Review of Anti-infective Therapy*, **220**, *18,* 5.
19. Sullivan, T. "A Tough Road: Cost to Develop One New Drug Is $2.6 Billion; Approval Rate for Drugs Entering Clincal Development is Less Than 12%," *Policy & Medicine*, **2019**, Accessed 17 April 2022.
20. Wright, G.D.; *Trends in Microbiol*, **2016**, *24*, 862.
21. Belete, T.M.; *Human Microbiome Journal*, **2019**, *11*, 100052.
22. Opitz, C.L.M.d.; Sass, P.; *Future Microbiol.*, **2020**, *15*, 703.
23. Matamoros-Recio, A.; Franco-Gonzalez, J.F.; Fergione, R.E.; Torres-Mozas, A.; Silipo, A.; Martin-Santamaria, S.; *ACS Omega,* **2021**, *6*, 6041.
24. Epand, R.M.; Walker, C.; Epand, R.F.; Margarvey N.A.; *Biochimica et Biophysica Acta*, **2016**, *1858*, 980.
25. Schrank, C.L.; Wilt, I.K.; Ortiz, C.M.; Haney, B.A.; Wuest, W.M.; *RSC Med. Chem.* , **2021**, *12*, 1312.
26. Taylor, T.A.; Unakal, C.G.; [Updated 14 Feb 2022]. In: StatPEarls [Internet]. Treasure Island: StatPearls Publishing. Accessed 19 Mar 2022
27. Chapot-Chartier, M.-P.; Kulakauskas, S.; *Microbial Cell Factories*, **2014**, *13(Suppl1):59*, 1.
28. Pasquina-Lemonche, L.; Burns, J.; Turner, R.D.; Kumar, S.; Tank, R.; Mullin N.; Wilson, J.S.; Chakrabarti, B.; Bullough, P.A.; Hobbs, J.K.; *Nature*, **2020**, *582*, 294.
29. Powers, MJ.; Trent, M.S.; *Prod. Natl. Acad. Sci.*, **2018**, *115,* E8518.
30. May, K.L.; Grabowicz, M.; *Prod. Natl. Acad. Sci.* **2018**, *115*, 8852.

Chapter 2: nTZDpa

Adapted from Kim, W.; Steele, A.D.; Zhu, W.; Csatary, E.E.; Fricke, N.; Dekarske, M.M.; Jayamani, E.; Pan, W.; Kwon, B.; Sinitsa, I.F.; Rosen, J.L.; Conery, A.L.; Fuch, B.B.; Vlahovska, P.M.; Ausubel, F.M.; Gao, H.; Wuest, W.M.; Mylonakis, E.; ACS Infect. Dis., ***2018****, 4, 1540; Kim, W.; Zou, G.; Hari, T.P.A.; Wilt, I.K.; Zhu, W.; Galle, N.; Faizi, H.A.; Hendricks, G.L.; Tori, K.; Pan, W.; Huang, X.; Steele, A.D.; Csatary, E.E.; Dekarske, M.M.; Rosen, J.L.; Ribeiro, N.d.Q.; Lee, K.; Port, J.; Fuchs, B.B.; Vlahovska, P.M.; Wuest, W.M.; Gao, H.; Ausubel, F.M.; Mylonakis, E.; Proc. Natl. Acad. Sci.* ***2019****, 116, 16529; Dekarske, M.M.; Felix, L.O.; Ortiz, C.M.; Csatary, E.E.; Mylonakis, E., Wuest, W.M.; Bioorg. Med. Chem. Lett.,* ***2022****, 64, 128678. Used with permission.*

2.1 Introduction

Staphylococcus aureus is the most clinically-relevant species of the *Staphylococcus* genus.[1-8] Within the general population, its prevalence in nasal mucous varies (about 20-40%) with the difference in survey sampling being largely responsible for the wide range.[1] Further, when the cutaneous or the mucosal membranes are sufficiently disturbed, this can allow *S. aureus* to enter the bloodstream and cause infection.[1] *S. aureus* infections can look innocuous as pimples or skin abrasions but can cause sepsis, pneumonia, or toxic shock syndrome.[1,2] While *S. aureus* infections are dangerous, methicillin-resistant *S. aureus* (MRSA) infections are worse because of their lack of response to first-line antibiotics.[1-8]

MRSA is classified by the Centers for Disease Control & Prevention (CDC) as a serious threat (**Fig. 2.1**).[2] As previously mentioned, MRSA (and other drug resistant cell lines of *S. aureus*)

Figure 2.1: Photo of MRSA cells and infection, which left untreated can lead to severe health issues and even death. MRSA photos from CDC, National Center for Emerging and Zoonotic Infectious Diseases (NCEZID), Division of Healthcare Quality Promotion (DHQP).

are resistant to first-line antibiotics (e.g. methicillin and gentamicin, which possess different bacterial targets).[1-4,10] According to the CDC, MRSA caused an estimated 323,700 infections, which resulted in 10,600 deaths in 2017 alone.[2] These infections culminated in $1.7 billion spent in healthcare costs.[2] While the CDC indicates that there is an overall decrease in the number of MRSA cases, infection prevention is stalling.[2,5-8,10] Furthermore, those who utilize drugs via injection methods have a higher risk (16x) of developing a MRSA infection, thus making them a vulnerable population.[2]

Additionally, there are two types of MRSA: community-acquired and hospital-acquired.[1] Hospital-acquired MRSA (HA-MRSA) is phenotypically and genetically different than community-acquired MRSA (CA-MRSA).[1] While misleading, HA-MRSA does indeed circulate outside of hospitals but is mostly concentrated within them.[1] CA-MRSA also manufactures a *Staphylococcal* virulence factor, PVL (Panton-Valentine leukocidin), that attacks white blood cells. Thus, MRSA is a serious threat, and we need more therapeutics that can kill both types of MRSA effectively.[1]

2.1.1 High-throughput screen

In investigating new compounds that can kill MRSA, the Mylonakis Lab at Brown University conducted a high throughput screen of more than 80,000 compounds (**Fig. 2.2**).[5-8] In their screen, they utilized *Caenorhabditis elegans* (nematodes) and SYTOX Orange dye.[5-8] They then infected the nematodes with MRSA and dosed with compound and SYTOX Orange dye to visualize their survival.[5-8] Alive nematodes would not fluoresce, while dead nematodes would.[5-7] Thus, the screen also acted as an initial toxicity screen.[5-8] Additionally in their high-throughput screen, they utilized vancomycin and DMSO as positive and negative controls, respectively.[5-8] In their screening efforts, Mylonakis and coworkers found that three compounds were able to rescue the nematodes from MRSA infection: nTZDpa, bithionol, and CD437 (**2.1**, **2.2**, and **2.3**, respectively), all of which spurred collaborations between our labs.[5-8]

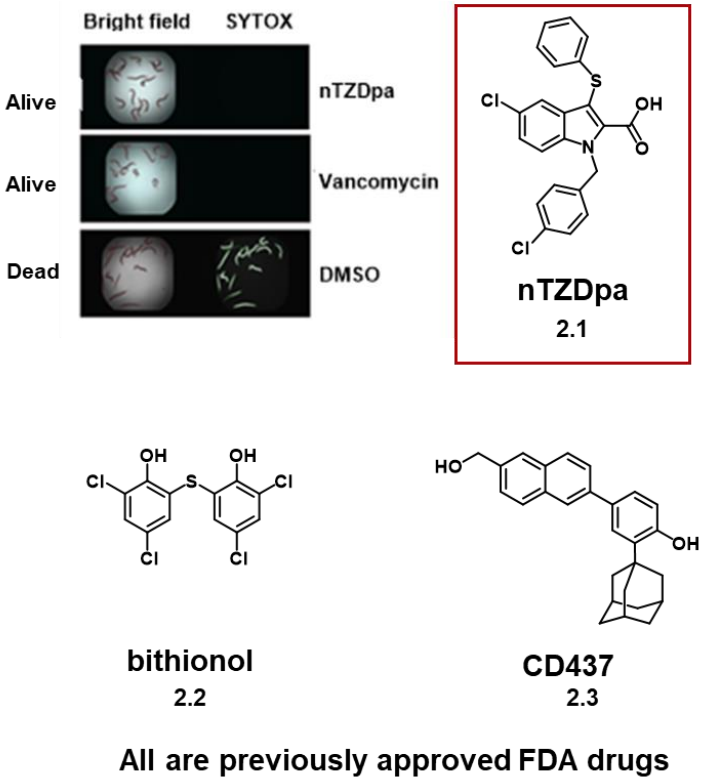

Figure 2.2: High throughput screen conducted by the Mylonakis Lab and structures of the three hits, which spurred three collaborations with our lab.

2.1.2 Resistance vs persistence

While nTZDpa is able to kill resistant *S. aureus*, the impetus for the project is its ability to kill persister cells (**Fig. 2.3**). To understand the implications of killing persister cells, one must examine the differences in resistance, tolerance, and persistence, which are three different terms to classify how bacteria survive antibacterial pressure.[9-12] Resistance is when bacteria can survive and proliferate despite high antibiotic concentrations and results in the change of the minimum inhibitory concentration (MIC) for that antibiotic (a genetic change).[9-12] Tolerance differs in that bacteria are still able to survive for a short-term antibacterial pressure but that there is no change in the MIC.[9-12] This typically is exemplified by bacteria slowing down cellular processes, such as cell wall synthesis.[9-12] For example, it is difficult for β-lactam antibiotics, which target cell wall synthesis, to then perform their mechanism of action.[9-12] Therefore, for the β-lactam antibiotic to produce the same killing level as in a non-tolerant strain, the bacteria must be subjected to the antibiotic for a longer period of time.[9-12]

Meanwhile, persistence is when a subpopulation of bacteria that are genetically the same to the rest of the population can survive high antibacterial concentrations, which killed the rest of the bacterial population.[11,12] Interestingly, this phenotype is not inheritable, unlike resistance and some tolerance.[11,12] Single cell studies indicated that slowed growth and dormancy may lead to persister cell survival in high antibiotic concentrations.[11,12]

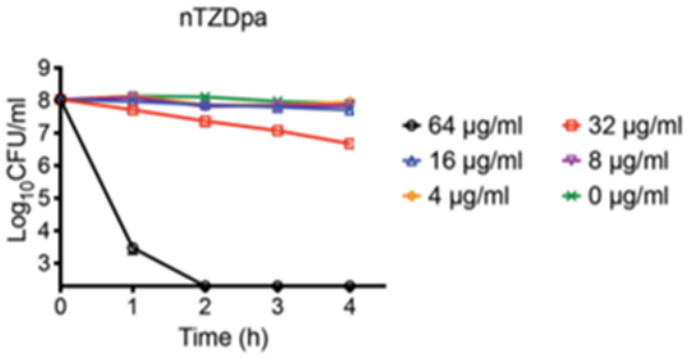

Figure 2.3: nTZDpa eradicates persister cells at high concentration.

Time-kill curves further illustrate the difference in tolerance and persistence.[11,12] The tolerance time-kill curve indicates that to achieve 99% cell death requires a much longer period of time.[11,12] The persistence time-kill curve contrasts in that it is biphasic.[11,12] So, while both tolerant and persistent bacteria have the same MIC as their susceptible strains, in persistent infections, the antibiotic is able to perform its mechanism of action well for a certain amount of the population.[11,12] Once the antibiotic has killed all but the persistent population, it approaches a limit to which killing the rest of the (persistent) bacteria population necessitates an exceedingly longer amount of time.[11,12] Thus, the impetus for this project is the ability of nTZDpa to kill persister cells.[5-8]

2.1.3 Resistance selection and mechanism studies

After determining that nTZDpa was able to kill both resistant and persistent *S. aureus*, Mylonakis and coworkers sought to determine its mechanism of action.[5] They first turned to a resistance selection assay (serial passage), which would give them information about what pathway nTZDpa affects from the mutant generated.[5] However, they were unable to produce a mutant, which is a hallmark of membrane mechanisms.[13]

To further probe the mechanism of action, they performed a membrane permeabilization assay that uses SYTOX Green dye and measures fluorescence (**Fig. 2.4**).[5,6] In this assay, bacterial cells uptake the SYTOX Green dye, and a base fluorescence is obtained.[5] Then, the cells are treated with compound at various concentrations, and the fluorescence is measured.[5]

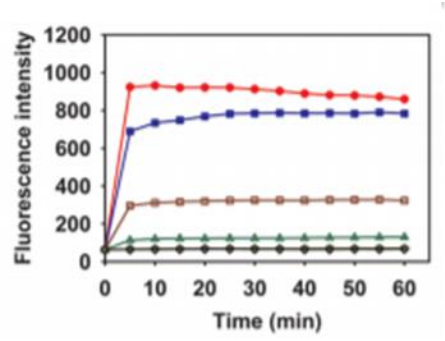

Figure 2.4: Graph highlighting membrane permeabilization induced by nTZDpa.

Compounds that cause membrane permeabilization (creating holes in the cell membrane, thus allowing the SYTOX Green dye to leech out) will read an increase in fluorescence intensity, which was indeed what the Mylonakis Lab observed.[5]

To further verify this membrane permeabilization, the Mylonakis Lab obtained TEM (transmission electron microscope) images (**Fig. 2.5**).[5] These microscopes utilize electron particle beams to achieve high magnification; thus, they can visualize bacterial cells.[5] The Mylonakis Lab then treated *S. aureus* cells with nTZDpa (or the DMSO negative control) and froze the cells with a chemical agent to have a snapshot of those cells at that particular time point.[5] From their images, they observed abnormal cell division as well as cell lysis, both indicative of membrane mechanisms.[5] However, the red arrows show mesosomes, which are artifacts of cell freezing in preparation for obtaining TEM images.

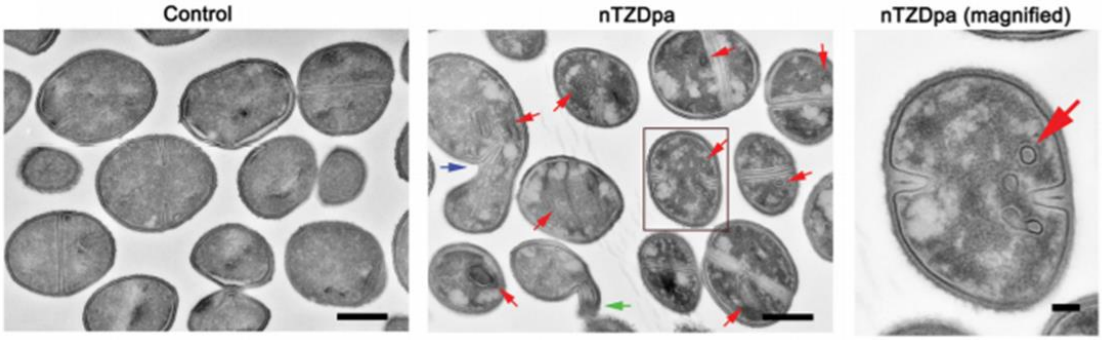

Figure 2.5: TEM images highlighting the abnormal cell division (blue arrow) and cell lysis (green arrow). Red arrows are mesosomes, which are artifacts of freezing the cells.

2.1.4 Restoring gentamicin activity

Further highlighting the importance of this project was the ability of nTZDpa to restore gentamicin activity.[5] Gentamicin is an aminoglycoside antibiotic that acts on the aminoacyl-tRNA recognition site within the 30S ribosomal subunit.[11,14] Thus, bacteria can no longer synthesize polypeptides, ultimately leading to cell death.[11,14] Resistance to gentamicin can be conferred in a multitude of methods. However, a popular mechanism of resistance is target modification via methylating the 30S subunit at the active site of the 16S rRNA, which then prevents gentamicin

binding.[14] While nTZDpa may not be able to aid in the methyltransferase resistance pathway, nTZDpa can assist gentamicin entry into the bacterial cell.[5] Thus, the Mylonakis Lab investigated combination therapy of gentamicin and nTZDpa and found that nTZDpa was able to act synergistically with gentamicin.[5]

2.1.5 Generation 1 SAR

Through the work done by the Mylonakis lab, it was determined that nTZDpa is able to kill resistant and persistent *S. aureus* at 4 μg/mL and 64 μg/mL, respectively, as well as restore gentamicin activity (**Fig. 2.6**).[5] Despite the promise of nTZDpa as a therapeutic, it possessed a key issue: red blood cell toxicity.[5] The Mylonakis Lab then reached out and formed a collaboration with our lab in order to perform a first round of structure-activity relationships (SAR) around the core scaffold.[5] This first generation of SAR was executed by Dr. Andrew Steele.

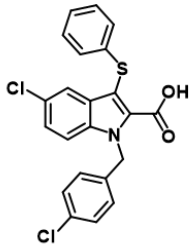

nTZDpa
2.1
MIC: 4 μg/mL
PKC: 64 μg/mL
HC_{50}: 50 μg/mL

Figure 2.6: nTZDpa: able to kill resistant and persister *S. aureus* but lyses red blood cells.

In Steele's work, he began with a precedented Buchwald-Hartwig-type coupling to form the indole core from 4-chloro-2-iodoaniline and pyruvic acid (**Fig. 2.7**).[5] Next, he protected the acid with thionyl chloride and ethanol to generate the ethyl ester.[5] Following this, he generated the thioether by forming the chlorothiol by stirring N-chlorosuccinimide and thiophenol.[5] Then, the indole starting material is added and acts as the nucleophile.[5] Next, Steele alkylated at the 1-position of the indole core via an S_N2 addition with potassium carbonate in DMF at 60 ºC with

TBAB as a phase transfer catalyst.[5] He subsequently hydrolyzed the ester to the acid with sodium hydroxide in a THF/ethanol solution.[5]

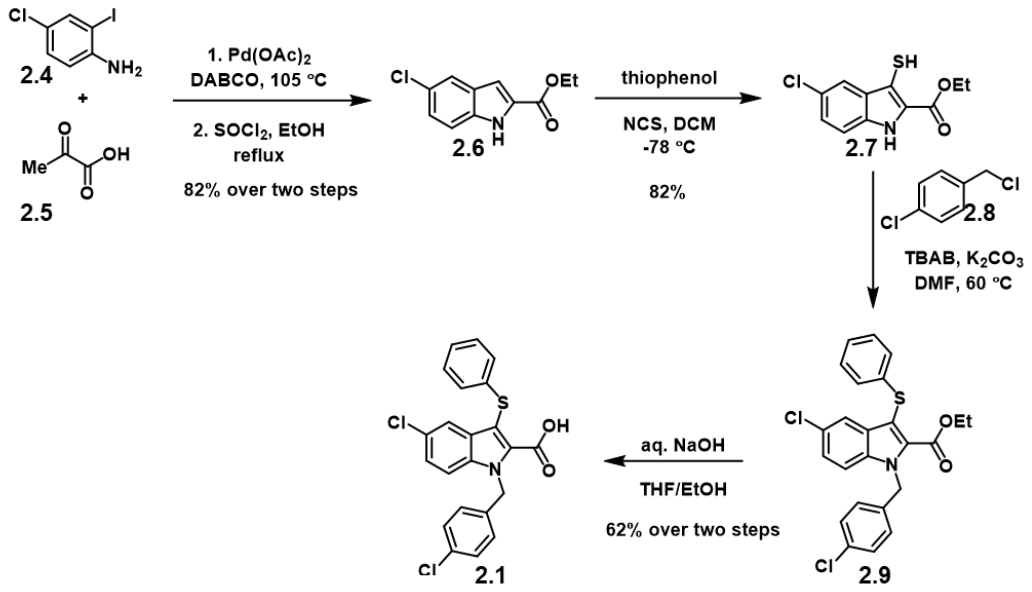

Figure 2.7: Dr. Steele's synthesis of nTZDpa (also utilized in Gen 1 SAR).

After devising a synthesis that is amenable to diversification, Steele began his SAR (**Fig. 2.8**).[5] From his SAR, he found that he could improve persister killing via adding a *t*-butyl or chloro- to the 4-position of the aryl sulfide.[5] He established that there was no improvement in activity when he functionalized with a 6-chloro, 5-fluoro, or 5-trifluoromethyl on the indole core itself.[5] He

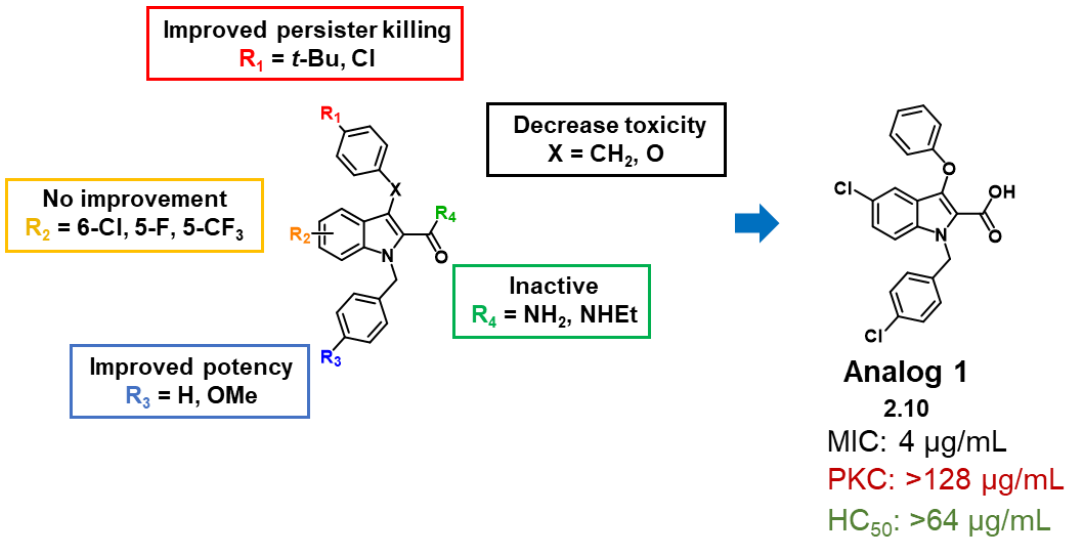

Figure 2.8: Highlights of Gen 1 SAR designed and synthesized by Dr. Andrew Steele, resulting in Analog 1, **2.1**.

could then improve the potency via changing the 4-chlorobenzyl to a nonfunctionalized benzyl or a 4-methoxylbenzyl.[5] Following this, he modified the acid to a primary or secondary amide, both of which were found to not be tolerated and lost all activity.[5] Lastly, he found changing the sulfide to an ether mitigated the red blood cell toxicity previously seen.[5] Thus, the best compound out of this first generation of SAR was Analog 1(**2.10**).[5] However, while Analog 1 was just as potent at killing resistant *S. aureus* and no longer lysed red blood cells, the persister killing ability was totally ablated, which was the impetus for the project.[5] This then resulted in a second round of SAR, in which Dr. Erika Csatary and I came onto the project.

2.1.6 Mechanism

However, before detailing our efforts in the second generation of SAR, the first round further informed the mechanism.[5] From Steele's work, we understand that the acid is necessary for activity.[5] At physiological pH, the acid should be deprotonated. The acid then anchors into the lipid bilayer, most likely through interactions with the divalent cations embedded within the membrane surface, and then folds over and disrupts the membrane (**Fig. 2.9**).[5] This "wrecking ball" action allows for the compound to sufficiently disturb and permeabilize the membrane, thus creating holes in the bacterial membrane, which enables the innards to leech out, ultimately leading to cell death.[5] Furthermore, the Gao Lab performed molecular modeling for how nTZDpa and its analogs function, and their modeling aligns with our hypothesis.[5]

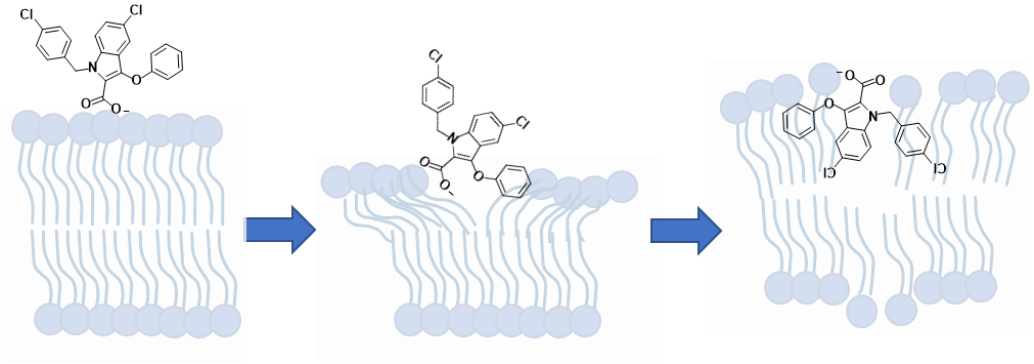

Figure 2.9: Proposed mechanism. nTZDpa anchors into the lipid bilayer with the rest of the molecule acting as a "wrecking ball" to create holes in the membrane, thus allowing the cell innards to leach out, ultimately leading to cell death.

2.2 Generation 2 SAR

2.2.1 Compounds

Because of the ether linkage at the 3-position of the core scaffold, this required a slightly different manner to synthesize analogs (**Fig. 2.10**).[5] Thus, Dr. Andrew Steele devised a route, in which we alkylate methyl 2-amino-5-chlorobenzoate to set up for the Dieckmann condensation, which was performed with freshly prepared sodium methoxide refluxing in THF.[5] After obtaining the indole core, we then protected the alcohol at the 3-position with dimethyl sulfate to prevent over-alkylation in the next step.[5] The next step was one of our main derivatization steps in which we performed a substitution at the 1-position of the indole.[5] Next, we de-methylated with boron

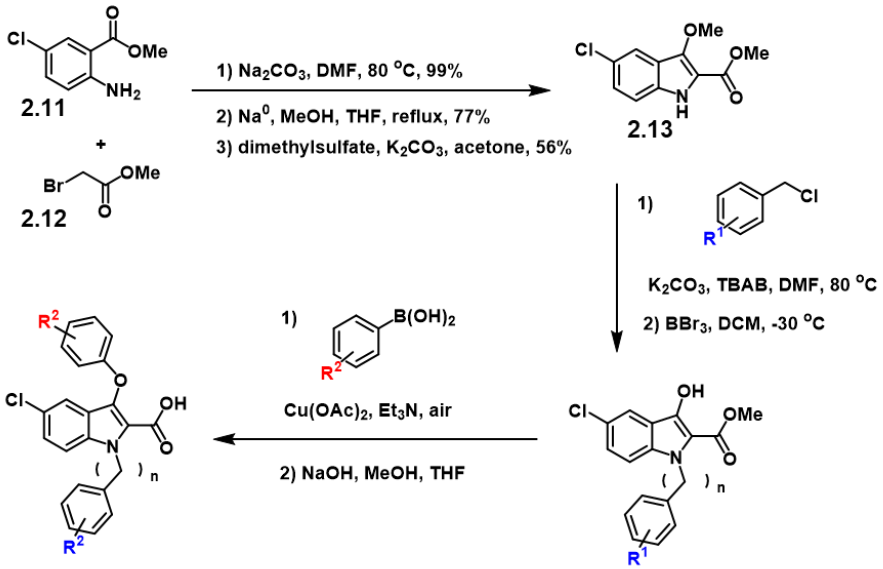

n =1: R^1 = 3-Cl	R^2 = 4-H	2.20	
= 2,4-Cl	= 4-H	2.21	
= 3,4-Cl	= 4-H	2.22	
= 4-Br	= 4-H	2.23	
= 4-F	= 4-H	2.24	
= 4-Cl	= 4-Cl	2.25	
= 4-Cl	= 4-F	2.26	
= 4-Cl	= 4-*t*-Bu	2.27	
= 4-Cl	= 4-OH	2.28	
= 4-Cl	= 4-Br	2.29	
= 4-Cl	= 4-I	2.30	
= 4-Cl	= 4-CF_3	2.31	
= 4-Cl	= 3,4-Cl	2.32	
= 4-Cl	O-Bn	2.33	
n = 2: R^1 = 4-Cl	R^2 = 4-H	2.34	

n =1: R^1 = 3-Cl	2.14	
= 2,4-Cl	2.15	
= 3,4-Cl	2.16	
= 4-Br	2.17	
= 4-F	2.18	
n = 2: R^1 = 4-Cl	2.19	

Figure 2.10: Route utilized in Gen 2 SAR (and partially used in Gen 3).

tribromide in DCM at -30 ºC, which then enabled us to perform a Chan-Lam coupling with the free alcohol to append the aryl fragment and form the phenylether.[5] Lastly, we saponified with sodium hydroxide in a 1:1 mixture of THF and methanol to obtain our desired acid. Dr. Csatary and I both built up grams of key intermediates (methylation **2.13** and demethylation **2.35** products) in order to enable our SAR campaign.[5]

In our SAR, we primarily investigated further functionalization to the benzyl fragment at the 1-position and the aryl piece at the 3-position (**Fig. 2.10**).[5] In our 1-position investigation, we examined 3-chlorobenzyl, 2,4-dichlorobenzyl, 3,4-dichlorobenzyl, 4-bromobenzyl, 4-fluorobenzyl, and an extra methylene spacer.[5] In our 3-position investigation, we made analogs containing 4-chlorophenyl, 4-fluorophenyl, 4-*t*-buylphenyl, 4-hydroxyphenyl, benzyl, 4-bromophenyl, 4-iodophenyl, 4-trifluoromethylphenyl, and 3,4-dichlorophenyl ethers.[5] Dr. Csatary also made three analogs examining the substituent at the 5-position on the indole scaffold, which were fluoro-, benzyl-, and bromo-, and additionally explored reducing the acid at the 2-position to an alcohol.[5] I was responsible for final analogs **2.29**, **2.30**, **2.31**, **2.33**, and **2.34** and their syntheses.[5]

2.2.2 Rationale & activity

The rationale behind our design was that changes to the aryl ether and the benzylic fragment were facile to incorporate (**Fig. 2.11**).[5] Furthermore, we focused on halogens not for their electron-withdrawing inductive effects, but instead for their spherical nature.[5] Re-examining our hypothesized mechanism, halogens would enhance the “wrecking ball” nature of our

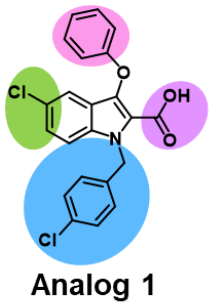

Analog 1

Figure 2.11: Zones that we focused on in our Gen 2 SAR. We primarily examined the aryl ether (pink) as well as the benzyl fragment at the 1-position of the indole core (blue), but we also made changes to the 5-position (green) and the acid (purple).

compounds and aid in disrupting the lipid bilayer.[5] The trifluoromethyl analog stemmed from industrial literature about the “magic methyl” and trifluoromethyl, and thus sticking to our previous success with halogens, we pursued the trifluoromethyl.[5] We also chose to not pursue many alkyl substituents in lieu of aryl fragments at the 3-position due to lack of potency previously observed by Dr. Steele.[5] The alcohol analog (reduction of the carboxylic acid at the 2-position of the indole core) originated from a sister project, CD437 and their success.[6]

Of these changes, we found we could improve potency for killing resistant and persistent *S. aureus* with the certain changes to the 3-position aryl ether: 3,4-dichlorophenyl, 4-bromophenyl, and 4-iodophenyl ether analogs.[5] Furthermore, we observed that the 4-chlorophenyl ether analog also was potent at killing resistant *S. aureus* but lost persister killing activity, similar to Analog 1.[5] We also could improve the potency by substituting the 4-chlorobenzyl fragment at the 1-position with more chlorines.[5] From this second round of SAR, we made the next lead, Analog 2 (**2.30**), which I designed and synthesized (**Fig. 2.12**).

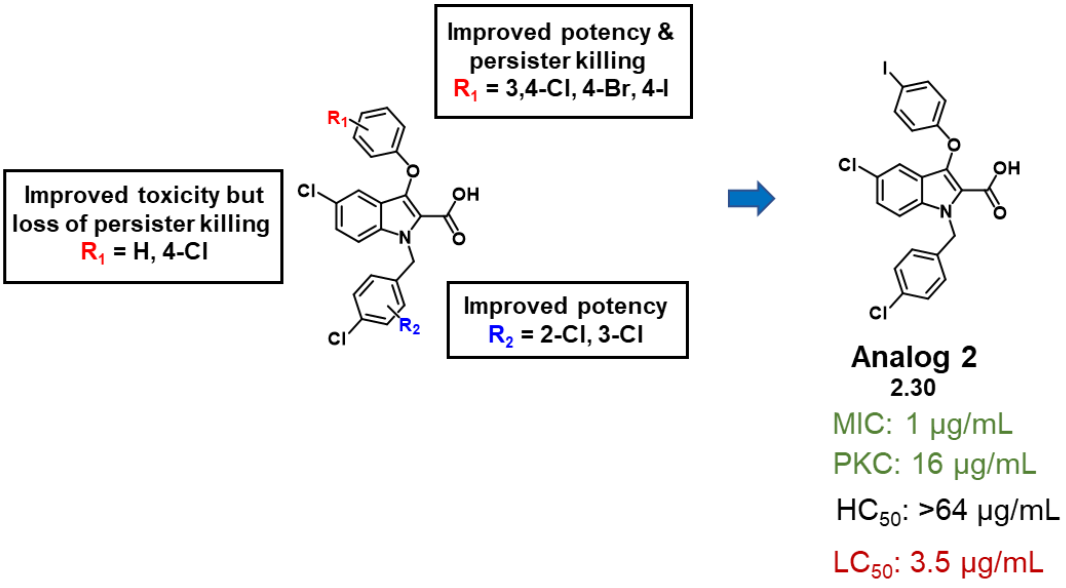

Figure 2.12: Gen 2 SAR highlights culminating in Analog 2: more potent at killing resistant and persistent *S. aureus* and nontoxic to red blood cells but toxic to renal (kidney) cells.

2.2.3 Renal toxicity

As previously mentioned, we generated a new lead compound, Analog 2, which is more potent at killing not only resistant *S. aureus* but also persistent *S. aureus* (**Fig. 2.12**).[5] It also does not lyse red blood cells.[5] In further testing to validate that this nTZDpa derivative could become a potential therapeutic, the Mylonakis Lab discovered that Analog 2 displays renal cell toxicity.[8] Because the kidneys are vital, we performed one last round of SAR in order to combat the renal cell toxicity, which is when I became the lead on this project.

2.2.4 Membrane fluidity

In a sister project to nTZDpa, the Mylonakis Lab investigated bithionol as a potential therapeutic against resistant and persistent *S. aureus*, and our lab designed SAR around the bithionol backbone.[7] In the biological investigation, the Mylonakis Lab found an interesting correlation between membrane permeability, membrane fluidity (cell membrane viscosity), and persister killing.[7] Because of their initial findings, they then utilized our nTZDpa analogs to further elucidate this relationship.[7] The Mylonakis lab found that while some nTZDpa analogs do induce a membrane permeabilization event with SYTOX Green, they do not induce a change in membrane fluidity.[7] Interestingly, these compounds also do not kill persisters.[7] They attribute this lack of persister killing to localized membrane damage that is enough to indicate a permeabilization event occurred but not enough to show an overall increase in membrane fluidity.[7] Furthermore, they noticed that persister killing occurred only when there was a significant change in the overall membrane fluidity.[7]

2.3 Generation 3 SAR

2.3.1 Hypotheses

In this final round of SAR, I endeavored to construct compounds with improved toxicity profiles by answering lingering questions about our scaffold (**Fig. 2.13**).[8] Hashimoto previously showed that flat, planar compounds tend to stack well and then precipitate out of solution, typically in the kidneys, which could account for the renal toxicity that we observed.[15] Therefore, I postulated that by increasing the sp^3 character of our compounds we could diminish this effect.[8] Furthermore, all the potent analogs that we had developed to date possessed an acid at the 2-position of the indole scaffold and were toxic to renal cells.[8] However, some previously derived analogs lacking the acid had improved renal toxicity numbers albeit with lower potency.[8] Therefore, I hypothesized that we could produce a less toxic, equally potent new lead compound via slightly increasing sp^3 character or by interchanging the acid for other known bioisosteres.[8,17] This work was completed by Dr. Erika Csatary, Carlos Monteagudo Ortiz (an undergraduate), and myself.[8]

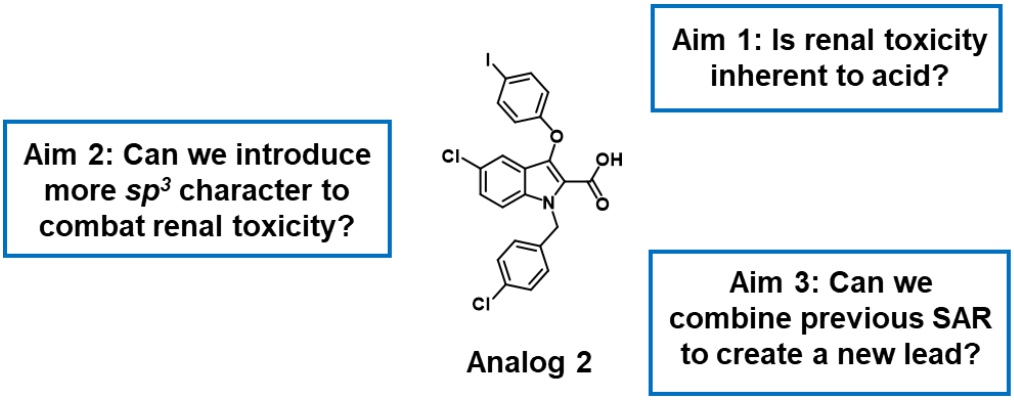

Figure 2.13: Questions leading into third and final generation of SAR.

2.3.2 Compounds & Renal toxicity

First, we examined if the renal toxicity could be improved by increasing sp^3 character (**Fig. 2.14**).[8] Using our previous synthetic route, which included a key Dieckmann condensation to form the indole core, we were able to obtain the methyl (**2.41**) and *t*-butyl (**2.42**) analogs in short order.[8] Methylation of the resulting indole alcohol, alkylation of the 1-position of the indole, and

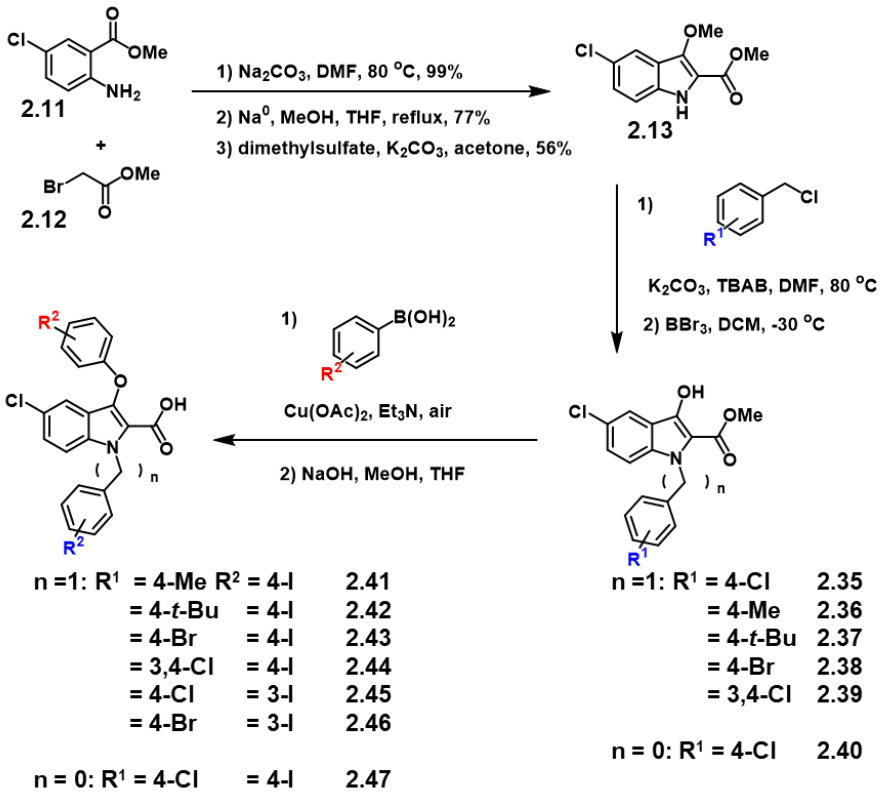

Figure 2.14: General scheme of some third generation compounds.

deprotection of the methyl ether with boron tribromide yields the penultimate intermediate.[8] A Chan-Lam coupling yields the phenolic ether, which following basic hydrolysis, provides analogs **2.41** and **2.42.**[8] Unfortunately, although the *para*-*t*-butyl analog (**2.42**) maintained its potency, there was no improvement to its renal toxicity (**Table 2.1**).[8]

I next focused on introducing bioisosteres to replace the acid, with the goal of improving the renal toxicity profile (**Fig. 2.15**).[8,17] I aimed to access a tetrazole analogs **2.48** and **2.49**, which would act as an acid bioisostere.[8,17] In addition, I sought to make the amide-acid analogs **2.50** and **2.51**, which would homologate the acid farther away from the indole core.[8] From our mechanism of action studies and previous SAR work, I knew that the acid was necessary for activity but wanted to see if the placement of the acid away from the indole core would retain activity while introducing more sp^3 character.[8,15] For both analogs, I used **2.4** (or **2.30** depending on desired phenolic ether functionality) as our starting material.[8] For the tetrazole analog, I first

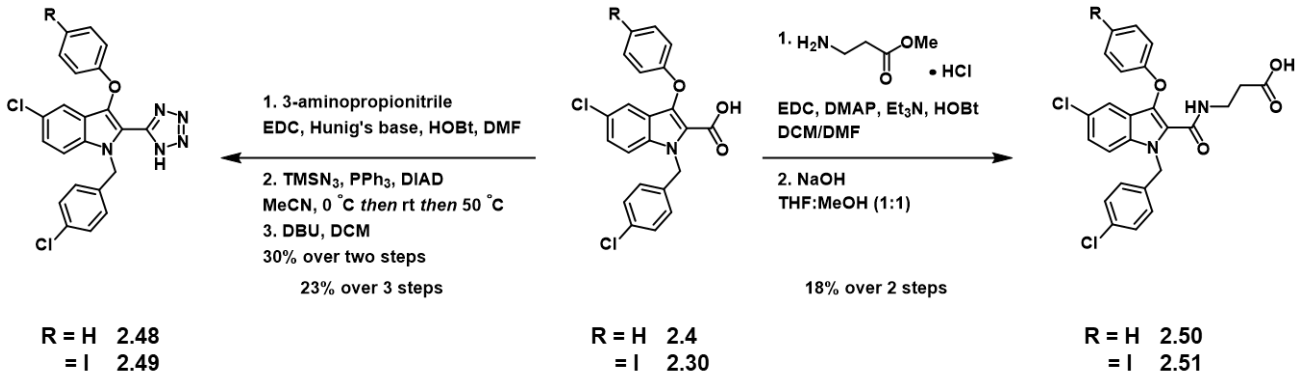

Figure 2.15: Routes to access acid isosteres.

amidated, cyclized with TMS-N_3, and then eliminated the alkyl chain with DBU to generate the free tetrazoles, **2.48** and **2.49**. With **2.50** and **2.51** (our amide-acid analogs), I amidated and then deprotected the methyl ester to obtain the desired analog.[8,17] Interestingly, the *p*-iodophenyl ether analogs (**2.48** and **2.49**) were inactive in both series, while the non-functionalized aryl ether analogs (**2.50** and **2.51**) were active.

In addition, to these compounds, we also synthesized five additional compounds by our general method presented in **Fig. 2.14**.[5,8] These compounds combined preferable aspects of previous analogs (i.e. location of heteroatoms) to test if these changes improved their renal toxicity.[8] These compounds largely retained their potency; however, none of these compounds significantly improved the renal toxicity. **Table 2.1** indicates who designed and made which compounds.[8]

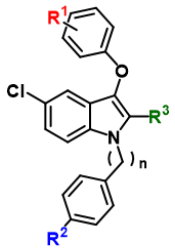

Cmpd #	R^1	R^2	R^3	n	MIC[a]	Renal Toxicity[b]
1 (prev. lead)	*p*-I	*p*-Cl	COOH	1	1	15%
2.41[c,d]	*p*-I	*p*-Me	COOH	1	8	15%
2.42[d,e]	*p*-I	*p*-*t*-Bu	COOH	1	1	10%
2.43[c,d]	*p*-I	*p*-Br	COOH	1	2	15%
2.44[c,d]	*p*-I	*m*, *p*-Cl	COOH	1	4	15%
2.45[e,f]	*m*-I	*p*-Cl	COOH	1	1	10%
2.46[c,d]	*m*-I	*p*-Br	COOH	1	8	15%
2.47[c,d]	*p*-I	*p*-Cl	COOH	0	16	20%
2.48[c,d]	*p*-H	*p*-Cl		1	8	20%
2.49[c,d]	*p*-I	*p*-Cl		1	>64	25%
2.50[c,d]	*p*-H	*p*-Cl	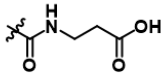	1	4	20%
2.51[c,d]	*p*-I	*p*-Cl	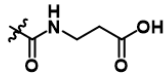	1	32	15%

[a] concentrations in μg/mL [b] % viability of cells at 64 μg/mL
Vancomycin and DMSO used as positive and negative controls, respectively. Vanco MIC: 1 μg/mL and 65% cells viable at 64 μg/mL. DMSO MIC: >64 μg/mL and 95% cells viable at 64μg/mL. [c] synthesized by MMD [d] designed by MMD [e] synthesized by CMO and EEC [f] designed by EEC

Table 2.1: Analogs made in third generation of SAR and their activity as well as who designed and synthesized which analogs.

2.3.3 Failed analogs

Because of successes seen in our lab toward optimizing the antimicrobial activity of CD437, I sought to incorporate an adamantyl in the Analog 2 scaffold in order to increase molecular surface area (**Fig. 2.16**).[6] I first endeavored to add the adamantyl via an S_N1 fashion with bromoadamantane at either the 1-position of the indole (in which nitrogen would act as the nucleophile) or at the 3-position of the indole (with the alcohol acting as the nucleophile) (**2.55**).

Unfortunately, I saw no success with either approach. I next thought to utilize cross coupling conditions, such as the Chan-Lam, to append the adamantyl fragment at the 3-position of the indole core. Much to my dismay, I never observed incorporation of the adamantyl, despite alkyl substituent competence in Chan-Lam couplings.[18]

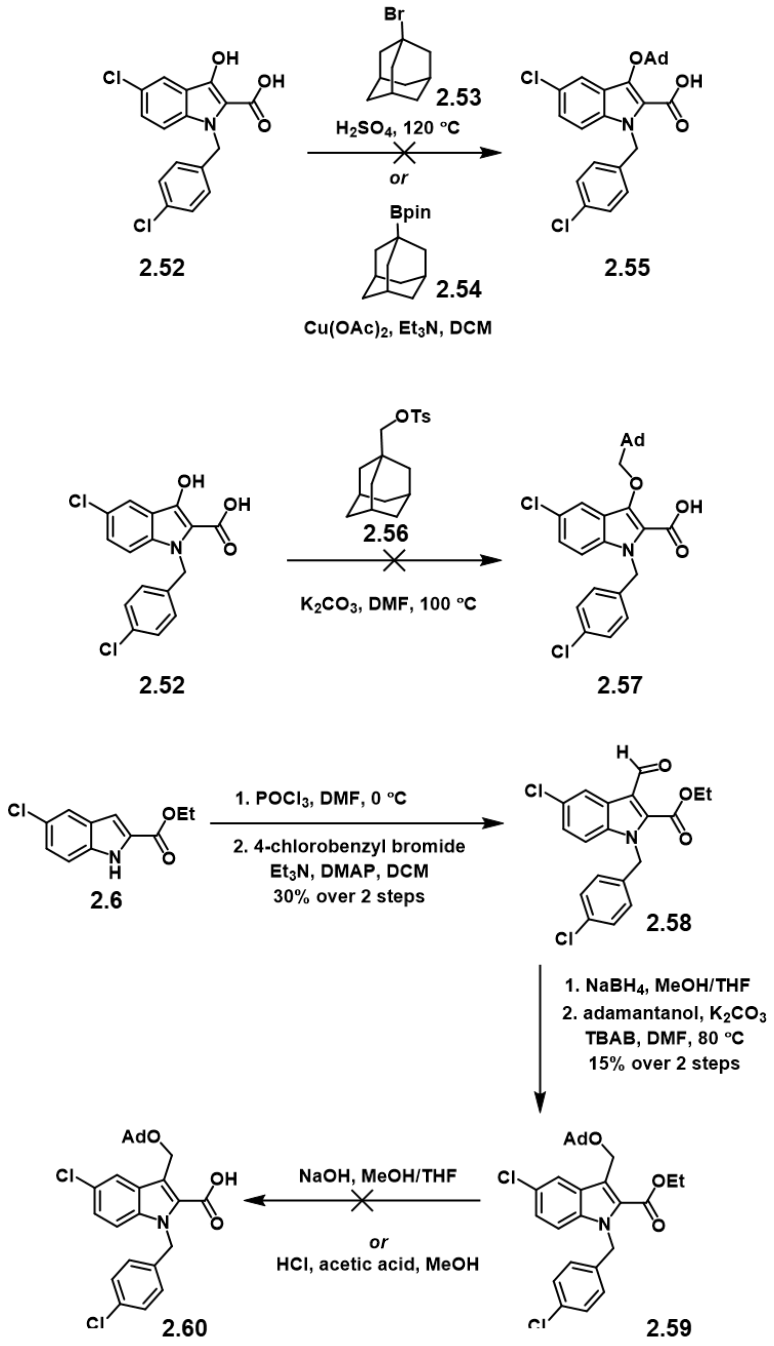

Figure 2.16: Routes tried to access an adamantyl analog.

I next turned to the homologated adamantyl derivatives (**2.57** and **2.60**). I decided to pursue both homologated adamantyl analogs in the hopes that one route would produce the desired adamantyl analog. Regarding the methylene adjacent to the adamantyl cage (**2.57**), I utilized **2.52** (our Chan-Lam starting material) and then activated the 1-adamantanemethanol via tosylation. To couple the activated adamantyl fragement and the alcohol, I used our alkylation conditions but did not observe product (**Fig. 2.16**). Rationalizing that the adamantyl reagent was most likely too bulky for addition into its σ^* orbital.

I also endeavored to access the other homologated adamantyl analog (methylene adjacent to the indole core, **2.60**) via Vilsmeier-Haack formylation of the commercially available indole ethyl ester (**Fig. 2.16**).[16] Alkylation of the nitrogen, reduction of the aldehyde with sodium borohydride, and alkylation would yield adamantyl ether **2.59**.[8] Much to my dismay, I was never able to realize this analog due to loss of adamantanol during ethyl ester hydrolysis (**Fig. 2.17**).[8] Under basic conditions, I observed both hydrolysis of the adamantyl ether and the ethyl ester (**2.61**).[8] Typically, in basic hydrolysis conditions, hydroxide addition into the ester forms a tetrahedral intermediate, which then eliminates methoxide affording the carboxylic acid.[8] With the homologated adamantyl ether analog, one could see two pathways that this hydrolysis goes awry.[8] In the first pathway, hydroxide could potentially add in an S_N2 fashion at the methylene bridge between the indole core and the adamantyl ether to expel adamantanoxide.[8] In a second pathway, one could see the hydrolysis of the methyl ester to provide the acid, which under basic conditions would then be deprotonated (**2.62**).[8] This carboxylate could add in to the σ^* orbital of

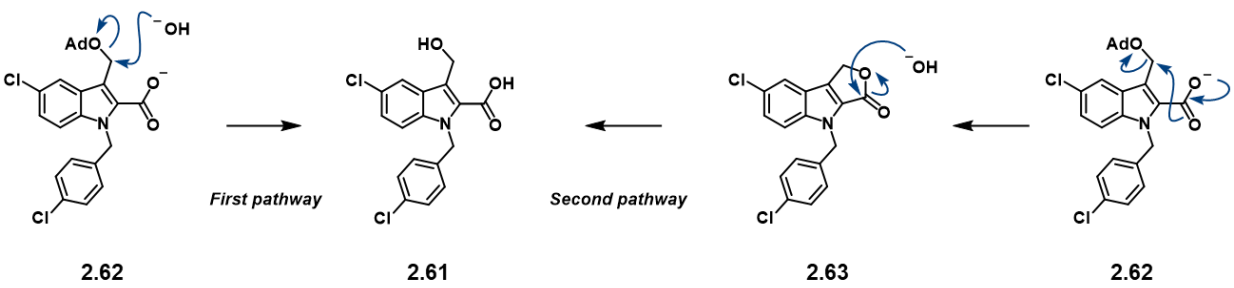

Figure 2.17: Failed saponification leading to unwanted hydrolysis product, **2.61**.

the adamantyl ether to form a 5-membered lactone **2.63** and kick out adamantanoxide.[8] This lactone could then undergo typical basic hydrolysis to reform the acid and create a homologated alcohol at the 3-position of the indole core.[8] Because of the issues I encountered with basic hydrolysis conditions, I next turned to acidic conditions.[8] However, in my studies, I was only able to isolate the homologated alcohol ethyl ester product under our acidic conditions, which indicates that the adamantyl ether is primed for extrusion before the ethyl ester can be hydrolyzed.[8]

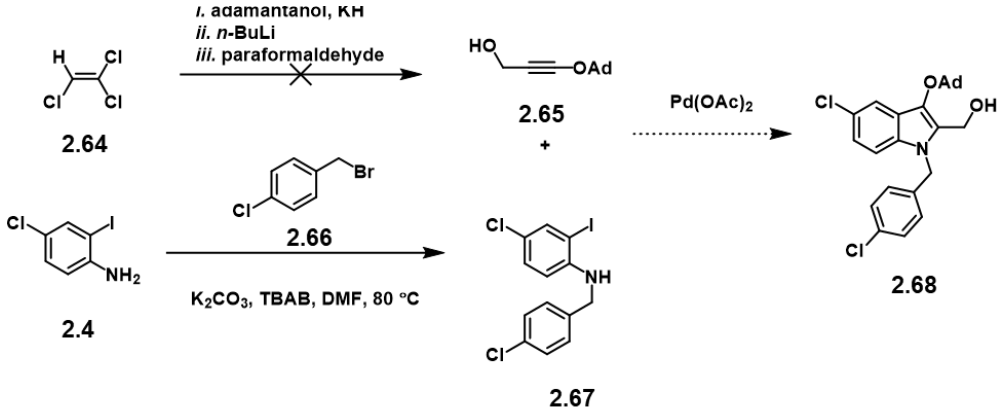

Figure 2.18: Route to non-homologated adamantyl analog using Larock indole synthesis. Had I obtained the desired regioisomer **2.68**, then I would have oxidized up to the carboxylic acid to obtain the adamantyl analog.

Despite attempting to access the homologated adamantyl ether analogs, I also continued to pursue the non-homologated adamantyl ether analog (**Fig. 2.18**). I designed a synthesis which would enable me to access this analog via the Larock indole synthesis. To build my starting materials, I needed to alkylate 4-chloro-2-iodoaniline with the 4-chlorobenzyl fragment to help push the adamantyl to the 3-position.[19,20] The Larock indole synthesis typically selects for the large substituent to go to the 2-position of the indole core, but this regioselectivity may be muddled with the 4-chlorobenzyl fragment on the aniline. Additionally, I needed to construct my alkyne starting material.[19,20] Porter and coworkers detail that they could obtain their alkyne starting material with a cyclohexyl ether directly on the alkyne.[20] Because of moderate substrate similarity and multiple literature example utilizing Porter's one-pot synthesis, I decided to use Porter's

conditions.[19,20] Unfortunately, I was unable to generate my desired alkyne and so was never able to explore the Larock cyclization and regioselectivity.

Finally, I also explored a quinoline analog. Most of our SAR focused around functionalizing the amine or the ether, changing the substituent at the 5- position, or exploring acid derivatives. However, we had not explored more major changes to the core itself, such as changing from indole to a quinoline. Thus, I designed a synthesis to access our quinoline analog, which utilized a Sonogashira to craft the alkyne starting material for the quinoline cyclization from 4-chloro-2-iodoaniline. Despite literature precedence, I was unable to achieve my alkyne starting material, and we decided to no longer pursue the analog due to initial difficulty and low promise.

2.4 My contributions

In my efforts to craft a potent, non-toxic nTZDpa derivative, I synthesized 16 analogs of 55 total across three generations of SAR (**Fig. 2.19**). I lead the last thrust of the project in order

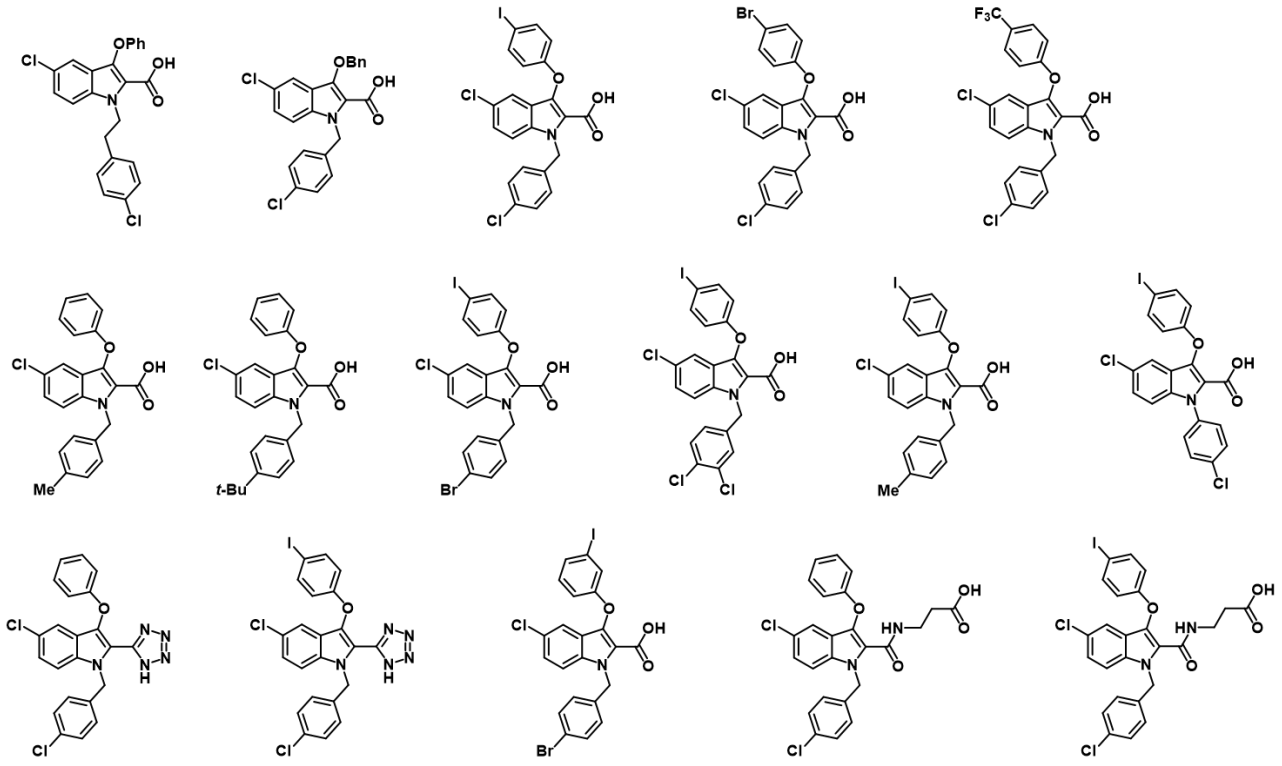

Figure 2.19: The sixteen compounds I made during our three rounds of SAR.

to develop a non-toxic derivative of Analog 2 that was just as potent. Unfortunately, we were unable to create an analog that was non-toxic but did synthesize two analogs that were just as potent at killing resistant and persistent *S. aureus* and published our results in *Bioorganic & Medicinal Chemistry Letters*.

Works Cited:

1. Lee, A.S.; Lencastre, H.d.; Garau, J.; Klytmans, J.; Malhotra-Kumar, S.; Peschel, A.; Harbarth, S.; *Nat. Rev. Dis. Primers*, **2018**, *4*, 1.
2. Centers for Disease Control & Prevention, “Antibiotic Resistance Threats in the United States 2019” **2019**, 1.
3. Centers for Disease Control and Prevention. “COVID-19 & Antibiotic Resistance.” **2021**. Accessed 17 Jan 2022
4. Centers for Disease Control and Prevention. “About Antibiotic Resistance.” **2021**. Accessed 9 Feb 2022.
5. Kim, W.; Steele, A.D.; Zhu, W.; Csatary, E.E.; Fricke, N.; Dekarske, M.M.; Jayamani, E.; Pan, W.; Kwon, B.; Sinitsa, I.F.; Rosen, J.L.; Conery, A.L.; Fuch, B.B.; Vlahovska, P.M.; Ausubel, F.M.; Gao, H.; Wuest, W.M.; Mylonakis, E.; *ACS Infect. Dis.*, **2018**, *4*, 1540.
6. Kim, W.; Zhu, W.; Hendricks, G.L.; Tyen, D.V.; Steele, A.D.; Keohane, C.E.; Fricke, N.; Conery, A.L.; Shen, S.; Pan, W.; Lee, K.; Rajamuthiah, R.; Fuchs, B.B.; Vlahovska, P.M.; Wuest, W.M.; Gilmore, M.S.; Gao, H.; Ausubel, F. M.; Mylonakis, E.; *Nature*, **2018**, *556*, 103.
7. Kim, W.; Zou, G.; Hari, T.P.A.; Wilt, I.K.; Zhu, W.; Galle, N.; Faizi, H.A.; Hendricks, G.L.; Tori, K.; Pan, W.; Huang, X.; Steele, A.D.; Csatary, E.E.; Dekarske, M.M.; Rosen, J.L.; Ribeiro, N.d.Q.; Lee, K.; Port, J.; Fuchs, B.B.; Vlahovska, P.M.; Wuest, W.M.; Gao, H.; Ausubel, F.M.; Mylonakis, E.; *Proc. Natl. Acad. Sci.* **2019**, *116*, 16529.
8. Dekarske, M.M.; Felix, L.O.; Ortiz, C.M.; Csatary, E.E.; Mylonakis, E., Wuest, W.M.; *Bioorg. Med. Chem. Lett.*, **2022**, *64*, 128678.
9. Fisher, R.A.; Gollan, B.; Helaine, S.; *Nat. Rev.: Microbiol.*, **2017**, *15*, 453.
10. Maisonneuve, E.; Gerdes, K.; *Cell*, **2014**, *157*, 539.
11. Reygaert, W.C.; *AIMS Microbio*, **2018**, *4(3)*, 482.
12. Brauner, A.; Fridman, O.; Gefen, O.; Balaban, N.Q.; *Nat. Rev. Microbiol.*, **2016**, *14*, 320.

13. Hurdle, J.G.; O'Neill, A.J.; Chopra, L.; Lee, R.E.; *Nat. Rev. Microbiol.*, **2011**, *9*, 62.

14. Doi, Y.; Wachino, J.-i.; Arakawa, Y.; *Infect. Dis. Clin. N. Am.,* **2016**, *30*, 523.

15. Ishikawa, M.; Hashimoto, Y.; *J. Med. Chem.*, **2011**, *54*, 1539.

16. Schmidt, M.A.; Simmons, E.M.; Wei, C.S.; Park, H.; Eastgate, M.D.; *J. Org. Chem.*, **2018**, *83*, 3928.

17. Lassalas, P.; Gay, B.; Lasfargeas, C.; James, M.J.; Tran, V.; Vijayendran, K.G.; Brunden, K.R.; Kozlowski, M.C.; Thomas, C.J.; Smith, III, A.B.; Huryn, D.M.; Ballatore, C.; *J. Med. Chem.*, **2016**, *59*, 3183.

18. Chen, J.-Q.; Li, J.-H.; Dong, Z.-B.; *Adv. Syn. Catal.*, **2020**, *362*, 3311.

19. Hashmi, A.S.K.; Rudolph, M.; Huck, J.; Frey, W.; Bats, J.W.; Hamzic, M.; *Angew. Chem. Int. Ed.,* **2009**, *48*, 5848.

20. Porter, N.A.; Dussault, P.; Breyer, R.A.; Kaplan, J.; Morelli, J.; *Chem. Res. Toxicol.*, **1990**, *3*, 236.

Chapter 3: Honokiol

*Adapted from Solinski, A.E.; Ochoa, C. Lee, Y.E.; Paniak, T.; Kozlowski, M.C.; Wuest, W.M.; ACS Infect. Dis., **2018**, 4, 118. Ochoa, C.; Solinski, A.E.; Nowlan, M.; Dekarske, M.M.; Wuest, W.M.; Kozlowski, M.C.; ACS Infect. Dis., **2020**, 6, 74. Used with permission.*

3.1 Introduction

3.1.1 Activity and Kozlowski Synthesis

The oral microbiome is rich in flora and as such plays host to commensal and pathogenic bacteria.[1-11] One such pathogenic bacterium is *Streptococcus mutans*, a Gram-positive bacterium that is the primary causative agent in dental caries.[1-11] According to Forssten and coworkers, dental caries and plaque are two of the most prevalent diseases in the world.[9] Furthermore, dental caries have been implicated as a causative agent of infective endocarditis (heart valve growth that encompasses bacteria and can ultimately lead to death).[6]

S. mutans causes tooth decay via metabolizing sucrose or fructose with glycosyltransferases into glucans, which producing lactic acid and causing tooth degradation of

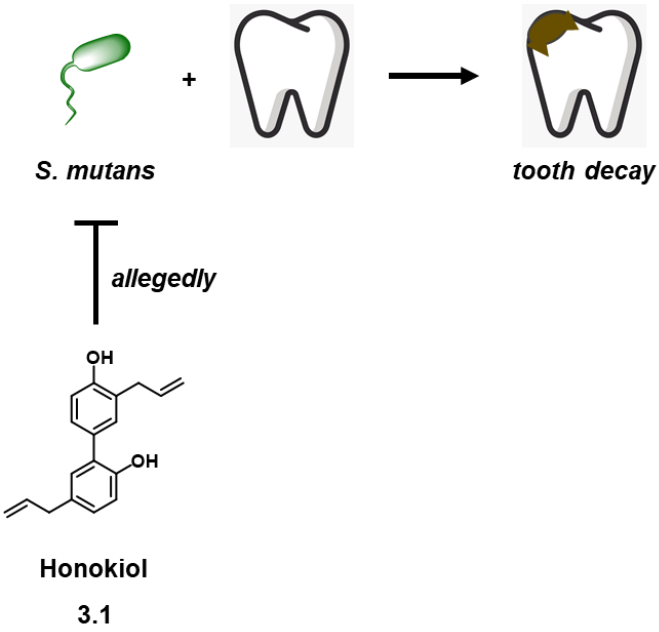

Figure 3.1: Namba and coworkers indicate that the natural product honokiol is able to kill planktonic *S. mutans*.

the enamel.[8-11] *S. mutans* is one of the primary cariogenic species in the mouth for three reasons: (i) uptake of extracellular polymers and conversion to glucan, which aids in adhering to hard surfaces; (ii) metabolism of carbohydrates into organic acids; and (iii) fitness in low pH environments.[8-10] Accumulation of biofilm (also known as plaque) causes a majority of the tooth damage.[8-10] *S. mutans* forms biofilm by adhering to the hard surface of the tooth and produces extracellular polysaccharide, which creates a niche environment and lowers the pH in the immediate area.[1-7] Furthermore, *S. mutans* exists in several different states within the oral environment: planktonic, adhered colonies, microcolonies, and then biofilm.[1-7] A majority of *S. mutans* research is toward investigating biofilm as that is the preferred state of *S. mutans*; however, this chapter shall only address planktonic *S. mutans* cell death.[1-7]

Honokiol is a natural product isolated from *Magnolia obovate* Thunb. by Fujita and coworkers in 1972 and played a role in traditional eastern medicine herbal mixes.[2,3,13] Namba and coworkers later reported its activity against *S. mutans* of 10 μg/mL in 1982 (**Fig. 3.1**).[12,13] The Kozlowski Lab highlighted their oxidative cross-coupling methodology with the total synthesis of honokiol (**Fig. 3.2**).[2,14] To assemble the two asymmetric phenol fragments, Ochoa and coworkers utilized a chromium-salen catalyst developed in the original methodology along with molecular oxygen and heated in DCE for several days.[2,14] Ochoa also performed SAR around the core scaffold to develop a more potent analog. Our lab then tested the compounds developed by Ochoa and coworkers.[2]

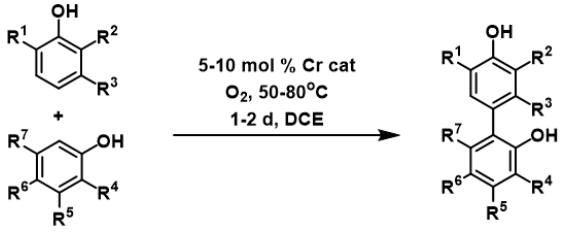

Figure 3.2: Methodology developed by the Kozlowski Lab and then featured in their honokiol total synthesis.

3.1.2 First Round of SAR

Interestingly, when Dr. Amy Solinski (Wuest Lab) tested honokiol and its derivatives synthesized by Ochoa for activity, she found that the natural product was inactive against *S. mutans* while some of its analogs, however, were (**Fig. 3.3**).[2] Because of her previous work with *S. mutans*, Solinski understood that *S. mutans* must be grown with a 5% supplemental CO_2 environment so as to best reflect oral microbiome conditions with CO_2 exhalation.[2-4,7] However, in 1982 study, Namba and coworkers did not grow *S. mutans* cultures with the supplemental CO_2, thus rendering their activity studies irrelevant to oral conditions.[2]

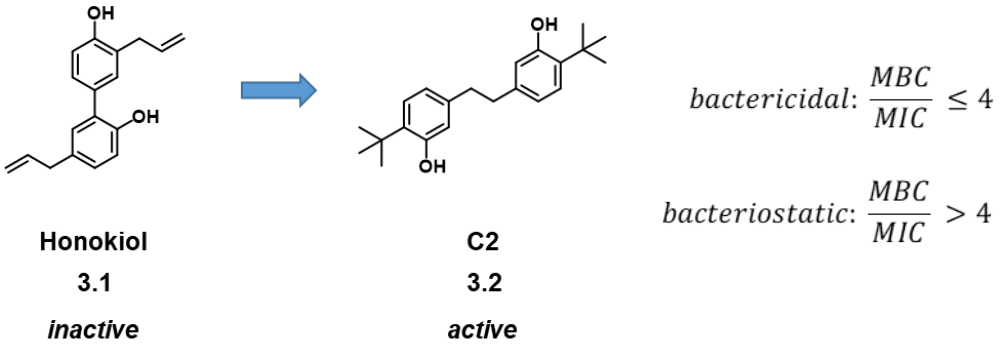

Figure 3.3: Honokiol is inactive against *S. mutans*, but fortunately the Kozlowski Lab developed **C2**, which kills planktonic *S. mutans*.

After Solinski established that honokiol was inactive under the supplemental CO_2 conditions, she still performed MIC (Minimum Inhibitory Concentration) and MBC (Minimum Bactericidal Concentration) assays to establish the activity of Ochoa's analogs.[2] The difference between bacteriostatic and bactericidal being that bacteriostatic prevents growth, while bactericidal kills the bacteria. The method to decide if the compound of interest is -static or -cidal is to obtain the MIC and MBC for the compounds and then divide the MBC by the MIC (formulas presented in **Fig. 3.3**). If the value obtained is less than or equal to four, the compound is bactericidal. If the quotient is greater than four, then the compound of interest is bacteriostatic. Fortunately, Solinski observed several compounds that were active with the best in class being **C2** with an MIC of 2 μM and was bactericidal with an MBC of 4 μM.[2]

3.1.2 Second Round of SAR

In the second round of SAR, Ochoa focused on the **C2** scaffold, since its activity was improved compared to the natural product.[3] Ochoa examined the length of carbon linker between the two phenolic rings, placement of the alcohols decorating the rings (*ortho*, *meta*, and *para* to the linker), steric influence of the alkyl chain (*t*-Bu on **C2**), alkyl capping of one or both phenols, and alkyl substitutions on the aryl rings.[3]

From this round of SAR, four notable compounds emerged: **3N**, **4G**, **4H**, and **C2p** (**Fig. 3.4**). **3N** and **4H** were just as potent as **C2**, and **4G** is one dilution less potent at 4 μM.[3] **C2p** seemed to also be as potent as **C2p**, but later studies proved its true MIC to be far higher; however, because of its initial activity, it was investigated in our mechanism studies (*vide infra*) as having an MIC of 2 μM.[3]

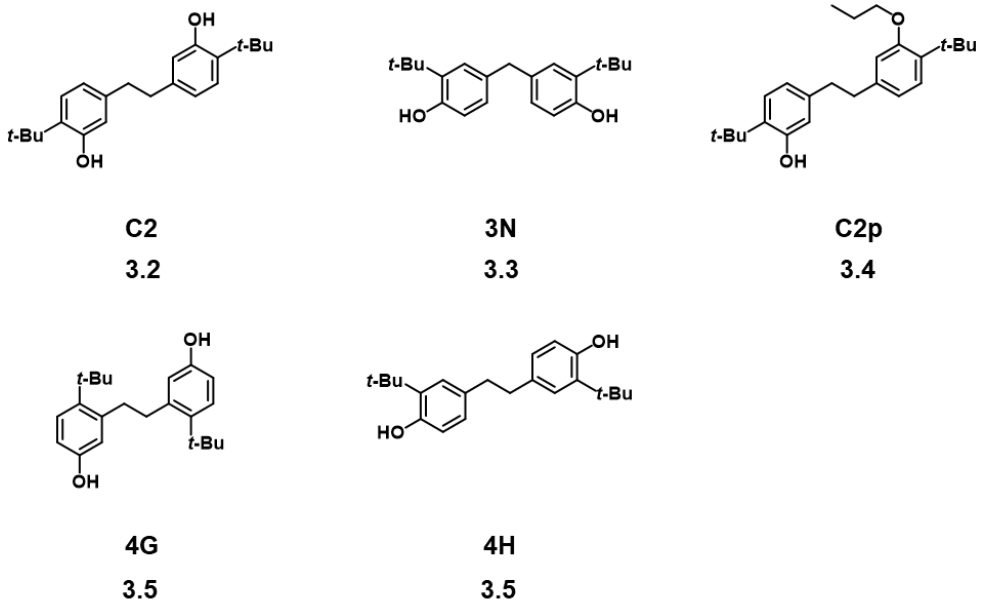

C2 **3.2** | **3N** **3.3** | **C2p** **3.4**

4G **3.5** | **4H** **3.5**

Figure 3.4: Active compounds from second generation of SAR.

3.2 Mechanism Studies

Our group next sought to elucidate the mechanism of action through implementation of our tool compounds in microbiological assays. Solinski next tried to generate a resistant mutant through serial passaging but she was unable to, which is a hallmark of membrane mechanisms.[15]

Because of my experience with membrane mechanisms, I was brought onto the project to aid in uncovering the mechanism of action.[16-18]

3.2.1 Polarization studies

Membrane potential was once previously thought to be homeostatic (or kept within certain limits so as to keep the cell functioning).[19] However, bacterial cells have recently been shown to utilize the electrical gradient across their membrane processes beyond ATP synthesis, including regulation of cellular processes (motility, cell division, antibiotic resistance, and membrane transport, etc) as well as information signaling.[19] Because membrane potential is so important for cell vitality, it is logical that membrane potential as hyperpolarization (more negative charge within the cell) or depolarization (less negative charge within the cell) events are first steps into investigating a membrane mechanism.[19]

Solinski had performed preliminary depolarization assays with $DIBAC_4(3)$ and observed a hyperpolarization effect and a difference in response between the mono-capped and free alcohol analogs (such as **C2p** and **C2**). Thus, we performed the $DIBAC_4(3)$ membrane depolarization assay in biological triplicate but could not replicate the initial response seen by Solinski.

In our studies, we utilized a few positive membrane potential controls: cetylpyridinium chloride, 12(3)2(3)12, chlorohexidine, and chlorogenic acid. Cetylpyridinium chloride (CPC) is a quaternary ammonium compound (QAC) that is one of the oral microbiome industry standards for cleaning and hygiene and is present in most mouthwashes as the active ingredient.[2] 12(3)2(3)12 is a structurally distinct QAC developed in collaboration by our lab and the Minbiole Lab at Villanova University.[20] Chlorohexidine (CHX) is a non-QAC industry standard to fight gingivitis, which also differs from CPC in structure.[2] We also utilized a positive control that more closely resembled our scaffold, chlorogenic acid (CGA), which was reported to hyperpolarize bacteria cell membranes, although the mechanism is not completely verified.[21] We also employed DMSO

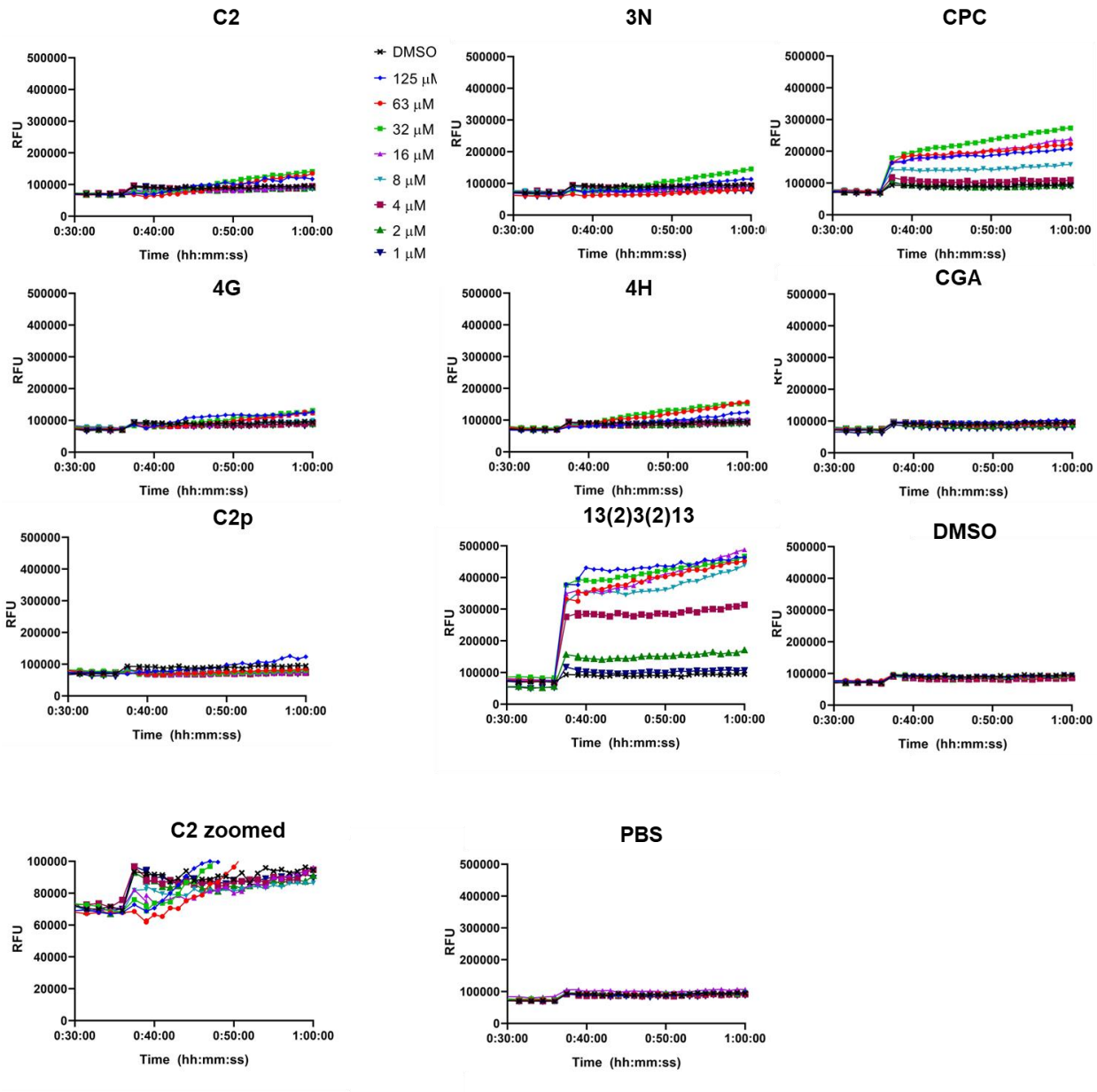

Figure 3.5: Graphs generated from membrane potential assay using $DIBAC_4(3)$.

(used to make the 10 mM stock solutions) and phosphate buffer saline (PBS, used to wash cells in the assay) as our two negative controls.

In our membrane potential studies, we observed what seems to be initial hyperpolarization at high concentration with **C2**, which eventually leads to a statistically insignificant depolarization response (when compared to in experiment negative DMSO control) (**Fig. 3.5**). This initial, small hyperpolarization response occurred for concentrations of 8 µM up to 125 µM but did not occur

at 1-4 μM or within experiment DMSO negative control.[3] Further, we observed significant depolarization response with our positive controls (12(3)2(3)12 and CPC) but interestingly did not see any polarization response with CGA.[3] Thus, the lack of response at MIC levels suggested that **C2** and analogs thereof do not act via a membrane potential mechanism.[3]

3.2.2 Permeabilization Studies

Because of the lack of response we observed with membrane potential studies, we next turned to examining membrane permeabilization (**Fig. 3.6**).[3,16-18,22] Permeabilization is the physical formation of holes within the bacterial cell membrane, resulting in leakage of cell contents, and ultimately cell death.[16-18,22] Thus, we measured the membrane permeabilization response with SYTOX Green dye (a nucleic acid stain) and found that **C2** and its analogs permeabilize cell membranes at high concentrations (32 μM to 125 μM) (**Fig. 3.6**).[3] Of our positive controls, we saw that 12(3)2(3)12 and CPC permeabilized from 8 μM to 125 μM.[3] CHX permeabilized similarly to **C2** (only 32 μM to 125 μM), and CGA did not induce a significant

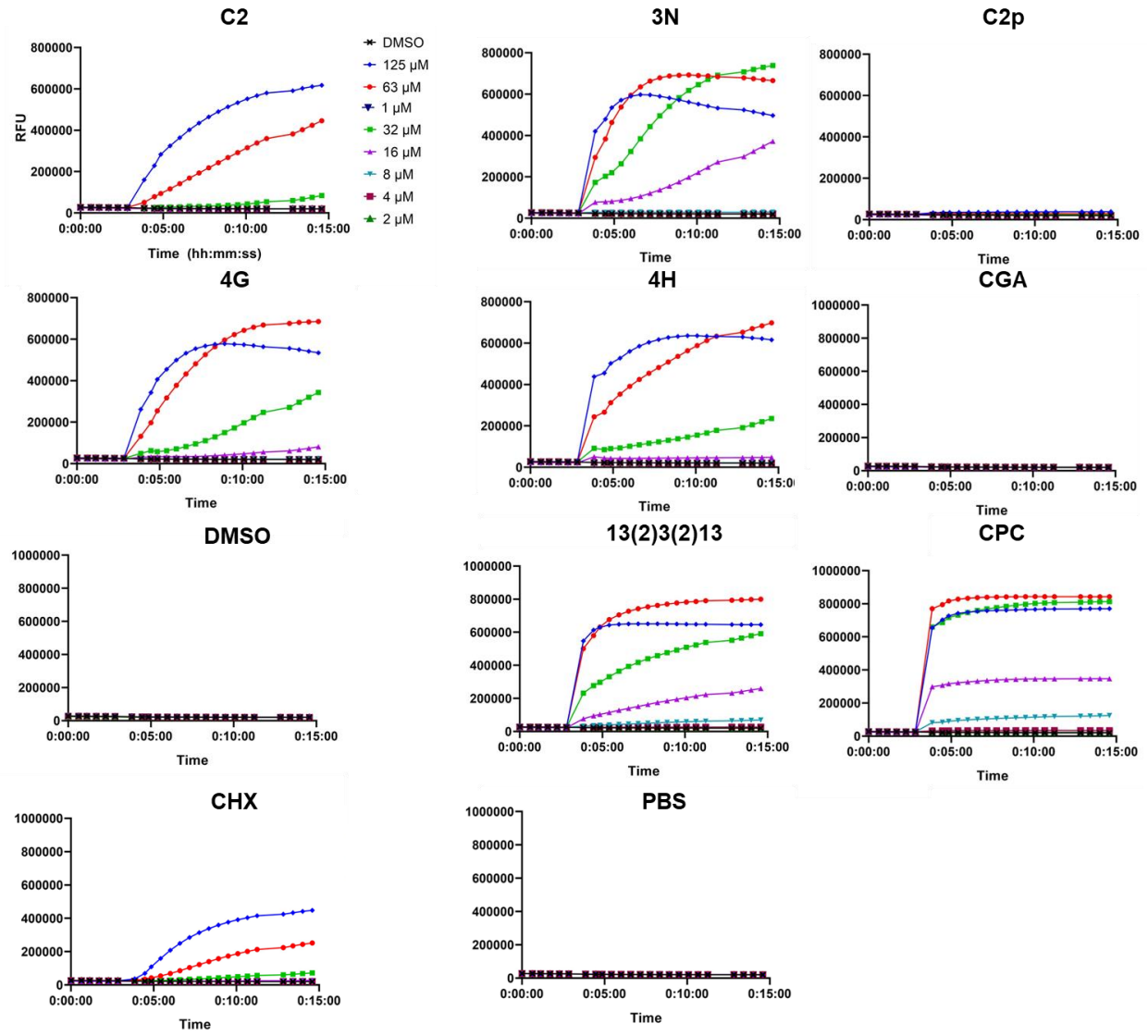

Figure 3.6: Permeabilization studies showing that **C2** and analogs thereof permeabilize *S. mutans* membranes at high concentrations.

membrane permeabilization event.[3] Interestingly, **C2p** did not show any permeabilization, which implied that it was operating under a different mechanism of action compared to **C2** and other analogs. Thus, the lack of response at MIC levels suggests that membrane permeabilization is not the main mechanism for **C2** and its free alcohol derivatives.

3.2.3 Therapeutic Index

After determining that **C2** permeabilizes *S. mutans* cell membrane at high concentrations, the next step is to explore the red blood cell toxicity, which can be quantified using therapeutic

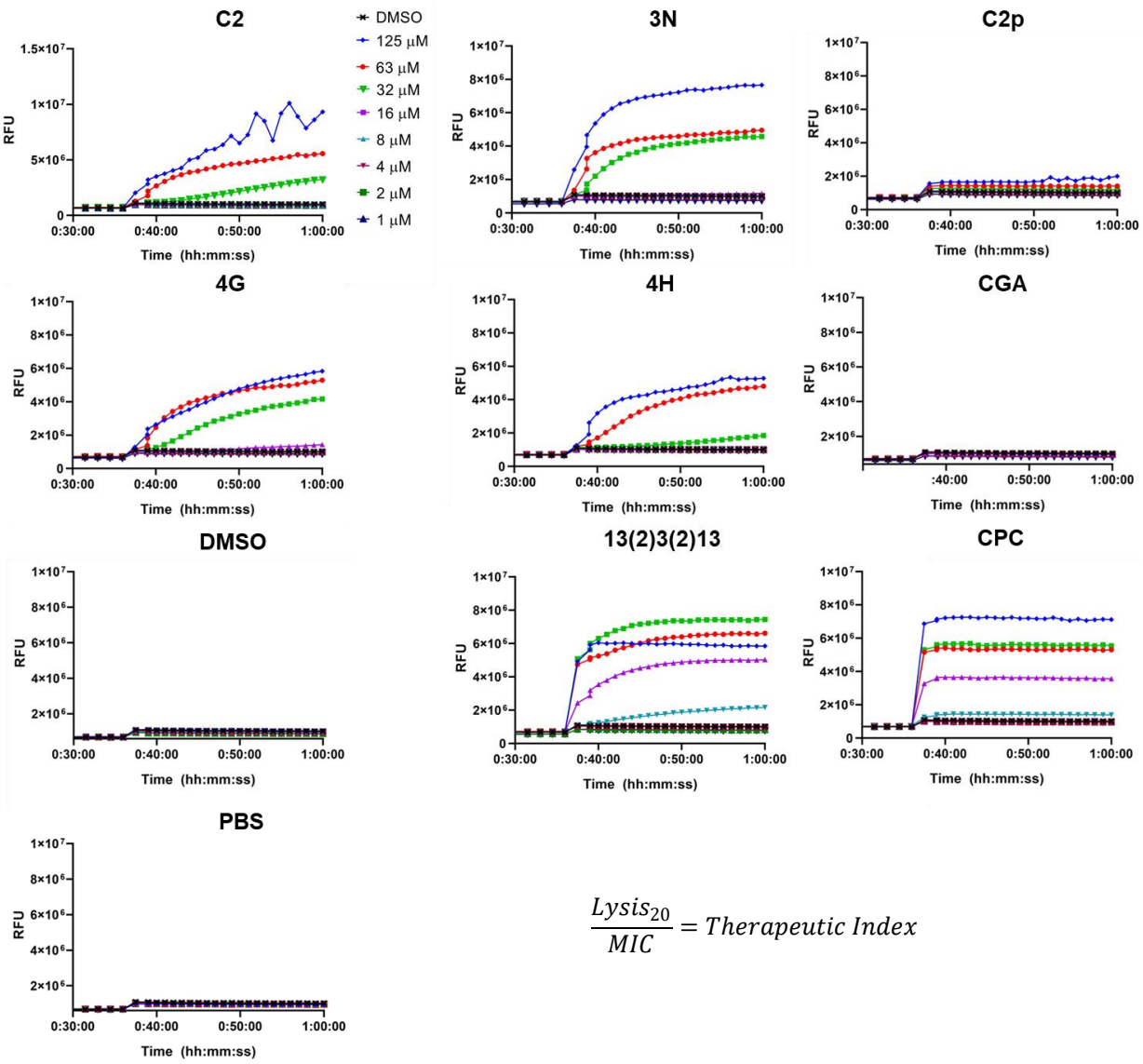

$$\frac{Lysis_{20}}{MIC} = Therapeutic\ Index$$

Figure 3.7: Hemolysis data indicating that **C2** and analogs thereof possess some hemolytic activity but also are less toxic than industry standard **CPC**.

index (**Fig. 3.7**).[3] Therapeutic index is typically measured by assessing the hemolytic activity with propidium iodide, which is dye that leeches out of the cell only if the cell membrane is compromised, which can lead to lysis.[3,22] The concentration at which 20% of the red blood cells lyse is divided by the MIC to obtain the therapeutic index.[3] Thus, the therapeutic index for **C2** is 32, while the therapeutic index for industry standard CPC is 8, implying that **C2** may be a better alternative to CPC.[3] We saw similar therapeutic indices for **3N** and **4H**, while **4G** possessed an index more similarly to CPC at 8.[3] Interestingly, **C2p** did not show much lytic activity, lending

further credence to a different, less toxic mechanism as membrane mechanisms tend to have off target mammalian cell toxicity issues.

3.2.4 TEM Images

Because of the membrane mechanism results we had previously seen, we wanted to examine the bacterial cells visually upon treatment with compound.[3] Thus, we obtained TEM images at 2 μM, 4 μM, 16 μM, 63 μM, 125 μM (**Fig. 3.8**).[3] DMSO was used as a negative control. At high concentration (63 μM and 125 μM), we noticed cell lysis, which is consistent with our propidium iodide (hemolytic activity) studies.[3] At 16 μM and below, we did not observe cell lysis and instead only saw normal cell division.[3]

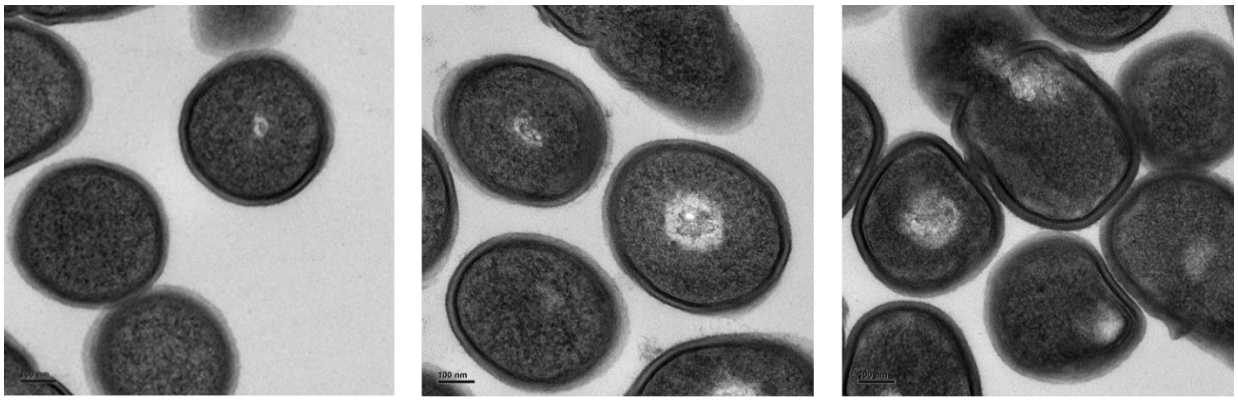

Figure 3.8: TEM images demonstrate that lysis occurs only at high concentrations.

3.2.5 Other Membrane Assays

Because we observed physical membrane permeabilization mechanism at only high concentration, we next endeavored to investigate the mechanism at and around the MIC. Furthermore, we were interested in the differences between **C2** and **C2p**, particularly in how capping of only one of the phenols led to stark differences in permeabilization and toxicity. Thus, we examined how **C2** and **C2p** affect intracellular pH, membrane protein changes, and internal calcium ion concentration.

We first analyzed *S. mutans* internal pH response to varying concentrations of **C2** and **C2p** via uncoupling proton motive force (**Fig. 3.9**). We observed that high concentrations (125 μM

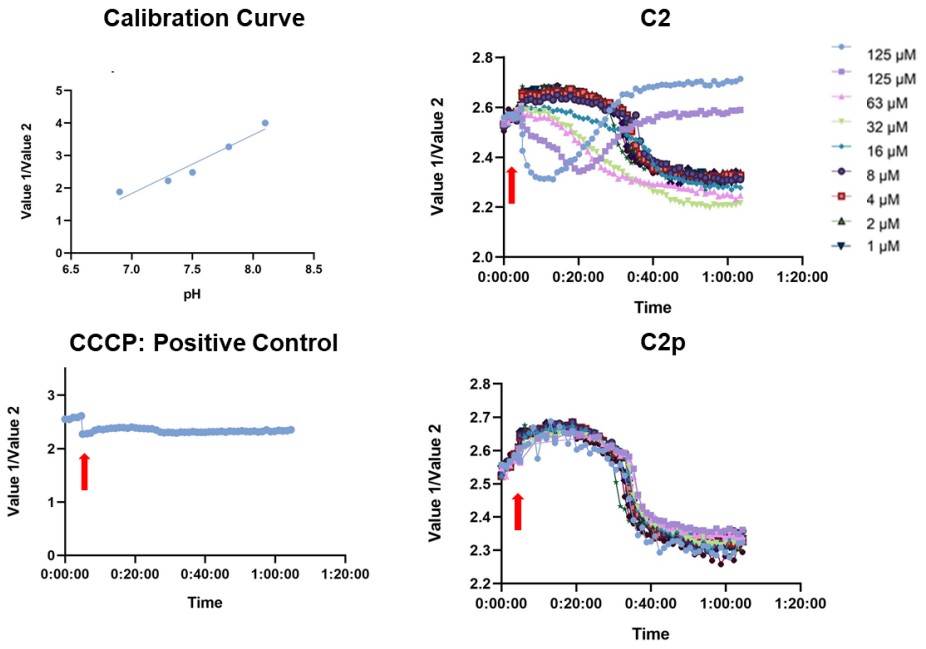

Figure 3.9: intracellular pH studies to investigate if **C2** or **C2p** affected *S. mutans* intracellular pH.

and 250 µM) of **C2** produced a decrease in intracellular pH that over the course of an hour reversed and increased, eventually leveling off around pH 2.7. At concentrations 63 µM and below of **C2**, the internal pH initially increased and eventually reversed and rapidly decreased, ultimately reaching its pH of around 2.2-2.3. The dichotomy of these two responses is interesting and would be expected if we had observed concentration dependent depolarization and hyperpolarization effects. However, we did not see a significant membrane potential effect. Instead, we had only observed membrane permeabilization at high concentrations, which is consistent with a decrease in pH as the cell leaks its internal contents, but the pH response reverses and increases over time for high concentration, providing conflicting data from which it is difficult to draw conclusions. Although we observe an initial increase in pH at and around the MIC, we do not see a

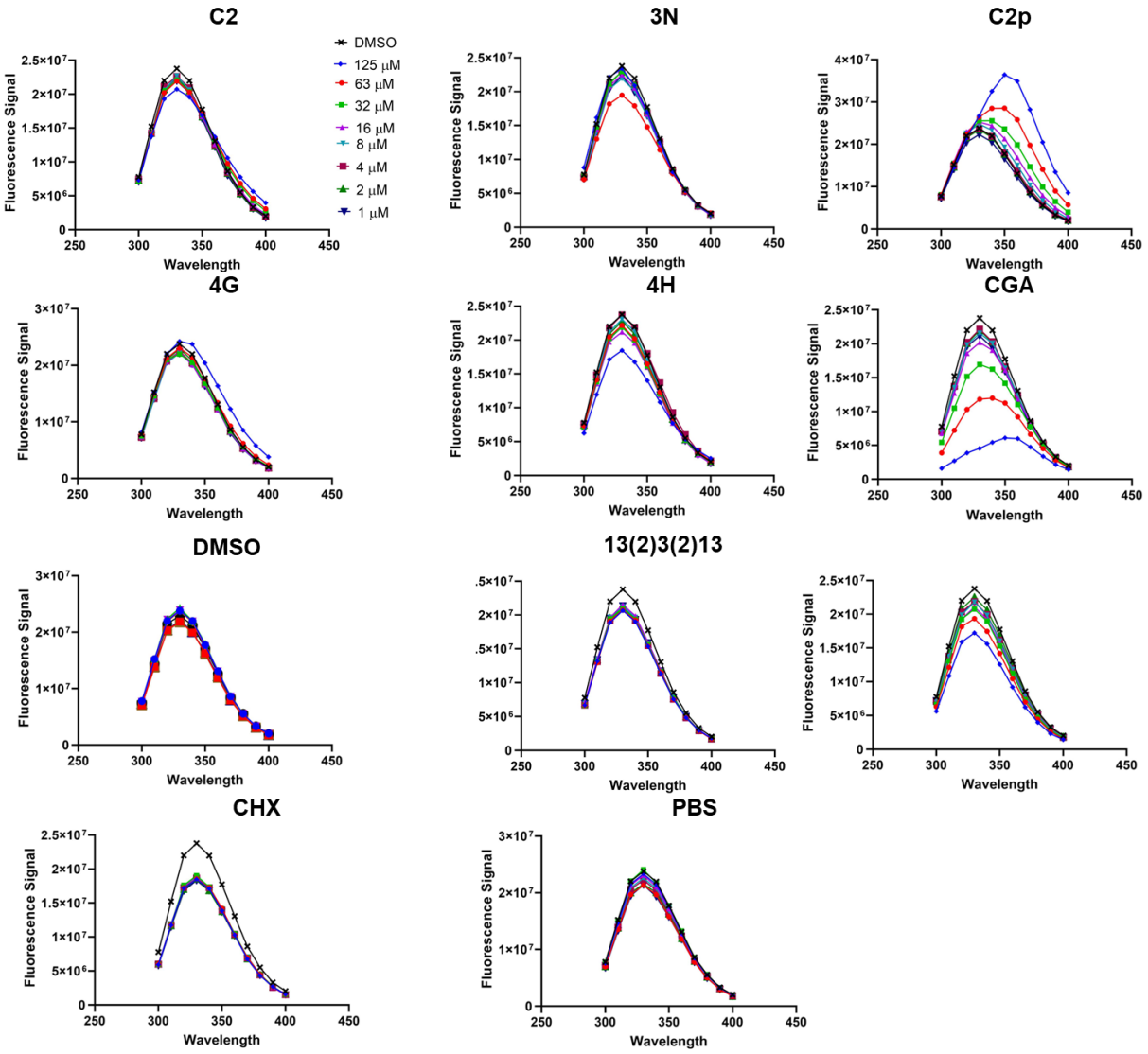

Figure 3.10: Examining membrane proteins and if **C2** and analogs thereof induced changes within the extracellular membrane proteins.

permeabilization response, lending further credence that **C2** operates in a different mechanism at its MIC.

Next, we examined changes to membrane proteins in an effort to detect if **C2** or **C2p** alter the membrane microenvironment (**Fig. 3.10**). From our studies, **C2**, **3N**, **4G**, **4H**, 12(3)2(3)12, CPC, CHX, PBS, and DMSO do not result in any changes to membrane proteins. However, CGA and **C2p** show an increase in wavelength (red shift), meaning that when they interact with the

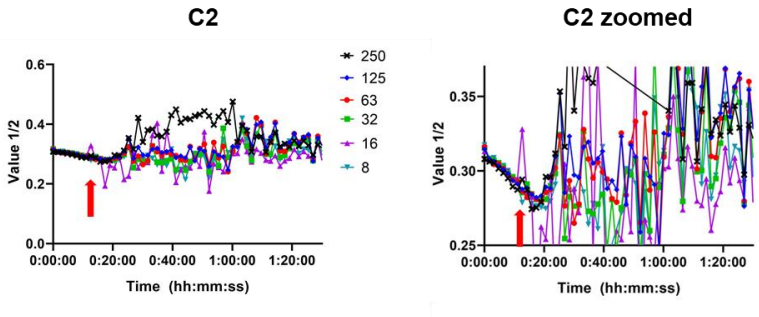

Figure 3.11: Examining the effect of **C2** on intracellular Ca^{2+} levels.

membrane, the microenvironment is changed. This provided further credence that **C2p** operates under a different mechanism than **C2**.

Furthermore, polyphenols have historically been metal chelators, and metal ions including Ca^{2+} are necessary for bacterial cell health.[23,24] Following our membrane protein assay, we measured the internal Ca^{2+} concentration in order to better understand our membrane mechanism results thus far (**Fig. 3.11**). From our results, at 250 μM of **C2**, it appears that there may be some initial interaction with [Ca^{2+}] but given that this interaction does not occur at or below 125 μM, the mechanism most likely does not involve the concentration of calcium ions within the bacterial cell. While we did not see a response with intracellular Ca^{2+} levels, this does not rule out a mechanism involving other divalent metals. Unfortunately, I was unable to perform assays to measure [Mg^{2+}] or [Zn^{2+}] due to prohibitive cost.

Thus, we understand what occurs with **C2** at high concentrations: permeabilization and lysis. However, we still do not understand exactly how **C2** kills *S. mutans* at or near its MIC of 2 μM, which lead to further studies that I performed.

3.3 Gen 3 SAR

Based on the results that mono-capped analogs, like **C2p**, possessed MIC data similar to **C2** but did not proceed through a membrane permeabilization-type of mechanism, we wanted to investigate the mechanism of **C2p** and its derivatives. Hanna Roenfranz of the Kozlowski Lab

synthesized a third generation of compounds on the **C2** scaffold in order to help elucidate the mechanistic differences in **C2** and **C2p** (**Fig. 3.12**).

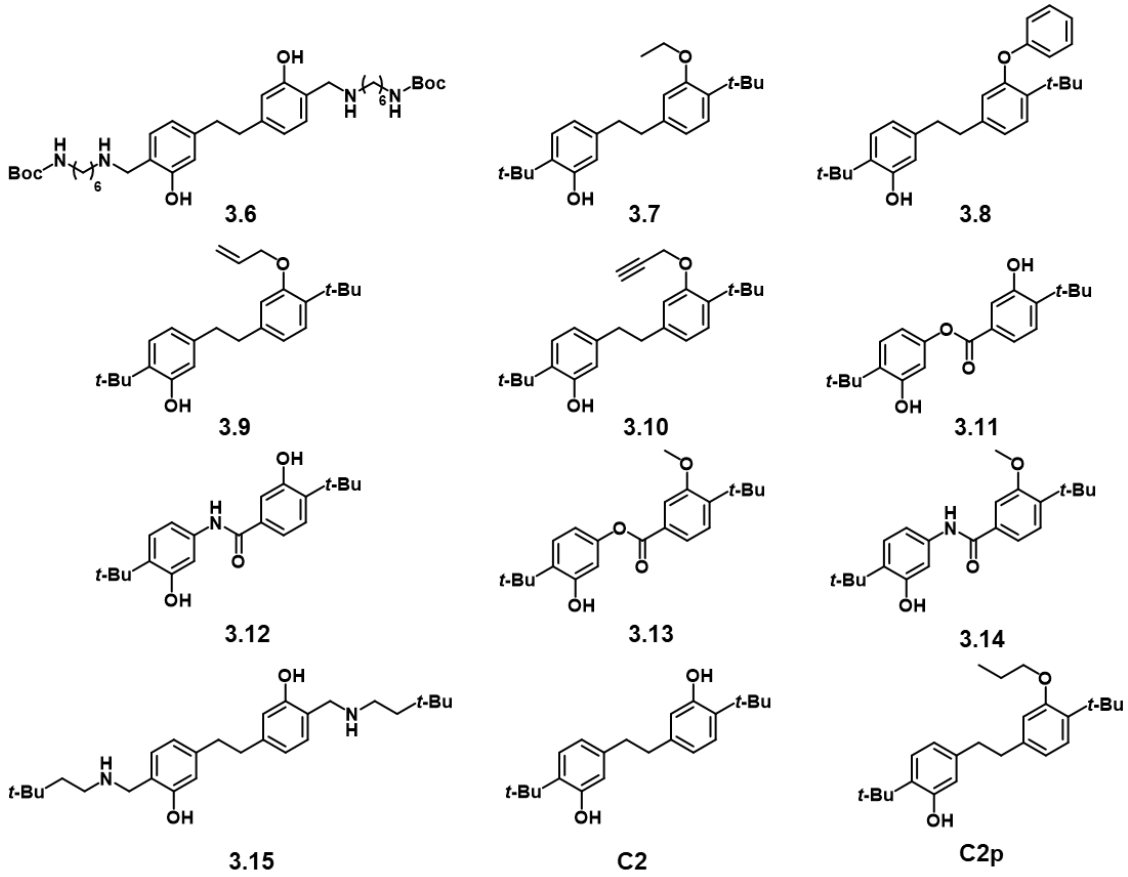

Figure 3.12: Structures of compounds tested in order to aid in **C2p** mechanism elucidation.

Initially, I obtained the MIC and MBC information to decide if the compounds were active, and whether they were bacteriostatic or bactericidal (**Fig. 3.13**). As previously stated, the difference being that bacteriostatic prevents cell division while bactericidal kills the bacteria (formulas re-presented in **Fig. 3.13**). In my MIC assay, I noticed a bizarre characteristic in some of the wells: there appeared to be either sediment or clumps of cells residing in the bottom of several clear wells. This did not occur across the entire plate (as in every well) and was only for certain compounds. In some of the compounds, the "sediment" would eventually stop before hitting the higher concentrations (63 and 125 μM), while with other compounds, the clumps would

Compound	MIC	MBC
3.6	8 μM	n.d.
3.7	125 μM*	-
3.8	>125 μM*	-
3.9	>125 μM*	-
3.10	63 μM*	63 μM
3.11	4 μM	16 μM
3.12	8 μM	8 μM
3.13	125 μM*	-
3.14	125 μM*	-
3.15	63 μM	63 μM
C2	1 μM	2 μM
C2p	>125 μM*	-
CPC	1 μM	4 μM
QAC	1 μM	2 μM
DMSO	>125 μM	-
THB	>125 μM	-

$$bactericidal: \frac{MBC}{MIC} \leq 4$$

$$bacteriostatic: \frac{MBC}{MIC} > 4$$

Figure 3.13: MICs and MBCs of new compounds with the definition of bactericidal and bacteriostatic. (*) denotes compounds that exhibited “sediment” at the bottom of the wells that upon further investigation proved to be viable cells. CPC and QAC are used as positive controls, and DMSO and THB are negative controls.

be present through every concentration tested. Thus, I ensured transfer of the “sediment” into the MBC experiment to investigate if motif was lysed or viable cells, which indeed indicated that they were viable cells. Reviewing the compounds that produced the motif of viable cells at the bottom of the well, I observed that all of them were monocapped compounds and that **C2p** also produced this effect (**Figure 3.13**). In fact, every monocapped compound exhibited this motif. Because the “sediment” at the bottom of the wells was actually viable cells, this indicates that the true MIC of the monocapped compounds is indeed much higher than originally thought, which could explain the difference in mechanism for the free hydroxyl and monocapped analogs.

3.4 My contributions & future directions

In our honokiol collaboration with the Kozlowski Lab, I worked alongside Dr. Solinski and Dr. Ochoa to complete all the mechanism of action studies, led our membrane permeabilization assay efforts, and performed data analysis for several assays in addition to all of our revision experiments. I also completed all the experiments requested by our reviewers for our 2020 *ACS Infectious Diseases* paper, in which the reviewers requested data for the additional compounds, **4B**, **4I**, **4K**, **4P**, and **4R** (**Fig. 3.14**). These compounds served as controls for the membrane permeabilization activity seen in our studies, which I was able to verify. Following our *ACS Infectious Diseases* publication, I performed initial screening assays (MIC and MBC) to assess the new compounds sent by Hanna Roenfanz of the Kozlowski Lab to aid in differentiating the mechanism of **C2** and **C2p**.

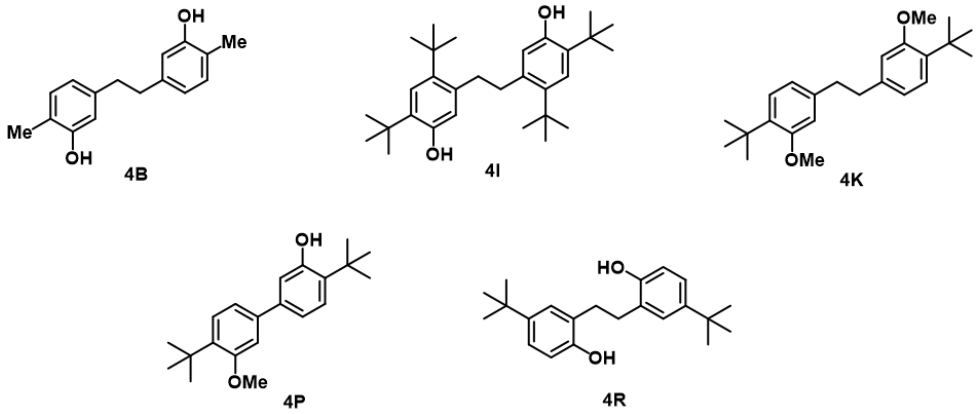

Figure 3.14: Structures of inactive compounds that required further experiments in revisions for our *ACS Infect. Dis.* 2020 publication.

Therefore, while we do not know how **C2** kills *S. mutans* at or near its MIC, we understand that it to act through membrane permeabilization at high concentrations. While the results do not tell the full picture, it is still important to comprehend what occurs at all concentrations for a potential therapeutic, especially because antibiotic dosing is typically much higher than the MIC. Currently, Hanna Roenfanz in the Kozlowski Lab has generated two resistant mutants through a serial passage resistance selection assay and is working to validate her results, which will tell us more about the mechanism of action of **C2** at its MIC.

Works Cited:

1. Kaspar, J.R.; Godwin, M.J.; Velsko, I.M.; Richards, V.P.; Burne, R.A.; *Antimicrob. Agents Chemothera*., **2019**, *63*, 1.
2. Solinski, A.E.; Ochoa, C. Lee, Y.E.; Paniak, T.; Kozlowski, M.C.; Wuest, W.M.; *ACS Infect. Dis.*, **2018**, *4*, 118.
3. Ochoa, C.; Solinski, A.E.; Nowlan, M.; Dekarske, M.M.; Wuest, W.M.; Kozlowski, M.C.; *ACS Infect. Dis.*, **2020**, *6*, 74.
4. Solinski, A.E.; Scharnow, A.M.; Fraboni, A.J.; Wuest, W.M.; *ACS Infect. Dis.*, **2019**, *5*, 1480.
5. Gross, E.L.; Beall, C.J.; Kutsch, S.R.; Firestone, N.D.; Leys, E.J.; Griffen, A.L.; *PLOS One*, **2012**¸*7*, e47722.
6. Nomura, R.; Matayoshi, S.; Otsugu, M.; Kitamura, T.; Teramoto, N.; Nakano, K.; *Infect. Immun.*, **2020**, *88*, 1.
7. Solinski, A.E.; Koval, A.B.; Brzozowski, R.S.; Morrison, K.R.; Fraboni, A.J.; Carson, C.E.; Eshraghi, A.R.; Zhou, G.; Quivey, Jr., R.G.; Voelz, V.A.; Buttaro, B.A.; Wuest, W.M.; *J. Am. Chem. Soc.*, **2017**, *139*, 7188.
8. Lemos, J.A.; Palmer, S.R.; Zeng, L.; Wen, Z.T.; Kajfasz, J.K.; Freires, I.A.; Abranches, J.; Brady, L.J.; *Microbiol. Spectrum*, **2019**, *7*, 1.
9. Forssten, S.D.; Bjorklund, M.; Ouwehand, A.C.; *Nutrients*, **2010**, *2*, 290.
10. Zayed, S.M.; Aboulwafa, M.M.; Hashem, A.M.; Saleh, S.E.; *AMB Expr.*, **2021**, *11*, 1.
11. Friedman, J.Y.; "The Role of Streptococcus Mutans in the Formation of Dental Caries: An Ecological Perspective." *The Science Journal of the Lander College of Arts and Sciences*, *5(1)*. 1.
12. Fujita, M.; Itokawa, H.; Sashida, Y.; *Chem. Pharm. Bull.*, **1972**, *20*, 212.
13. Namba, T.; Hattori, M.; Tsunezuka, M.; Yamagishi, T.; Konishi, K.; *Shoyakugaku Zasshi*, **1982**, *36*, 222.

14. Lee, Y.E.; Cao, T.; Torruellas, C.; Kozlowski, M.C.; *J. Am. Chem. Soc.*, **2014**, *136*, 6782.
15. Hurdle, J.G.; O'Neill, A.J.; Chopra, L.; Lee, R.E.; *Nat. Rev. Microbiol.*, **2011**, *9*, 62.
16. Kim, W.; Steele, A.D.; Zhu, W.; Csatary, E.E.; Fricke, N.; Dekarske, M.M.; Jayamani, E.; Pan, W.; Kwon, B.; Sinitsa, I.F.; Rosen, J.L.; Conery, A.L.; Fuchs, B.B.; Vlahovska, P.M.; Ausubel, F.M.; Gao, H.; Wuest, W.M.; Mylonakis, E.; *ACS Infect. Dis.*, **2018**, *4*, 1540.
17. Kim, W.; Zou, G.; Hari, T.P.A.; Wilt, I.K.; Zhu, W.; Galle, N.; Faizi, H.A.; Hendricks, G.L.; Tori, K.; Pan, W.; Huang, X.; Steele, A.D.; Csatary, E.E.; Dekarske, M.M.; Rosen, J.L., Ribeiro, N.d.Q. Lee, K.; Port, J.; Fuchs, B.B.; Vlahovska, P.M.; Wuest, W.M.; Gao, H.; Ausubel, F.M.; Mylonakis, E.; *Prod. Natl. Acad. Sci*., **2019**, *116*, 16529.
18. Dekarske, M.M.; Felix, L.O.; Ortiz, C.M.; Csatary, E.E.; Mylonakis, E., Wuest, W.M.; *Bioorg. Med. Chem. Lett.*, **2022**, *64*, 128678.
19. Benarroch, J.M.; Asally, M.; *Trends in Microbiol*., **2020**, *28*, 304.
20. Morrison, K.R.; Allen, R.A.; Minbiole, K.P.C.; Wuest, W.M.; *Tet. Lett*., **2019**, *60*, 150935.
21. Santana-Galvez, J.; Cisneros-Zevallos, L.; Jacobo-Velzquez, D.A.; *Molecules*, **2017**, *22*, 358.
22. Winkel, J.D.t.; Gray, D.A.; Seistrup, K.H.; Hamoen, L.W.; Strahl, H.; *Front. Cell Dev. Biol.*, **2016**, *4*, 1.
23. Hider, R.C.; Liu, Z.D.; Khodr, H.H.; *Methods in Enzymol.*¸**2001**, *17*, 190.
24. Lakey-Beitia, J.; Burillo, A.M.; Penna, G.L.; Hegde, M.L.; Rao, K.S.; *J. Alzheimer's Dis.*, **2021**, *82*, 5335.

Chapter 4: Ogipeptins

This work was performed by Madeline Dekarske and Wanli Zhang, and their contributions are clearly defined.

4.1 Introduction

4.1.1 Gram-negative bacteria and Lipid A

Gram-negative bacteria possess an asymmetrical lipid bilayer and are harder to kill due to their second membrane, called the outer membrane(**Fig. 4.1**).[1-4] The outer membrane stops small molecular entry to the cell as well as insulates the peptidoglycan from lysozyme degradation.[3] Furthermore, the outer membrane consists of 60-80% lipopolysaccharide, and Lipid A is a key component that binds the lipopolysaccharide to the outer membrane (**Fig. 4.2**).[1-4] While the sugars comprising the tail of lipopolysaccharide can vary across different bacterial species, Lipid A remains the same and is a vital component to bacterial health, such that there exist only three bacterial strains that can simply endure without Lipid A: *Moraxella catarrhalis*, *Neisseria meningitidis*, and *Acinetobacter baumannii*.[1,5,6] These three strains can survive without Lipid A (and in essence, lipopolysaccharide), but they do not thrive.[1,6] They are typically more susceptible to antibiotics and are overall less virulent, thus highlighting the importance of Lipid A to Gram-negative bacterial vitality.[1,6]

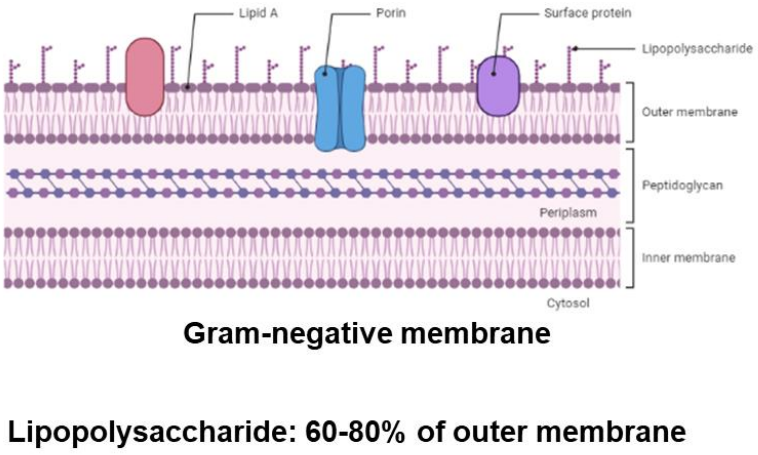

Figure 4.1: Depiction of the membrane of Gram-negative bacteria, highlighting the outer membrane, lipid A, and porins. Figure made with BioRender.

Because of the three strains that can survive without Lipid A, the essential role of Lipid A in other Gram-negative bacteria has been questioned, particularly with *Escherichia coli*.[6] *E. coli* is typically a nonpathogenic bacterial strain that is present in over 90% of the general population's gut microbiome but is also a primary cause of urinary-tract infections.[7] However, previous studies of *E. coli* focused on pathogenic or antibiotic-resistant strains, severely limiting the knowledge of more common *E. coli* strains.[7] *E. coli* is also one of the first bacteria to exist in the gut microbiome as it is present in neonatal populations (which is where it was first discovered).[7] Because of the discrepancy in lipopolysaccharide necessity, experts further probed the requirement of Lipid A for cell survival and proposed more nuanced explanations to account for the apparent essential role

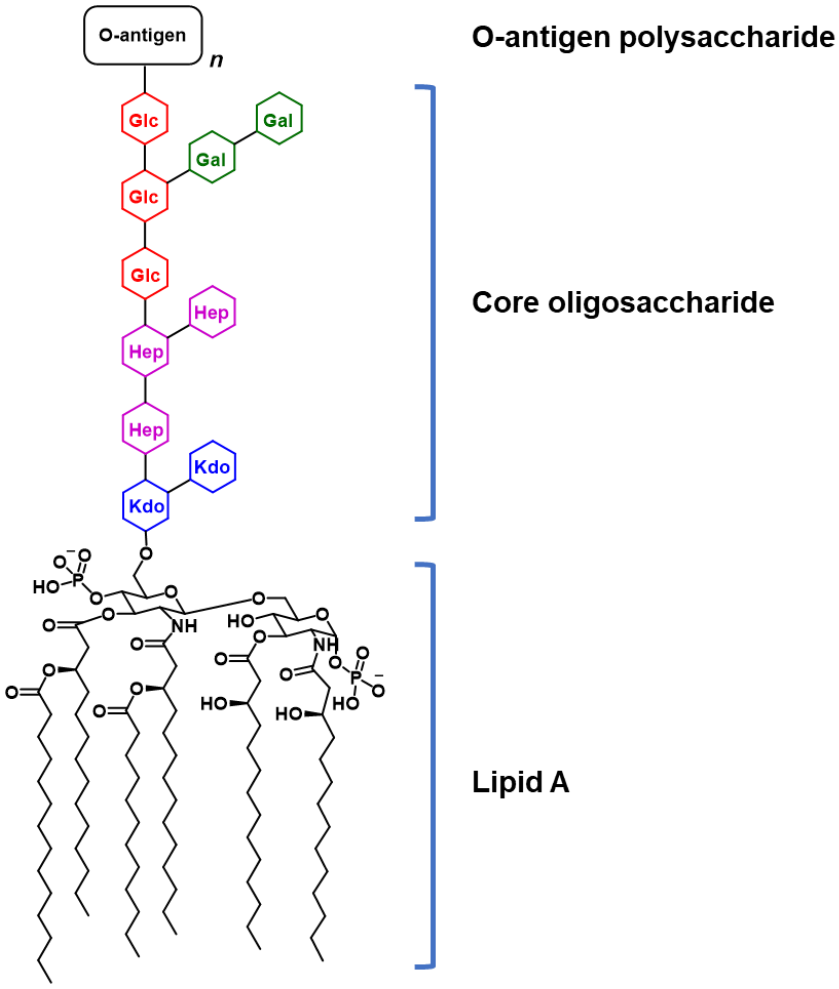

Figure 4.2: The three components of lipopolysaccharide: Lipid A (ties lipopolysaccharide to the membrane), the core saccharide, and the O-antigen polysaccharide. Only three bacterial strains can exist without Lipid A.

Lipid A plays for *E. coli* (and other strains) vitality and how the *Acinetobacter*, *Neisseria*, and *Moraxella* genera are able to survive without lipopolysaccharide.[1,5-7]

While Kahne and coworkers note that Lipid A itself may not be necessary for Gram-negative bacterial survival, they detail the implications of lipopolysaccharide removal, exemplified in the loss of functioning in the cell envelope, which ultimately leads to cell death.[6] They mention that inhibition of Lipid A biosynthesis can lead to accrual of cell envelope components (Und-PP O-antigen precursors) in undesirable locations, propelling the cell to its death unless it possesses mechanisms to treat stalled cellular processes.[6] Furthermore, lipopolysaccharide aids in porin assembly and function; porins enable nonspecific small molecule nutrients entry into the cell and are necessary for cell survival.[6] Several broad-spectrum porins, like BamA, have been shown to be essential for cell vitality.[6] Another protein necessary for *E. coli* survival is LptD. Interestingly, LptD is not essential in *N. meningitidis*, which could account for the discrepancy between the two bacterial strains in regard to Lipid A and cell survival.[6] Finally, Kahne and coworkers specify that

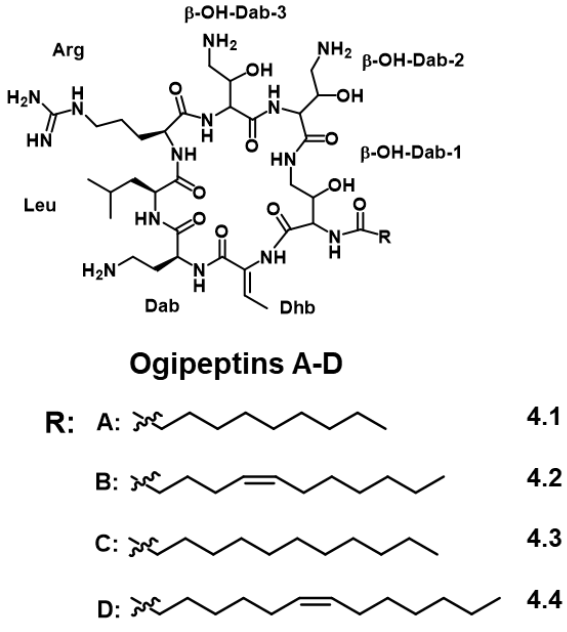

Figure 4.3: The ogipeptins possess activity against only Gram-negative bacteria.

losing lipopolysaccharide can prompt stress pathways, which leads to growth inhibition of the strain itself, in a sort of “friendly fire” aspect.[6] Thus, while *A. baumannii*, *N. meningitidis*, and *M. catarrhalis* are able to survive without Lipid A (and thus lipopolysaccharide), this is abnormal. In order to explain how loss of lipopolysaccharide specifically affects a bacterial strain, one must explore that strain specifically, as the Kahne Lab explored *E. coli*.[6] The development of a specific chemical tool compound that targets Lipid A would have the potential to expand this hypothesis to other bacteria.

4.1.2 Ogipeptins and polymyxin B

The ogipeptins are a class of macrocyclic peptides with activity against *E. coli*, a Gram-negative bacterial strain (**Fig. 4.3**).[8,9] Ando and coworkers tested the ogipeptins against *Staphylococcus aureus* and found the ogipeptins to be inactive against the Gram-positive strain.[8,9]

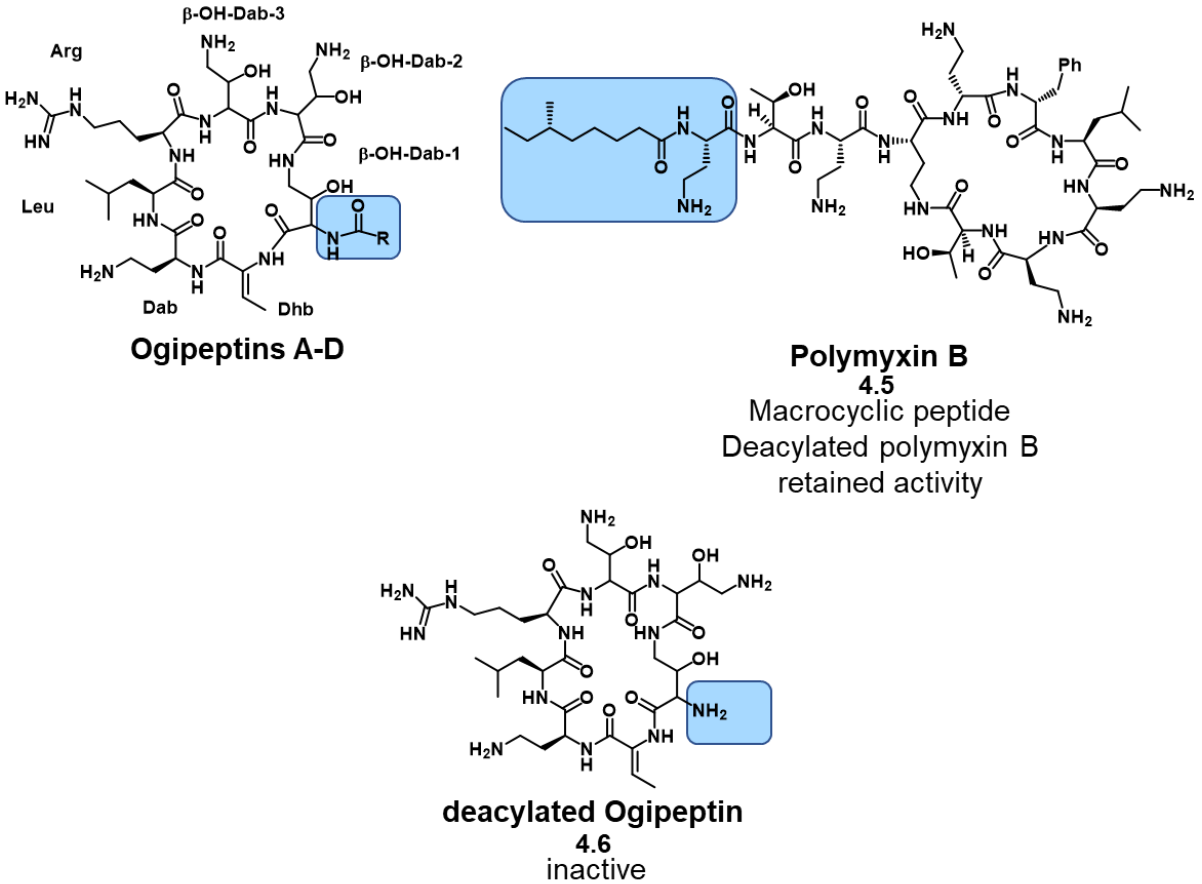

Figure 4.4: Deacylated ogipeptins are inactive, unlike deacylated polymyxin B, indicated the ogipeptins operate under a different mechanism than polymyxin B.

This difference in activity hints at an outer membrane mechanism. As previously mentioned, Gram-negative bacteria are harder to kill because of the outer membrane, which is a secondary layer that prevents small molecule entry into the cell.[1-6] The ogipeptins possess a side chain (R) that is an all-carbon backbone with no or one point of unsaturation. Furthermore, while there are nine stereocenters in the ogipeptin macrocycle, only three have been unambiguously assigned (**Fig. 4.3**).

In their attempts to unravel the mechanism of action of the ogipeptins, Ando and coworkers compared the ogipeptins to polymyxin B, which is in the colistin family (a drug of last resort in order to limit the rise of resistance) (**Fig 4.4**).[8,9] Polymyxin B operates via binding to lipopolysaccharide and displacing the embedded divalent cations (Ca^{2+} and Mg^{2+}) that provide stabilization to the membrane.[3,10] This displacement leads to disruption of the membrane, which ultimately culminates in cell death.[3,10] In Ando and coworkers' studies, they deacylated both the ogipeptins and polymyxin B at their side chains.[8,9] Polymyxin B is a mixture of several similar compounds (B_{1-4}) all varying at the side chain, which makes them an apt comparison for the ogipeptins, in which the side chain is their diversification point.[10] However, Polymyxin B retained activity, but the deacylated ogipeptins did not, highlighting the necessity of the side chain for activity (**Fig. 4.4**).[8,9]

4.1.3 LpxC

Investigating other outer membrane mechanisms, I found the metalloenzyme, LpxC, which is a popular outer membrane target.[2,11-18] LpxC catalyzes the first committed step in Lipid A biosynthesis, and Lipid A anchors lipopolysaccharide to the outer membrane (**Fig 4.5**).[2,11-18]

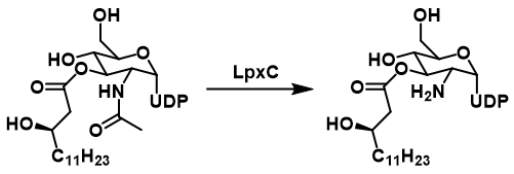

4.7 **4.8**

Figure 4.5: LpxC catalyzes the first committed step in Lipid A biosynthesis.

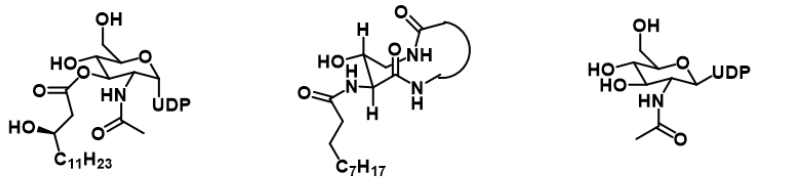

Native LpxC substrate **4.9** | **Ogipeptin A** **4.10** | **Deacylated native LpxC substrate** **4.11** inactive

Figure 4.6: Ogipeptin A: modeled similar to the myr-UDP-GlcNAc (native LpxC substrate) which may explain the importance of the side chain of the ogipeptins.

Specifically, the LpxC metalloenzyme catalyzes the removal of an acetate from myr-UDP-GlcNAc to produce myr-UDP-$GlcNH_2$ (**Fig. 4.5**).[11-16] Furthermore, the hydroxylmyristoyl side chain is important for substrate recognition, based on the Michaelis-Menten steady-state kinetics, in which LpxC has low binding affinity for UDP-GlcNAc and high binding affinity for myr-UDP-GlcNAc.[13] One can base this hydroxylmyristoyl side chain necessity on the crystal structure of LpxC with its natural substrate.[13] In the crystal structure, there is a structural fold in which one β-sheet is flat while the other β-sheet is kinked such that the Insert II requires hydrophobic interactions for binding.[13] Thus, I believe the acyl side chain of the ogipeptins is similar to that of the natural substrate, myr-UDP-GlcNAc, which enables substrate recognition by LpxC biosynthesis (**Fig. 4.6**). Therefore, I hypothesize that the ogipeptins mimic the LpxC natural substrate to inhibit Lipid A. Additionally, I hypothesize that while the acyl side chain is important for substrate recognition, the dehydrobutyrine (Dhb, Michael acceptor) residue is responsible for acting as the warhead of the natural product.

Because of its role in Lipid A biosynthesis, and subsequently lipopolysaccharide binding, LpxC is a popular target for Gram-negative bacterial inhibition.[2,17,18] There exist several reviews of LpxC inhibitor patent literature. Kalinin and Holl note commonalities in structure: a divalent zinc chelating moiety and lipophilic side chain, both of which are present in the ogipeptins.[18] Merck and co also filed several patents detailing their LpxC inhibitors (**Fig. 4.7**).[18] They note that

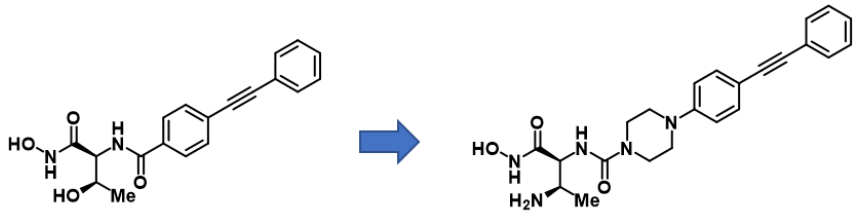

4.12 4.13

Figure 4.7: Two compounds from Merck and co. LpxC patents from 2009 and 2010.

benzolactams were not as active (due to inability to form a hydrogen-bonding interaction with the enzyme) but were able to mitigate some of this lack of inhibitory activity via incorporation of a longer lipophilic chain.[18] In an ensuing patent, Merck describes the incorporation of a urea to provide the necessary hydrogen-bonding activity with Thr179.[18] In their SAR, they prepared analogs with piperazine and piperidine rings, and piperazine analogs were more active.[18] This can be rationalized because the piperazine analogs are more polar and therefore more likely to be able to permeate the cell.[18] In their studies, Merck tested their compounds against not only susceptible and multidrug-resistant *E. coli* but also against ESKAPE pathogens, *Klebsiella pneumoniae* and *Pseudomonas aeruginosa,* and observed activity across the board.[18]

Merck is not the only pharma company to pursue LpxC inhibitors. Their competitors are Achaogen, Pfizer, AstraZeneca, Actelion, and Novartis. Achaogen developed butadiyne inhibitors with hydroxamates as the Zn^{2+}-binding motif.[18] Their compound, ACHN-975, is first in class in human trials.[18] It possessed excellent activity (<1 μg/mL) against colistin- and β-lactam-resistant *P. aeruginosa*.[18] It also exhibited activity against many other Gram-negative bacteria, except for *A. baumannii*, which as detailed previously, can exist without lipopolysaccharide.[1,5-7,18] Achaogen developed several formulations for ACHN-975 of varying stabilities but ultimately withdrew ACH-975 from trials after injection site inflammation despite the pre-clinical trial promise.[18] The candidates filed by the other pharma companies display similar activity on the same bacteria (*P.*

aeruginosa, *K. pneumoniae*, *E. coli*, and *A. baumannii*) and present resembling structures (hydroxamate derivatives for Zn^{2+} binding-motif and a lipophilic moiety).[18]

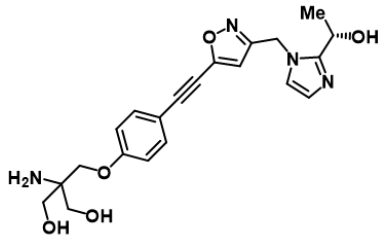

4.14

Figure 4.8: Another LpxC inhibitor lead compound published by Hubbard and coworkers in *J. Med. Chem.* in 2020.

These are not the only published examples. Hubbard and coworkers from Taisho Pharmaceuticals and Vernalis (R&D) Ltd. published in *J. Med. Chem*. on their SAR toward their lead imidazole scaffold with activity against *P. aeruginosa* (**Fig. 4.8**).[19] Interestingly, their imidazole lead does not contain a hydroxamate as the zinc-binding moiety but an isoxazole.[19] It also possesses three free alcohols and one free amine.[19] The synthesis is six steps with relatively mild conditions and includes two Sonogashira couplings.[19] In their SAR, the authors not only test their compounds against *P. aeruginosa* but also against *E. coli* and *K. pneumoniae*.[19] Intriguingly, the authors describe attempting to optimize their scaffold for *P. aeruginosa* but observe more activity with *E. coli* and *K. pneumoniae*.[19] Furthermore, the compound that they appoint as their preferred series possesses the best activity against *P. aeruginosa* but only at 4 or 8 μg/mL (± HSA), which is much worse than previously patented compounds.[2, 17-19] Hubbard and coworkers indicate that their next steps are to perform further SAR around their imidazole scaffold in order to generate a more potent lead and to investigate the *in vivo* efficacy of their compounds.[19] In their publication, they did not detail toxicity nor cell permeability, which is typically performed simultaneously as activity studies so as to better understand the scaffold and its properties as well as better plan the next target compounds. Thus, while this publication was interesting from an academic perspective, it is lacking from a pharmaceutical development perspective.

4.1.4 Stereochemistry

As previously stated, the ogipeptins contain nine chiral centers and only three of which have been unambiguously assigned.[8,9] Thus, in order to synthesize the natural product, one must also elucidate the stereochemistry. All six unspecified stereocenters are contained within three of four unnatural amino acids within the macrocycle: β-OH Dab-1,-2, and -3 (**Fig. 4.9**). After identifying key moieties for activity within the natural product, we can model ogipeptin A after the natural substrate, myr-UDP-GlcNAc.[11-16] Thus, we orient the lipophilic side chains similarly and form a chair-like conformation with ogipeptin A (**Fig. 4.6**). This then allows for prediction of both stereocenters within β-OH Dab-1, which would be (*2S,3R*) (**Fig. 4.10**). While we are confident in our prediction, we still intend to access the other three stereoisomers to validate that (*2S,3R*) is the correct stereochemistry of the natural product via comparing NMR samples of the isolated natural product and our synthesized material. Finally, we also aim to examine the biological activity of the four stereoisomers of β-OH Dab-1 to ascertain if the stereochemistry surrounding the lipophilic side chain affects activity.

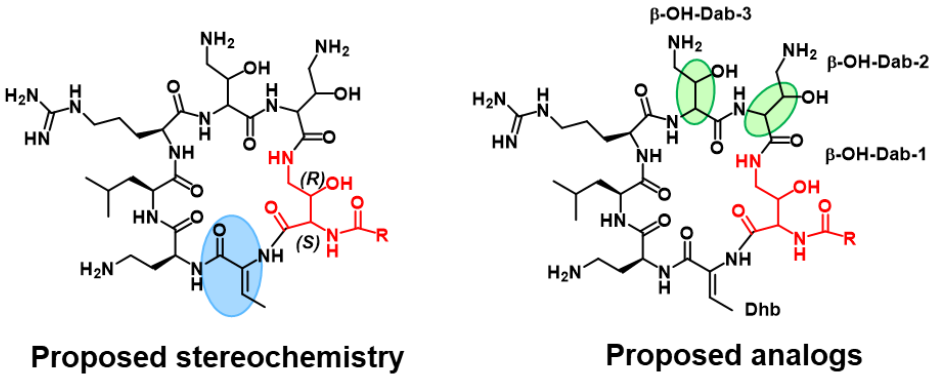

Figure 4.9: Depiction showing the key Michael acceptor of the Dhb, the proposed stereochemistry at β-OH Dab-1 (in red), and potential stereochemical permutations that can be made at β-OH Dab-2 and -3.

Because there are six unspecified stereocenters within the ogipeptins, this would be 64 possible isomers (2^6). However, we can curtail the number of isomers by hypothesizing that the three β-OH Dab residues possess identical relative stereochemistry, narrowing the list to 4 isomers (2^2). We can test this hypothesis via synthesizing other β-OH Dab stereocenter variations,

such as (*2S, 3S*), at β-OH Dab-2 and β-OH Dab-3 and identifying how the different stereocenters affect antibacterial activity (**Fig. 4.9**).

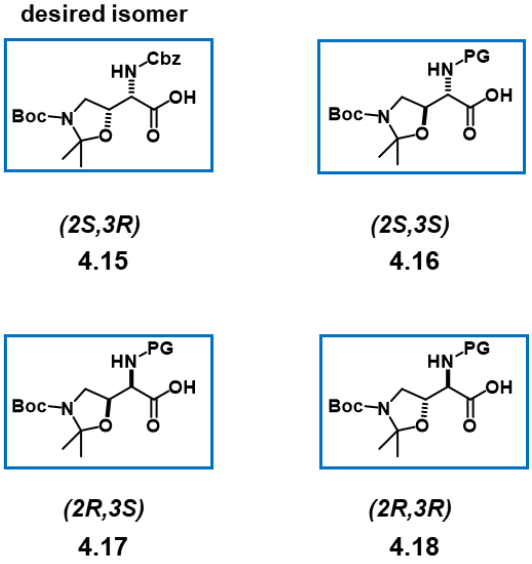

Figure 4.10: The four β-OH Dab isomers.

4.1.5 Previous β-OH Dab residue syntheses

β-OH Dab residues are not commercially available, but there currently exist two methods to access protected versions of these unnatural amino acids.[20,21] Stepan and coworkers utilized a method focused on accessing all four isomers that relies on chiral resolution in the penultimate step to separate the isomers.[20] Racine and coworkers specifically pursued the (*2S,3S*) isomer.[21]

In Stepan and coworkers' synthesis, they first start with propargylamine, which is expensive ($30/g) and acutely toxic (**Fig. 4.11**).[20] They then perform a reductive amination to append a *p*-methoxybenzene (PMB) to the free amine, protect with di-*t*-butyl dicarbonate to affix a second protecting group (Boc) to the mono-protected amine, and react the terminal alkyne with strong base (*n*-butyl lithium) and methyl chloroformate in order to access the alkynyl methyl ester.[20] Following this, they performed a reduction with Lindlar's catalyst to access the *cis*-alkene, which can be funneled into a racemic dihydroxylation with osmium tetroxide, a compound known to be acutely toxic and whose fumes can cause blindness.[20] Next, Stepan and coworkers trapped the racemic dihydroxylated material with thionyl chloride and then opened the five-membered ring

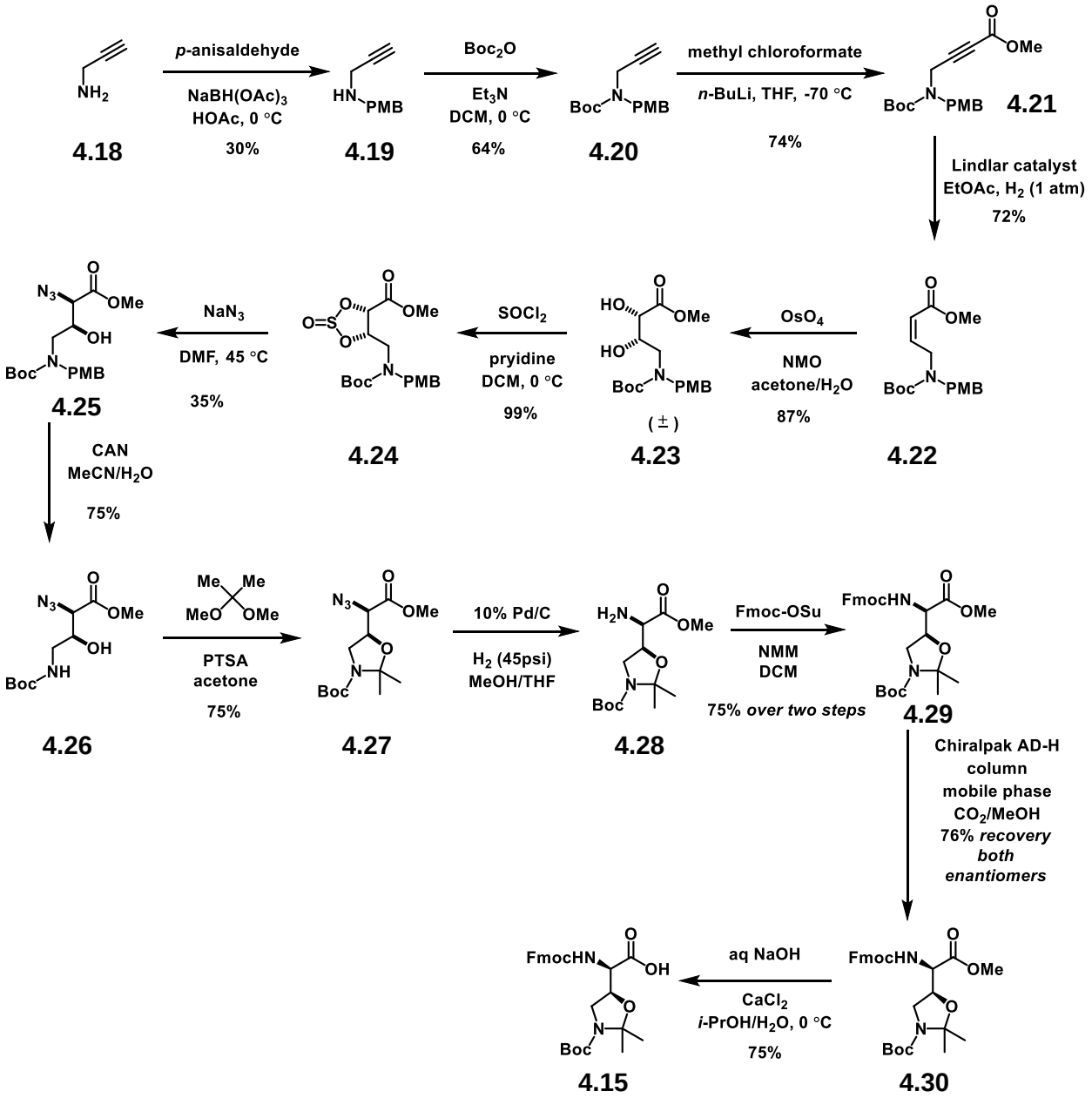

Figure 4.11: Stepan and coworkers' route to access all four β-OH Dab isomers.

with sodium azide by heating in dimethylformamide overnight in low to moderate yield.[20] Following the introduction of the azide, Stepan and coworkers mono-deprotected the γ-amine with cerium ammonium nitrate (CAN) to remove the PMB.[20] The monoprotected amine and the β-alcohol were then protected via formation of a hemiaminal with 2,2-dimethoxypropane and catalytic *p*-toluene sulfonic acid in acetone overnight.[20] After obtaining the hemiaminal, Stepan and coworkers reduced the azide to the amine with palladium on carbon in the presence of H_2 and pressure (45

psi) and then protected the α-amine with Fmoc.[20] Then, they performed a chiral resolution and hydrolyzed the ester to obtain the separated desired *syn* β-OH Dab building blocks, which is ready for amidation.[20]

The synthetic route by Stepan and coworkers' employs thirteen steps and multiple protecting group manipulations to access their desired β-OH Dab building blocks (**Fig. 4.11**).[20] They are able to access the other two isomers (*anti*-) in identical conditions but with the *trans*-alkene from the alkynyl reduction.[20] They also utilize vibrational circular dichroism as a method to assign the absolute configuration of their dihydroxylated intermediates, which is not an easily accessible tool.[20] While their method enables access to all four β-OH Dab stereoisomers, it relies on chiral resolution in order to separate the racemic mixtures, which is another limitation.[20]

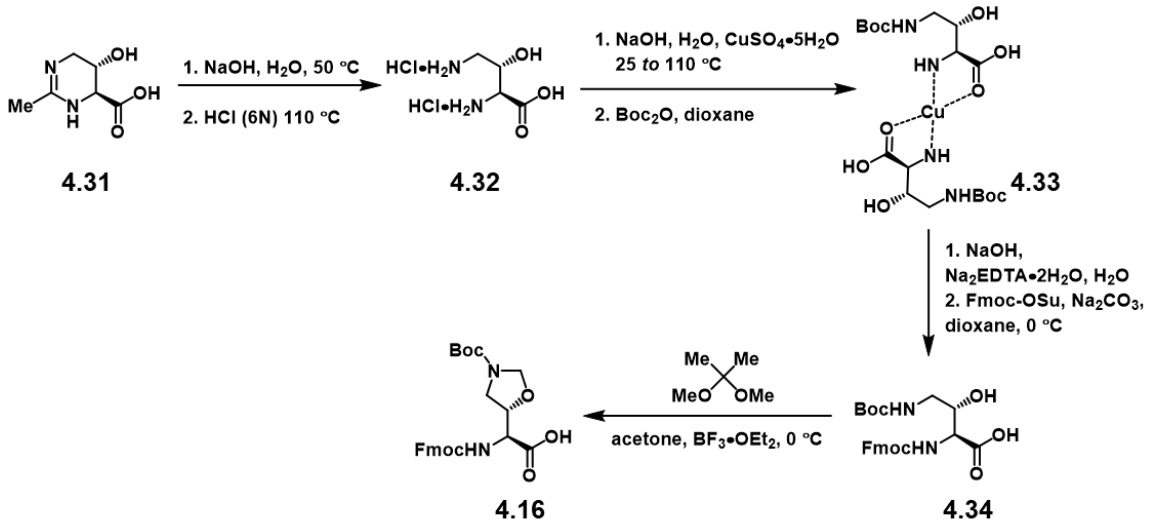

Figure 4.12: Racine and coworkers' route to access (*2S,3S*) and (*2S,3R*) β-OH Dab isomers.

In Racine and coworkers' route, they utilize 5-hydroxyectoin (~$30/g) and capitalize on pre-set stereocenters (**Fig. 4.12**).[21] They first saponify to access the mono-acetylated intermediate, which was telescoped into a further saponification to afford free amine **4.32** that could be salted out to obtain the β-OH Dab hydrochloride salt.[21] After this first step, Racine and coworkers analyzed the diastereomeric ratio (d.r.) of their crude mixture and observed a 3:1 ratio of (*2S,3S*) and (*2S,3R*) isomers, respectively.[21] They attempted to improve the observed d.r. but unfortunately were unable to do so and thus telescoped the β-OH Dab hydrochloride salt into the

next reaction: copper-complex formation.[21] This copper-complex formation enabled selective protection of the γ-amine in the next step with di-*t*-butyl dicarbonate in 40% yield over four steps.[21] Following Boc protection, Racine and coworkers dismantled the copper complex with EDTA to free the α-amine, which could then be protected with Fmoc.[21] Finally, they formed the hemiaminal with 2,2-dimethoxypropane and acetone in the presence of a Lewis Acid (BF_3•OEt_2).[21]

Racine and coworkers' synthesis utilizes seven steps efficiently (telescoping) to afford the desired protected β-OH Dab residue in 29% yield overall (**Fig. 4.12**).[21] It does not require the use of a chiral column as diastereomers can be separated via achiral chromatography and makes use of fairly mild reagents.[21] However, utilizing 5-hydroxyectoin as the starting material is a double-edged sword: both stereocenters are already set (and the β-OH Dab backbone is formed) but the α-stereocenter cannot be easily and efficiently modified to produce the (*R*) stereocenter.[21] Furthermore, Racine and coworkers' synthesis is difficult to reproduce (reproduction experiments performed by Dr. Wanli Zhang). Thus, the synthesis for a protected β-OH Dab residue designed by Racine and coworkers is efficient but lacking.

4.2 Epoxidation Methods

Because of the issues surrounding both Stepan and Racine's syntheses, we endeavored to design syntheses that are more amenable for our goals: no chiral resolution requirement, access to the (*2R,3S*) and *(2R,3R*) isomers, fewer than thirteen steps, and less toxic reagents. Thus, in my first thought process, I wanted to install the β-alcohol from an enantioselective epoxidation (**Fig. 4.13**). After obtaining the chiral epoxide, I envisioned opening it with an amine like ammonia or with an azide to install the γ-functionality before performing several protecting group manipulations to access the desired protected β-OH Dab residue. While this route would enable access of the (*2S,3R*) isomer and its enantiomer, it would not afford the diastereomers. Despite this limitation, I still pursued this route due to literature precedence of several steps, which should enable facile access to the protected β-OH Dab residue and allow us to proceed to

synthesizing the linear chain of amino acids and performing macrocyclization to obtain the natural product.

4.2.1 Alkyne

Thus, in my quest to access the alkene starting material for the epoxidation, I was inspired from the previously published racemic route and chose to start with Boc-protected propargylamine (**Fig. 4.13**).[20] I could then append the ester with ethyl chloroformate at low temperature.[20-22] While precedented, this method provided double addition to the terminal alkyne and the carbamate. Because of this, I then turned to a precedented one-pot synthesis that protected the carbamate, underwent the ethyl chloroformate addition, and then deprotected to provide the mono-carbamate.[22] Unfortunately, these conditions did not provide the desired product. We next thought of other conditions to protect the carbamate, further functionalize the terminal alkyne, and then selectively deprotect. In our literature searches, we found reductive amination conditions to

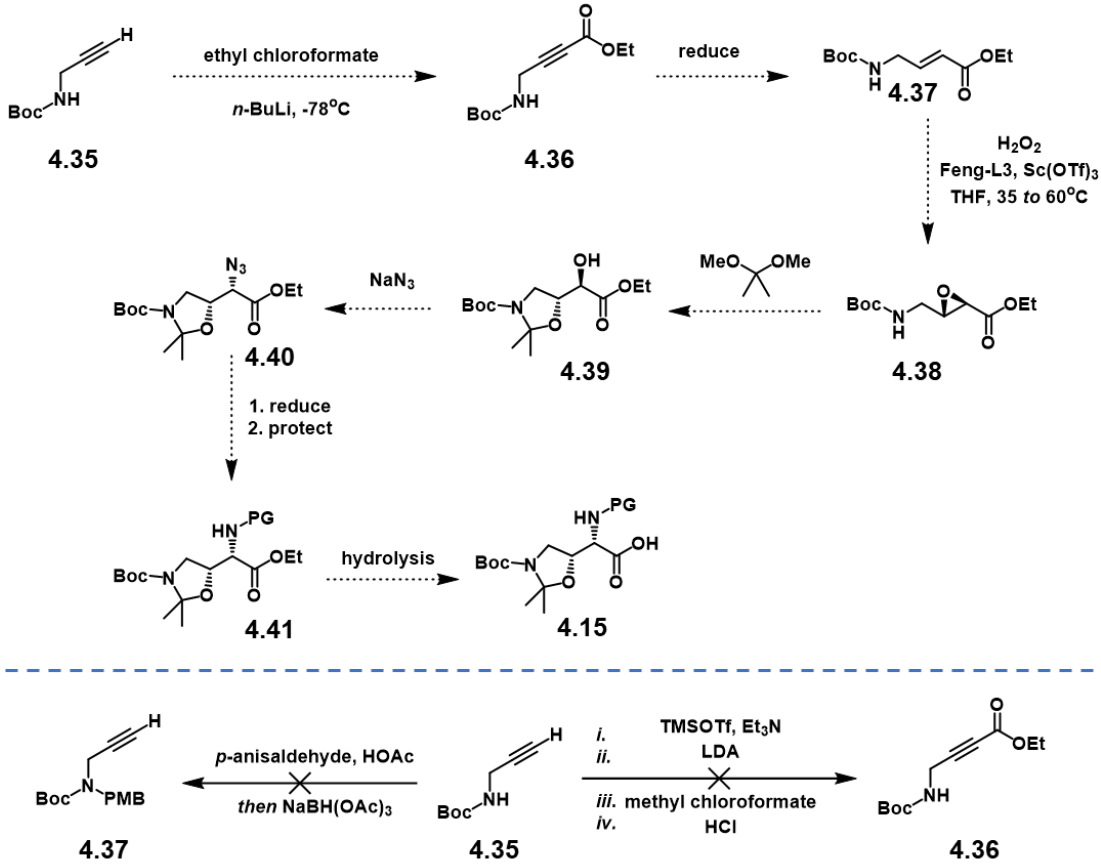

Figure 4.13: Epoxidation route.

protect the carbamate with PMB, but acetic acid with a reducing agent such as STAB is enough to remove the Boc protecting group. Thus, because of these limitations, we turned to a new method to access our key α,β-unsaturated ester.

4.2.2 Reduction and Wittig

Instead of utilizing an alkyne starting material, I chose to use the inexpensive, commercially available Boc-protected glycine methyl ester (**Fig. 4.14**). Then, I reduced the methyl ester with the bulky reducing agent, DIBAL-H, to obtain the aldehyde and funneled it crude after workup into the Wittig to obtain desired α,β-unsaturated ester.[23] While this method is only two steps, it does require low temperature and patience while adding the reducing agent in order to minimize over-reduction to the alcohol. Furthermore, the Wittig produces both the *cis* and *trans* isomers in a 1:2 ratio, which can be separated by careful column chromatography.

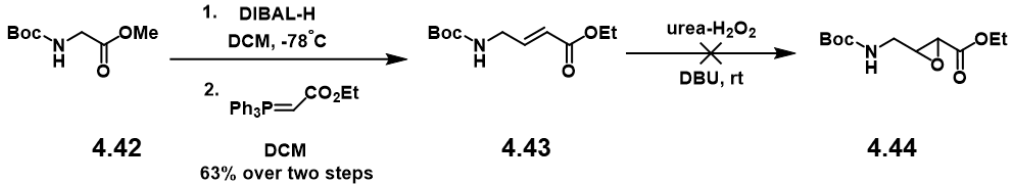

Figure 4.14: Reduction and Wittig to obtain key α,β-unsaturated ester, and the racemic epoxidation did not give epoxide product.

4.2.3 Epoxidation

Now that I had the key α,β-unsaturated ester in hand, I next wanted to investigate the enantioselective epoxidation (**Fig. 4.14**). In my initial efforts, I employed 30% hydrogen peroxide in THF and observed no reaction—most likely because the starting material is an electronically deficient alkene.[24] Thus, I heated the reaction mixture to 66 ºC and observed decomposition with the current starting material as well as a PMB-protected starting material. Because of the results seen with hydrogen peroxide despite literature precedent, I consulted epoxidation reviews.[25,26] The Sharpless epoxidation is typically for that of allylic alcohols and so would be immediately unhelpful.[25] The Shi epoxidation, while promising, requires use of perchloric acid to generate the ligand from *D*-fructose.[26] Finally, in a review specifically on enantioselective epoxidation of

electron-deficient alkenes, Porter and Skidmore cite that urea-H_2O_2 with DBU and poly-*L*-leucine in THF is able to enantioselectively epoxidize an α,β-unsaturated ester with the desired stereoselectivity (**Fig. 4.14**).[26] Before synthesizing the ligand, I decided to attempt the epoxidation racemically, and it did not work. While exciting as this indicates that the ligand was necessary for the epoxidation, due to supply chain issues, I instead pursued other routes while waiting on starting materials.

4.3 Aminohydroxylation

4.3.1 Literature precedent

Because of the supply chain difficulties with the epoxidation, I decided to explore other routes and pivoted to the aminohydroxylation, because it would decrease the step-count from eight steps to five. The aminohydroxylation is typically performed on α,β-unsaturated esters with an aryl ring at the β-position (**Fig. 4.15**).[28] The literature surrounding the reaction indicates that it can be very difficult, prone to dihydroxylation and hydrolysis side products, and typically produces moderate yields of 50-70%.[28]

The aminohydroxylation would set both the α and β stereocenters simultaneously and also highlights the beauty of utilizing the key α,β-unsaturated ester as a linchpin in two ways. In the aminohydroxylation, I can access both the (*2S,3R*) and (*2R,3S*) isomers by exchanging the ligand ($(DHQ)_2AQN$ and $(DHQD)_2AQN$). I can also achieve the (*2R,3R*) and (*2S,3S*) isomers via Sharpless dihydroxylation, which enables us to attain all four protected Dab stereoisomers to aid in our biological investigation.

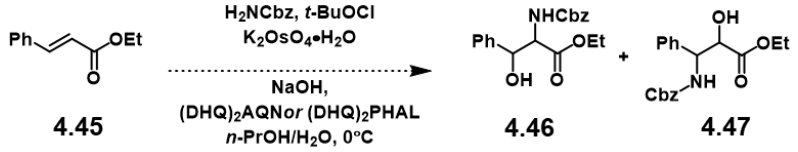

Figure 4.15: General reaction conditions and substrate for the aminohydroxylation.

4.3.2 Alkyl ester & Chen precedent

However, when I was first searching through the literature, I encountered conflicting reports of within substrates that deviated from the typical starting material (alkyl chain or alkyl amine at the β-position) (**Fig. 4.16**).[29,30] Furthermore, there was little consensus within the literature on the procedure to perform the aminohydroxylation at the bench. Panek and coworkers detailed in 1999 that with an alkyl backbone (as opposed to the typical aryl substituent off the β position) and an ethyl ester, the produced regioisomer will be the α-alcohol and β-carbamate.[29] Moreover, the alkyl backbone was an isopropyl off the β position.[29] In their 2004 mitomycin synthesis, Chen and coworkers note that in a system very similar to our desired substrate, but with a di-protected amine and a methyl ester, they observed the carbamate at the desired α-position.[30] Thus, based on substrate similarity, I decided to utilize the conditions specified in the 2004 Chen paper.

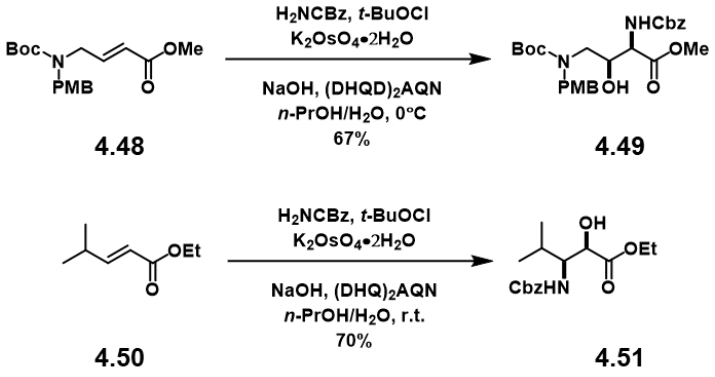

Figure 4.16: Chen precedent indicates an α-carbamate regioisomer (**4.49**), while Panek details that they obtained the α-alcohol (**4.51**).

In order to obtain my desired regioisomer, the approach of the alkene to the osmium(VIII) complex was important (**Fig. 4.17**). If the alkene approached in which the ester overlapped with the carbamate of the osmium(VIII) complex, then I would obtain my desired regioisomer with the carbamate at the α-position. However, if the carbamate of the osmium complex and the carbamate of the starting material instead overlap, giving the undesired transition state, this will

produce the undesired regioisomer with the α-alcohol. A steric argument seems to support the desired transition state (giving α-carbamate product).

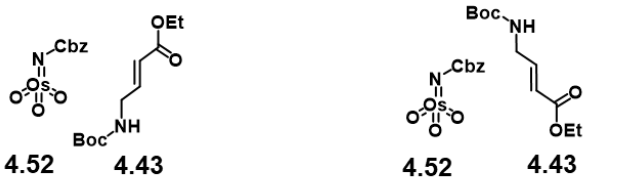

Figure 4.17: Schematics detailing approach of the alkene to the osmate(VIII) catalyst, **4.52**.

4.3.3 Aminohydroxylation optimization

I first began my studies via following the Chen procedure of a 1:2 ratio of *n*-PrOH to water with benzyl carbamate as the nucleophile and obtained dihydroxylated and hydrolyzed products in addition to recovery of starting material (**Table 4.1, entry 1**).[30] I next explored temperature as the literature possesses inconsistencies in whether the reaction should be performed at 0 ºC or room temperature (**Table 4.1, entry 2**). While I did see starting material conversion both cold and at room temperature, I did not observe aminohydroxylated products and instead obtained dihydroxylation and hydrolysis products. I also examined the order of addition (**Table 4.1, entry 3**). According to several literature procedures, potassium osmate(VI) dihydrate is added last to the reaction mixture, which is how I had performed my reaction setup. I postulated that it should be added earlier based on the mechanism, which indicates that the chloroamine generated *in situ* from *t*-butyl hypochlorite and benzyl carbamate needs to interact with the potassium osmate(VI) dihydrate in order to form the active osmium(VIII) species that performs the [3+2] cycloaddition with the alkene of interest. Thus, I added my safer form of osmium tetroxide following *t*-butyl hypochlorite addition. Unfortunately, I again did not obtain aminohydroxylated product. Next, I examined catalyst and ligand equivalence and utilized 0.08 and 0.10 equivalents of potassium osmate(VI) dihydrate and $(DHQ)_2AQN$, respectively, which doubled the previous equivalents (**Table 4.1, entry 4**). However, this only produced dihydroxylation and hydrolysis products.

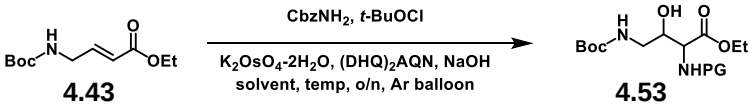

4.43 **4.53**

	Solvent	Temp	Order of Addition	Eq. Cat; Ligand	Nucleophile	Product	Yield
1	*n*-PrOH/H_2O (1:2)	0°C	ligand, alkene, osmium source	0.04; 0.05	$CbzNH_2$	dihydroxyl; hydrolysis; SM	--
2	*n*-PrOH/H_2O (1:2)	rt	ligand, alkene, osmium source	0.04; 0.05	$CbzNH_2$	dihydroxyl; hydrolysis; SM	--
3	*n*-PrOH/H_2O (1:2)	0°C	osmium source, ligand, alkene	0.04; 0.05	$CbzNH_2$	dihydroxyl; hydrolysis; SM	
4	*n*-PrOH/H_2O (1:2)	0°C	ligand, alkene, osmium source	0.08;0.10	$CbzNH_2$	dihydroxyl; hydrolysis; SM	--
5	*n*-PrOH/H_2O (1:1)	0°C	ligand, alkene, osmium source	0.04; 0.05	$CbzNH_2$	dihydroxyl; hydrolysis; SM	--
6	DMF/H_2O (1:2)	0°C	ligand, alkene, osmium source	0.04; 0.05	$CbzNH_2$	dihydroxyl; hydrolysis; SM	--
7	*i*-PrOH/H_2O (1:2)	0°C	ligand, alkene, osmium source	0.04; 0.05	$CbzNH_2$	dihydroxyl; hydrolysis; SM	--
8	MeCN/H_2O (1:2)	0°C	ligand, alkene, osmium source	0.04; 0.05	$CbzNH_2$	dihydroxyl; hydrolysis; SM	--
9	acetone/H_2O (1:2)	0°C	ligand, alkene, osmium source	0.04; 0.05	$CbzNH_2$	dihydroxyl; hydrolysis; SM	--
10	*n*-PrOH/acetone/H_2O (1:1:1)	0°C	ligand, alkene, osmium source	0.04; 0.05	$CbzNH_2$	dihydroxyl; hydrolysis; SM	--
11	*n*-PrOH/H_2O (1:2)	0°C	ligand, alkene, osmium source	0.04; 0.05	$BnNH_2$	dihydroxyl; hydrolysis; SM	--
12[a]	*n*-PrOH/H_2O (1:2)	0°C	ligand, alkene, osmium source	0.04; 0.05	$CbzNH_2$	SM	--
13[a,b]	*n*-PrOH/H_2O (1:2)	0°C	ligand, alkene, osmium source	0.04; 0.05	$CbzNH_2$	SM	--
14[a]	*n*-PrOH/H_2O (2:1)	0°C	ligand, alkene, osmium source	0.04; 0.05	$CbzNH_2$	aminohydroxyl	9%
15[a]	MeCN/H_2O (1:1)	0°C	ligand, alkene, osmium source	0.04; 0.05	$CbzNH_2$	aminohydroxyl	52%[c]

[a] accounted for hydroxide from $K_2OsO_4 \bullet 2H_2O$ [b] Rigorously degassed solvents [c] Performed in triplicate

Table 4.1: Aminohydroxylation conditions screen.

I next examined if a different solvent ratio would enable access to the aminohydroxylated product. In my solvent screen, I examined a 1:1 mixture of *n*-PrOH and water, a 1:2 mixture of MeCN and water, a 1:2 mixture of DMF and water, a 1:2 mixture of *i*-PrOH and water, a 1:2 mixture of acetone and water, and a 1:1:1 mixture of *n*-PrOH, acetone, and water (**Table 4.1, entries 5-10**). In my studies, I seemed to observe aminohydroxylation by LCMS but was never able to isolate the aminohydroxylated product, instead isolating dihydroxylated and hydrolysis products in addition to recovering starting material. Because of the products obtained, I questioned the nucleophilicity of benzyl carbamate in generating the active osmium(VIII) complex needed to perform the aminohydroxylation (**Table 4.1, entry 11**). When I substituted to benzyl amine, I still observed dihydroxylation and hydrolysis products and recovered starting material.

In attempts to understand how to produce aminohydroxylated material, I reexamined the literature and found additional information from the Sharpless Lab at Scripps, who designed the reaction (**Table 4.1**).[31] In their troubleshooting guide, they detailed accounting for all the hydroxide in the reaction in order to prevent dihydroxylation and hydrolysis products (**Table 4.1, entry 12**).[31] Thus, I accounted for the hydroxide produced in creating the active osmium(VIII) complex from the potassium osmate(VI) dihydrate (from 3 eq sodium hydroxide to 2.96 eq sodium hydroxide) and only recovered starting material, which was a step forward. Furthermore, to ensure accurate sodium hydroxide addition, I also switched from weighing out solid sodium hydroxide (and thus eliminating balance error) to making a fresh solution of 0.5M sodium hydroxide. Gratifyingly, the suggestions proved true, and I was able to arrest dihydroxylation and hydrolysis side products. However, I still did not observe aminohydroxylation.

In the same troubleshooting article, Sharpless and coworkers also detailed how rigorously degassing the solvent can aid the reaction proceeding, since oxygen dissolved in the solvent can interfere with the reaction.[31] I degassed according to the freeze-pump-thaw method for water and *n*-PrOH (and used a dry ice/acetone bath and liquid nitrogen, respectively) (**Table 4.1, entry 13**). However, I still only recovered starting material. While examining a spent vial which had originally contained a solution of starting material in *n*-PrOH, I noticed persistent starting material, which I then questioned if the compound was actually soluble in the solvent system I had been using. I decided to increase my solvent ratio to 2:1 *n*-PrOH to water from 1:2 *n*PrOH to water (as I had already examined a 1:1 mixture) and observed aminohydroxylated product in a 9% yield (**Table 4.1, entry 14**). In the same troubleshooting manual previously mentioned, Sharpless and coworkers also describe that, in instances of solubility issues with the starting material, acetonitrile is competent within the reaction but will result in a decrease in enantioselectivity.[31] I switched to a 1:1 mixture of acetonitrile to water and obtained the aminohydroxylated product in a 52% yield, in triplicate (**Table 4.1, entry 15**).

4.3.4 Higher order spectroscopy

Now that I had aminohydroxylated product in hand, I needed to determine which regioisomer I had synthesized. I obtained the COSY for the aminohydroxylated material, because COSY should be the easiest method to differentiate the two regioisomers. COSY will indicate which proton (geminal to the benzyl carbamate or the alcohol) is at the β-position by its proximity to the protons at the γ-carbon.[32] While NOESY would give through space information, NOESY would be not allow us to definitively prove which regioisomer was obtained as both protons (at the α- and β-positions) of each regioisomer would show a coupling with the protons on the γ-carbon.[32] HMBC would provide further validation as the technique suppresses one-bond coupling and would allow observance of coupling between the proton at the α-position and γ-carbon.[32] While this information would be useful in proving the regioisomer obtained, I was unable to collect this information due to time constraints. In seeking confirmation for regioselectivity, I investigated

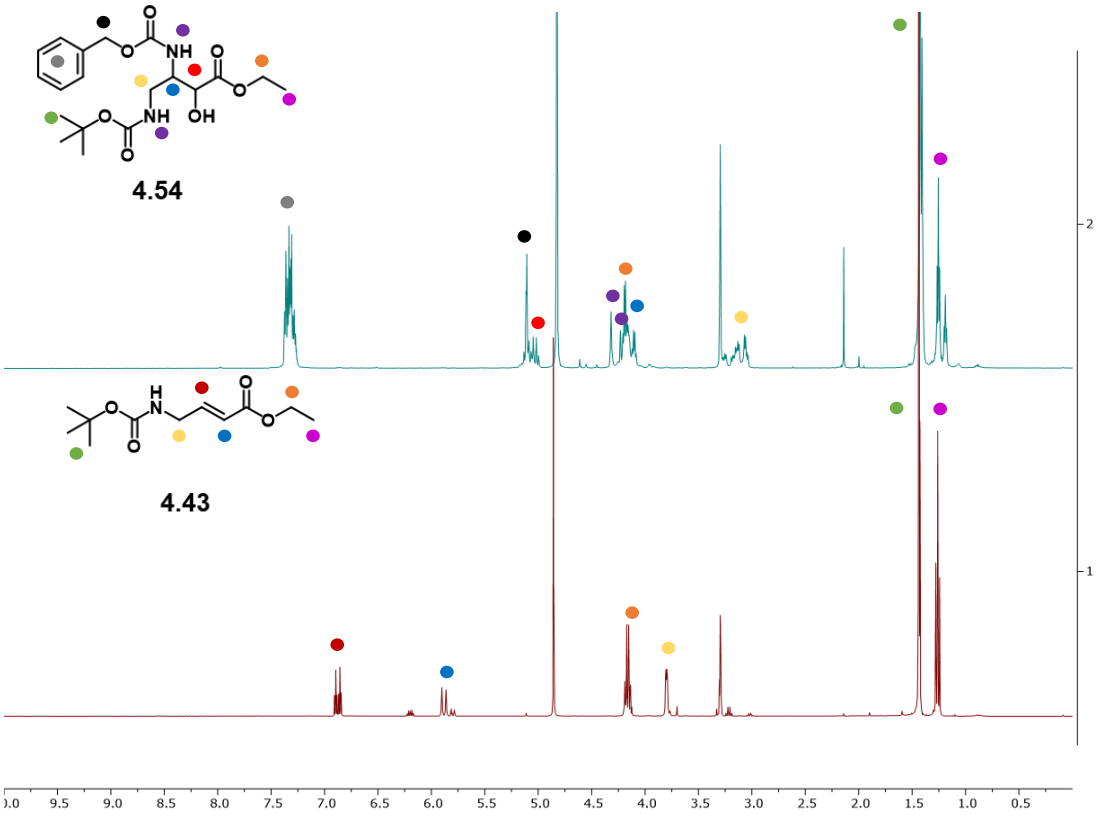

Figure 4.18: Stacked ^{1}H-NMRs of the aminohydroxylated product (top) and starting material (bottom).

reported data from Chen and coworkers, but unfortunately, no higher order spectra were reported.[30]

Based on ChemDraw predicted shifts, I expected the proton geminal to the alcohol to be more downfield than the proton geminal to the benzyl carbamate and between 5 - 6 ppm (**Fig. 4.18**). The ethyl (ester) and *t*-butyl (carbamate) peaks should not shift, and the methylene of the benzyl carbamate should be 5.1 – 5.3 ppm, which is indeed what occurs. The protons of the γ-position located at 3.8 ppm should shift upfield, which I observe with a shift to 3.0 - 3.2 ppm, and become diastereotopic as chirality is introduced into the scaffold. The proton geminal to the benzyl carbamate should be in the range of 4 - 5 ppm and close to the methylene of the ethyl ester, which I observe overlapping from 4.1 – 4.3 ppm in my ^{1}H-NMR spectrum.

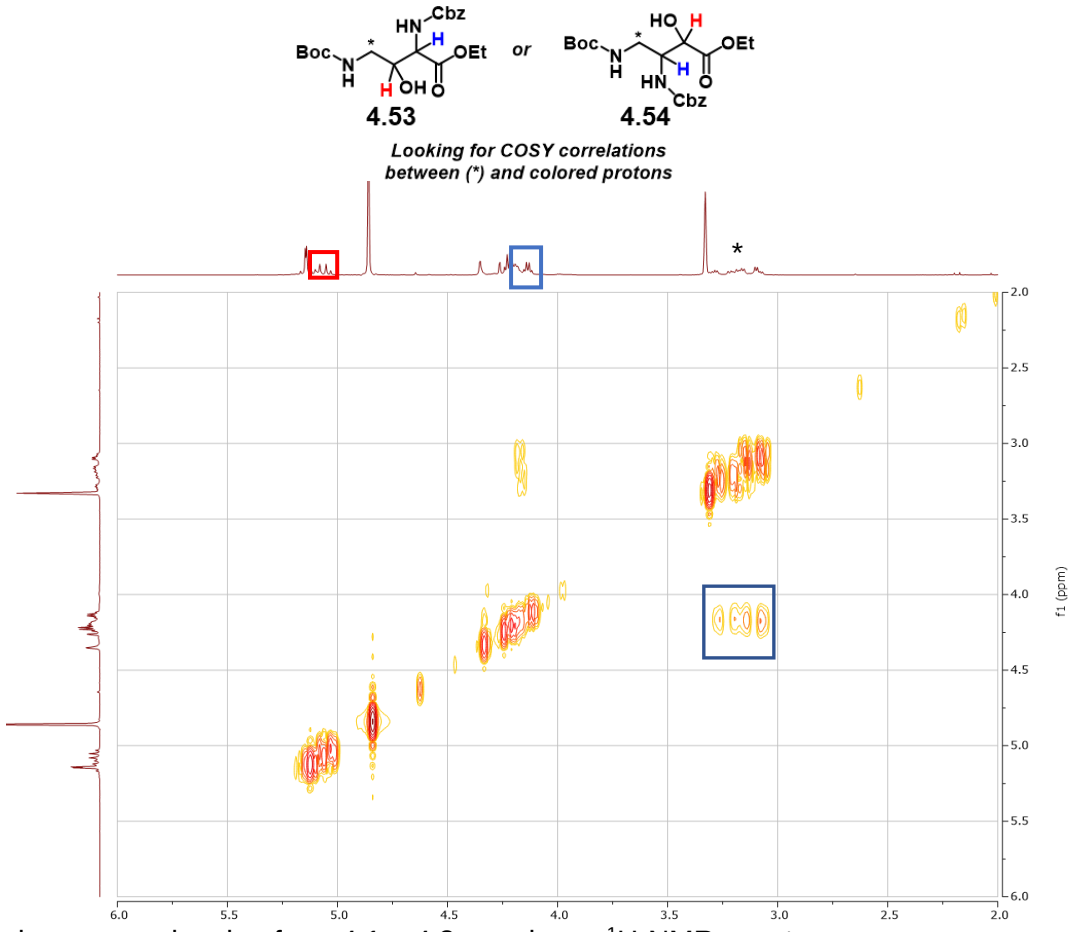

Figure 4.19: COSY for the aminohydroxylated alkyl ester. The protons of the γ-carbon show a correlation with the proton of the carbamate, indicating that the product most likely is the α-alcohol regioisomer.

After assigning all proton peaks, I can then use their location relative to the γ-carbon protons to assign regioisomer obtained (**Fig. 4.19**). In the COSY spectrum, I observe a correlation between the protons on the γ-carbon (3.0 – 3.2 ppm) and the proton geminal to the benzyl carbamate (4.1 – 4.3 ppm, **Fig. 4.18**). Though the correlation is convoluted by the overlap between the diastereotopic (β) proton and the ester methylene, a correlation with the ester is unlikely due to proximity and so this correlation is assigned to the (β) proton. This strongly suggests that I obtained the undesired α-alcohol regioisomer based on my previous peak assignments. My ^{1}H-NMR seems consistent with the spectrum obtained by Chen and coworkers, but my conclusion that I obtained the α-alcohol regioisomer conflicts with their reported results. Thus, Dr. Wanli Zhang performed the aminohydroxylation on the substrate utilized by Chen and coworkers with their specified conditions, and he also identified the α-alcohol regioisomer, leading us to conclude that Chen and coworkers may not have correctly identified the structure. However, this conclusion should be further evaluated through HMBC and, if possible, single crystal X-ray analysis.

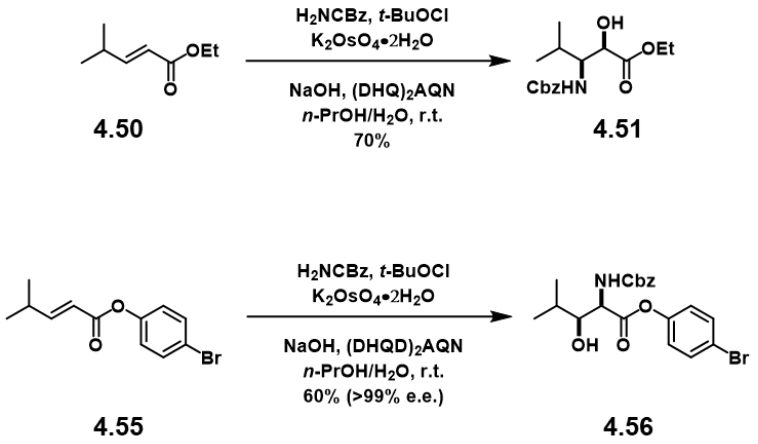

Figure 4.20: Panek and coworkers published that alkyl esters resulted in the α-alcohol, but they were able to reverse the regioselectivity via changing to an aryl ester.

4.3.5 Aryl ester & Panek precedent

Because I obtained the undesired α-alcohol regioisomer with Chen and coworkers' method, I pivoted to the procedure developed by Panek and coworkers published in the *Journal of Organic Chemistry* in 1999, in which they describe how to reverse the regioselectivity of the aminohydroxylation via changing the alkyl ester to an aryl ester (**Fig. 4.20**).[29] In their work, they describe that aryl esters, particularly *p*-bromophenyl esters, give 7:1 selectivity (20:1 after two recrystallizations) for the α-carbamate over the α-alcohol.[29] The authors rationalized the selectivity of the aryl esters over alkyl esters with a π-stacking interaction between the benzyl carbamate and the aryl ester, which forces the benzyl carbamate to add to the α-position.[29]

Due to the issues associated with Chen's work and the precedent from Panek, I synthesized the aryl ester from hydrolyzing ester **4.43** to the acid and then esterifying to **4.57**. I then performed the aminohydroxylation on the aryl ester substrate but obtained the undesired α-alcohol, which I also identified via similar correlations in the COSY (**Fig. 4.21**). Rationalizing this result, I postulated that there may be a hydrogen-bonding network between the mono-protected amine of the starting material and the nitrogen within the osmium(VIII) complex. Thus, to test this hypothesis, I decided to cap the amine with a methyl, because I needed an alkyl protecting group to avoid the aryl protecting group coordinating with the benzyl carbamate, producing the undesired regioisomer.[33]

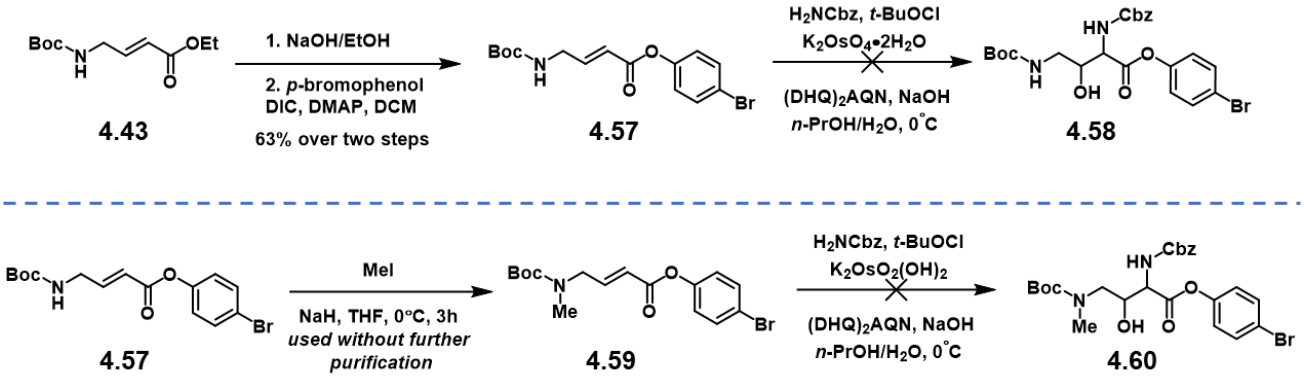

Figure 4.21: Access to both aryl esters (**4.57** and **4.59**) for aminohydroxylation, but both produced the α-alcohol.

4.3.6 Methyl-capped intermediate higher order spectroscopy

After obtaining the methyl-capped product by reaction with methyl iodide, I performed the aminohydroxylation (**Fig. 4.21**). As previously stated, I utilized COSY to determine the regioselectivity. In the methyl-capped intermediate, I observed a correlation between the proton geminal to the carbamate and the protons of the γ-carbon, indicating that I obtained the undesired α-alcohol again.

4.3.7 Outcomes

Thus, while the aminohydroxylation would allow for a short synthesis and access of both enantiomers via varying the ligand choice, it seems to not permit access of the desired α-carbamate regioisomer. To further validate these results, an HMBC spectrum and possibly a crystal structure should be obtained to definitively confirm the correct regioselectivity of the product. While the aminohydroxylation does not seem to produce the desired regioisomer, the literature surrounding my starting materials (without an aryl ring at the β-position) was lacking. Herein, I have demonstrated that the reaction is more nuanced than previously thought (rationalizing my results in combination with Panek and coworkers' publication). Interestingly, the reaction seemed to produce the α-alcohol despite ester modification to the starting material, which contained a mono- and then di- protected amine. For future advancement, it would be worthwhile to probe if this is specific to this backbone or if other amine-containing starting materials will face the same regioselectivity issues.

4.4 Vinylglycine route

4.4.1 Route to access vinylglycine

Due to the inherent uncertainty associated with the aminohydroxylation, I concurrently worked on another route to access the desired protected Dab residue. From *L*-vinylglycine, my route utilized an epoxidation to set the β-stereocenter, which could then be opened with ammonia.

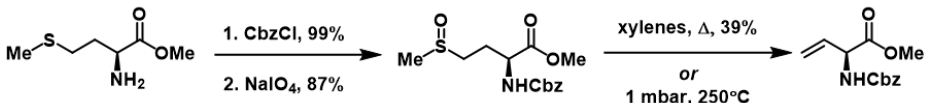

Figure 4.22: Route to access *L*-vinylglycine.

Next, I planned to form the hemiaminal and hydrolyze the ester to obtain the protected β-OH Dab building block. While the starting material, *L*-vinylglycine, is commercially available, it is also expensive; however, there is a well-precedented method to access it (**Fig. 4.22**).[34] Rapoport and coworkers utilize methionine methyl ester hydrochloride as the starting material, protect the amine with benzyl chloroformate, oxidize the thioether to sulfoxide, and eliminate the sulfoxide to form the vinylglycine.[34] The sulfoxide can be eliminated through two methods: by refluxing in xylenes overnight or by employing a kugelrohr at 250 ºC under 1 mbar vacuum for three hours.[33] Both conditions worked, but the kugelrohr elimination significantly increased the yield.

4.4.2 Route to (2S,3R) isomer

Once I had *L*-vinylglycine in hand, I epoxidized with *m*CPBA (**Fig. 4.23**).[35] Rapoport and coworkers detail that while the epoxidation gives both diastereomers, it is selective for the *syn* isomer in a 4:1 ratio over the *anti* isomer.[34] They rationalize this selectivity by postulating that the nitrogen of the carbamate exhibits hydrogen-bonding with the *m*CPBA, similar to acyclic allylic alcohols.

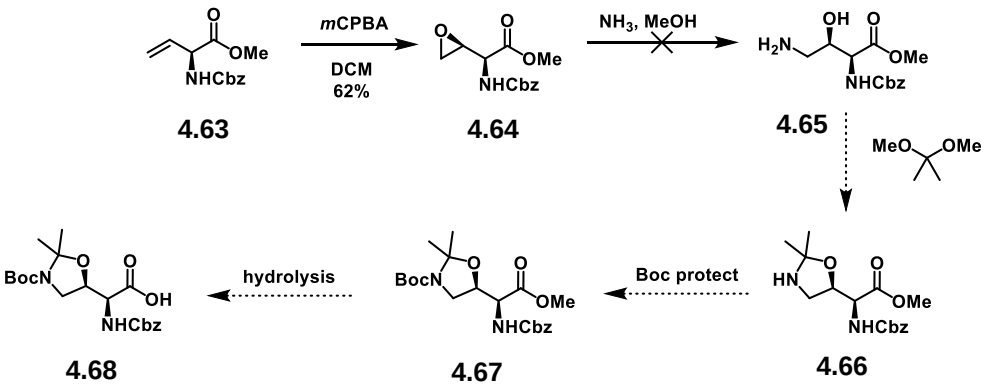

Figure 4.23: Route to access β-OH Dab isomer.

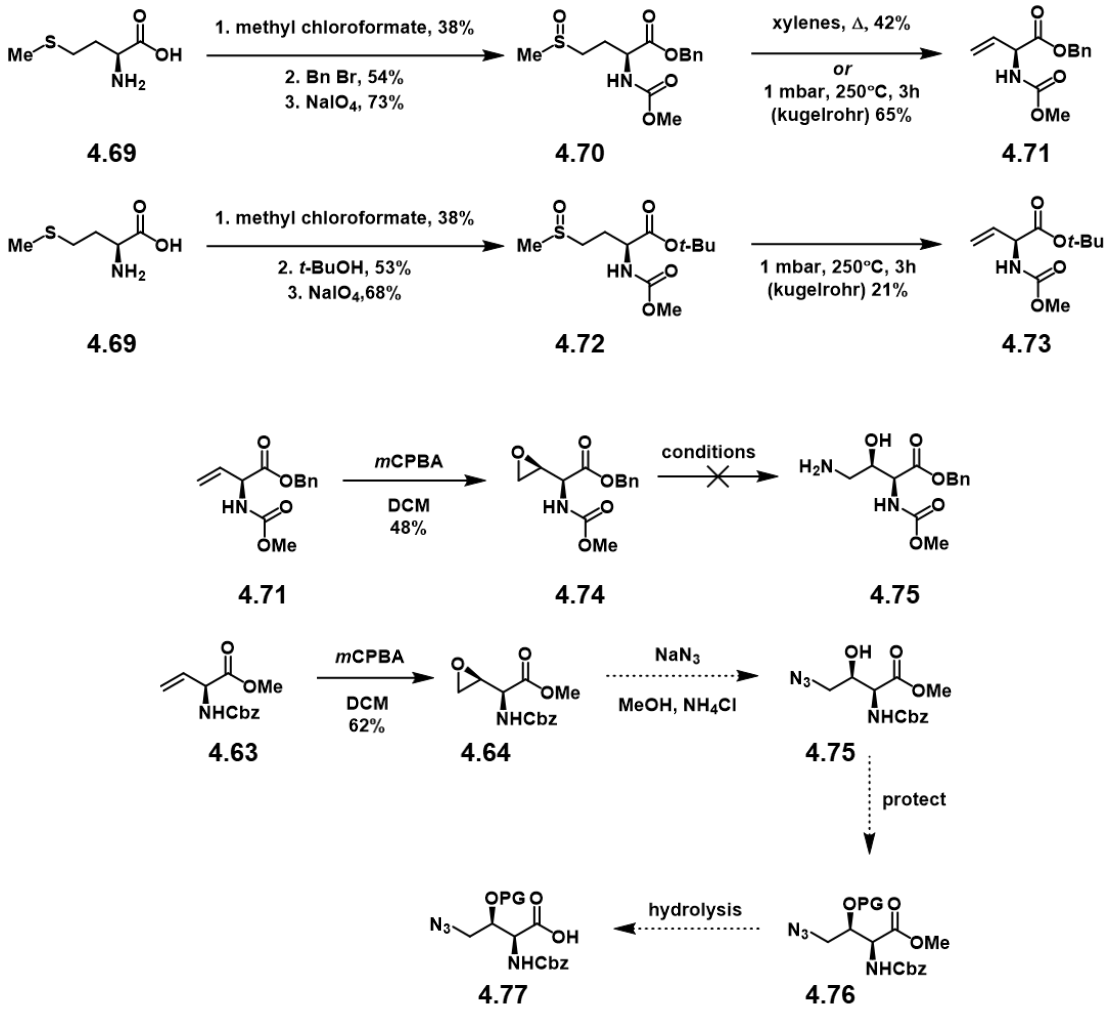

Figure 4.24: After the previous protecting groups proved incompetent in the ammonia-mediated opening of the epoxide, I consulted Greene's Protecting Groups in Organic Synthesis and exchanged protecting groups to a methyl carbamate for the α-amine and either a *t*-butyl ester or benzyl ester. Following the protecting group exchange and obtaining the epoxide of the benzyl ester, I could not produce the opened epoxide. However, there is precedent to open the epoxide with buffered sodium azide.

4.4.3 Ring-opening with ammonia

With the epoxide in hand, I next explored the ring-opening with ammonia. The first set of conditions tried lead to hydrolysis products, because benzyl carbamate and methyl esters are sensitive to ammonia.[36] I then turned to other protecting groups (using Greene's textbook as a reference) and found that methyl carbamates and benzyl (and *t*-butyl) esters exhibit low reactivity to ammonia (**Fig. 4.24**).[36] I made the appropriate epoxide with new protecting groups and tried to open the epoxide via ammonia (7N in methanol) with methanol as the solvent. Unfortunately, I

only observed elimination products. In protic solvents, a base-catalyzed elimination predominates after ammonia has opened the epoxide. I decided to utilize a different ammonia source as well as solvent and employed ammonia (0.5 M in dioxane) in THF at room temperature as my new conditions. From this, I only recovered starting material. Consequently, I thought to try to activate the epoxide with a Lewis acid like $FeCl_3$ at -30 ºC as epoxides are poor electrophiles and need a Lewis acid for activation but still only observed starting material. Because of these difficulties with ammonia, I accordingly attempted a different nucleophile, like benzylamine, and obtained new spots by TLC, but neither spot was the product by NMR analysis.

4.4.4 Outcomes & next steps

Following all these unsuccessful attempts, my next thought was to use sodium azide to open the epoxide. However, further literature review indicated that sodium azide would also present the same elimination issues that I had already witnessed earlier in my studies. Nonetheless, Rapoport and coworkers noted that they were able to circumvent these elimination products and ensure smooth opening of the epoxide with sodium azide if they also utilized ammonium chloride as an additive.[35] This can be rationalized as ammonium chloride is mildly acidic and thus arrests this base-catalyzed elimination. Thus, while I did not perform this reaction, because of the Rapoport precedent, this pathway to access the desired protected Dab residue is still viable albeit dangerous with the high nitrogen content and low carbon count. To further address the safety of this reaction, one should perform the reaction dilute as well as properly quench the reaction mixture with sodium nitrite.

4.5 Dihydroxylation route

4.5.1 Purpose

While the aminohydroxylation is no longer a viable pathway for producing the desired (*2S,3R*) isomer and its enantiomer, the dihydroxylation can still provide the diastereomers, (*2S,3S*) and (*2R,3R*). We are interested in the diastereomers, because they will both serve as controls in our NMR studies and also provide flexibility in the synthetic efforts when we attempt to

elucidate the stereochemistry of the natural product. Furthermore, they will also act as controls in our biological assays. After confirming the stereochemistry of the β-OH Dab residues, we can examine how stereochemistry affects activity via synthesizing several analogs incorporating various permutations of the enantiomer and diastereomers at not only β-OH Dab-2 and -3 as previously stated but also at β-OH Dab-1 to confirm activity of the natural product. Thus, we are interested in synthesizing the diastereomers, (*2S,3S*) and (*2R,3R*), via dihydroxylation.

Because of the commonality of the 1,2-*syn*-diol, there are several methods to dihydroxylate.[37] One of the most common is through osmium tetroxide, the hazards of which were already mentioned.[37] Another reagent commonly utilized is ruthenium tetroxide, which is significantly less expensive than osmium tetroxide.[37] However, ruthenium tetroxide oxidations contend with over-oxidation and progress to form α-hydroxyketones.[37] Because of this over-oxidation power, ruthenium tetroxide is also employed in oxidative cleavage reactions.[37] While the ketohydroxylation seems to be an issue in ruthenium(VIII)-catalyzed dihydroxylations, there have been attempts to circumvent the over-oxidation.[37] Plietker and coworkers demonstrated that the turnover-limiting step is the hydrolysis of the ruthenate ester to the diol, which they indicated could be accelerate through addition of a Bronsted or redox-active Lewis acid.[37] Interestingly, ruthenium-catalyzed oxidations can also be performed in tandem with ring-closing metathesis with added sodium periodate and Lewis acid for the dihydroxylation event (**Fig. 4.25**).[37] Furthermore, Che and coworkers demonstrated that they can prevent over-oxidation and cleavage pathways via the addition of bulky ligands to ruthenium tetroxide to generate a new ruthenium catalyst.[37] Che also found that, in the absence of the two system solvent typically used in dihydroxylations and in just acetonitrile, their ruthenium catalyst actually favored oxidative

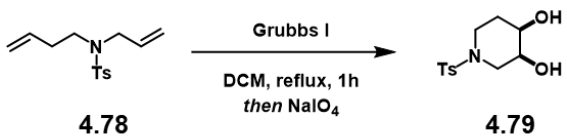

Figure 4.25: Tandem ring closing metathesis and dihydroxylation.

cleavage. However, in the presence of a water and acetonitrile solvent system, their catalyst favored dihydroxylation.[37] The previously mentioned methods are all racemic, but there are ruthenium-catalyzed asymmetric dihydroxylations utilizing chiral auxiliaries to induce enantioselectivity.[37] There are also several dihydroxylation methods that employ permanganate as the oxidant alone or in combination with a phase transfer catalyst (to transfer to organic media), but these oxidations typically also form MnO_2, which can be difficult to remove from the reaction mixture.[37] The above examples are not the only methods present in the literature as there are several that utilize other metals (cerium, palladium, technetium, molybdenum), are metal-free (Prevost-Woodward-type, selenium, oxone), or employ enzymes.[37] For our purposes, I elected to apply the Upjohn and Sharpless conditions as they employ potassium osmate(VI) dihydrate as the catalyst, which is commercially available, relatively inexpensive, well-precedented, and does not result in over-oxidation. Furthermore, we already owned the reagents to perform both the Upjohn and Sharpless oxidations, which was a necessary factor to consider due to supply chain issues stemming from world events and the Covid-19 pandemic.

4.5.2 Upjohn (racemic)

The Upjohn is a racemic dihydroxylation and would produce both diastereomers. I desired to perform the Upjohn, because my first attempts to dihydroxylate under Sharpless conditions were unsuccessful. My aminohydroxylation studies demonstrated that I was able to obtain dihydroxylated material, but only under the aminohydroxylation conditions. Thus, I thought that procedures incorporating AD mix were more nuanced, and while I searched the literature, I performed the Upjohn to obtain dihydroxylated material in order to further scout my route and not

4.43 *race*-4.80

Figure 4.26: Upjohn dihydroxylation conditions.

waste precious material (**Fig. 4.26**).[38] The Upjohn conditions utilize *N*-methylmorpholine *N*-oxide as an oxidant for the osmium to oxidize it from Os(VI) back to the active catalyst of Os(VIII).[39] The reaction differs from most Sharpless conditions in that the solvent ratio is not a 1:1 or 2:1 mixture but 9:1 acetone to water and performed overnight at room temperature under an inert atmosphere.

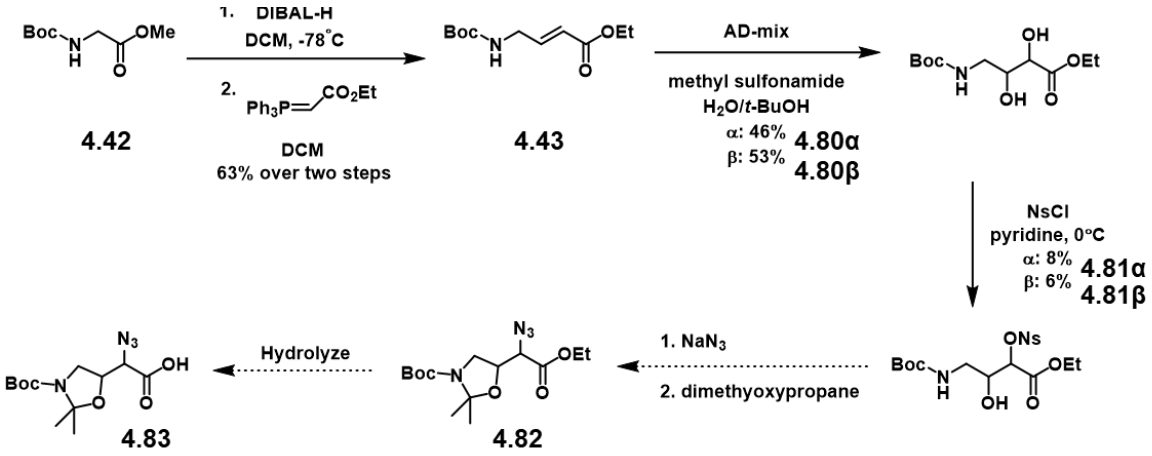

Figure 4.27: Route to access β-OH Dab diastereomers, (*2S,3S*) and (*2R,3R*).

4.5.3 Sharpless (asymmetric)

During my literature review of Sharpless dihydroxylation conditions, I found a few literature procedures, but the procedure that produced dihydroxylated material called for a specific reaction sequence.[40] Claudel and coworkers indicate that after adding the AD mix-α and methane sulfonamide to the 1:1 solution of *t*-BuOH to water that one should cool to 0 ºC and stir until an orange precipitate forms before adding the starting material (**Fig. 4.27**). Next, the reaction should be stirred at 0 ºC for one hour before warming to room temperature and stirring overnight under inert atmosphere.[40] If the orange precipitate does not form, one should not add starting material as the reaction most likely will not proceed.[40] I originally did not observe the orange precipitate in my studies, indicating that the bottle of AD mix-α used was most likely off-spec.[40] Thus, after obtaining a new bottle of AD mix-α, I was able to synthesize dehydroxylated product. I also was able to perform the reaction with AD mix-β successfully.[41] Unfortunately, due to time limitations, I

was unable to confirm absolute stereochemistry of the products. However, I had planned to assign stereochemistry by utilizing Birman's *S*-HBTM and *R*-HBTM catalysts to aid in the assignment.[42,43]

4.5.4 Nosylation

After acquiring dihydroxylated product, I next attempted to form the hemiaminal, knowing that I would most likely obtain a mixture of the hemiaminal and the acetal (**Fig. 4.27**). Unfortunately, I only procured the acetal. Thus, I next endeavored to perform a Mitsunobu to access the α-azide, which would prevent acetal formation and allow access to the hemiaminal. This also did not work, and I next turned to activating the α-alcohol with a selective mesylation.[41] Fortunately, I was able to achieve mono-mesylation, but upon further reflection, the literature indicated preferred activation of the alcohol for a Mitsunobu by nosylation over mesylation.[41] Thus, I nosylated the α-alcohol for both dihydroxylated products (from AD-mix α and AD-mix β).[41] While the yields for both nosylations were low, this may be because nosyl chloride was not entirely soluble in the small amount of dry pyridine utilized (in order to make a 0.3 M reaction mixture) and that the reaction was performed in the fridge overnight as per the literature procedure. [41]

4.5.5 Future Directions

While the yield of the nosylation reactions leave much to be desired, they can be optimized, or instead of utilizing nosyl as an activating group, there is significantly more literature surrounding sulfoxides as diol activating groups. Furthermore, Stepan and coworkers already demonstrated the selectivity and success of employing thionyl chloride to generate the activated α-alcohol for azide addition.[20] Thus, it may be more fruitful to pursue this avenue instead of nosylation.[41] Furthermore, despite being unable to finish the syntheses of the protected (*2R,3R*) and (*2S,3S*) isomers, I had planned to utilize the azide as protecting group, which decreases step count. Then, the hemiaminal could be formed, and the ester hydrolyzed, which would provide a protected Dab diastereomer, ready for the solid phase peptide synthesizer.

4.6 Future Directions

4.6.1 Dr. Zhang's synthesis

As previously mentioned, Dr. Wanli Zhang joined my project when I started my β-OH Dab isomer syntheses. He developed and worked on different syntheses so as to improve the likelihood for a successful synthesis. Zhang endeavored to replicated Racine's method to produce the (*2S,3S*) and (*2S,3R*) isomers.[21] He also pursued a synthesis that utilized phthalimide as a protecting group for the γ-amine instead but employed the Crimmins aldol in order to create the main backbone (α-amine and β-alcohol) as previously demonstrated by Boger (**Fig. 4.28**).[44] This method is asymmetric and allows for both enantiomers.[44] While elegant, this synthesis suffers from its explosion hazard as the carbon to nitrogen count is below the threshold of 3, making it particularly dangerous.

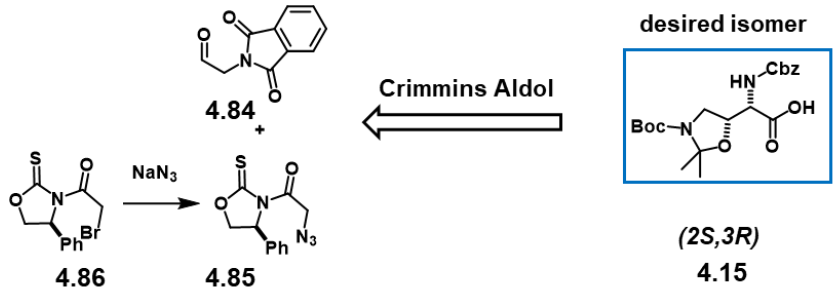

Figure 4.28: Dr. Zhang's Crimmins aldol route.

4.6.2 Peptide synthesis and LpxC binding assay

Following synthesis of the β-OH Dab isomers, Dr. Wanli Zhang and Martina Golden, currently a second-year graduate student in our lab, will synthesize the linear peptide either with the departmental solid phase peptide synthesizer or via a solid phase peptide synthesis vessel (in the event the departmental synthesizer is unavailable). Furthermore, several analogs will be made in order to verify necessity of the stereochemistry of the Dab residues as well as the Michael acceptor hypothesis (that β-OH Dab-1 is necessary for substrate recognition but that the Michael acceptor of the Dhb adjacent to the β-OH Dab-1 residue is the actual warhead of the natural

product). In order to verify the biological hypothesis that the ogipeptins bind LpxC (and thus inhibit Lipid A biosynthesis), we plan to employ a well-precedent LpxC competition binding assay that measures our natural product binding versus positive control ligand binding through fluorescence polarimetry.[14] This is also the assay utilized by industry to test for LpxC inhibitors.[2,18,19]

Works Cited

1. Powers, M.J.; Trent, M.S.; *Prod. Natl. Acad. Sci.*, **2018**, *115*, E8518.
2. Tomaras, A.P.; McPherson, C.J.; Kuhn, M.; Carifa, A.; Mullins, L.; George, D.; Desbonnet, C.; Eidem, T.M.; Montgomery, J.I.; Brown, M.F.; Reilly U.; Miller, A.A.; O'Donnell, J.P.; *MBio*, **2014**, *5*, 1.
3. May, K.L.; Grabowicz, M.; *Prod. Natl. Acad. Sci.* **2018**, *115*, 8852.
4. Hobot, J.A.; "Chapter 2: Bacterial Ultrastruture," Molecular Medical Microbiology Vol 1, 2nd Ed, Elsevier: London, **2015**, 7.
5. Raetz, C.R.H.; Reynolds, C.M.; Trent, M.S.; Bishop, R.E.; *Annu. Rev. Biochem.*, **2007**, *76*, 295.
6. Zhang, G.; Meredith, T.C.; Kahne, D.; *Curr. Opinion Microbiol.*, **2013**, *16*, 779.
7. Martinson, J.N.V.; Walk, S.T.; *EcoSal Plus*, **2020**, *9*(1).
8. Hirota-Takahata, Y.; Kozuma, S.; Kuraya, N.; Fukuda, D.; Nakajima, M.; Takatsu, T.; Ando, O.; *J. Antibiot*, **2017**, *70*, 84.
9. Kozuma, S.; Hirota-Takahata, Y.; Fukuda, D.; Kuraya, N.; Nakajima, M.; Ando, O.; *J. Antibiot*., **2017**, *70*, 79.
10. Zavascki, A.P.; Goldani, L.Z.; Li, J.; Nation, R.L.; *J. Antimicrob. Chemothera.*, **2007**, *60*, 1206.
11. Barb, A.W.; Zhou, P.; *Curr. Pharm. Biotechnol.*, **2008**, *9*, 9.
12. Cote, J.M.; Taylor, E.A.; *Int. J. Mol. Sci.*, **2017**, *18*, 1.
13. Clayton, G.M.; Klein, D.J.; Rickert, K.W.; Patel, S.B.; Kornienko, M.; Zugay-Murphy, J.; Reid, J.C.; Tummala, S.; Sharma, S.; Singh, S.B.; Miesel, L.; Lumb, K.J.; Soisson, S.M.; *J. Biol. Chem.*, **2013**, *288*, 34073.
14. Hernick, M., "Ch. 11: Fluorescence Based Methods to Assay Inhibitors of Lipopolysaccharide Synthesis," Methods in Molecular Biology: Microbial Toxins: Methods and Protocols, Humana Press: New York, **2011**, 123.

15. Jackman, J.E.; Raetz, C.R.H.; Fierke, C.A.; *Biochem*., **1999**, *38*, 1902.

16. Hernick, M.; Fierke, C.A.; *Biochem.*, **2006**, *45*, 15240.

17. Krause, K.M.; Haglund, C.M.; Hebner, C.; Serio, A.W.; Lee, G.; Nieto, V.; Cohen, F.; Kane, T.R.; Machajewski, T.D.; Hildebrandt, D.; Pillar, C.; Thwaites, M.; Hall. D.; Miesel, L.; Hackel, M.; Burek, A.; Andrews, L.D.; Armstrong, E.; Swem, L.; Jubb, A.; Cirz, R.T.; *Antimicrob. Agents Chemothera.,* **2019**, *63*, 1.

18. Kalinin, D.V.; Holl, R.; *Exp. Opinion Therap. Patents*, **2017**, *27*, 1227.

19. Yamada, Y.; Takashima, H.; Walmsley, D.L.; Ushiyama, F.; atsuda, Y.; Kanazawa, H.; Yamaguchi-Saski, T.; Tanaka-Yamamoto, N.; Yamagishi, J.; Kurimoto-Tsuruta, K.; Ogata, Y.; Ohtake, N.; Angove, H.; Baker, L.; Harris, R.; Macias, A.; Robertson, A.; Surgenor, A.; Watanabe H.; Nakano K.; Mima, M.; Iwamoto, K.; Okada, A.; Takata, I.; Hitaka, K.; Tanaka, A.; Fujita, K.; Sugiyama, H.; Hubbard, R.E.; *J. Med. Chem.*, **2020**, *63*, 14805.

20. Stepan A.F.; Nguyen, T.-T.; Anderson, D.; Liang, H.; Zhanshan, Q.; Magee, T.V.; *Synlett*, **2011**, *17*, 2499.

21. Sarciaux, M.; Pantel, L.; Midrier, C.; Serri, M.; Gerber, C.; de Figueiredo, R.M..; Campagne, J.-M.; Villain-Guillot, P.; Gualtieri, M.; Racine, E.; *J. Med. Chem.*, **2018**, *61*, 7814.

22. Cabre, A.; Khaziourane, H.; Garcon, M.; Verdaguer, X.; Riera, A.; *Org. Lett.*, **2018**, *20*, 3953.

23. Trost, B.M.; Taft, B.R.; Masters, J.T.; Lumb, J.-P.; *J. Am. Chem. Soc.*, **2011**, *133*, 8502.

24. Powell, D.A.; Batey, R.A.; *Org. Lett.*, **2002**, *4*, 2913.

25. Ji, J.; Lin, L.; Tang, Q.; Kang, T.; Liu, X.; Feng, X.; *ACS Catal.*, **2017**, *7*, 3763.

26. Carrea, G.; Colonna, S.; Kelly, D.R.; Lazcano, A.; Ottolina, G.; Roberts, S.M.; *TRENDS in Biotech*, **2005**, *23*, 507.

27. Porter, M.J.; Skidmore, J.; “Chapter 3: Asymmetric Epoxidation of Electron-Deficient Alkenes” Organic Reactions, John Wiley & Sons, **2009**, *74*, 425.

28. Bodkin, J.A.; McLeod, M.D.; *J. Chem. Soc. Perkin Trans. 1*, **2002**, 2733.

29. Morgan, A.J.; Masse, C.E.; Panek, J.S.; *Org. Lett.*, **1999**,*1*, 1949.

30. Coleman, R.S.; Felpin, F.-X.; Chen, W.; *J. Org. Chem.*, **2004**, *69*, 7309.

31. "Asymmetric Aminohydroxylation (AA)" Sharpless Group. < https://www.scripps.edu/sharpless/backup/research/aa.html>. Accessed 10 June 2021.

32. Claridge, T.D.W.; High-Resolution NMR Techniques in Organic Chemistry, 2nd Ed, Elsevier: Amsterdam, **2016**.

33. Ohta, Y.; Kamijyo, Y.; Fujii, S.; Yokoyama, A.; Yokozawa, T.; *Macromolec.*, **2011**, *44*, 5112.

34. Carrasco, M.; Jones, R.J.; Kamel, S.; Rapoport, H.; Truong, T.; *Org. Syn.*, **1998**, *9*, 29.

35. Shaw, K.J.; Luly, J.R.; Rapoport, H.; *J. Org. Chem.*, **1985**, *50*, 4515.

36. Wutz, P.G.M.; Greene, T.W.; "Chapter 10: Reactivities, Reagents, and Reactivity Charts," Greene's Protective Groups in Organic Synthesis, 4th Ed, John Wiley & Sons: Hoboken, **2006**, 986.

37. Bataille, C.J.R.; Donohoe, T.J.; *Chem. Soc. Rev.*, **2011**, *40*, 114.

38. Wang, J.; Hsung, R.P.; Ghosh, S.K.; *Org. Lett.*, **2004**, *6*, 1939.

39. Ager, D. "Synthetic Methods II – Chiral Auxiliaries," Comprehensive Chirality, **2012**, *3*, 223.

40. Claudel, S.; Olszewski, T.K.; Mutzenardt, P.; Aroulanda, C.; Coutrot, P.; Grison, C.; *Tetrahedron*, **2006**, *62*, 1787.

41. Fleming, P.R.; Sharpless, K.B.; *J. Org. Chem.*, **1991**, *56*, 2869.

42. Wagner, A.J.; David, J.G.; Rychnovsky, S.D.; *Org. Lett.*, **2011**, *13*, 4470.

43. Ott, A.A.; Goshey, C.S.; Topczewski, J.J.; *J. Am. Chem. Soc.*, **2017**, *139*, 7737.

44. Moore, MJ.; Qu, S.; Tan, C.; Cai, Y.; Mogi, Y.; Keith, D.J.; Boger, D.L. *J. Am. Chem. Soc.*, **2020**, *142*, 16039.

Chapter 5: Supplementary Information

General Methods:

NMR spectra were recorded on Bruker Ascend (600/150 MHz), INOVA (500/125 MHz), INOVA (400/100 MHz), INOVA (600/150 MHz), and VNMR (400/100 MHz) and at ambient temperature. Chemical shifts are quoted in ppm relative to solvent used: (^{1}H: δ = 2.05 and ^{13}C: δ = 30.12 and 205.87 for residual d_6-acetone and ^{1}H: δ = 2.50 for residual d_6-DMSO). The following abbreviations are used to describe splitting: s (singlet), d (doublet), t (triplet), q (quartet), m (multiplet), dd (doublet of doublets), dt (doublet of triplets), *etc*.

Non-aqueous reactions occur in frame-dried glassware, under an argon atmosphere, and with HPLC-grade solvents that were purified on a Pure Process Technology purification system. Amine bases were freshly distilled with CaH_2 before use. Brine refers to a saturated aqueous solution of sodium chloride. Column chromatography refers to utilization of a Biotage Isolera One Automated system for purification. Reactions were monitored via thin-layer chromatography (TLC) with EMD Millipore® TLC silica gel glass plates stained with vanillin, *p*-anisaldehyde, or $KMnO_4$. The products were purified via column chromatography unless denoted otherwise.

Chapter 2: nTZDpa

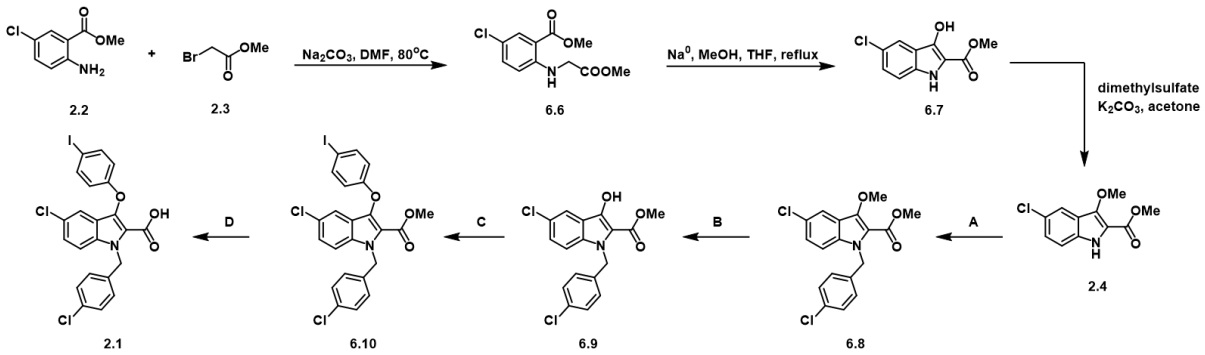

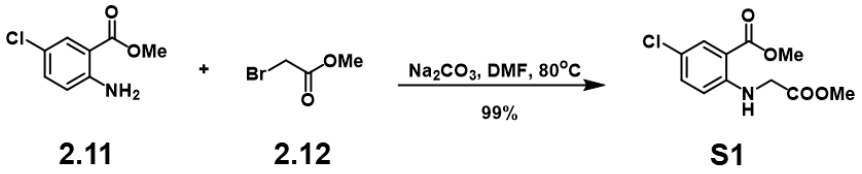

Methyl 5-chloro-2-((2-methoxy-2-oxoethyl)amino)benzoate (S1). Na_2CO_3 (1.5 equiv) was dried under vacuum at 105°C for 30 minutes and then allowed to cool to room temperature. Methyl-2-aminobenzoate starting material (**2.11**) (1 equiv) was added in DMF to the flask, and then methyl bromoacetate (1.2 equiv) was added. The reaction was allowed to stir overnight at 80°C. Then, the reaction was cooled to room temperature and filtered. The filtrate was concentrated, diluted with EtOAc, washed with H_2O and brine, dried with Na_2SO_4, filtered, and concentrated to yield the title compound in 99% yield. **^{1}H-NMR:** (300 MHz, Chloroform-*d*) δ 7.86 (ddd, *J* = 23.3, 2.6, 0.8 Hz, 1H), 7.39 – 7.04 (m, 1H), 6.72 – 6.32 (m, 1H), 4.00 (d, *J* = 5.2 Hz, 2H), 3.88 (s, 3H), 3.79 (s, 3H).

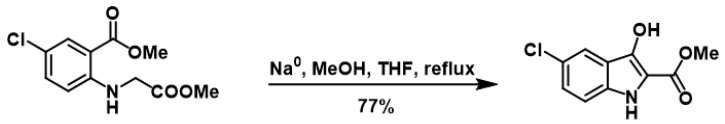

S1 **S2**

Methyl 5-chloro-3-hydroxy-1H-indole-2-carboxylate (S2). Sodium metal (2 equiv) was added slowly to MeOH that was cooled to 0°C. To a solution of (**S1**) starting material in THF, *in situ* NaOMe was added, and the reaction was refluxed to 70°C. The reaction was allowed to run for 3 hours, and then H_2O was added. The reaction was then acidified with 1N HCl, concentrated, extracted with EtOAc (x3), washed with brine, dried with Na_2SO_4, filtered, concentrated, and purified by column chromatography to yield the indole in 77% yield.[8] **^{1}H-NMR:** (300 MHz, Acetone-d_6) δ 10.26 (s, 1H), 8.29 (s, 1H), 7.73 – 7.58 (m, 1H), 7.50 – 7.19 (m, 1H), 3.91 (s, 3H).

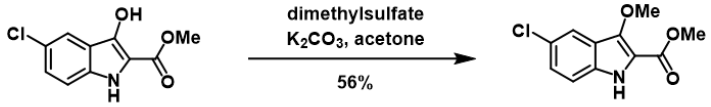

S2 **2.13**

Methyl 5-chloro-3-methoxy-1H-indole-2-carboxylate (2.13). To a solution of indole (**S2**) (1 equiv) starting material (**S2**) in acetone, K_2CO_3 (1.1 equiv) and dimethylsulfate (1.2 equiv) were added. The reaction was stirred overnight, and then H_2O was added to quench the reaction. Then, the reaction mixture was separated with EtOAc (x3), dried with Na_2SO_4, filtered, concentrated, and purified by column chromatography to yield the methyl ether product in 56% yield.[8] **^{1}H-NMR:** (300 MHz, Chloroform-*d*) δ 8.34 (s, 1H), 7.95 – 7.65 (m, 1H), 7.33 (s, 1H), 7.19 (s, 1H), 4.11 (d, J = 0.8 Hz, 3H), 3.97 (d, J = 0.7 Hz, 3H).

General Procedure for A: Alkylation: To a suspension of K_2CO_3 (2 equiv) in DMF, methyl ether starting material (1 equiv) was added. Then, 4-chlorobenzyl chloride (2 equiv) and TBAB (0.1 equiv) were added, and DMF was added until all materials dissolved. The reaction was heated overnight at 80°C. Then, the reaction was cooled, and then H_2O was added. The reaction was then extracted with EtOAc (x3) and washed with brine (x3). The organic layer was dried with Na_2SO_4, filtered, concentrated, and purified by column chromatography, which yielded the alkylated indole.

General Procedure for B: Deprotection: To a solution of alkylated methyl ether starting material (1 equiv) in CH_2Cl_2 at -30°C, BBr_3 (1.01 equiv) was added. The reaction was allowed to stir at -30°C for 2 hours and then reverse quenched with $NaHCO_3$. The reaction mixture was then extracted with CH_2Cl_2 (x3), washed with brine (x3), dried with Na_2SO_4, filtered, concentrated, and purified by column chromatography to yield the alcohol.

General Procedure for C: Chan-Lam coupling: 4Å molecular sieves were added and activated. Phenylboronic acid and copper (II) acetate were added to the flask, and then alcohol starting material was added in CH_2Cl_2. Then, triethylamine was added, and the reaction was vented and allowed to stir overnight. The crude reaction mixture was then filtered over celite with EtOAc, concentrated, and purified by column chromatography to yield the title compound.

General Procedure for D: Saponification: To a solution of ester starting material in equal parts THF and MeOH, NaOH was added. The reaction was vented and stirred overnight. Then the reaction was neutralized with HCl, extracted with EtOAc, dried with Na_2SO_4, filtered, concentrated, and purified by column chromatography to yield the acid.

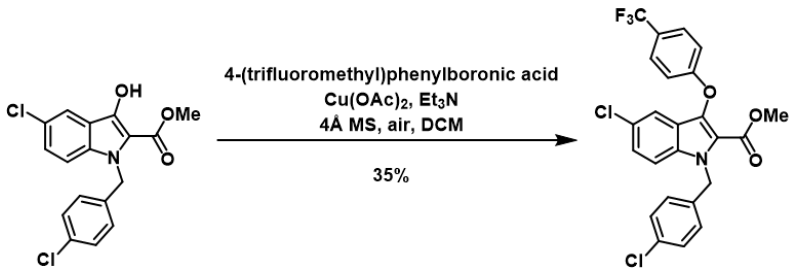

2.35 **S4**

Methyl 5-chloro-1-(4-chlorobenzyl)-3-(4-(trifluoromethyl)phenoxy)-1H-indole-2-carboxylate (S4). Using general procedure C, hydroxyindole (**2.35**) (100 mg, 0.286 mmol) yielded the title compound as a white solid (50 mg, 35% yield). **1H NMR** (400 MHz, Acetone) δ 7.79 – 7.60 (m, 3H), 7.50 (dd, J = 2.1, 0.6 Hz, 1H), 7.44 – 7.27 (m, 2H), 7.24 – 7.10 (m, 3H), 5.94 (s, 2H), 3.68 (s, 3H); **13C NMR** (150 MHz, Acetone) δ 160.76, 159.18, 138.50, 137.83, 137.15, 135.03, 132.55, 128.62, 128.15, 126.69, 126.43, 120.54, 118.99, 118.37, 118.06, 113.21, 84.21, 51.27, 47.19; **HRMS** ESI (m/z): [M+H] + calcd for C24H17O3NCl2F3 494.0532, found 494.0536.

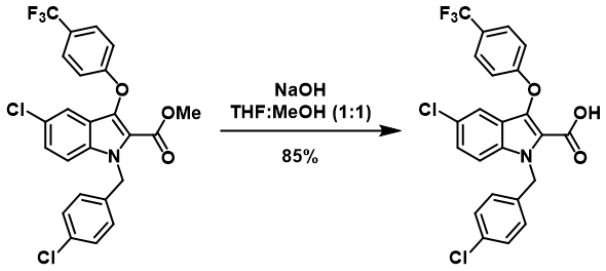

S4 **2.31**

5-chloro-1-(4-chlorobenzyl)-3-(4-(trifluoromethyl)phenoxy)-1H-indole-2-carboxylic acid (2.31). Using general procedure D, methyl ester **S4** (25 mg, 0.051 mmol) yielded the title compound as a white solid (21 mg, 85% yield). **1H NMR** (600 MHz, Acetone) δ 7.68 (dd, J = 8.8, 6.2 Hz, 3H), 7.48 (d, J = 2.1 Hz, 1H), 7.42 – 7.27 (m, 3H), 7.17 (dd, J = 8.5, 4.4 Hz, 4H), 5.96 (s, 2H); **13C NMR** (150 MHz, Acetone) δ 161.79, 160.91, 137.24, 135.04, 132.53, 128.61, 128.19,

127.08 (q, J = 3.8 Hz), 125.59, 124.56 (q, J = 270.6 Hz), 123.67 (q, J = 32.5 Hz), 120.51, 119.55, 118.22, 115.83, 113.24, 47.10; **HRMS** ESI (m/z): [M+Na]+ calcd for C23H14O3NCl2F3Na 502.0201, found 502.0198.

2.35 **S5**

Methyl 3-(4-bromophenoxy)-5-chloro-1-(4-chlorobenzyl)-1H-indole-2-carboxylate (S5). Using general procedure C, hydroxyindole **2.35** (100 mg, 0.286 mmol) yielded the title compound as a white solid (29 mg, 20% yield). **1H NMR** (400 MHz, Acetone) δ 7.68 (dd, J = 9.0, 0.7 Hz, 1H), 7.51 – 7.46 (m, 2H), 7.44 (dd, J = 2.1, 0.6 Hz, 1H), 7.38 (d, J = 2.1 Hz, 1H), 7.35 – 7.32 (m, 2H), 7.18 – 7.12 (m, 2H), 6.98 – 6.92 (m, 2H), 5.92 (s, 2H), 3.70 (s, 3H); **13C NMR** (150 MHz, Acetone) δ 160.77, 158.40, 137.93, 137.15, 135.03, 132.55, 132.45, 128.62, 128.15, 126.70, 126.43, 120.53, 118.96, 118.39, 117.62, 114.07, 113.21, 51.30, 47.19; HRMS ESI (m/z): [M+H]+ calcd for C23H17BrCl2NO3 503.9769, found 503.9764.

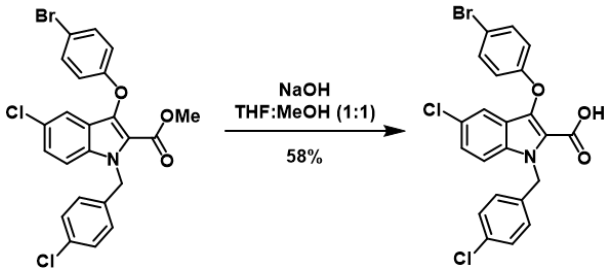

S5 **2.29**

3-(4-bromophenoxy)-5-chloro-1-(4-chlorobenzyl)-1H-indole-2-carboxylic acid (2.29). Using general procedure D, methyl ester **S5** (25 mg, 0.050 mmol) yielded the title compound as a white

solid (14 mg, 58% yield). **1H NMR** (400 MHz, Acetone) δ 7.67 (d, J = 9.0 Hz, 1H), 7.51 – 7.41 (m, 3H), 7.38 – 7.31 (m, 3H), 7.20 – 7.13 (m, 2H), 6.99 – 6.94 (m, 2H), 5.95 (s, 2H); **13C NMR** (150 MHz, Acetone) δ 161.08, 158.38, 137.68, 137.31, 135.00, 132.49, 132.38, 128.58, 128.20, 126.46, 126.29, 120.54, 119.63, 118.33, 117.59, 113.90, 113.17, 47.04; **HRMS** ESI (m/z): [M+H]+ calcd for C22H15O3NBrCl2 489.9607 and 491.9607, found 489.9611 and 491.9582.

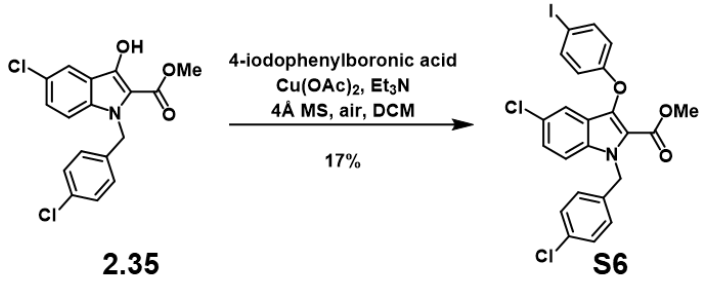

2.35 **S6**

Methyl 5-chloro-1-(4-chlorobenzyl)-3-(4-iodophenoxy)-1H-indole-2-carboxylate (S6). Using general procedure C, hydroxyindole **2.35** (100 mg, 0.286 mmol) yielded the title compound as a white solid (27 mg, 17% yield). **1H NMR** (400 MHz, Acetone) δ 7.70 – 7.61 (m, 3H), 7.44 (dd, J = 2.1, 0.6 Hz, 1H), 7.36 (dd, J = 9.0, 2.1 Hz, 1H), 7.35 – 7.30 (m, 2H), 7.17 – 7.12 (m, 2H), 6.86 – 6.81 (m, 2H), 5.91 (s, 2H), 3.70 (s, 3H); **13C NMR** (100 MHz, Acetone) δ 161.63, 160.04, 139.37, 138.69, 138.02, 135.90, 133.42, 129.49, 129.02, 127.57, 127.30, 121.40, 119.84, 119.26, 118.93, 114.08, 85.11, 52.18, 48.06; **HRMS** ESI (m/z): [M+H]+ calcd for C23H17O3NCl2I 551.9625, found 551.9628.

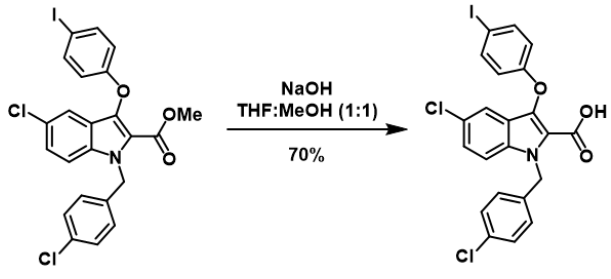

S6 **2.30**

5-chloro-1-(4-chlorobenzyl)-3-(4-iodophenoxy)-1H-indole-2-carboxylic acid (2.30). Using general procedure D, methyl ester **S6** (27 mg, 0.049 mmol) yielded the title compound as a white solid (18 mg, 70% yield). **1H NMR** (600 MHz, Acetone) δ 7.73 – 7.60 (m, 3H), 7.44 (d, J = 2.1 Hz, 1H), 7.39 – 7.31 (m, 3H), 7.20 – 7.13 (m, 2H), 6.91 – 6.82 (m, 2H), 5.96 (s, 2H); **13C NMR** (150 MHz, Acetone) δ 161.01, 159.16, 138.45, 137.65, 137.29, 135.04, 132.49, 128.59, 128.17, 126.52, 126.31, 120.52, 119.47, 118.35, 118.03, 113.18, 84.02, 47.04; **HRMS** ESI (m/z): [M+H]+ calcd for C22H15O3NCl2I 537.9474, found 537.9471.

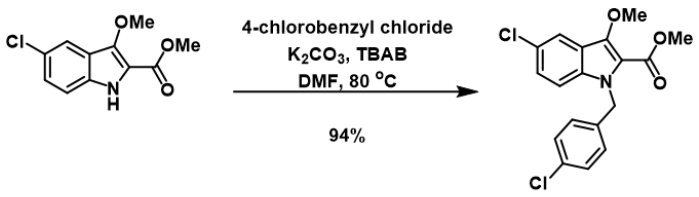

2.13 **S7**

Methyl 5-chloro-1-(4-chlorobenzyl)-3-methoxy-1H-indole-2-carboxylate (S7). Using general procedure A, methyl 5-chloro-3-methoxy-1H-indole-2-carboxylate (**2.13**) (100 mg, 0.417 mmol) yielded the title compound as a yellow solid (143 mg, 94%).[8] **^{1}H-NMR:** ^{1}H NMR (399 MHz, Acetone-d_6) δ 7.76 (dd, *J* = 2.1, 0.6 Hz, 1H), 7.52 (dd, *J* = 9.0, 0.6 Hz, 2H), 7.44 – 7.39 (m, 1H), 7.31 – 7.19 (m, 4H), 7.16 – 6.98 (m, 3H), 5.78 (s, 3H), 4.02 (d, *J* = 0.5 Hz, 4H), 3.86 (d, *J* = 0.5 Hz, 5H).

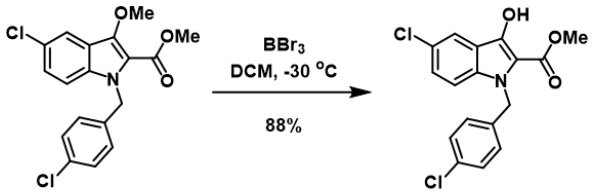

S7 **2.35**

Methyl 5-chloro-1-(4-chlorobenzyl)-3-hydroxy-1H-indole-2-carboxylate (2.35). Using general procedure B, methyl 5-chloro-1-(4-chlorobenzyl)-3-methoxy-1H-indole-2-carboxylate (**S7**) (143 mg, 0.392 mmol) yielded the title compound as a green solid (121 mg, 88%).[8] **^{1}H-NMR:** ^{1}H NMR (399 MHz, Acetone-d_6) δ 8.66 (s, 1H), 7.67 (d, *J* = 2.1 Hz, 1H), 7.56 – 7.37 (m, 1H), 7.34 – 7.21 (m, 2H), 7.05 (d, *J* = 8.5 Hz, 2H), 5.67 (s, 2H), 3.89 (s, 3H).

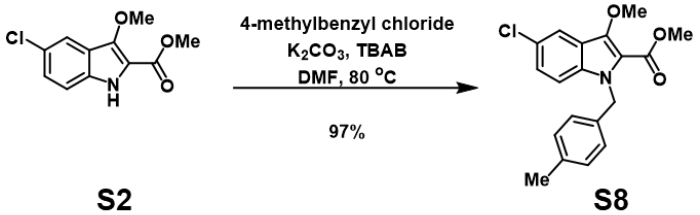

S2 **S8**

Methyl 5-chloro-3-methoxy-1-(4-methylbenzyl)-1H-indole-2-carboxylate (S8). Using general procedure A, methyl 5-chloro-3-methoxy-1H-indole-2-carboxylate (**S2**) (50 mg, 0.209 mmol) yielded the title compound as a white solid (69.5 mg, 97%).**^{1}H-NMR:** (399 MHz, Acetone-d_6) δ 7.74 (dd, *J* = 2.1, 0.6 Hz, 1H), 7.52 (dd, *J* = 9.0, 0.6 Hz, 2H), 7.27 (ddd, *J* = 9.0, 2.1, 0.5 Hz, 1H), 7.12 – 6.74 (m, 6H), 5.74 (s, 3H), 4.01 (s, 2H), 3.86 (s, 2H). **^{13}C-NMR:** (100 MHz, Acetone-d_6) δ 136.63, 135.41, 129.04, 126.36, 126.01, 125.34, 120.67, 118.77, 112.88, 51.07, 47.23, 20.09. **MS** ESI (m/z): $[M+H]^+$ calcd for $C_{19}H_{19}O_3N^{35}Cl$ 344.1048, found 344.1043.

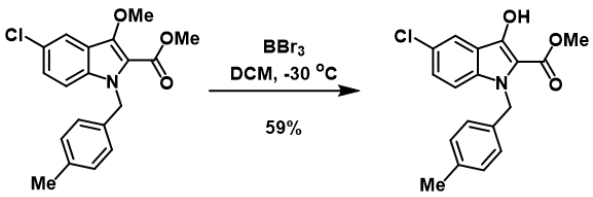

S8 **2.36**

Methyl 5-chloro-3-hydroxy-1-(4-methylbenzyl)-1H-indole-2-carboxylate (2.36). Using general procedure B, methyl 5-chloro-3-methoxy-1-(4-methylbenzyl)-1H-indole-2-carboxylate (**S8**) (114 mg, 0.332 mmol) yielded the title compound as a yellow product (64.1 mg, 59%). **^{1}H-NMR:** ^{1}H NMR (399 MHz, Acetone-d_6) δ 8.68 (s, 1H), 7.68 (d, J = 0.6 Hz, 1H), 7.57 – 7.22 (m, 3H), 7.17 – 6.74 (m, 8H), 5.66 (s, 4H), 3.92 (s, 5H). **^{13}C-NMR:** (100 MHz, Acetone-d_6) δ 136.62, 135.77, 135.54, 129.03, 127.14, 126.33, 124.49, 118.83, 112.62, 51.05, 51.03, 47.28, 20.09. **MS** ESI (m/z): $[M+H]^+$ calcd for $C_{18}H_{15}O_3N^{35}Cl$ 328.0746, found 328.0751.

2.36 **S9**

Methyl 5-chloro-3-(4-iodophenoxy)-1-(4-methylbenzyl)-1H-indole-2-carboxylate (S9). Using general procedure C, methyl 5-chloro-3-hydroxy-1-(4-methylbenzyl)-1H-indole-2-carboxylate (**2.36**) (75.2 mg, 0.229 mmol) yielded the title compound as a white solid (67 mg, 55%). **^{1}H-NMR:** (500 MHz, Acetone-d_6) δ 7.74 – 7.58 (m, 3H), 7.51 – 7.38 (m, 1H), 7.38 – 7.31 (m, 1H), 7.30 – 7.14 (m, 1H), 7.15 – 6.96 (m, 4H), 6.90 – 6.71 (m, 1H), 5.87 (s, 2H), 3.70 (s, 3H). **^{13}C-NMR:** (126 MHz, Acetone-d_6) δ 160.80, 159.25, 138.49, 136.83, 135.12, 135.05, 129.18, 128.37, 126.47, 126.37, 126.28, 120.49, 118.27, 118.03, 113.39, 84.14, 51.22, 47.52, 20.12. **MS** ESI (m/z): $[M+H]^+$ calcd for $C_{20}H_{16}ON_7{}^{35}Cl^{127}I$ 532.0144, found 532.0163.

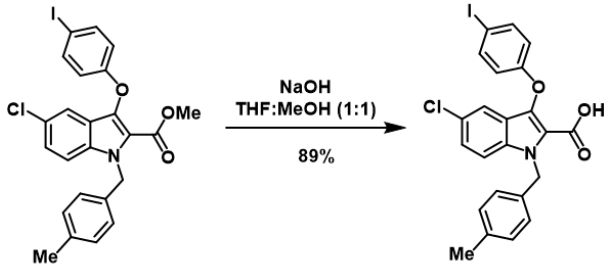

S9 **2.41**

5-chloro-3-(4-iodophenoxy)-1-(4-methylbenzyl)-1H-indole-2-carboxylic acid (2.41). Using general procedure D, methyl 5-chloro-3-(4-iodophenoxy)-1-(4-methylbenzyl)-1H-indole-2-carboxylate (**S9**) (67 mg, 0.126 mmol) yielded the title compound as a white solid (58 mg, 89%). **^{1}H-NMR:** (500 MHz, Acetone-d_6) δ 7.72 – 7.61 (m, 3H), 7.42 (dt, *J* = 2.1, 0.6 Hz, 1H), 7.34 (dd, *J* = 9.0, 2.1 Hz, 1H), 7.15 – 6.97 (m, 4H), 6.87 – 6.79 (m, 2H), 5.90 (s, 2H). **^{13}C-NMR:** (151 MHz, Acetone-d_6) δ 161.61, 159.28, 138.43, 136.74, 135.36, 134.88, 129.16, 126.45, 126.11, 120.55, 120.22, 118.02, 113.38, 83.91, 61.06, 47.33, 40.46. **MS** ESI (m/z): $[M+H]^+$ calcd for $C_{23}H_{16}O_3N^{35}Cl^{127}I$ 515.9869, found 515.9873.

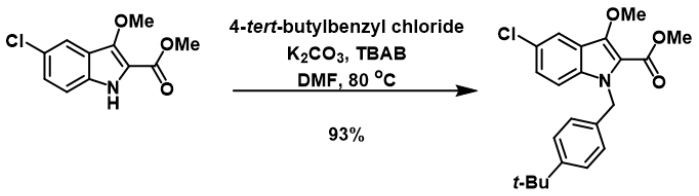

2.13 **S10**

Methyl 1-(4-(tert-butyl)benzyl)-5-chloro-3-methoxy-1H-indole-2-carboxylate (S10). Using general procedure A, methyl 5-chloro-3-methoxy-1H-indole-2-carboxylate (**2.13**) (500 mg, 2.086

mmol) yielded the title compound as a white solid (749.6 mg, 93%). **^{1}H-NMR:** (600 MHz, Acetone-d_6) δ 8.21 (s, 1H), 7.99 (d, J = 8.4 Hz, 1H), 7.76 (s, 1H), 7.55 (dd, J = 8.8, 5.4 Hz, 1H), 7.31 – 7.28 (m, 3H), 5.78 (s, 2H), 4.07 – 3.98 (m, 3H), 3.89 (d, J = 3.8 Hz, 3H).**^{13}C-NMR:** (100 MHz, Acetone-d_6) δ 149.84, 135.42, 134.88, 126.12, 126.07, 125.38, 125.32, 120.65, 118.83, 112.86, 62.20, 51.11, 47.12, 34.05, 30.71. **MS** ESI (m/z): $[M+H]^+$ calcd for $C_{22}H_{25}O_3N^{35}Cl$ 386.1518, found 386.151.

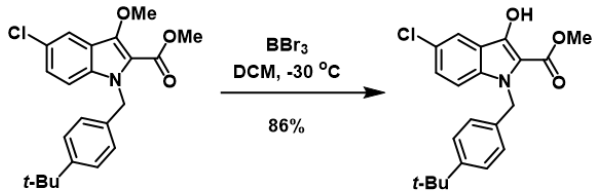

S10 **2.37**

Methyl 1-(4-(tert-butyl)benzyl)-5-chloro-3-hydroxy-1H-indole-2-carboxylate (2.37). Using general procedure B, methyl 1-(4-(tert-butyl)benzyl)-5-chloro-3-methoxy-1H-indole-2-carboxylate (**S10**) (300 mg, 0.777 mmol) yielded the title compound as a yellow solid (249 mg, 86%). **^{1}H-NMR:** (399 MHz, Acetone-d_6) δ 8.66 (d, J = 1.4 Hz, 1H), 7.67 (dd, J = 2.1, 0.6 Hz, 1H), 7.47 (dd, J = 9.0, 0.7 Hz, 1H), 7.36 – 7.20 (m, 4H), 7.05 – 6.88 (m, 2H), 5.66 (s, 3H), 3.91 (s, 3H), 1.22 (s, 9H). **^{13}C-NMR:** (100 MHz, Acetone-d_6) δ 163.13, 149.85, 146.41, 135.74, 135.52, 127.18, 126.11, 125.29, 124.52, 118.88, 117.93, 112.55, 54.06, 51.08, 47.17, 34.04, 30.70. **MS** ESI (m/z): $[M+H]^+$ calcd for $C_{21}H_{21}O_3N^{35}Cl$ 370.1215, found 370.1215.

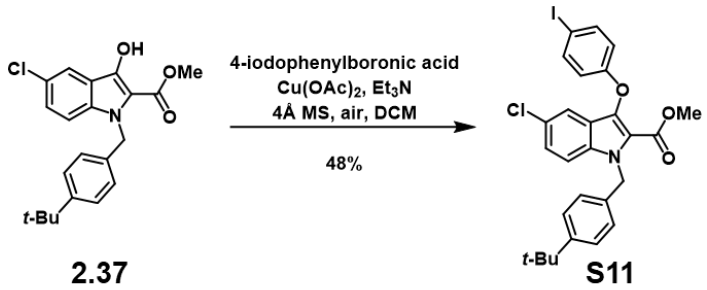

2.37 **S11**

Methyl 1-(4-(tert-butyl)benzyl)-5-chloro-3-(4-iodophenoxy)-1H-indole-2-carboxylate (S11). Using general procedure H, hydroxyindole (**2.37**) (189 mg, 0.508 mmol) yielded the title compound as a brittle light pink solid (139 mg, 48% yield). **^{1}H NMR** (500 MHz, Acetone) δ 7.70 – 7.62 (m, 3H), 7.43 (dd, *J* = 2.2, 0.7 Hz, 1H), 7.38 – 7.30 (m, 3H), 7.09 – 7.02 (m, 2H), 6.87 – 6.80 (m, 2H), 5.89 (s, 2H), 3.71 (s, 3H), 1.26 (s, 9H); **^{13}C NMR** (150 MHz, Acetone) δ 161.74, 160.15, 150.94, 139.40, 138.54, 136.02, 135.95, 127.40, 127.19, 126.98, 126.34, 121.38, 120.01, 119.18, 118.94, 114.31, 85.05, 52.14, 48.28, 34.98, 31.58; **HRMS** APCI (*m/z*): $[M+H]^+$ calcd for $C_{27}H_{26}ClINO_3$ 574.0640, found 574.0636.

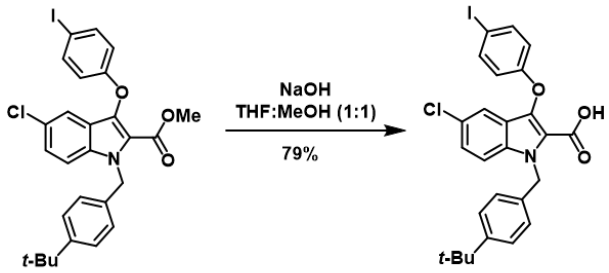

S11 **2.42**

1-(4-(tert-butyl)benzyl)-5-chloro-3-(4-iodophenoxy)-1H-indole-2-carboxylic acid (2.42). Using general procedure I, methyl ester (**S11**) (70 mg, 0.122 mmol) yielded the title compound as a white solid (54 mg, 79% yield). **^{1}H NMR** (500 MHz, Acetone) δ 7.67 – 7.63 (m, 3H), 7.42 (d, *J* = 2.0 Hz, 1H), 7.35 – 7.31 (m, 3H), 7.09 – 7.05 (m, 2H), 6.88 – 6.81 (m, 2H), 5.92 (s, 2H), 1.26 (s, 9H); **^{13}C NMR** (125 MHz, Acetone) δ 161.98, 160.12, 150.89, 139.34, 138.37, 136.17, 135.96, 127.23, 127.08, 127.01, 126.31, 121.36, 120.55, 119.15, 118.93, 114.26, 84.86, 48.17, 34.98, 31.59; **HRMS** APCI (*m/z*): $[M+H]^+$ calcd for $C_{26}H_{24}ClINO_3$ 560.0484, found 560.0480.

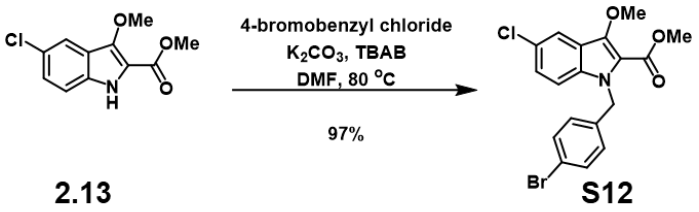

2.13 **S12**

Methyl 1-(4-bromobenzyl)-5-chloro-3-methoxy-1H-indole-2-carboxylate (S12). Using general procedure A, methyl 5-chloro-3-methoxy-1H-indole-2-carboxylate (**2.13**) (75 mg, 0.300 mmol) yielded the title compound as a yellow solid (118 mg, 97%). **^{1}H-NMR:** (500 MHz, Acetone-d_6) δ 7.77 (dd, *J* = 2.1, 0.7 Hz, 1H), 7.54 (dd, *J* = 9.0, 0.7 Hz, 1H), 7.44 (d, *J* = 8.5 Hz, 2H), 7.30 (dd, *J* = 9.0, 2.1 Hz, 1H), 7.05 – 6.93 (m, 1H), 5.78 (s, 1H), 4.03 (s, 3H), 3.87 (s, 3H). **^{13}C-NMR:** (126 MHz, Acetone-d_6) δ 161.40, 145.48, 137.96, 134.89, 131.49, 128.45, 126.27, 125.54, 120.75, 120.46, 118.92, 117.42, 112.69, 62.19, 51.11, 47.02. **MS** ESI (m/z): $[M+H]^+$ calcd for $C_{19}H_{13}ON_7{}^{79}Br^{35}Cl^{127}I$ 595.9093, found 595.9118.

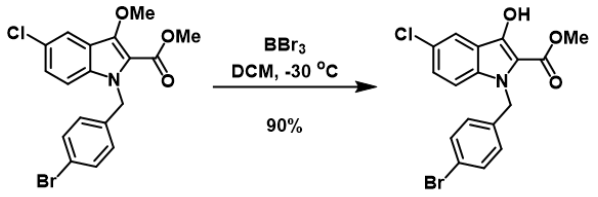

S12 **2.38**

Methyl 1-(4-bromobenzyl)-5-chloro-3-hydroxy-1H-indole-2-carboxylate (2.38). Using general procedure B, methyl 1-(4-bromobenzyl)-5-chloro-3-methoxy-1H-indole-2-carboxylate (**S12**) (117 mg, 0.286 mmol) yielded the title compound as a green solid (102 mg, 90%). **^{1}H-NMR:** (500 MHz, Acetone-d_6) δ 8.67 (s, 1H), 7.69 (d, *J* = 0.6 Hz, 1H), 7.59 – 7.47 (m, 2H), 7.37 – 7.25 (m, 2H), 7.02 (d, *J* = 8.6 Hz, 2H), 5.70 (s, 3H), 3.91 (s, 4H). **^{13}C-NMR:** (126 MHz, Acetone-d_6) δ 162.95,

146.39, 138.08, 135.74, 131.49, 128.43, 127.35, 124.71, 120.46, 118.94, 118.08, 112.41, 51.09, 47.00. **MS** ESI (m/z): $[M+H]^+$ calcd for $C_{22}H_{13}O_3N^{79}Br^{35}Cl^{127}I$ 579.8818, found 579.8821.

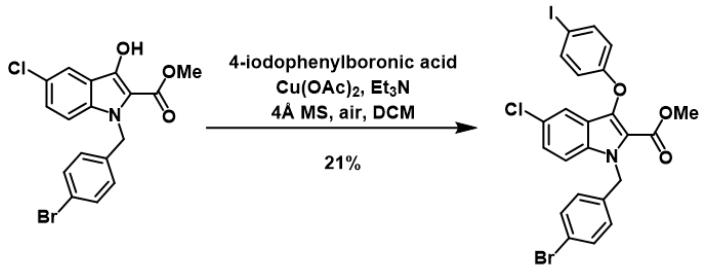

2.38 **S13**

Methyl 1-(4-bromobenzyl)-5-chloro-3-phenoxy-1H-indole-2-carboxylate (S13). Using general procedure C, methyl 1-(4-bromobenzyl)-5-chloro-3-hydroxy-1H-indole-2-carboxylate (**2.38**) (101 mg, 0.256 mmol) yielded the title compound as a white solid (32 mg, 21%). **^{1}H-NMR:** (500 MHz, Acetone-d_6) δ 7.82 – 7.72 (m, 1H), 7.71 – 7.62 (m, 3H), 7.52 – 7.45 (m, 2H), 7.37 (ddd, J = 9.0, 2.0, 0.7 Hz, 1H), 7.14 – 7.07 (m, 2H), 7.04 – 6.91 (m, 1H), 6.90 – 6.77 (m, 2H), 5.90 (d, J = 38.0 Hz, 2H), 3.70 (d, J = 0.8 Hz, 3H).**^{13}C-NMR:** (126 MHz, Acetone-d_6) δ 138.50, 138.39, 137.65, 131.61, 128.47, 126.70, 126.44, 124.28, 120.61, 120.54, 118.38, 118.06, 113.20, 84.22. **MS** ESI (m/z): $[M+H]^+$ calcd for $C_{19}H_{12}ON_7{}^{35}Cl_3{}^{127}I$ 585.9208, found 585.9228.

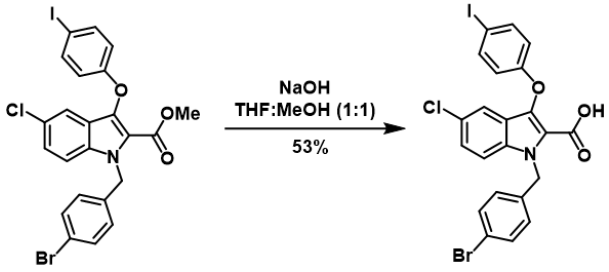

S13 **2.43**

1-(4-bromobenzyl)-5-chloro-3-phenoxy-1H-indole-2-carboxylic acid (2.43). Using general procedure D, methyl 1-(4-bromobenzyl)-5-chloro-3-phenoxy-1H-indole-2-carboxylate (**S13**) (31 mg, 0.052 mmol) yielded the title compound as a white solid (16 mg, 53 %). **^{1}H-NMR:** (600 MHz, Acetone-d_6) δ 7.77 – 7.55 (m, 4H), 7.55 – 7.28 (m, 3H), 7.10 (d, J = 8.0 Hz, 2H), 6.84 (d, J = 8.2 Hz, 2H), 5.93 (s, 2H). **^{13}C-NMR:** (151 MHz, Acetone-d_6) δ 160.97, 159.17, 138.47, 137.79, 135.08, 131.60, 128.51, 126.57, 126.35, 120.57, 118.37, 118.04, 113.19, 84.05, 76.37, 55.05, 47.11. **MS** ESI (m/z): $[M+H]^+$ calcd for $C_{22}H_{12}O_3N^{35}Cl_3{}^{127}I$ 569.8933, found 569.8935.

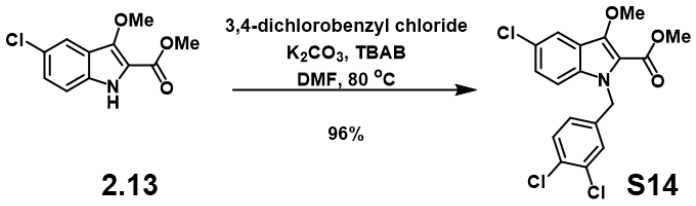

2.13 **S14**

Methyl 5-chloro-1-(3,4-dichlorobenzyl)-3-methoxy-1H-indole-2-carboxylate (S14). Using general procedure A, methyl 5-chloro-3-methoxy-1H-indole-2-carboxylate (**2.13**) (75 mg, 0.313 mmol) yielded the title compound as a yellow solid (120 mg, 96%). **^{1}H-NMR:** (399 MHz, Acetone-d_6) δ 7.77 (dd, J = 2.1, 0.6 Hz, 1H), 7.54 (dd, J = 9.0, 0.7 Hz, 2H), 7.44 (d, J = 8.3 Hz, 1H), 7.34 – 7.26 (m, 2H), 6.98 (dd, J = 8.3, 2.1 Hz, 1H), 5.79 (s, 3H), 4.03 (s, 3H), 3.86 (s, 4H).

^{13}C-NMR: (126 MHz, Acetone-d_6) δ 161.42, 139.65, 134.89, 130.64, 130.63, 128.48, 128.47, 126.44, 126.42, 125.70, 120.79, 119.04, 119.02, 112.57, 67.76, 62.19, 51.16, 46.65.

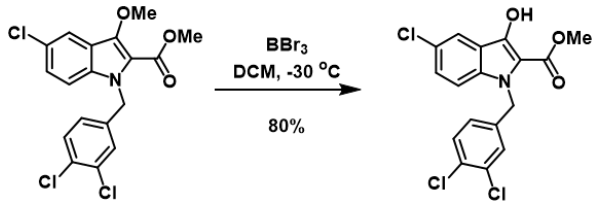

S14 **2.39**

Methyl 5-chloro-1-(3,4-dichlorobenzyl)-3-hydroxy-1H-indole-2-carboxylate (2.39). Using general procedure B, methyl 5-chloro-1-(3,4-dichlorobenzyl)-3-methoxy-1H-indole-2-carboxylate (**S14**) (120 mg, 0.302 mmol) yielded the title compound as a red solid (93 mg, 80%). **^{1}H-NMR:** (500 MHz, Acetone-d_6) δ 8.67 (s, 1H), 7.70 (dd, *J* = 2.1, 0.6 Hz, 1H), 7.57 – 7.43 (m, 2H), 7.34 (dd, *J* = 9.0, 2.1 Hz, 1H), 7.30 (d, *J* = 2.1 Hz, 1H), 7.09 – 6.92 (m, 1H), 5.73 (s, 2H), 3.91 (s, 2H). **^{13}C-NMR:** (126 MHz, Acetone-d_6) δ 162.84, 146.35, 139.79, 135.70, 131.84, 130.66, 130.44, 128.43, 127.49, 126.40, 124.87, 119.02, 118.20, 112.29, 51.13, 46.57.

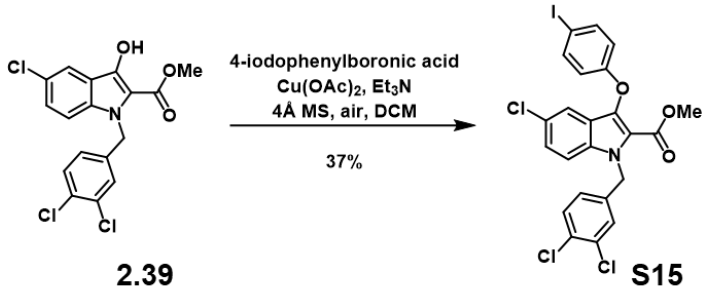

2.39 **S15**

Methyl 5-chloro-1-(3,4-dichlorobenzyl)-3-(4-iodophenoxy)-1H-indole-2-carboxylate (S15). Using general procedure C, methyl 5-chloro-1-(3,4-dichlorobenzyl)-3-hydroxy-1H-indole-2-carboxylate (**2.39**) (90mg, 0.234 mmol) yielded the title compound as a light yellow solid (51 mg, 37%). **^{1}H-NMR:** (600 MHz, Acetone-d_6) δ 7.80 – 7.74 (m, 3H), 7.70 (dd, *J* = 9.0, 0.6 Hz, 1H), 7.69 – 7.65 (m, 2H), 7.51 (d, *J* = 8.3 Hz, 1H), 7.47 (dd, *J* = 2.0, 0.6 Hz, 1H), 7.41 – 7.38 (m, 2H), 5.94 (d, *J* = 0.8 Hz, 2H), 3.72 (s, 3H). **^{13}C-NMR:** (126 MHz, Acetone-d_6) δ 160.77, 159.15, 139.32, 138.51, 137.99, 135.05, 131.97, 130.77, 130.61, 128.55, 126.87, 126.59, 126.43, 120.62, 118.93, 118.50, 118.09, 113.08, 84.29, 51.34, 46.88. **MS** ESI (m/z): $[M+H]^+$ calcd for $C_{19}H_{12}ON_7{}^{35}Cl_3{}^{127}I$ 585.9208, found 585.9228.

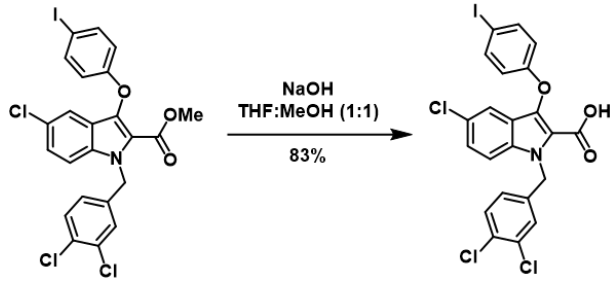

S15 **2.44**

5-chloro-1-(3,4-dichlorobenzyl)-3-(4-iodophenoxy)-1H-indole-2-carboxylic acid (2.19). Using general procedure D, methyl 5-chloro-1-(3,4-dichlorobenzyl)-3-(4-iodophenoxy)-1H-indole-2-carboxylate (**6.22**) (25 mg, 0.043 mmol) yielded the title compound as a white solid (21 mg, 83%). **^{1}H-NMR:** (600 MHz, Acetone-d_6) δ 7.99 – 7.57 (m, 1H), 7.60 – 7.32 (m, 2H), 7.21 – 6.99 (m, 1H), 6.87 (d, J = 8.9 Hz, 1H), 5.97 (s, 1H). **^{13}C-NMR:** (151 MHz, Acetone-d_6) δ 161.00, 159.14, 139.48, 138.47, 137.84, 135.09, 131.92, 130.77, 130.56, 128.61, 126.73, 126.49, 120.60, 118.46, 118.06, 113.09, 84.10, 46.73. **MS** ESI (m/z): $[M+H]^+$ calcd for $C_{22}H_{12}O_3N^{35}Cl_3{}^{127}I$ 569.8933, found 569.8935.

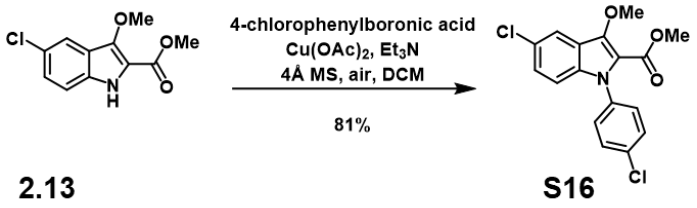

2.13 **S16**

Methyl 5-chloro-1-(4-chlorophenyl)-3-methoxy-1H-indole-2-carboxylate (S16). Using general procedure C, methyl 5-chloro-3-methoxy-1H-indole-2-carboxylate (**2.13**) (100 mg, 0.417 mmol) yielded the title compound as a pink solid (118 mg, 81%). **^{1}H-NMR:** (600 MHz, Acetone-d_6) δ 7.81 (dd, J = 2.1, 0.6 Hz, 1H), 7.57 (s, 1H), 7.40 (s, 1H), 7.29 (d, J = 2.1 Hz, 1H), 7.11 (dd, J = 8.9, 0.7 Hz, 1H), 4.10 (s, 3H), 3.73 (s, 3H). **^{13}C-NMR:** (151 MHz, Acetone-d_6) δ 160.36, 146.06, 137.26, 135.71, 133.14, 129.44, 129.21, 126.64, 126.11, 121.23, 118.90, 112.91, 62.20, 50.97.

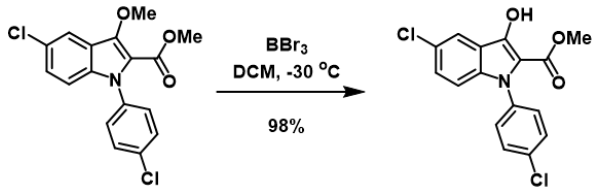

S16 **2.40**

Methyl 5-chloro-1-(4-chlorophenyl)-3-hydroxy-1H-indole-2-carboxylate (2.40). Using general procedure B, methyl 5-chloro-1-(4-chlorophenyl)-3-methoxy-1H-indole-2-carboxylate (**S13**) (59 mg, 0.169 mmol) yielded the title compound as a white solid (56 mg, 98%). **^{1}H-NMR:** (399 MHz, Acetone-d_6) δ 8.86 (s, 1H), 7.72 (d, J = 2.1 Hz, 1H), 7.48 (dd, J = 56.1, 8.7 Hz, 4H), 7.31 (dd, J = 9.0, 2.1 Hz, 1H), 7.09 (d, J = 9.0 Hz, 2H), 3.73 (s, 6H). **^{13}C-NMR:** (126 MHz, Acetone-d_6) δ 162.67, 147.49, 137.10, 136.58, 132.95, 129.54, 129.05, 127.79, 125.48, 118.87, 118.69, 112.71, 50.95.

2.40 **S17**

Methyl 5-chloro-1-(4-chlorophenyl)-3-(4-iodophenoxy)-1H-indole-2-carboxylate (S17). Using general procedure C, methyl 5-chloro-1-(4-chlorophenyl)-3-hydroxy-1H-indole-2-carboxylate (**2.40**) (56 mg, 0.166 mmol) yielded the title compound as a yellow solid (21.6 mg, 24%). **^{1}H-NMR:** (399 MHz, Acetone-d_6) δ 7.71 – 7.59 (m, 4H), 7.53 – 7.48 (m, 2H), 7.46 (dd, J = 2.0, 0.6 Hz, 1H), 7.34 (ddd, J = 9.0, 2.1, 0.5 Hz, 1H), 7.19 (dt, J = 9.0, 0.6 Hz, 1H), 6.96 – 6.88 (m, 2H), 3.63 – 3.53 (m, 3H).. **^{13}C-NMR:** (151 MHz, Acetone-d_6) δ 159.71, 159.05, 138.52, 136.68, 135.93, 133.64, 129.75, 129.29, 126.99, 126.85, 120.82, 120.57, 118.34, 118.25, 113.38, 84.41, 51.12. **MS** ESI (m/z): $[M+H]^+$ calcd for $C_{22}H_{15}O_3N^{35}Cl_2{}^{127}I$ 537.9468, found 537.947.

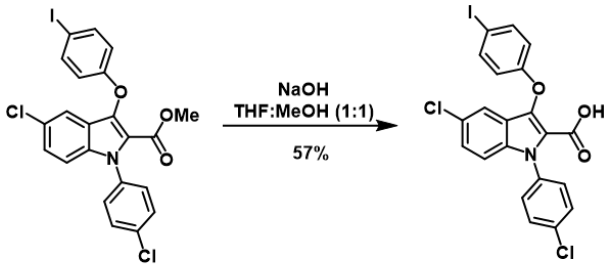

S17 **2.47**

5-chloro-1-(4-chlorophenyl)-3-(4-iodophenoxy)-1H-indole-2-carboxylic acid (2.47). Using general procedure D, methyl 5-chloro-1-(4-chlorophenyl)-3-(4-iodophenoxy)-1H-indole-2-carboxylate (**S17**) (21 mg, 0.040 mmol) yielded the title compound as a white solid (12 mg, 57%). **^{1}H-NMR:** (399 MHz, Acetone-d_6) δ 7.70 – 7.62 (m, 2H), 7.62 – 7.49 (m, 4H), 7.46 (dd, *J* = 2.1, 0.6 Hz, 1H), 7.34 (dd, *J* = 9.0, 2.1 Hz, 1H), 7.20 (dd, *J* = 8.9, 0.7 Hz, 1H), 6.98 – 6.88 (m, 2H). **^{13}C-NMR:** (151 MHz, Acetone) δ 159.06, 138.46, 136.89, 135.92, 133.48, 129.76, 129.22, 126.78, 126.73, 120.87, 118.28, 118.24, 113.32, 84.22. **MS** ESI (m/z): $[M+H]^+$ calcd for $C_{21}H_{13}O_3N^{35}Cl_2{}^{127}I$ 523.9312, found 523.9312.

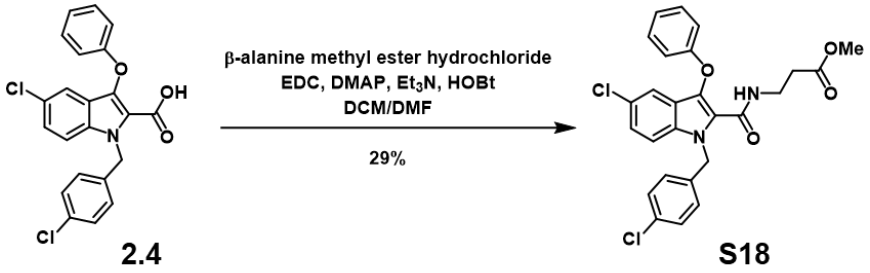

2.4 **S18**

Methyl 3-(5-chloro-1-(4-chlorobenzyl)-3-phenoxy-1H-indole-2-carboxamido)propanoate (S18). To a solution of acid starting material (**2.4**) (30 mg, 0.073 mmol, 1 equiv) in DMF, EDC (4 equiv), DMAP (4 equiv), and HOBt (4 equiv) were added to the reaction flask. β-alanine methylester hydrochloride (1.2 equiv) was pre-mixed with triethylamine. Then, the β-alanine

methyl ester solution was added to the reaction flask, making a light yellow reaction mixture. The reaction was allowed to stir overnight, and then the reaction mixture was concentrated and purified by column chromatography to give the title compound as a white solid (10.6 mg, 29%). **^{1}H-NMR:** (399 MHz, Acetone-d_6) δ 7.84 (s, 1H), 7.66 – 7.54 (m, 1H), 7.41 – 7.33 (m, 2H), 7.31 (dq, *J* = 9.0, 2.2 Hz, 2H), 7.25 (dd, *J* = 8.9, 2.1 Hz, 1H), 7.23 – 7.17 (m, 2H), 7.14 (dtd, *J* = 4.7, 2.5, 1.2 Hz, 2H), 7.06 (dtd, *J* = 6.5, 2.5, 0.9 Hz, 2H), 5.99 (d, *J* = 3.5 Hz, 2H), 3.63 – 3.53 (m, 2H), 3.49 (d, *J* = 4.1 Hz, 3H), 2.48 (td, *J* = 6.5, 3.4 Hz, 2H).**^{13}C-NMR:** (126 MHz, Acetone-d_6) δ 171.86, 157.60, 137.57, 134.18, 129.83, 129.67, 128.94, 128.50, 128.48, 125.74, 125.26, 123.35, 118.18, 116.19, 112.98, 50.85, 46.88, 34.55, 33.54. **MS** ESI (m/z): $[M+H]^+$ calcd for $C_{26}H_{23}O_4N_2{}^{35}Cl_2$ 497.1029, found 497.1026.

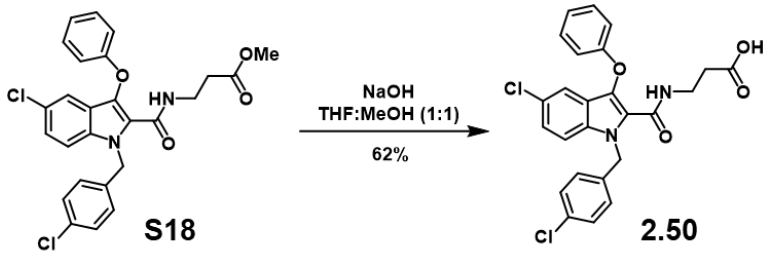

Methyl 3-(5-chloro-1-(4-chlorobenzyl)-3-phenoxy-1H-indole-2-carboxamido)propanoate (2.50). Using general procedure D, methyl 3-(5-chloro-1-(4-chlorobenzyl)-3-phenoxy-1H-indole-2-carboxamido)propanoate (**S18**) (10 mg, 0.020 mmol) yielded the title compound as a white solid (15.3 mg, xx %). **^{1}H-NMR:** (600 MHz, Acetone-d_6) δ 7.89 (s, 1H), 7.61 (d, *J* = 8.9 Hz, 2H), 7.40 – 6.88 (m, 8H), 6.01 (s, 2H), 3.59 (s, 3H), 2.49 (d, *J* = 6.6 Hz, 2H). **^{13}C-NMR:** (151 MHz, Acetone-d_6) δ 172.50, 157.62, 137.59, 134.50, 134.15, 132.42, 129.82, 128.54, 128.49, 125.73, 125.22, 123.31, 119.82, 118.20, 116.18, 113.01, 76.36, 55.04, 46.88. **MS** ESI (m/z): $[M+H]^+$ calcd for $C_{25}H_{19}O_4N_2{}^{35}Cl_2$ 481.0727, found 481.0727.

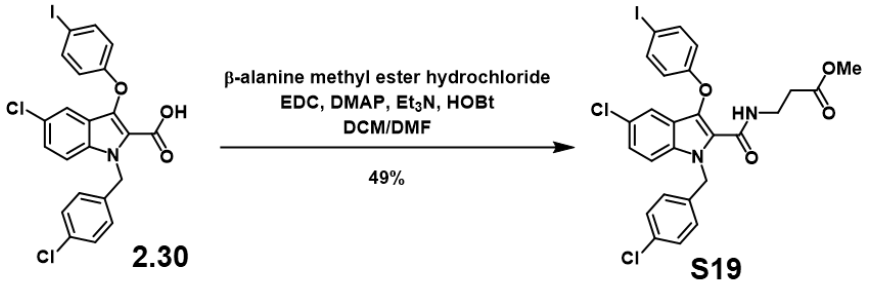

Methyl 3-(5-chloro-1-(4-chlorobenzyl)-3-(4-iodophenoxy)-1H-indole-2-carboxamido)propanoate (S19). To a solution of acid starting material (**2.30**) (58 mg, 0.108 mmol, 1 equiv) in DMF, EDC (4 equiv), DMAP (4 equiv), and HOBt (4 equiv) were added to the reaction flask. β-alanine methylester hydrochloride (1.2 equiv) was pre-mixed with triethylamine. Then, the β-alanine methyl ester solution was added to the reaction flask, making a light yellow reaction mixture. The reaction was allowed to stir overnight, and then the reaction mixture was concentrated and purified by column chromatography to give the title compound as a white solid (33 mg, 49%). **^{1}H-NMR:** ^{1}H NMR (500 MHz, Acetone-d_6) δ 7.79 (s, 1H), 7.75 – 7.68 (m, 2H), 7.68 – 7.59 (m, 3H), 7.37 – 7.17 (m, 10H), 6.96 – 6.81 (m, 3H), 5.99 (d, *J* = 3.6 Hz, 2H), 3.61 – 3.56 (m, 2H), 3.54 (d, *J* = 3.8 Hz, 3H), 2.50 (td, *J* = 6.4, 3.5 Hz, 2H). Intermediate exists as rotomers, which we see resolution with high temperature NMR (at 80ºC). **^{13}C-NMR:** (126 MHz, Acetone-d_6) δ 171.89, 138.73, 138.59, 128.96, 128.58, 128.52, 128.49, 125.37, 124.21, 118.55, 118.14, 117.98, 117.55, 113.06, 112.55, 50.87, 46.90, 34.59, 33.47. **MS** ESI (m/z): $[M+H]^+$ calcd for $C_{22}H_{18}O_2N_8{}^{35}Cl_2{}^{127}I$ 622.9969, found 622.9995.

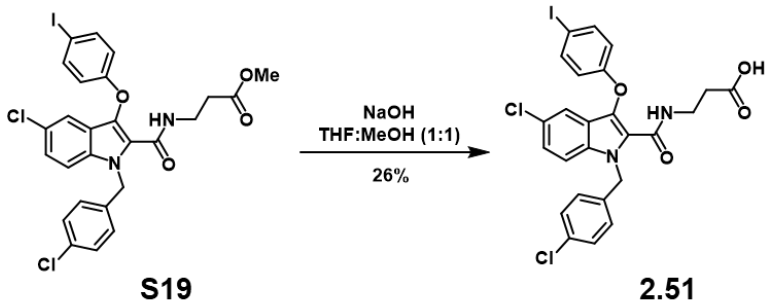

S19 **2.51**

3-(5-chloro-1-(4-chlorobenzyl)-3-(4-iodophenoxy)-1H-indole-2-carboxamido)propanoic acid (2.51). Using general procedure D, methyl 3-(5-chloro-1-(4-chlorobenzyl)-3-phenoxy-1H-indole-2-carboxamido)propanoate (**S19**) (33 mg, 0.053 mmol) yielded the title compound as a white solid (8 mg, 26%). **^{1}H-NMR:** (600 MHz, Acetone-d_6) δ 7.72 – 7.68 (m, 2H), 7.64 (dd, J = 9.0, 0.6 Hz, 1H), 7.35 – 7.31 (m, 2H), 7.29 (dd, J = 8.9, 2.1 Hz, 1H), 7.26 – 7.22 (m, 2H), 6.95 – 6.89 (m, 2H), 6.01 (s, 2H), 3.64 – 3.56 (m, 2H), 2.52 (t, J = 6.5 Hz, 3H). **^{13}C-NMR:** (151 MHz, Acetone-d_6) δ 159.91, 157.78, 138.72, 137.48, 134.09, 133.72, 132.45, 128.56, 128.50, 125.98, 125.33, 122.17, 119.65, 118.56, 118.01, 113.09, 85.44, 46.90, 34.58, 34.46, 33.25.

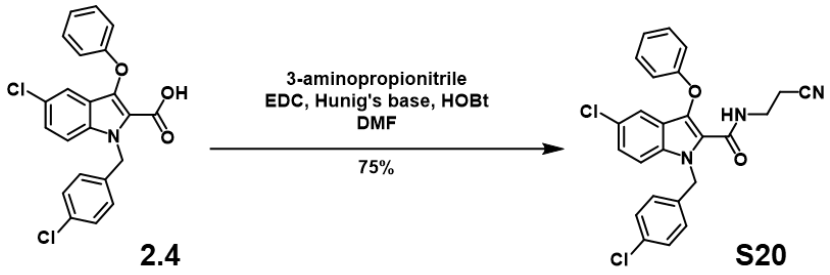

2.4 **S20**

5-chloro-1-(4-chlorobenzyl)-N-(2-cyanoethyl)-3-phenoxy-1H-indole-2-carboxamide (S20). To a solution of EDC (2.5 equiv) and HOBt (2.8 equiv) in DMF, acid starting material (**2.4**) (29 mg, 0.071 mmol, 1 equiv) was added in DMF. Then, Hunig's base (4 equiv) was added dropwise, and the reaction mixture was allowed to stir for 5 minutes. Then, 3-aminopropionitrile (2.5 equiv) was added. The reaction was allowed to stir overnight, and then 1N HCl was added to neutralize the

reaction mixture. Then, the reaction was extracted with EtOAc, washed with brine and saturated aqueous $NaHCO_3$, dried with Na_2SO_4, filtered, concentrated, and purified by column chromatography to produce the title compound as a white solid (25 mg, 75%). **^{1}H-NMR:** (399 MHz, Acetone-d_6) δ 8.06 (s, 1H), 7.62 (dd, *J* = 9.0, 0.6 Hz, 1H), 7.49 – 7.17 (m, 4H), 7.17 – 6.91 (m, 2H), 5.98 (s, 2H), 3.65 (td, *J* = 6.7, 6.1 Hz, 2H), 2.68 (t, *J* = 6.7 Hz, 2H). **^{13}C-NMR:** (151 MHz, Acetone-d_6) δ 157.60, 137.48, 134.35, 132.48, 129.86, 128.60, 128.52, 125.73, 125.43, 123.52, 119.58, 118.36, 117.98, 116.59, 113.06, 46.92, 35.33, 17.51. **MS** ESI (m/z): $[M+H]^+$ calcd for $C_{25}H_{20}O_2N_3{}^{35}Cl_2$ 464.0927, found 464.0923.

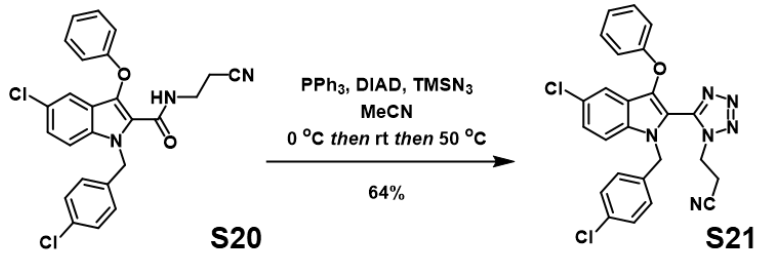

3-(5-(5-chloro-1-(4-chlorobenzyl)-3-phenoxy-1H-indol-2-yl)-1H-tetrazol-1-yl)propanenitrile (S21). A suspension of amide starting material (**S20**) (21 mg, 0.045 mmol, 1 equiv) and triphenylphosphine (2.5 equiv) in acetonitrile was cooled to 0°C and stirred for 10 minutes. Then, diisopropyl azodicarboxylate (2.5 equiv) was added dropwise, and the reaction was allowed to stir at 0°C for 5 minutes. Then, trimethylsilyl-azide was added dropwise over 5 minutes, and the reaction was stirred at 0°C for 1 hour. Then, the reaction stirred at room temperature for 2 hours, and then at 50°C overnight. Afterward, the reaction was cooled and quenched with 3M aq. $NaNO_2$ (1 equiv) at 0°C and stirred for 30 minutes. Then, 0.5M aq. CAN (1.4 equiv) was added, and the reaction was allowed to stir for 30 minutes. Then, the reaction was diluted with H_2O, extracted with EtOAc, dried with $MgSO_4$, filtered, concentrated, and purified by column chromatography to yield the title compound (14 mg, 64%). **^{1}H-NMR:** (399 MHz, Acetone-d_6) δ 8.06 (s, 1H), 7.62 (dt, *J* = 9.0, 0.6 Hz, 1H), 7.37 (dddd, *J* = 8.7, 7.3, 1.9, 0.8 Hz, 2H), 7.32 – 7.28 (m, 2H), 7.26 (ddt, *J* =

8.9, 2.0, 0.7 Hz, 1H), 7.24 – 7.21 (m, 2H), 7.14 (dddd, *J* = 8.4, 7.0, 1.6, 0.9 Hz, 1H), 7.09 (dtq, *J* = 2.8, 1.4, 0.6 Hz, 2H), 7.08 – 7.06 (m, *J* = 1.0 Hz, 1H), 5.98 (s, 2H), 3.69 – 3.60 (m, 2H), 2.68 (tt, *J* = 6.7, 0.7 Hz, 2H).**^{13}C-NMR:** (151 MHz, Acetone-d_6) δ 129.94, 129.86, 128.77, 128.60, 128.54, 128.52, 125.50, 125.43, 123.53, 123.47, 118.36, 118.13, 116.60, 115.92, 113.30, 113.05, 47.31, 46.92, 44.13, 35.33, 17.76, 17.52.

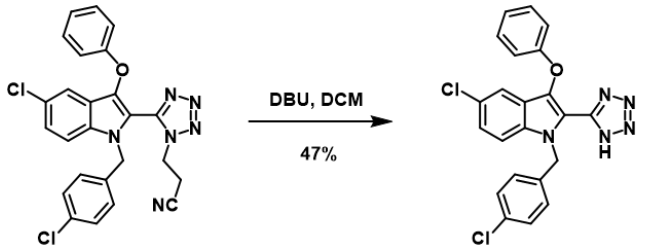

S21 **2.48**

5-chloro-1-(4-chlorobenzyl)-3-phenoxy-2-(1H-tetrazol-5-yl)-1H-indole (2.48). Base was added to a stirring solution of tetrazole starting material (**S21**) in dichloromethane. The reaction was allowed to stir overnight at room temperature and then the reaction was diluted with dichloromethane and washed with 1N HCl solution and brine. Then, the reaction mixture was dried with Na_2SO_4, filtered, concentrated, and purified by column chromatography to yield the title compound as a white solid (3 mg, 47%). **^{1}H-NMR** (399 MHz, Acetone-d_6) δ 7.66 (d, *J* = 8.9 Hz, 1H), 7.41 – 7.26 (m, 4H), 7.19 (d, *J* = 8.2 Hz2H), 7.10 (d, *J* = 8.5 Hz, 4H), 6.15 (s, 2H). **^{13}C-NMR:** (151 MHz, Acetone-d_6) δ 157.64, 136.84, 135.15, 132.61, 129.74, 129.32, 128.61, 128.32, 125.89, 125.27, 123.37, 120.04, 118.06, 116.70, 115.20, 113.18, 47.55. **MS** ESI (m/z): $[M+H]^+$ calcd for $C_{22}H_{16}ON_5{}^{35}Cl_2$ 436.0726, found 436.0722.

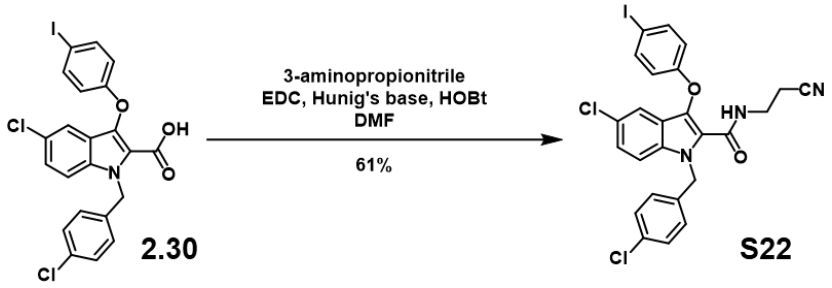

5-chloro-1-(4-chlorobenzyl)-N-(2-cyanoethyl)-3-(4-iodophenoxy)-1H-indole-2-carboxamide (S22). To a solution of EDC (2.5 equiv) and HOBt (2.8 equiv) in DMF, acid starting material (**2.30**) (58 mg, 0.108 mmol, 1 equiv) was added in DMF. Then, Hunig's base (4 equiv) was added dropwise, and the reaction mixture was allowed to stir for 5 minutes. Then, 3-aminopropionitrile (2.5 equiv) was added. The reaction was allowed to stir overnight, and then 1N HCl was added to neutralize the reaction mixture. Then, the reaction was extracted with EtOAc, washed with brine and saturated aqueous $NaHCO_3$, dried with Na_2SO_4, filtered, concentrated, and purified by column chromatography to produce the title compound as a white solid (39 mg, 61%). **^{1}H-NMR:** ^{1}H NMR (600 MHz, Acetone-d_6) δ 8.01 (s, 1H), 7.73 – 7.68 (m, 2H), 7.64 (dd, J = 8.9, 0.6 Hz, 1H), 7.34 – 7.27 (m, 3H), 7.25 – 7.20 (m, 3H), 6.94 – 6.90 (m, 2H), 5.97 (s, 2H), 3.65 (q, J = 6.6 Hz, 2H), 2.69 (t, J = 6.7 Hz, 2H). **^{13}C-NMR:** (151 MHz, Acetone-d_6) δ 160.44, 157.79, 138.76, 137.36, 134.27, 132.52, 128.62, 128.54, 126.01, 125.54, 119.49, 118.85, 118.15, 117.97, 113.14, 85.62, 46.94, 35.36. **MS** ESI (m/z): $[M+H]^+$ calcd for $C_{21}H_{15}N_9{}^{35}Cl_2{}^{127}I$ 589.98667, found 589.98856.

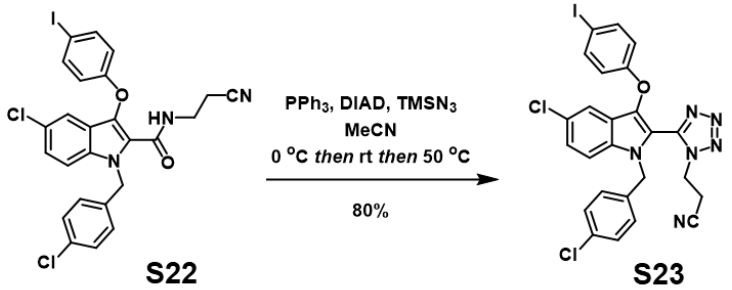

3-(5-(5-chloro-1-(4-chlorobenzyl)-3-(4-iodophenoxy)-1H-indol-2-yl)-1H-tetrazol-1-yl)propanenitrile (S23). A suspension of amide starting material (**S22**) (39 mg, 0.066 mmol, 1 equiv) and triphenylphosphine (2.5 equiv) in acetonitrile was cooled to 0ºC and stirred for 10 minutes. Then, diisopropyl azodicarboxylate (2.5 equiv) was added dropwise, and the reaction was allowed to stir at 0ºC for 5 minutes. Then, trimethylsilyl-azide was added dropwise over 5 minutes, and the reaction was stirred at 0ºC for 1 hour. Then, the reaction stirred at room temperature for 2 hours, and then at 50^{0}C overnight. Afterward, the reaction was cooled and quenched with 3M aq. $NaNO_2$ (1 equiv) at 0ºC and stirred for 30 minutes. Then, 0.5M aq. CAN (1.4 equiv) was added, and the reaction was allowed to stir for 30 minutes. Then, the reaction was diluted with H_2O, extracted with EtOAc, dried with $MgSO_4$, filtered, concentrated, and purified by column chromatography to yield the title compound (33 mg, 80%). **^{1}H-NMR:** (500 MHz, Acetone-d_6) δ 8.97 (s, 1H), 8.04 (s, 1H), 7.76 – 7.58 (m, 3H), 7.39 – 7.16 (m, 6H), 6.96 – 6.86 (m, 2H), 5.97 (t, *J* = 1.3 Hz, 2H), 3.73 – 3.57 (m, 2H), 2.70 (tt, *J* = 6.7, 1.3 Hz, 2H). **^{13}C-NMR:** (126 MHz, Acetone-d_6) δ 160.44, 157.78, 138.75, 137.34, 128.61, 128.53, 126.00, 125.53, 119.48, 118.84, 118.14, 117.96, 113.12, 85.61, 68.61, 46.94, 35.36, 21.11, 17.50.

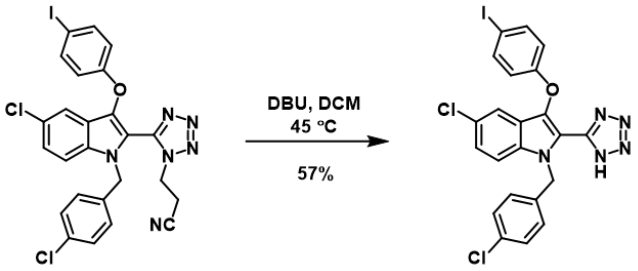

S23 **2.49**

5-chloro-1-(4-chlorobenzyl)-3-(4-iodophenoxy)-2-(1H-tetrazol-5-yl)-1H-indole (2.49). Base was added to a stirring solution of tetrazole starting material (**S23**) in dichloromethane. The reaction was allowed to stir overnight at 45ºC and then the reaction was cooled and diluted with

dichloromethane and washed with 1N HCl solution and brine. Then, the reaction mixture was dried with Na_2SO_4, filtered, concentrated, and purified by column chromatography to yield the title compound as a white solid (4 mg, 57%). **^{1}H-NMR:** (600 MHz, Acetone-d_6) δ 7.79 (d, J = 4.1 Hz, 1H), 7.56 (s, 2H), 7.44 (s, 1H), 7.31 (s, 2H), 7.09 (s, 2H), 6.96 – 6.83 (m, 4H), 5.82 (s, 2H). **^{13}C-NMR:** ^{13}C NMR (151 MHz, Acetone-d_6) δ 161.42, 137.49, 134.90, 132.40, 128.50, 128.13, 126.26, 125.59, 125.54, 120.76, 118.91, 117.44, 112.73, 62.19, 61.86, 51.11, 46.96.

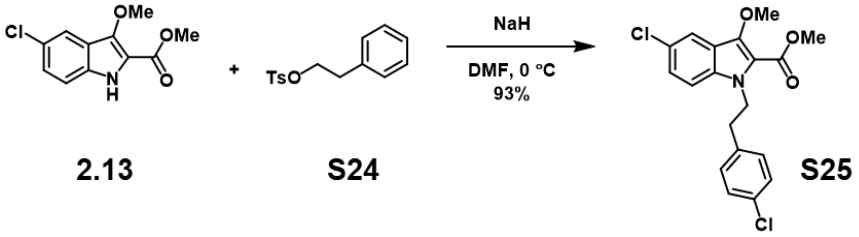

2.13 **S24** **S25**

.Methyl 5-chloro-1-(4-chlorophenethyl)-3-methoxy-1H-indole-2-carboxylate (S25). Indole **2.13** (200 mg, 0.835 mmol) dissolved in DMF (2 mL) was added to a suspension of NaH (60% in mineral oil, 43 mg, 1.086 mmol) in DMF (3 mL) at 0 ºC. The reaction was stirred for 30 minutes, then 4-chlorophenethyl-4-methylbenzenesulfonate (Cheng, K. et al, Org. Biomol. Chem. 2007, 5, 1177. 389 mg, 1.253 mmol) was added. The ice bath was removed, and the reaction was stirred for 72 hours. The reaction was poured into EtOAc and water, and the aqueous layer was extracted with EtOAc 3x. The combined organic layers were washed with water and brine, dried over Na 2SO4, filtered, concentrated, and purified by column chromatography, yielding the title compound as a yellow solid (293 mg, 93%). **1H NMR** (400 MHz, CDCl3) δ 7.71 (dd, J = 2.0, 0.5 Hz, 1H), 7.25 – 7.21 (m, 2H), 7.21 – 7.19 (m, 1H), 7.17 – 7.13 (m, 1H), 7.05 – 7.01 (m, 2H), 4.67 – 4.60 (m, 2H), 4.00 (s, 3H), 3.93 (s, 3H), 3.02 – 2.92 (m, 2H); **13C NMR** (100 MHz, CDCl3) δ 161.95, 145.14, 136.87, 134.32, 132.55, 130.38, 128.70, 126.44, 125.79, 120.38, 119.39, 117.10, 111.52, 62.94, 51.91, 46.22, 36.32; **HRMS** ESI (m/z): [M+Na]+ calcd for C19H17Cl2NO3Na 400.0483, found 400.0481.

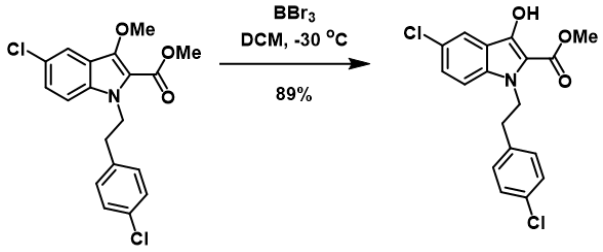

S25 **2.19**

Methyl 5-chloro-1-(4-chlorophenethyl)-3-hydroxy-1H-indole-2-carboxylate (2.19). Using general procedure B, methyl ether **S25** (243.1 mg, 0.643 mmol) yielded the title compound as a yellow solid (208.4 mg, 89% yield). **1H NMR** (400 MHz, CDCl3) δ 8.39 (br s, 1H), 7.71 (d, J = 2.1 Hz, 1H), 7.25 – 7.18 (m, 3H), 7.04 – 6.95 (m, 3H), 4.53 – 4.45 (m, 2H), 3.97 (s, 3H), 2.96 – 2.89 (m, 2H); **13C NMR** (150 MHz, Acetone) δ 163.13, 146.15, 137.64, 135.18, 131.73, 130.68, 128.24, 126.84, 124.19, 118.70, 117.56, 112.16, 109.96, 51.12, 45.87, 35.79; **HRMS** ESI (m/z): [M+Na]+ calcd for C24H19Cl2NO3Na 462.0640, found 462.0634.

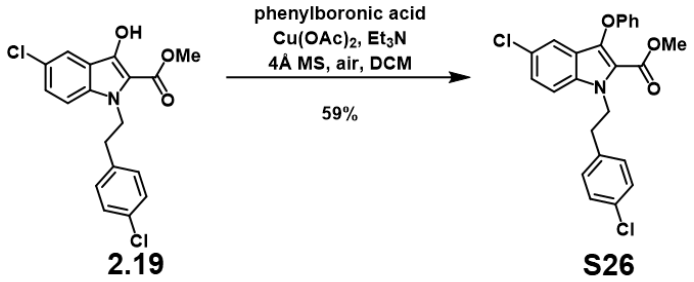

2.19 **S26**

Methyl 5-chloro-1-(4-chlorophenethyl)-3-phenoxy-1H-indole-2-carboxylate (S26). Using general procedure C, hydroxyindole **2.19** (243 mg, 0.643 mmol) yielded the title compound as a yellow solid (208 mg, 89% yield). 1H NMR (400 MHz, Acetone) δ 7.65 – 7.59 (m, 1H), 7.43 – 7.23 (m, 6H), 7.20 – 7.15 (m, 2H), 7.08 – 7.01 (m, 1H), 6.94 – 6.88 (m, 2H), 4.94 – 4.82 (m, 2H), 3.68 (s, 3H), 3.17 – 3.05 (m, 2H); **13C NMR** (150 MHz, Acetone) δ 160.99, 159.11, 137.77, 137.35,

134.41, 131.85, 130.77, 129.51, 128.28, 125.97, 125.72, 122.18, 120.37, 118.95, 118.29, 115.54, 112.92, 51.07, 45.69, 35.69; **HRMS** ESI (m/z): [M+H]+ calcd for C23H20O3NCl2 440.0815, found 440.0822.

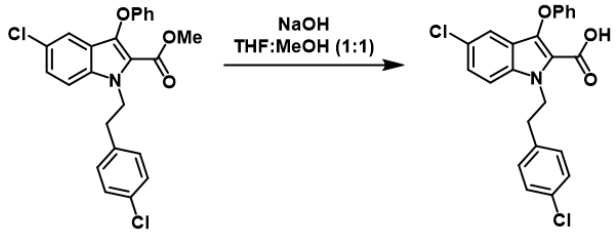

S26 **2.34**

5-chloro-1-(4-chlorophenethyl)-3-phenoxy-1H-indole-2-carboxylic acid (2.34). Using general procedure D, methyl ester **S26** (46 mg, 0.132 mmol) yielded the title compound as a white solid (34 mg, 53% yield). **1H NMR** (400 MHz, Acetone) δ 7.65 – 7.54 (m, 1H), 7.39 – 7.10 (m, 8H), 7.02 (tt, J = 7.2, 1.1 Hz, 1H), 6.92 (dt, J = 7.9, 1.0 Hz, 2H), 4.88 (t, J = 7.3 Hz, 2H), 3.12 (t, J = 7.3 Hz, 2H); **13C NMR** (150 MHz, Acetone) δ 161.23, 159.06, 137.79, 137.44, 134.57, 131.80, 130.73, 129.48, 128.29, 125.86, 125.58, 122.07, 120.24, 119.21, 118.27, 115.51, 112.89, 45.69, 35.77; **HRMS** ESI (m/z): [M+H]+ calcd for C23H18O3NCl2 426.0658, found 426.0666.

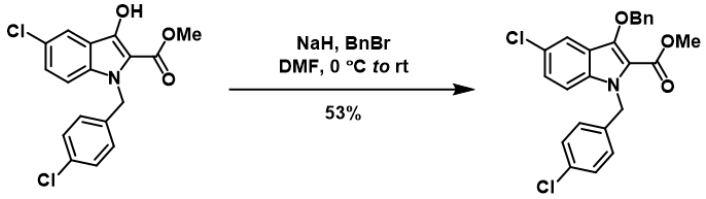

2.35 **S27**

Methyl 3-(benzyloxy)-5-chloro-1-(4-chlorobenzyl)-1H-indole-2-carboxylate (S27). To a suspension of NaH (40 mg, 0.984 mmol) in DMF (5 mL) at 0 °C was added hydroxyindole **2.35**

(265 mg, 0.757 mmol) dissolved in DMF (3 mL). The reaction mixture was stirred at room temperature for 30 minutes. Benzyl bromide (0.13 mL, 1.136 mmol) was added and the reaction was stirred for 2 hours at room temperature. The reaction was quenched with water, and the aqueous layer was extracted with EtOAc 3x. The combined organic layers were washed with water and brine, dried over Na 2SO4, filtered, concentrated, and purified by column chromatography, yielding the title compound as a yellow solid (178 mg, 53% yield). **1H NMR** (600 MHz, CDCl3) δ 7.63 (dd, J = 2.0, 0.5 Hz, 1H), 7.47 – 7.42 (m, 2H), 7.41 – 7.35 (m, 3H), 7.25 (dd, J = 8.9, 2.0 Hz, 1H), 7.23 – 7.18 (m, 3H), 6.93 – 6.88 (m, 2H), 5.67 (s, 2H), 5.19 (s, 2H), 3.84 (s, 3H); **13C NMR** (150 MHz, CDCl3) δ 161.81, 144.09, 137.03, 136.57, 135.01, 133.21, 128.95, 128.60, 128.52, 128.48, 127.62, 126.94, 126.36, 121.37, 119.56, 118.13, 111.93, 77.70, 51.90, 47.58; **HRMS** ESI (m/z): [M+H]+ calcd for C24H20Cl2NO3 440.0820, found 440.0814.

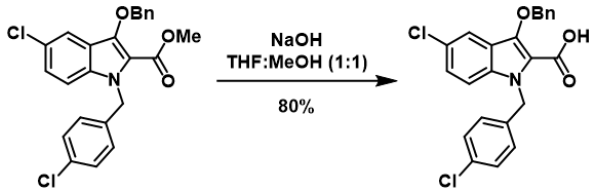

S27 **2.33**

3-(benzyloxy)-5-chloro-1-(4-chlorobenzyl)-1H-indole-2-carboxylic acid (2.33). Using general procedure D, methyl ester **S27** (65.1 mg, 0.148 mmol) yielded the title compound as a pale yellow solid (50 mg, 80% yield). **1H NMR** (400 MHz, Acetone) δ 7.69 (d, J = 1.7 Hz, 1H), 7.61 – 7.50 (m, 3H), 7.43 – 7.33 (m, 3H), 7.33 – 7.26 (m, 3H), 7.09 – 7.02 (m, 2H), 5.86 (s, 2H), 5.35 (s, 2H); **13C NMR** (150 MHz, Acetone) δ 161.29, 143.80, 137.56, 137.36, 134.87, 132.34, 128.56, 128.47, 128.29, 128.16, 128.10, 126.22, 125.57, 121.10, 119.10, 118.11, 112.69, 76.98, 46.80; **HRMS** ESI (m/z): [M+Na]+ calcd for C23H17Cl2NO3Na 448.0483, found 448.0482.

Chapter 3: Honokiol

Materials: The bacterial strain Streptococcus mutans wild-type strain UA159 was provided by Dr. Bettina Buttaro from Temple University Medical School, Philadelphia, PA.. Bacteria were routinely maintained on in BactoTM Todd- Hewitt (TH) agar plates and liquid cultures were grown in in BactoTM Todd-Hewitt broth (THB). Incubation was stagnant at 37 °C with 5% CO2. Optical density (OD) measurements were performed on a Molecular Devices SpectraMax iD3 plate reader for S. mutans.

Minimum Inhibitory Concentration (MIC) Assay: Stock solution of bibenzyl analogs, 10 mM, were serial diluted in THB media in flat-bottom 96-well microtiter plates (total volume 100 µL). Bacterial cultures were grown to mid-exponential phase, back diluted to an OD of 0.1 and then inoculated into the 96-well plate to reach a final volume of 200 µL. Plates were incubated at 37 °C in 5% CO2 for 20-24 hours upon which time wells are evaluated visually for bacterial growth. The MIC is determined as the lowest concentration of compound resulting in no bacterial growth visible to the naked eye. DMSO controls corresponding to each test concentration were performed. Biological triplicates were performed to confirm results.

S. mutans MBC assay: MIC assay is performed (above) and each well is diluted (log-dilution) into a new 96-well microtiter plate. 5 µL from each dilution is then plated on THB agar plates and incubated for 24 hours. Colony counts are performed to determine MBC which is defined as the concentration which there is a 3-log reduction in CFU count which corresponds to 99.9% bacterial death.

Hemolysis Assay (Lysis20): Hemolysis assays were performed on mechanically defibrinated sheep blood (Hemostat Labs: DSB030). 1.5 mL of blood was placed into a microcentrifuge tube and centrifuged at 10,000 rpm for ten minutes. The supernatant was removed and then the cells

were resuspended with 1 mL of phosphate-buffered saline (PBS). The suspension was centrifuged as previously, the supernatant was removed, and cells were resuspended two more times. The final cell suspension was diluted twentyfold with PBS. The twentyfold suspension dilution was then aliquoted into microcentrifuge tubes containing compound serially diluted in PBS. TritonX (1% by volume) served as a positive control (100% lysis marker) and sterile PBS served as a negative control (0% lysis marker). Samples were then placed in an incubator at 37 ◦C and shaken at 200 rpm. After 1 hour, the samples were centrifuged at 10,000 rpm for ten minutes. The absorbance of the supernatant was measured with a UV spectrometer at a 540 nm wavelength. Adapted from: Peng, L.; DeSousa, J.; Su, Z.; Novak, B.M.; Nevzorov, A.A.; Garland, E.R.; Melander, C. *Chem. Comm*. **2011**, *47*, 4896-4898.

SYTOX Assay: Bacterial overnight cultures were regrown to mid-log phase in THB media and the culture was centrifuged, and washed with PBS three times. Cells were then suspended in the same volume of PBS corresponding to the original regrow volume, and SYTOX green solution (5 mM in DMSO) was added to reach a final concentration of 5 μM. Cells were incubated at room temperature and in the dark for 30 minutes. 150 μL of cells were then added to a black, clear bottom 96-well plate. Fluorescence was recorded S18 for 10 minutes in plate reader to allow equilibration (excitation wavelength 485 nm and emission wavelength 525 nm). In a new 96-well plate, test compounds (10 mM DMSO stock solutions) were serially diluted in PBS. 50 μL of serially diluted compound was added to the SYTOX prepared cells in the plate reader and fluorescence was recorded overtime (excitation wavelength 485 nm, emission wavelength 525 nm). Biological triplicates were completed. Controls: DMSO vehicle control, PBS control, and CPC positive control. Adapted from Steele, A. D.; Ernouf, G.; Lee, Y. E. and Wuest W.M. *Org. Lett., **2018**, 20*, 1126-1129.

Detecting Membrane Depolarization and Rupture: Bacterial overnight cultures were regrown to mid-log phase in THB media and the culture was centrifuged, and washed with PBS three times. Cells were then suspended in the same volume of PBS corresponding to the original regrow volume. To 20 mLs of cell suspension, 500 µl of 1 M sterile filter glucose solution was added (Final glucose concentration = 24.4 mM). Cells were incubated for 15 minutes at 37˚C. Then 100 µl of 50 µM solution of DIBAC4(3) was added (Final concentration = 243 nM). Next, 400 µl of 2 mg/ml solution of PI was added (Final concentration 19 µg/ml). The sample was mixed thoroughly and 150 µL of sample was added into the wells of a black, clear bottom 96-well plate. The plate was then placed in a pre-warmed (37˚C) fluorescence detection plate reader. The measurements were recorded until readings stabilized (~40 mins). In a new 96-well plate, test compounds (10 mM DMSO stock solutions) were serially diluted in PBS. The fluorescence plate was ejected, 50 µl of test compound was added and then quickly returned to the plate reader. Fluorescence was recorded overtime (measurements below). Biological triplicates were completed. Controls: DMSO vehicle control, PBS control, and CPC positive control. Measurements 1. DiBAC4(3) measures changes in polarity. (490 nm excitation and 516 nm emission) detection 2. PI measures cell rupture. (535 nm excitation and 617 nm emission) detection Adapted from Clementi, E. A., Marks, L. R., Roche-Håkansson, H., Håkansson, A. P. *J. Vis. Exp.* (84), e51008.

TEM Imaging: Cells were grown to mid-log phase in THB media, centrifuged, and washed with PBS three times. Cells were then suspended to the original volume with PBS. The cells were then incubated with test compound for 30 minutes at 37˚C. Following treatment, cells were collected, washed, and prepared for transmission electron microscopy by fixing the cells in 2.5% glutaraldehyde in 0.1 M cacodylate buffer. Images were recorded on a JEOL JEM-1400 Transmission electron microscope at the Integrated Cellular Imaging Core at Emory University.

Intracellular pH Assay: Cells were grown to mid-log phase in THB media, centrifuged, and washed with PBS three times. Then, cells were diluted to make a 4x suspension, and 1 mL of cells was added to the 2x Loading Buffer (40 uL of 100x PowerLoad, 20 uL of 5mM ion-sensitive dye directly into PowerLoad, vortex, add 900 uL PBS, and then 100 uL of 100x probenecid, vortex, and wrap in foil). Cells were incubated in 30 ºC water bath for 40 min and protected from light (to minimize dye efflux). Next, cells are pelleted for 10 min in centrifuge (2400 x g) to remove excess dye. Then, cells are resuspended in 4 mL of 2x probenecid and 1 mM glucose to reenergize bacteria. Repeat pelleted and re-energization twice. Resuspend cells in 4 mL of 2 x probenecid and 1 mM glucose to reenergize bacteria. Incubate at 37 ºC for 5 min. Establish background fluorescence and create calibration curve. Then, place 200 uL of loaded and energized cells in wells of plate. Record fluorescence for 5 min. Eject plate and add 10 uL of carbonyl cyanide 3-chlorophenylhydrazone (positive control) to one well. Add 10 uL of experimental reagent to other wells. Record fluorescence for 10 min. Adapted from Clementi, E. A., Marks, L. R., Roche-Håkansson, H., Håkansson, A. P. *J. Vis. Exp.* (84), e51008.

Detecting Changes in Membrane Protein: Incubate *S. mutans* (UA159) overnight. Pellet bacterial cells at 2400 x g for 10 min and remove supernatant. Resuspend at final density of 1 x 10^9 CFU/mL in 0.85% saline solution. An amount of 0.3 mL of bacterial suspensions was added to 2.7 mL of compound solution with different concentrations. After incubation for 1 h at room temperature, the fluorescence was measured. Adapted from *Molecules*, **2016**, *21*, 1084.

Detecting Changes in Intracellular Ca^{2+} Concentrations: Incubate *S. mutans* (UA159) overnight. Pellet bacterial cells at 2400 x g for 10 min and remove supernatant. Resuspend with 1x PBS solution, pellet, and repeat 3 times. Remove supernatant and resuspend with PBS to 0.5 original volume. Add 1 mL of 2x cells to loading buffer (20 uL of 100x PowerLoad concentrate, 2 uL of 5mM ion-sensitive dye, vortex, 960 uL of PBS, then 20 uL of 100x probenecid, vortex, wrap

in foil to protect from light). Incubate cells for 75 min at 37 ºC protected from light. Pellet cells at 2400 x g for 10 min and remove supernatant. Resuspend with 2 mL 1x probenecid PBS solution, pellet, and repeat 3 times. Incubate cells for 30 min at 37 ºC with 2 mL 1x probenecid PBS solution, pellet, and repeat 3 times. Pellet cells at 2400 x g for 10 min and remove supernatant. Resuspend with 2 mL probenecid PBS solution, pellet, and repeat 3 times. Pipette 150 uL into wells of 96-well black/clear bottom plate. Place plate in pre-warmed (37 ºC) fluorescence detection plate reader. Equilibrate and read measurements for 1 minute, taking readings every second. Eject plate and add experimental reagent (50 uM). Divide value 1/value 2 to determine ratio of fluorescence. Adapted from Clementi, E. A., Marks, L. R., Roche-Håkansson, H., Håkansson, A. P. *J. Vis. Exp.* (84), e51008.

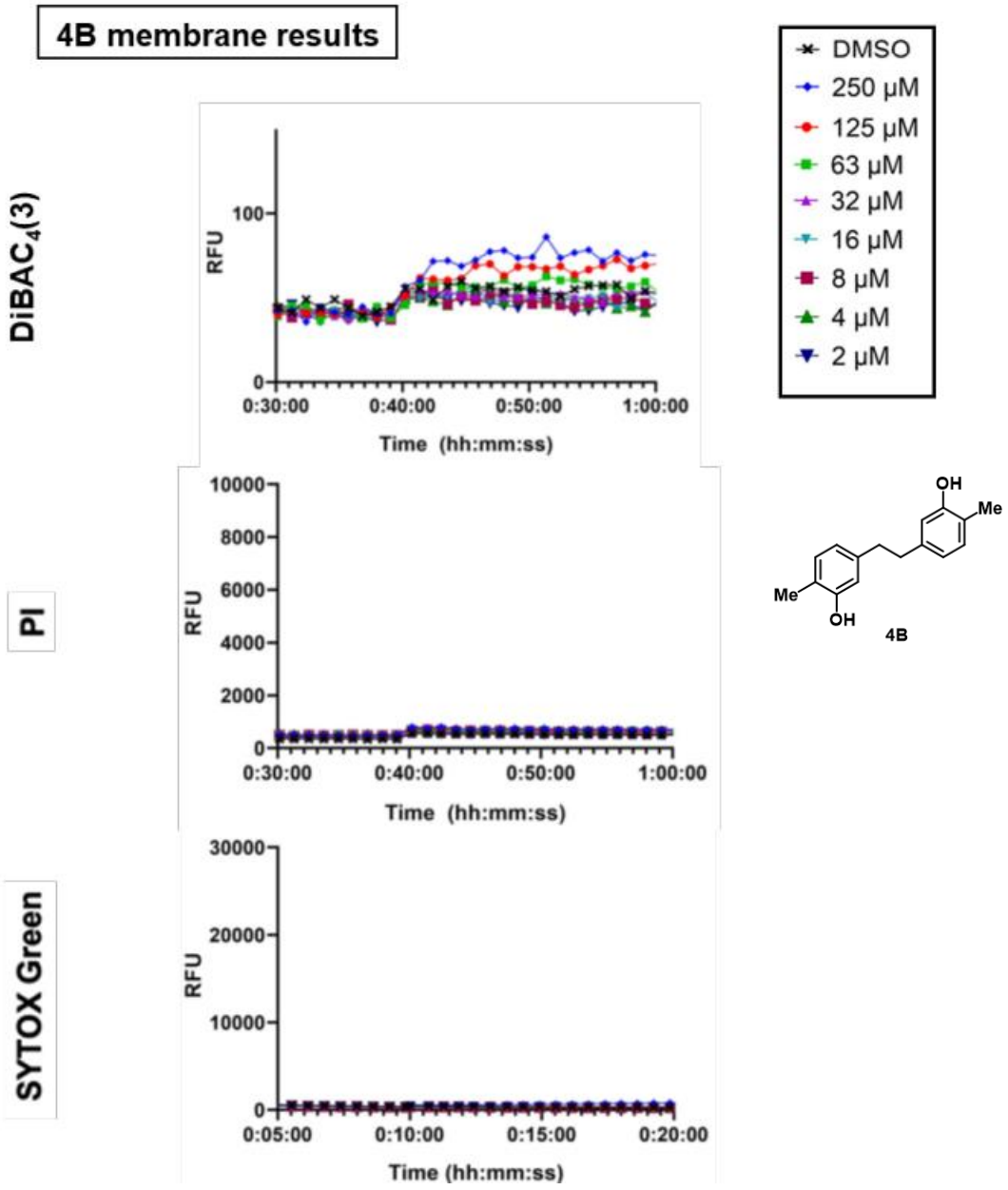
4B membrane results
DMSO
250 µM
125 µM
63 µM
32 µM
16 µM
8 µM
4 µM
2 µM
DiBAC4(3)
RFU
100
0
0:30:00
0:40:00
0:50:00
1:00:00
Time (hh:mm:ss)
PI
RFU
10000
8000
6000
4000
2000
0
0:30:00
0:40:00
0:50:00
1:00:00
Time (hh:mm:ss)
OH
Me
Me
OH
4B
SYTOX Green
RFU
30000
20000
10000
0
0:05:00
0:10:00
0:15:00
0:20:00
Time (hh:mm:ss)

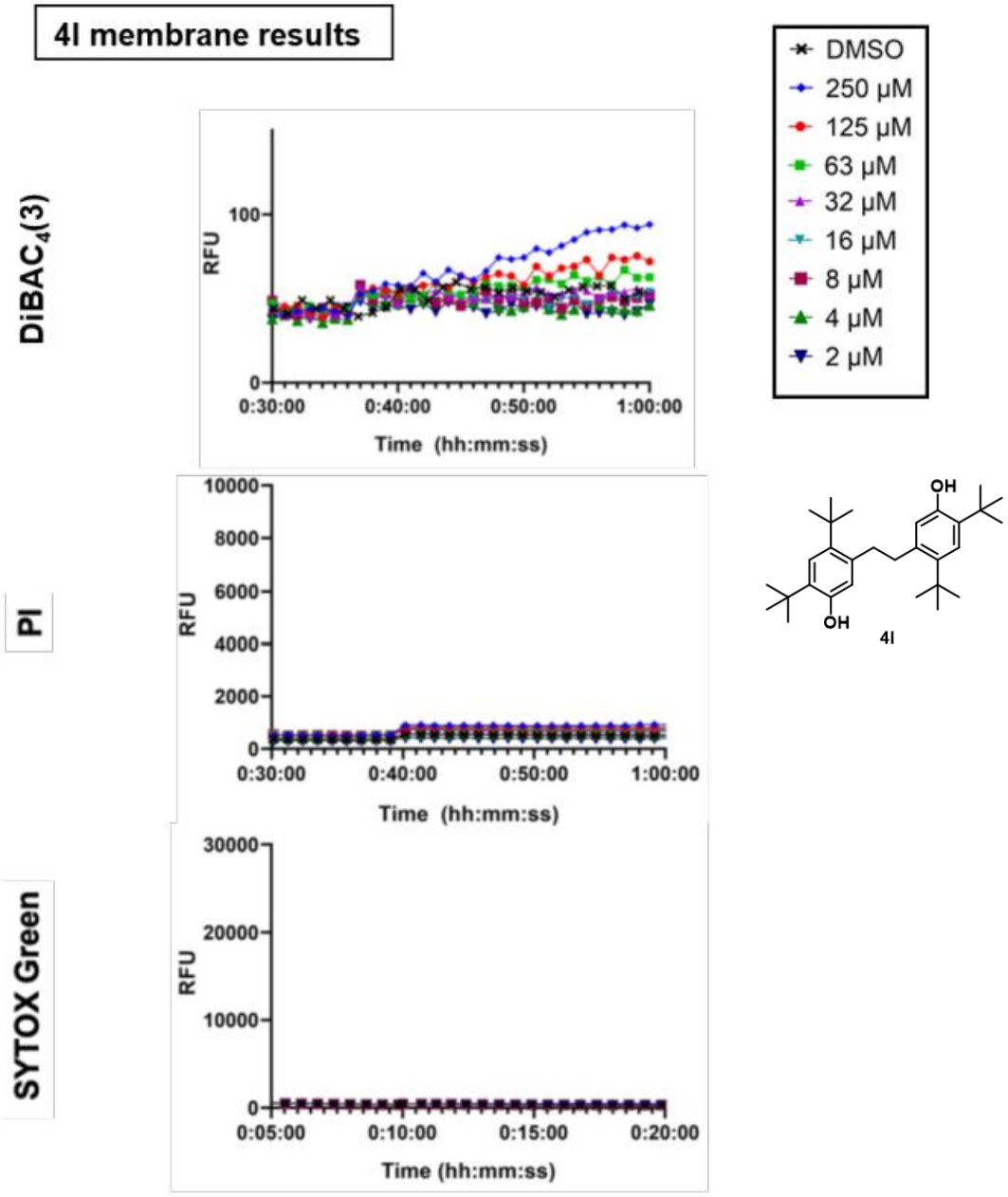
4l membrane results
DMSO
250 µM
125 µM
63 µM
32 µM
16 µM
8 µM
4 µM
2 µM
DiBAC4(3)
RFU
100
0
0:30:00
0:40:00
0:50:00
1:00:00
Time (hh:mm:ss)
PI
RFU
10000
8000
6000
4000
2000
0
0:30:00
0:40:00
0:50:00
1:00:00
Time (hh:mm:ss)
OH
OH
4l
SYTOX Green
RFU
30000
20000
10000
0
0:05:00
0:10:00
0:15:00
0:20:00
Time (hh:mm:ss)

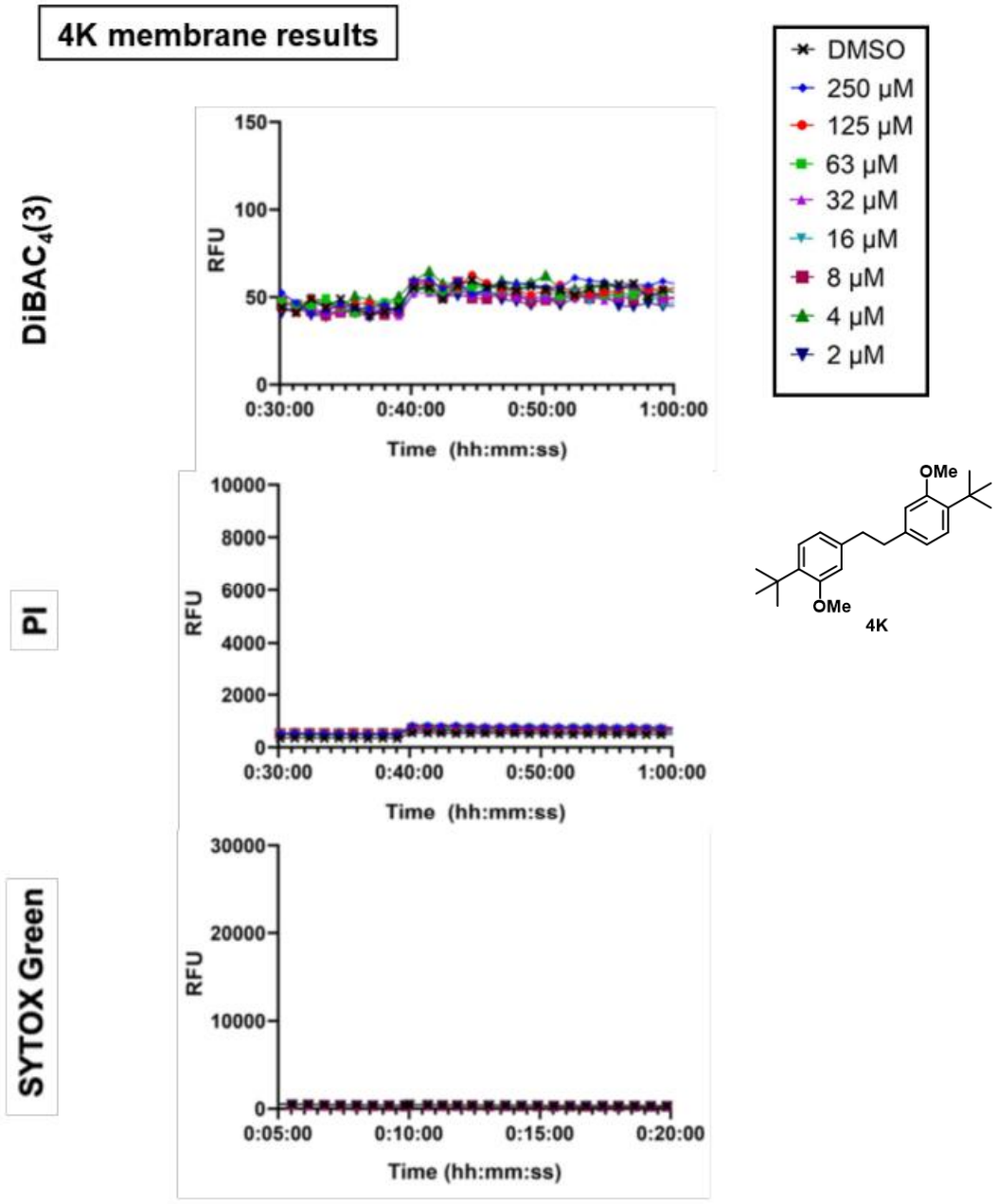
4K membrane results
DMSO
250 µM
125 µM
63 µM
32 µM
16 µM
8 µM
4 µM
2 µM
DiBAC4(3)
RFU
Time (hh:mm:ss)
PI
SYTOX Green
OMe
4K

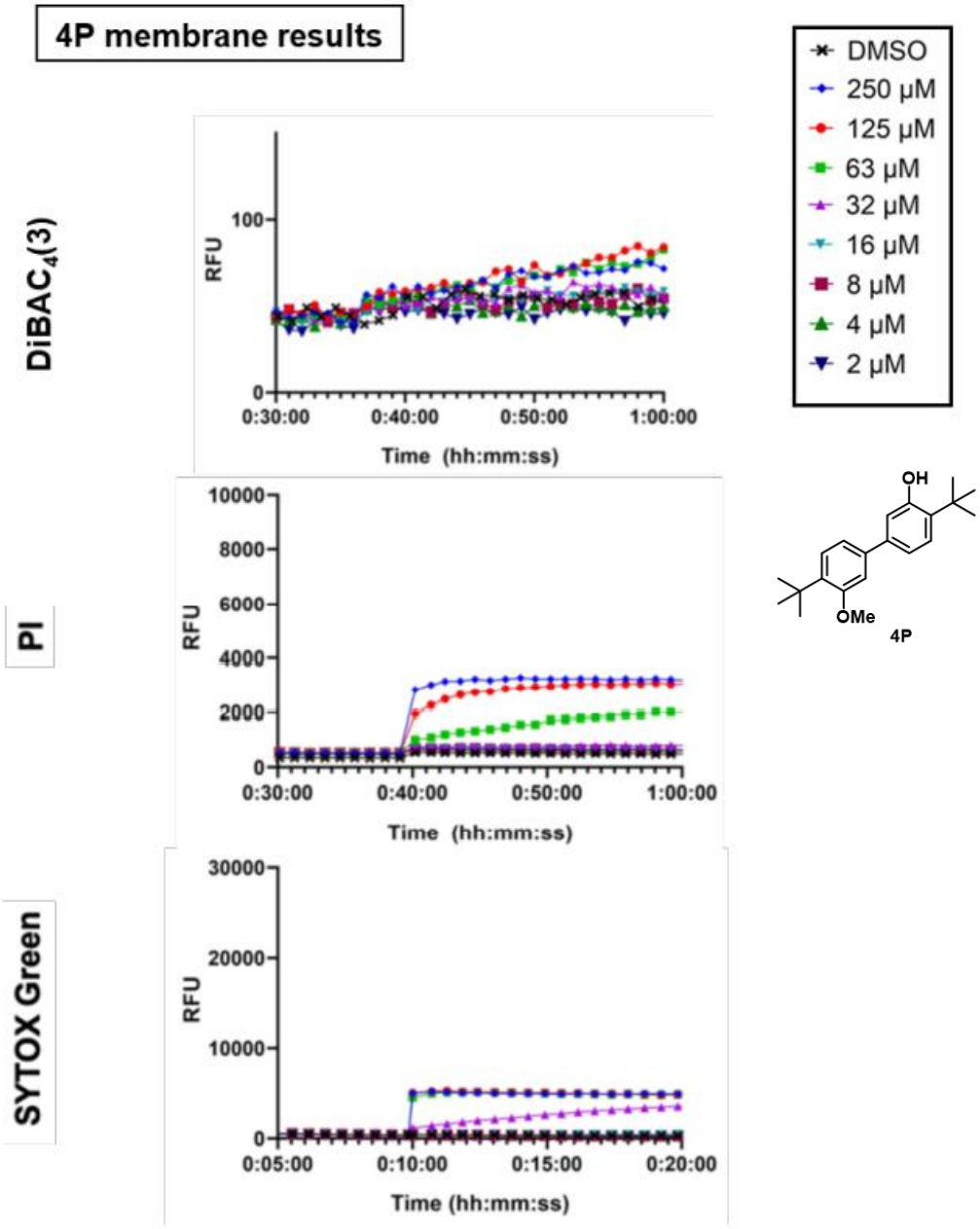
4P membrane results
DMSO
250 µM
125 µM
63 µM
32 µM
16 µM
8 µM
4 µM
2 µM
DiBAC4(3)
RFU
Time (hh:mm:ss)
PI
SYTOX Green
OH
OMe
4P

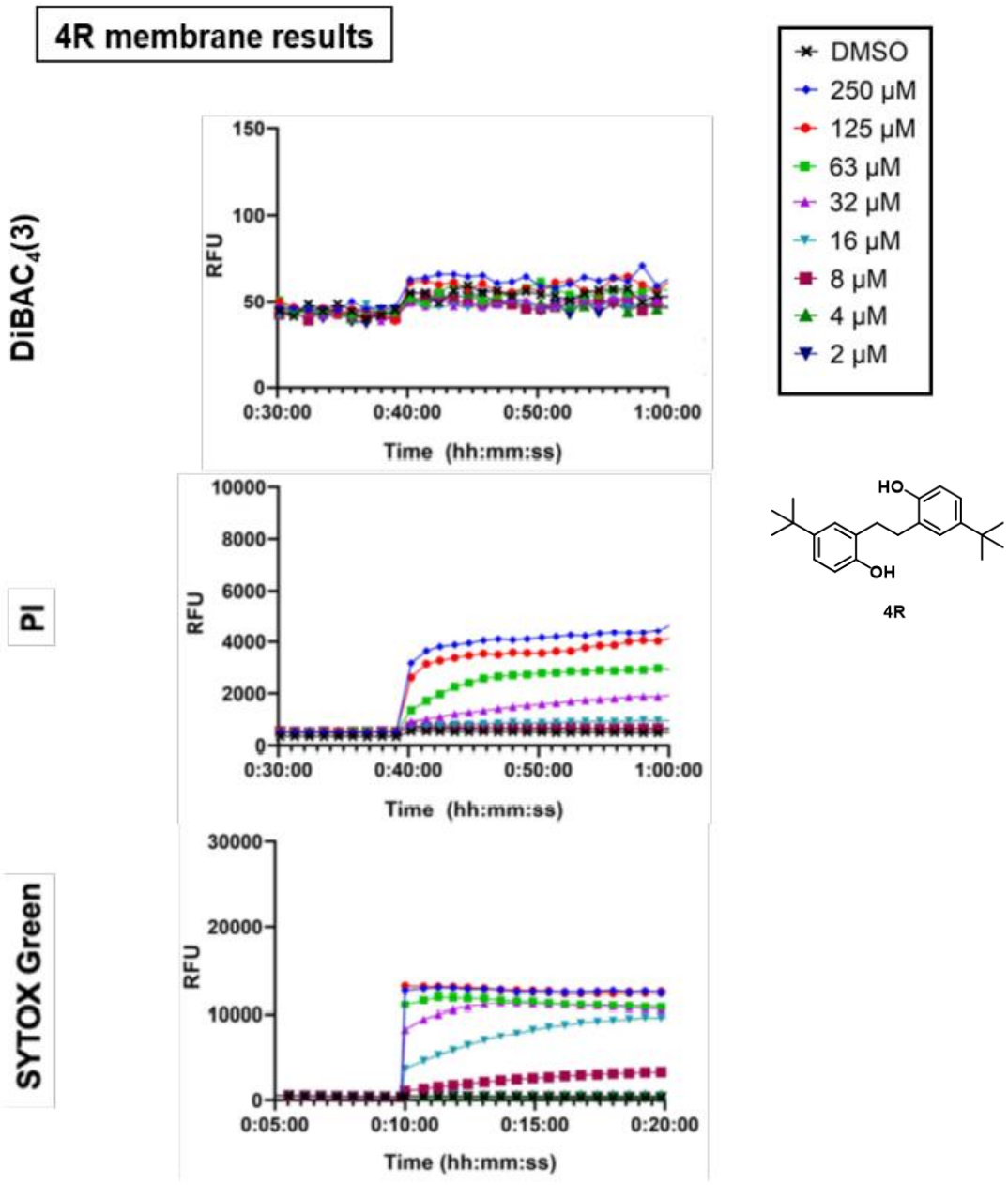
4R membrane results
DMSO
250 µM
125 µM
63 µM
32 µM
16 µM
8 µM
4 µM
2 µM
DiBAC4(3)
RFU
Time (hh:mm:ss)
PI
SYTOX Green
HO
OH
4R

Chapter 4: Ogipeptins

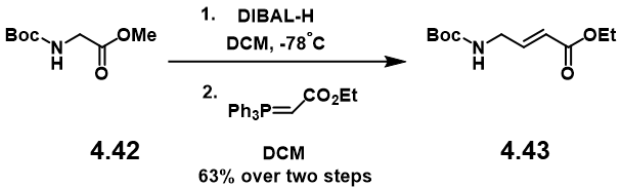

Ethyl (E)-4-((tert-butoxycarbonyl)amino)but-2-enoate (4.43). In flame dried round-bottom flask, atmosphere was exchanged (x3), and starting material (**4.42**, 404 mg, 2.135 mmol, 1 eq) was dissolved in dichloromethane. The septum was sealed to the reaction vessel with parafilm and then cooled to -78 ºC. Then, DIBAL-H (1.0 M in DCM) (1.5 eq) was added dropwise over the course of 30 min to prevent over-reduction. The reaction was allowed to stir at -78 ºC for 2 hours or until done under an argon balloon. The reaction mixture was TLC'ed in 3:1 Hex/EtOAc and stained in $KMnO_4$. The reaction was quenched at -78 ºC with 10 mL of methanol and then allowed to warm to room temperature. Next, it was quenched with 10 mL of water and allowed to stir for 30 min at room temperature. The reaction mixture was then concentrated down to remove dichloromethane and methanol. Following, the reaction mixture was gravity filtered, and the filtrate was extracted with EtOAc (x3), washed with brine (x3), dried over $MgSO_4$, filtered, and concentrated down to yield the title compound as a colorless oil. The worked up reaction mixture was taken crude into the Wittig after two hours on the hi-vac. In flame dried round-bottom flask, atmosphere was exchanged, and then ethyl 2-(triphenyl-λ^5-phosphaneylidene)acetate (1.1 eq) was added and dissolved in dichloromethane. Then, aldehyde was added in dichloromethane slowly, and the reaction was allowed to stir overnight at room temperature under an argon balloon. The reaction was TLC'ed in 3:1 Hex/EtOAc and stained in $KMnO_4$. The reaction mixture was concentrated down to remove the dichloromethane. Then, it was suspended in diethyl ether, filtered, and concentrated thrice to give a yellow oil that was purified via column chromatography. In order to achieve separation of the *cis* and *trans* isomers, the crude oil should be loaded in

toluene and a slow gradient of 0-45% EtOAc in hexanes performed to yield the title compound as a colorless oil (318 mg, 65% yield). ^{1}H NMR (399 MHz, Acetone-d_6) δ 6.89 (dt, J = 15.7, 4.8 Hz, 1H), 6.34 (s, 1H), 5.90 (dt, J = 15.7, 1.9 Hz, 1H), 4.14 (q, J = 7.1 Hz, 2H), 3.93 – 3.79 (m, 2H), 1.42 (s, 9H), 1.24 (t, J = 7.1 Hz, 3H).

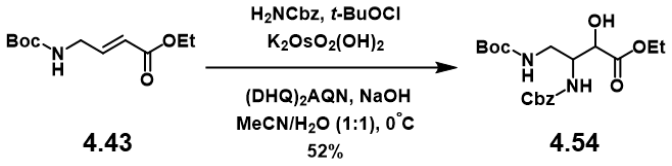

Ethyl 3-(((benzyloxy)carbonyl)amino)-4-((tert-butoxycarbonyl)amino)-2-hydroxybutanoate (4.54). In flame dried round-bottom flask, atmosphere was exchanged (x3). Then, 2 mL of MeCN and 2 mL of water were added to make a 1:1 solution of MeCN to water. Then, a 0.5 M solution of sodium hydroxide was added (2.96 eq, very important to not add more than necessary). Following that, benzyl carbamate (3.1 eq) is added to the reaction flask, and the reaction mixture is stirred until the solid benzyl carbamate totally dissolves. Once dissolved, the reaction is run in the dark: the reaction vessel is foiled and hood and overhead lights are turned off. Then, *t*-butyl hypochlorite (3 eq) is added to generate the chloroamine *in situ*. Then, the reaction is cooled to 0 ºC, and ligand ($(DHQ)_2AQN$, 0.05 eq) is added as a solid. Then, the alkene starting material (**4.43**, 129 mg, 0.563 mmol, 1 eq) is added in 3 mL MeCN (2 mL to add and 1 mL to wash). Then, K_2OsO_4•$2H_2O$ (0.04 eq) is added in 3 mL water (2 mL to add and 1 mL to wash). The reaction is sealed in the cooler under an argon balloon and run overnight. The reaction is then TLC'ed in 2:1 Hex/EtOAc and stained in ninhydrin. Next, the reaction is quenched with 2 crystals of thiosulfate (depending on scale), and the reaction mixture is stirred for 30 min at room temperature. The reaction mixture is then dilute and extracted with EtOAc (x3), dried over $MgSO_4$, filtered, concentrated, and purified by column chromatography (0 to 75% EtOAc in hexanes) to give a white solid (**4.54**, 118 mg, 53%). ^{1}H NMR (400 MHz, Methanol-d_4) δ 7.44 – 7.28 (m, 5H), 5.14 (d,

J = 1.8 Hz, 2H), 5.13 – 5.02 (m, 1H), 4.35 (s, 1H), 4.27 – 4.19 (m, 3H), 3.19 – 3.04 (m, 2H), 1.46 (s, 9H), 1.34 – 1.26 (t, 3H). ^{13}C NMR (151 MHz, Methanol-d_4) δ 128.08, 127.47, 48.03, 47.89, 47.75, 47.60, 47.46, 47.32, 47.18, 27.33, 13.04.

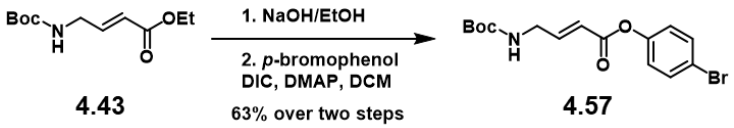

4.43 4.57

4-bromophenyl (E)-4-((tert-butoxycarbonyl)amino)but-2-enoate (4.57). In flame dried round bottom flask, atmosphere was exchanged and then vented. Then, starting material (**4.43**, 164 mg, 0.175 mmol, 1 eq) is dissolved in 4.3 mL ethanol. Then, the reaction mixture is cooled to 0 ºC and sodium hydroxide (1N, 1.2 eq) is added slowly. The reaction is vented and stirred overnight at 0 ºC. The reaction mixture is then TLC'ed in 3:1 Hex/EtOAc and stained with ninhydrin. The reaction mixture is then worked up via concentration down to dryness, cooled to 0 ºC, dissolved in water and EtOAc, and quenched slowly with 5% HCl solution. Then, the reaction mixture is extracted with EtOAc (x3), dried over $MgSO_4$, filtered, concentrated, and taken crude into the esterification. In a flame dried round bottom flask, atmosphere was exchanged (x3), and 4-bromophenol (1.5 eq) is added to the flask. Acid starting material (116 mg, 0.576 mmol, 1 eq) is dissolved in dichloromethane and transferred to the reaction vessel. Then, DIC (4 eq) is added to the flask, the contents allowed to stir for 5 min, and then DMAP (0.5 eq) is added. The reaction is stirred overnight under an argon balloon at room temperature. The reaction was then TLC'ed in 3:1 Hex/EtOAc and stained in ninhydrin. The reaction mixture was then concentrated down and purified by column chromatography to give the title compound as a white solid (55 mg, 84%). ^{1}H NMR (600 MHz, Methanol-d_4) δ 7.57 – 7.42 (m, 2H), 7.12 (dt, *J* = 15.7, 4.6 Hz, 1H), 7.09 – 7.02 (m, 2H), 6.10 (d, *J* = 15.6 Hz, 1H), 3.90 (dd, *J* = 4.8, 2.0 Hz, 2H), 1.47 (d, *J* = 4.5 Hz, 9H).

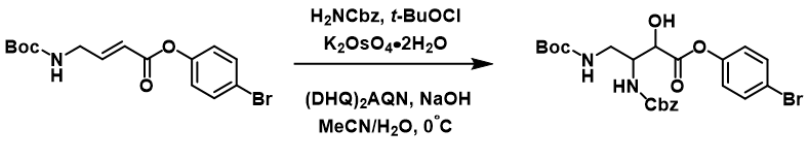

4.57 **S28**

4-bromophenyl 3-(((benzyloxy)carbonyl)amino)-4-((tert-butoxycarbonyl)amino)-2-hydroxybutanoate (S28). In flame dried round-bottom flask, atmosphere was exchanged (x3). Then, 2 mL of MeCN and 2 mL of water were added to make a 1:1 solution of MeCN to water. Then, a 0.5 M solution of sodium hydroxide was added (2.96 eq, very important to not add more than necessary). Following that, benzyl carbamate (3.1 eq) is added to the reaction flask, and the reaction mixture is stirred until the solid benzyl carbamate totally dissolves. Once dissolved, the reaction is run in the dark: the reaction vessel is foiled and hood and overhead lights are turned off. Then, *t*-butyl hypochlorite (3 eq) is added to generate the chloroamine *in situ*. Then, the reaction is cooled to 0 ºC, and ligand ($(DHQ)_2AQN$, 0.05 eq) is added as a solid. Then, the alkene starting material (**4.57**, 78 mg, 0.219 mmol, 1 eq) is added in 3 mL MeCN (2 mL to add and 1 mL to wash). Then, $K_2OsO_4•2H_2O$ (0.04 eq) is added in 3 mL water (2 mL to add and 1 mL to wash). The reaction is sealed in the cooler under an argon balloon and run overnight. The reaction is then TLC'ed in 2:1 Hex/EtOAc and stained in ninhydrin. Next, the reaction is quenched with 2 crystals of thiosulfate (depending on scale), and the reaction mixture is stirred for 30 min at room temperature. The reaction mixture is then dilute and extracted with EtOAc (x3), dried over $MgSO_4$, filtered, concentrated, and purified by column chromatography (0 to 75% EtOAc in hexanes) to give a white solid (**4.57**, 25 mg, 22%). ^{1}H NMR (400 MHz, Methanol-d_4) δ 7.60 – 7.51 (m, 1H), 7.43 – 7.32 (m, 5H), 7.13 – 7.06 (m, 1H), 5.27 – 5.21 (m, 1H), 5.19 – 5.12 (m, 2H), 5.07 (s, 1H), 4.59 (dd, *J* = 32.4, 2.3 Hz, 1H), 4.37 (td, *J* = 6.8, 2.4 Hz, 1H), 3.26 – 3.13 (m, 1H), 1.46 (d, *J* = 4.7 Hz, 9H).

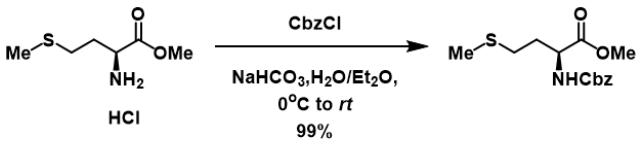

4.61 **S29**

Methyl ((benzyloxy)carbonyl)-L-methioninate (S29). In a flame dried round bottom flask, atmosphere was exchanged (x3). Then, starting material (**4.61**, 3140 mg, 15.724 mmol, 1 eq) and sodium bicarbonate (5 eq) were dissolved in water, and an equal amount of diethyl ether was added to the reaction flask. The reaction was cooled to 0 ºC and benzyl chloroformate (1.25 eq) was added slowly over a period of about one hour. The reaction was stirred for a few hours under an argon balloon and then TLC'ed in 9:1 DCM/MeOH (methanol used contains 2% ammonium hydroxide) and stained in ninhydrin. Then after the reaction was done, glycine (0.2 eq) was added to quench the reaction mixture. Then, the reaction was extracted with diethyl ether (x3), and the organic layer was washed with 0.01 M HCl, water, and brine. Then, the organic layer was dried over $MgSO_4$, filtered, concentrated, and carried crude into the oxidation as a light yellow oil (4652 mg, 99%). ^{1}H NMR (600 MHz, Chloroform-*d*) δ 7.41 – 7.30 (m, 5H), 5.39 (d, *J* = 7.9 Hz, 1H), 5.12 (s, 2H), 4.51 (q, *J* = 7.2 Hz, 1H), 3.76 (s, 3H), 2.58 – 2.47 (m, 2H), 2.16 (d, *J* = 7.0 Hz, 1H), 2.09 (s, 3H), 1.97 (dq, *J* = 14.6, 7.4 Hz, 1H).

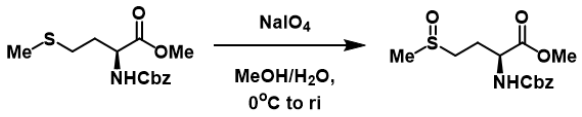

S29 **4.62**

Methyl (2S)-2-(((benzyloxy)carbonyl)amino)-4-(methylsulfinyl)butanoate (4.62). In a flame dried Morton flask, atmosphere was exchanged (x3). Then, starting material (**S29**, 683 mg, 2.297 mmol, 1 eq) was dissolved in methanol and cooled to 0ºC. Then, sodium periodate (1.1 eq) in

water was added dropwise via addition funnel. Cooling bath was removed, and the reaction was allowed to stir overnight under an argon balloon at room temperature. The reaction was TLC'ed in 9:1 DCM/MeOH (methanol used contains 2% ammonium hydroxide) and stained in ninhydrin. The reaction mixture was then filtered through celite, extracted with dichloromethane (x3), washed with water and brine, dried over $MgSO_4$, filtered, concentrated, and purified by column chromatography to yield the title compound as a white solid (623 mg, 88%). ^{1}H NMR (600 MHz, Chloroform-*d*) δ 7.38 (d, *J* = 2.7 Hz, 5H), 5.65 (s, 1H), 5.14 (s, 2H), 4.54 (d, *J* = 16.0 Hz, 1H), 3.80 (s, 3H), 2.78 (d, *J* = 39.6 Hz, 2H), 2.64 – 2.50 (m, 3H), 2.43 (s, 2H).

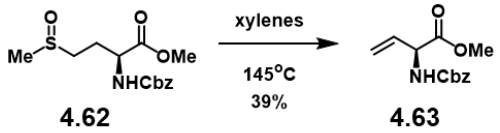

4.62 **4.63**

Methyl (S)-2-(((benzyloxy)carbonyl)amino)but-3-enoate (4.63). In a flame dried round bottom flask, atmosphere was exchanged (x3), and starting material (**4.62**, 718 mg, 2.291 mmol, 1eq) was dissolved in xylenes. The reaction mixture was then heated to reflux and allowed to reflux overnight under an argon balloon. The reaction was TLC'ed in 2:1 Hex/EtOAc and stained with ninhydrin. The reaction mixture was then allowed to cool to room temperature, concentrated down (with bleach rotovap setup), and purified by column chromatography to give a yellow oil (225 mg, 39%). ^{1}H NMR (600 MHz, Deuterium Oxide) δ 7.43 – 7.25 (m, 5H), 5.91 (s, 1H), 5.34 – 5.27 (m, 2H), 5.08 (s, 2H), 3.69 (s, 3H).

Methyl (S)-2-(((benzyloxy)carbonyl)amino)-2-((S)-oxiran-2-yl)acetate (4.64). In flamed dried

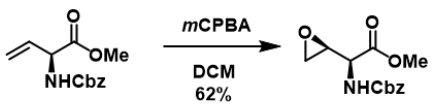

4.63 **4.64**

round bottom flask, atmosphere was exchanged (x3). Then, the starting material (**4.63**, 171 mg, 0.686 mmol, 1 eq) was dissolved in dichloromethane, and *m*CPBA added (5 eq). The reaction

was stirred overnight at room temperature under an argon balloon. The reaction was then TLC'ed in 2:1 Hex/EtOAc and stained in ninhydrin. The reaction mixture was then poured into a saturated aqueous solution of sodium bicarbonate and separated. The reaction mixture was then extracted with dichloromethane (x3), washed with sat. aq. sodium bicarbonate, water, and brine. Then, the mixture was dried over $MgSO_4$, filtered, concentrated, and purified by column chromatography to yield the title compound as a white solid (113 mg, 62%). ^{1}H NMR (600 MHz, Chloroform-*d*) δ 7.43 – 7.31 (m, 5H), 5.34 – 5.21 (m, 1H), 5.19 – 5.07 (m, 2H), 4.74 (dd, *J* = 8.9, 2.3 Hz, 1H), 3.83 (d, *J* = 8.6 Hz, 3H), 2.85 – 2.65 (m, 2H).

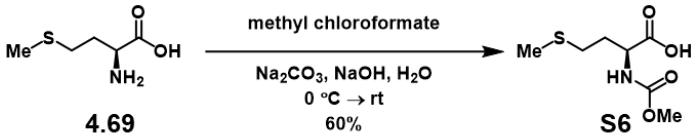

(Methoxycarbonyl)-L-methionine (S30). In flame dried RBF, atmosphere was exchanged (x3). Then, acid (**4.69**, 1000 mg, 6.702 mmol, 1 eq) was added to the RBF, followed by NaOH. Then, sodium carbonate was added. The reaction was cooled to 0 ºC and methyl chloroformate was added dropwise. The cooling bath was then removed and the reaction was stirred at room temperature under inert atmosphere overnight. Then, the reaction was diluted and separated with diethyl ether. The aqueous phase was cooled with an ice bath and acidified with concentrated HCL to pH of 1-2 to give the product (**S30**, 828 mg, 60%), which was telescoped into its next reactions (benzyl or *t*-butyl ester protection).

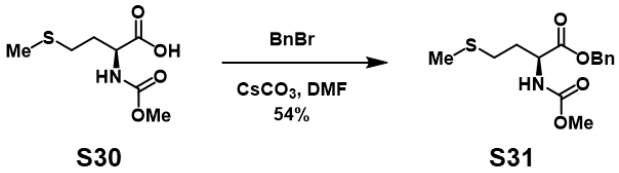

Benzyl (methoxycarbonyl)-L-methioninate (S31). In flame dried RBF, atmosphere was exchanged (x3). Then acid starting material (**S30**, 409 mg, 1.974 mmol, 1 equiv) was added and dissolved in DMF. Then, $CsCO_3$ was added and the mixture stirred for 30 min. Next, benzyl bromide was added and stirred overnight under inert atmosphere. The reaction mixture was then diluted with ethyl acetate and washed with saturated aqueous lithium bromide solution (x3), saturated sodium bicarbonate solution (x3), and brine (x2). Then, the organic layer was dried over magnesium sulfate, filtered, and concentrated. The crude product was then purified via column chromatography to give the product as a yellow oil (**S31**, 318 mg, 54%). ^{1}H NMR (600 MHz, Methanol-d_4) δ 7.42 – 7.25 (m, 5H), 5.25 – 5.06 (m, 2H), 4.37 (p, J = 7.2, 5.9 Hz, 1H), 3.65 – 3.59 (m, 3H), 2.59 – 2.40 (m, 2H), 2.07 (tt, J = 9.4, 8.1, 3.2 Hz, 1H), 2.04 – 2.01 (m, 3H), 1.95 – 1.88 (m, 1H).

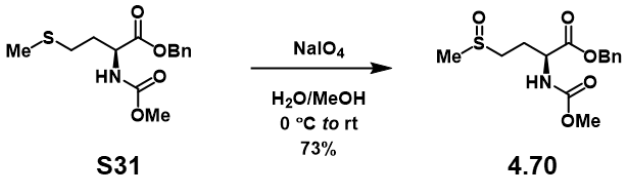

S31 **4.70**

Benzyl (2S)-2-((methoxycarbonyl)amino)-4-(methylsulfinyl)butanoate (4.70). In flame dried RBF, atmosphere was exchanged (x3). Then, benzyl ester (**S31**, 312 mg, 1.049 mmol, 1 equiv) was added in methanol and then cooled to 0 ºC. Next, sodium periodate was added in water dropwise via addition funnel. The reaction mixture was stirred under inert atmosphere overnight at room temperature. Next, the reaction mixture was filtered through celite and concentrated down. It was then diluted with DCM and separated (x3), washed with water and brine, dried over magnesium sulfate, filtered, and concentrated. It was then purified by column chromatrography. ^{1}H NMR (400 MHz, Methanol-d_4) δ 7.44 – 7.31 (m, 6H), 5.26 – 5.16 (m, 2H), 4.39 (dt, J = 9.3, 5.1

Hz, 1H), 3.67 (s, 3H), 2.90 – 2.77 (m, 2H), 2.63 (d, *J* = 3.5 Hz, 3H), 2.32 (tt, *J* = 10.5, 5.3 Hz, 1H), 2.10 (ddt, *J* = 15.2, 10.2, 5.3 Hz, 1H).

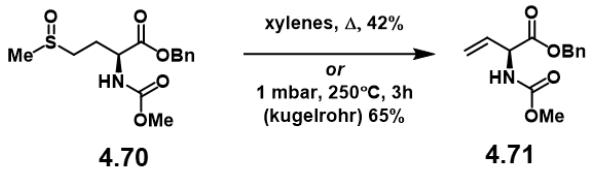

4.70 **4.71**

Benzyl (S)-2-((methoxycarbonyl)amino)but-3-enoate (4.71). In a flame dried round bottom flask, atmosphere was exchanged (x3), and starting material (**4.70**, 451 mg, 1.439 mmol, 1 equiv) was dissolved in xylenes. The reaction mixture was then heated to reflux and allowed to reflux overnight under an argon balloon. The reaction was TLC'ed in 2:1 Hex/EtOAc and stained with ninhydrin. The reaction mixture was then allowed to cool to room temperature, concentrated down (with bleach rotovap setup), and purified by column chromatography to give a yellow oil (149 mg, 42%). ^{1}H NMR (400 MHz, Methanol-d_4) δ 7.43 – 7.29 (m, 6H), 5.95 (ddd, *J* = 16.7, 10.4, 6.0 Hz, 1H), 5.35 (ddd, *J* = 17.2, 1.8, 0.9 Hz, 1H), 5.31 – 5.22 (m, 1H), 3.66 (s, 3H).

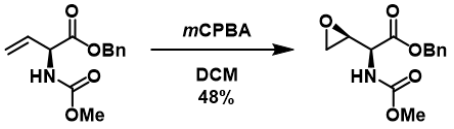

4.71 **4.74**

Benzyl (S)-2-((methoxycarbonyl)amino)-2-((S)-oxiran-2-yl)acetate (4.74). In flamed dried round bottom flask, atmosphere was exchanged (x3). Then, the starting material (**4.71**, 149 mg, 0.598 mmol, 1 eq) was dissolved in dichloromethane, and *m*CPBA added (5 eq). The reaction was stirred overnight at room temperature under an argon balloon. The reaction was then TLC'ed in 2:1 Hex/EtOAc and stained in ninhydrin. The reaction mixture was then poured into a saturated aqueous solution of sodium bicarbonate and separated. The reaction mixture was then extracted with dichloromethane (x3), washed with sat. aq. sodium bicarbonate, water, and brine. Then, the mixture was dried over $MgSO_4$, filtered, concentrated, and purified by column chromatography to

yield the title compound (76 mg, 48%). ^{1}H NMR (600 MHz, Methanol-d_4) δ 7.44 – 7.29 (m, 4H), 5.31 – 5.18 (m, 2H), 4.39 – 4.30 (m, 1H), 4.12 (q, *J* = 7.1 Hz, 1H), 3.67 (d, *J* = 5.1 Hz, 3H), 2.85

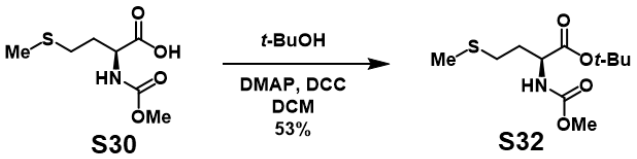

– 2.66 (m, 2H).

***tert*-butyl (methoxycarbonyl)-L-methioninate (S32)**. In flame dried RBF, atmosphere was exchanged (x3). Then, DCC was added and dissolved in DCM. Then, the reaction was cooled to 0 ºC and DMAP and *t*-BuOH were added to the RBF. Next, acid starting material (**S30**, 409 mg, 1.974 mmol, 1 equiv) was added to the flask in DCM over about 15 min. Then, the reaction was stirred at 0 ºC for 1 hour. Then, the reaction was stirred overnight at room temperature under inert atmosphere. Next, the reaction mixture was concentrated down, dissolved in ethyl acetate, filtered through celite, diluted with water, and washed with 10% citric acid solution, saturated aqueous sodium bicarbonate solution (x2), and brine. The mixture was then dried over magnesium sulfate, filtered, concentrated, and then purified via column chromatography to give the product (**S32**, 273 mg, 53%). ^{1}H NMR (600 MHz, Methanol-d_4) δ 4.20 (dd, *J* = 9.9, 5.4 Hz, 1H), 3.65 (s, 3H), 2.60 – 2.46 (m, 2H), 2.11 – 2.06 (m, 3H), 2.06 – 2.00 (m, 1H), 1.89 (ddt, *J* = 13.2, 8.7, 4.4 Hz, 1H), 1.49 – 1.43 (m, 9H).

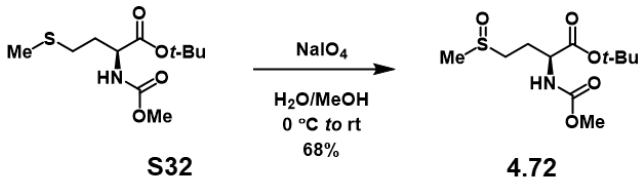

***tert*-butyl (2S)-2-((methoxycarbonyl)amino)-4-(methylsulfinyl)butanoate (4.72)**. In flame dried RBF, atmosphere was exchanged (x3). Then, benzyl ester (**S32**, 599 mg, 2.275 mmol, 1 equiv) was added in methanol and then cooled to 0 ºC. Next, sodium periodate was added in water dropwise via addition funnel. The reaction mixture was stirred under inert atmosphere overnight at room temperature. Next, the reaction mixture was filtered through celite and concentrated down. It was then diluted with DCM and separated (x3), washed with water and brine, dried over magnesium sulfate, filtered, and concentrated. It was then purified by column chromatrography to give the product (**4.72**, 431 mg, 68%). ^{1}H NMR (600 MHz, Methanol-d_4) δ 5.25 – 5.10 (m, 2H), 4.36 (s, 1H), 3.70 – 3.57 (m, 3H), 2.90 – 2.68 (m, 1H), 2.66 – 2.47 (m, 2H), 2.32 (d, *J* = 28.5 Hz, 1H), 2.10 (d, *J* = 9.6 Hz, 1H).

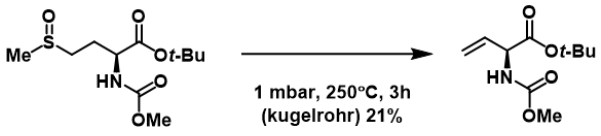

4.72 **4.73**

***tert*-butyl (S)-2-((methoxycarbonyl)amino)but-3-enoate (4.73)**. Use nomograph to confirm temperature at currently measured pressure from hi-vac needed to distill elimination product. Transfer starting material (**4.72**, 601 mg, 2.151 mmol, 1 equiv) into small round bottom and dry on hi-vac overnight before performing procedure. Next, set kugelrohr to temperature (260 ºC). Cool receiving flask with ice bath (product collects at mouth of receiving flask when dry ice/acetone used, which is not ideal). Spin at 20 rpm under 1 mbar of pressure to force elimination and obtain product (**4.73**, 95 mg, 21%, product impure). Perform in hood due to evolution of sulfur gas. ^{1}H NMR (400 MHz, Methanol-d_4) δ 5.42 – 5.14 (m, 1H), 4.19 (td, *J* = 9.0, 4.9 Hz, 1H), 3.67 – 3.65 (m, 5H), 1.49 – 1.46 (m, 9H).

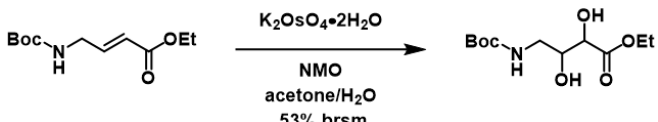

4.43 ***race*-4.80**

Ethyl 4-((tert-butoxycarbonyl)amino)-2,3-dihydroxybutanoate (*race*-4.80). In a flame dried round bottom flask, atmosphere was exchanged (x3). Then, starting material (**4.43**, 368 mg, 1.605 mmol, 1 eq) was dissolved in acetone. Water was added to make a 9:1 solution acetone to water. Then, NMO (1 eq) was added to the flask. The reaction mixture was stirred, and then potassium osmium tetroxide dihydrate (0.1 eq) was added. The reaction was allowed to stir overnight at room temperature under an argon balloon. The reaction was TLC'ed in 9:1 DCM/MeOH (methanol was 2% triethylamine) and stained in ninhydrin. The reaction was quenched with saturated aqueous sodium metabisulfite (100 mL), extracted with EtOAc (x3), washed with brine, dried over $MgSO_4$, filtered, concentrated, and purified via column chromatrography to yield the title racemic compound (209 mg, 49%). ^{1}H NMR (600 MHz, Methanol-d_4) δ 4.22 (qd, J = 7.1, 2.3 Hz, 2H), 4.13 (d, J = 2.3 Hz, 1H), 4.00 – 3.90 (m, 1H), 3.28 – 3.10 (m, 2H), 1.44 (s, 9H), 1.28 (t, J = 7.1 Hz, 3H).

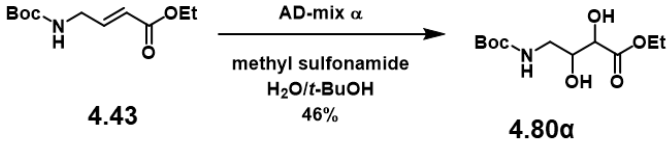

4.43 4.80α

Ethyl 4-((tert-butoxycarbonyl)amino)-2,3-dihydroxybutanoate (4.80α). In flame dried round bottom flask, atmosphere was exchanged (x3). Then, a 1:1 solution of *t*-BuOH and water was prepared in the flask, and AD mix (1.8 eq) and methyl sulfonamide (1 eq) were added to the reaction vessel. The reaction was stirred until the mixture was homogeneous. Then, the reaction was cooled to 0 ºC and stirred until an orange precipitate formed (about 15 min). Then, starting material (**4.43**, 246 mg, 1.073 mmol, 1 eq) was added, and the reaction stirred for 1 h at 0 ºC. Then, the reaction was stirred overnight at room temperature under an argon balloon. The reaction was TLC'ed in 2:1 Hex/EtOAc and stained in ninhydrin. The reaction was quenched with

1.8 eq of sodium thiosulfate and stirred for 1 h. Then, the reaction mixture was extracted with EtOAc(x3), dried over $MgSO_4$, filtered, concentrated, and purified by column chromatography to yield the title compound as a white solid (131 mg, 46%). ^{1}H NMR (500 MHz, Methanol-d_4) δ 7.70 – 7.53 (m, 1H), 4.22 (qd, *J* = 7.1, 1.8 Hz, 2H), 4.14 (d, *J* = 2.2 Hz, 1H), 4.01 – 3.92 (m, 1H), 3.29 – 3.12 (m, 2H), 1.44 (s, 9H), 1.29 (t, *J* = 7.1 Hz, 3H).

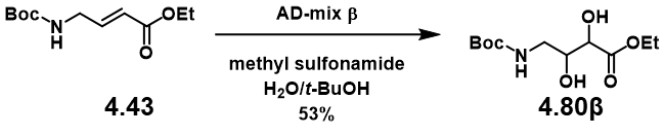

4.43 4.80β

Ethyl 4-((tert-butoxycarbonyl)amino)-2,3-dihydroxybutanoate (4.80β). In flame dried round bottom flask, atmosphere was exchanged (x3). Then, a 1:1 solution of *t*-BuOH and water was prepared in the flask, and AD mix (1.8 eq) and methyl sulfonamide (1 eq) were added to the reaction vessel. The reaction was stirred until the mixture was homogeneous. Then, the reaction was cooled to 0 ºC and stirred until an orange precipitate formed (about 15 min). Then, starting material (**4.43**, 189 mg, 0.824 mmol, 1 eq) was added, and the reaction stirred for 1 h at 0 ºC. Then, the reaction was stirred overnight at room temperature under an argon balloon. The reaction was TLC'ed in 2:1 Hex/EtOAc and stained in ninhydrin. The reaction was quenched with 1.8 eq of sodium thiosulfate and stirred for 1 h. Then, the reaction mixture was extracted with EtOAc(x3), dried over $MgSO_4$, filtered, concentrated, and purified by column chromatography to yield the title compound as a white solid (114 mg, 53%). ^{1}H NMR (600 MHz, Methanol-d_4) δ 4.28 – 4.17 (m, 2H), 4.13 (t, *J* = 2.6 Hz, 1H), 3.97 (d, *J* = 8.7 Hz, 1H), 3.28 – 3.12 (m, 2H), 1.43 (d, *J* = 4.6 Hz, 9H), 1.31 – 1.23 (m, 3H).

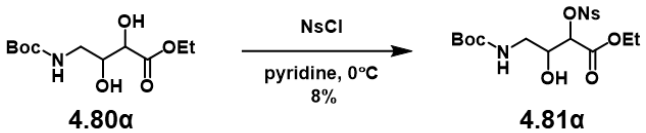

4.80α 4.81α

Ethyl 4-((tert-butoxycarbonyl)amino)-3-hydroxy-2-(((4-nitrophenyl)sulfonyl)oxy)butanoate (4.81α). In a vial, atmosphere was exchanged (x3). Starting material (**4.80α**, 65 mg, 0.247 mmol, 1 eq) was added to the vial. The reaction flask was cooled to 0 ºC and dry pyridine was added to make a 0.3M solution. After stirring for 10 min, nosyl chloride (1 eq) was added to the vial, and the vial was capped and placed inside the fridge overnight. The reaction was TLC'ed in 2:1 Hex/EtOAc and stain in ninhydrin. Afterward, the reaction was quenched with ice chips and then water was added. The reaction mixture was then extracted with diethyl ether (x3), washed with sat. aq. copper sulfate to remove pyridine (x3), and a water wash. The reaction mixture was then dried over $MgSO_4$, filtered, concentrated, and immediately purified via column chromatography to prevent rearrangement to yield the title compound (9 mg, 8%). ^{1}H NMR (600 MHz, Methanol-d_4) δ 8.46 (tq, *J* = 7.4, 2.6 Hz, 2H), 8.24 (dq, *J* = 9.8, 2.6 Hz, 2H), 5.15 (d, *J* = 2.8 Hz, 1H), 4.25 – 4.04 (m, 3H), 3.10 (ddd, *J* = 47.7, 13.8, 6.6 Hz, 2H), 1.49 – 1.36 (m, 9H), 1.19 (td, *J* = 7.4, 2.1 Hz, 3H).

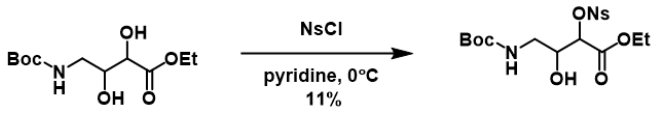

4.80β **4.81β**

Ethyl 4-((tert-butoxycarbonyl)amino)-3-hydroxy-2-(((4-nitrophenyl)sulfonyl)oxy)butanoate (4.81β). In a vial, atmosphere was exchanged (x3). Starting material (**4.80β**, 37 mg, 0.141 mmol, 1 eq) was added to the vial. The reaction flask was cooled to 0 ºC and dry pyridine was added to make a 0.3M solution. After stirring for 10 min, nosyl chloride (1 eq) was added to the vial, and the vial was capped and placed inside the fridge overnight. The reaction was TLC'ed in 2:1 Hex/EtOAc and stain in ninhydrin. Afterward, the reaction was quenched with ice chips and then water was added. The reaction mixture was then extracted with diethyl ether (x3), washed with sat. aq. copper sulfate to remove pyridine (x3), and a water wash. The reaction mixture was then

dried over $MgSO_4$, filtered, concentrated, and immediately purified via column chromatography to prevent rearrangement to yield the title compound (7 mg, 11%). ^{1}H NMR (600 MHz, Methanol-d_4) δ 8.51 – 8.40 (m, 2H), 8.29 – 8.16 (m, 2H), 5.17 – 5.09 (m, 1H), 4.19 – 4.03 (m, 3H), 3.22 – 2.98 (m, 2H), 1.43 (d, *J* = 6.0 Hz, 9H), 1.19 (dd, *J* = 7.7, 6.5 Hz, 3H).

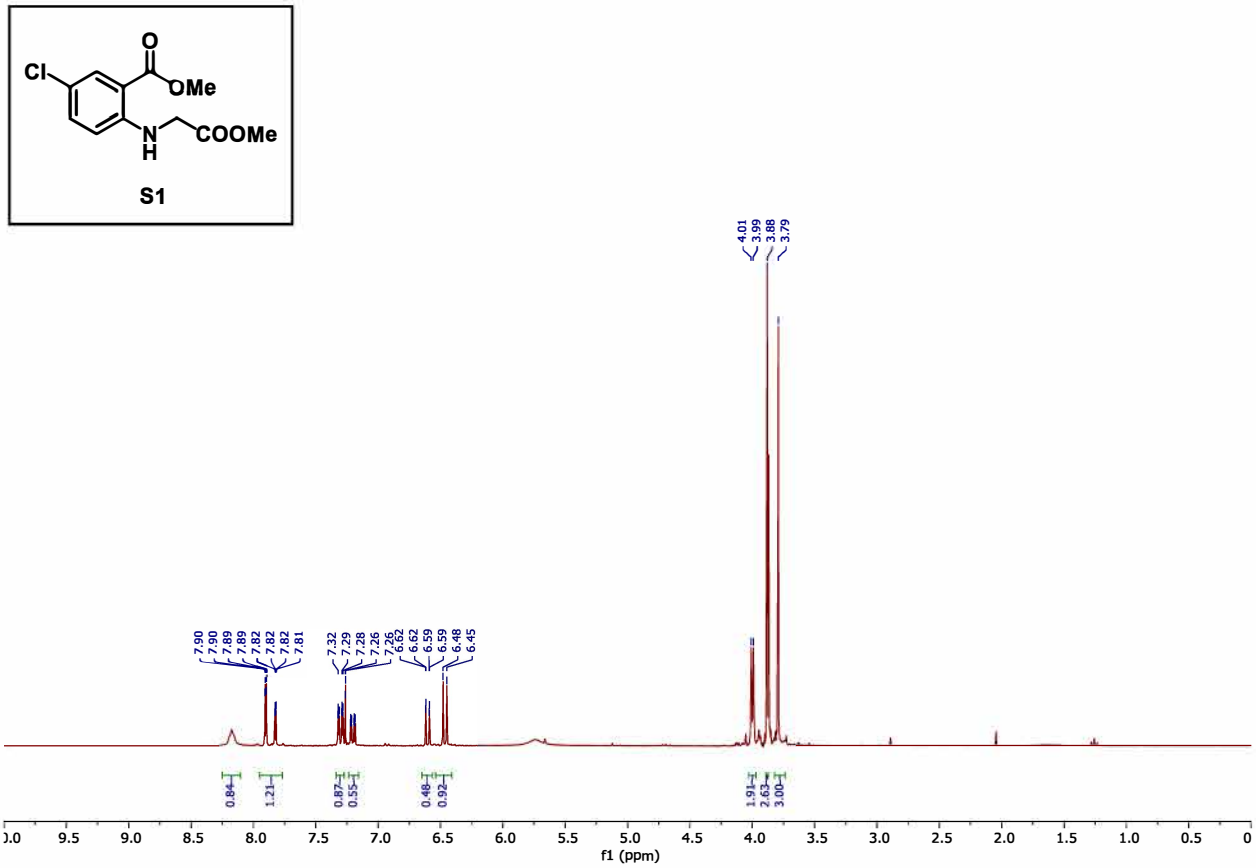
Cl
O
OMe
N
H
COOMe
S1
4.01
3.99
3.88
3.79
7.90
7.90
7.89
7.89
7.82
7.82
7.82
7.81
7.32
7.29
7.28
7.26
7.26
6.62
6.59
6.59
6.48
6.45
0.84
1.21
0.87
0.55
0.48
0.92
1.91
2.63
3.00
f1 (ppm)

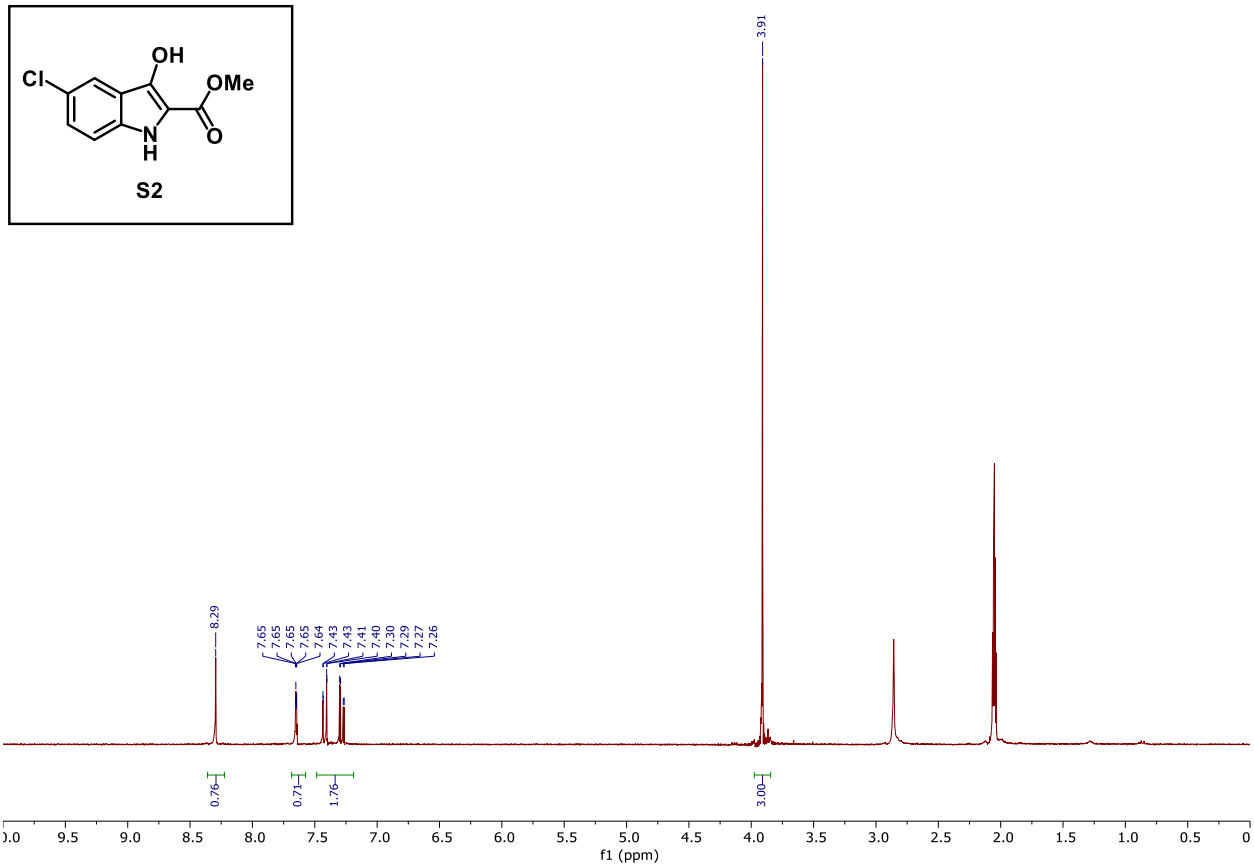
OH
Cl
OMe
N
H
O
S2
3.91
8.29
7.65
7.65
7.65
7.65
7.64
7.43
7.43
7.41
7.40
7.30
7.29
7.27
7.26
0.76
0.71
1.76
3.00
f1 (ppm)

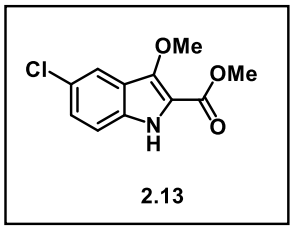
OMe
Cl
OMe
N
H
O

2.13

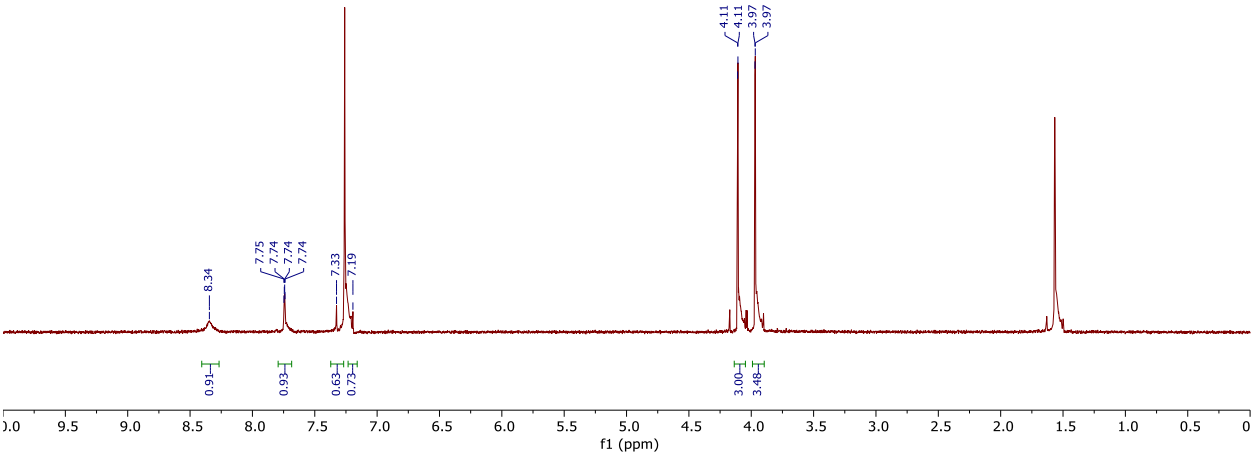
8.34
7.75
7.74
7.74
7.74
7.33
7.19
4.11
4.11
3.97
3.97
0.91
0.93
0.63
0.73
3.00
3.48
f1 (ppm)

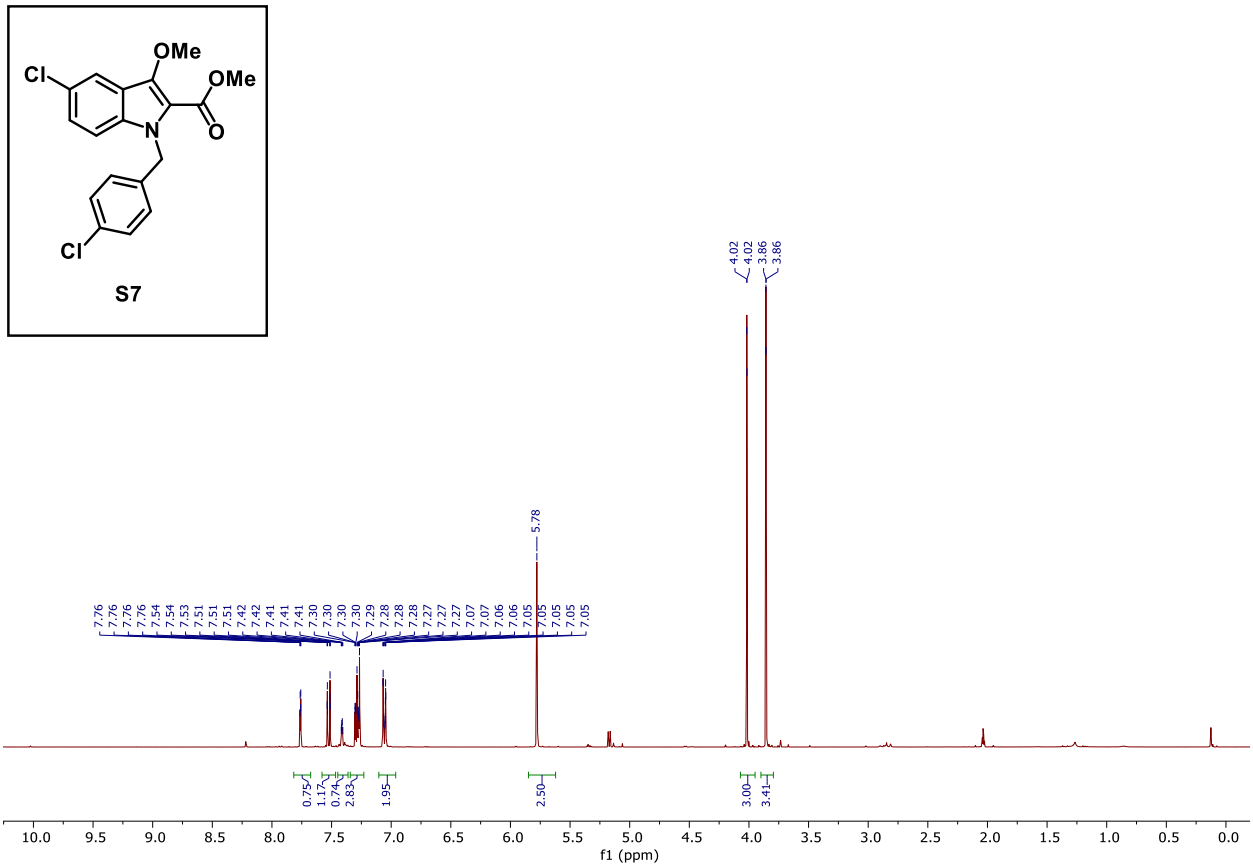
OMe
Cl
OMe
N
O
Cl
S7
4.02
4.02
3.86
3.86
5.78
7.76
7.76
7.76
7.76
7.54
7.54
7.53
7.51
7.51
7.51
7.42
7.42
7.41
7.41
7.41
7.30
7.30
7.30
7.29
7.28
7.28
7.27
7.27
7.27
7.07
7.07
7.06
7.06
7.05
7.05
7.05
7.05
0.75
1.17
0.74
2.83
1.95
2.50
3.00
3.41
10.0
9.5
9.0
8.5
8.0
7.5
7.0
6.5
6.0
5.5
5.0
4.5
4.0
3.5
3.0
2.5
2.0
1.5
1.0
0.5
0.0
f1 (ppm)

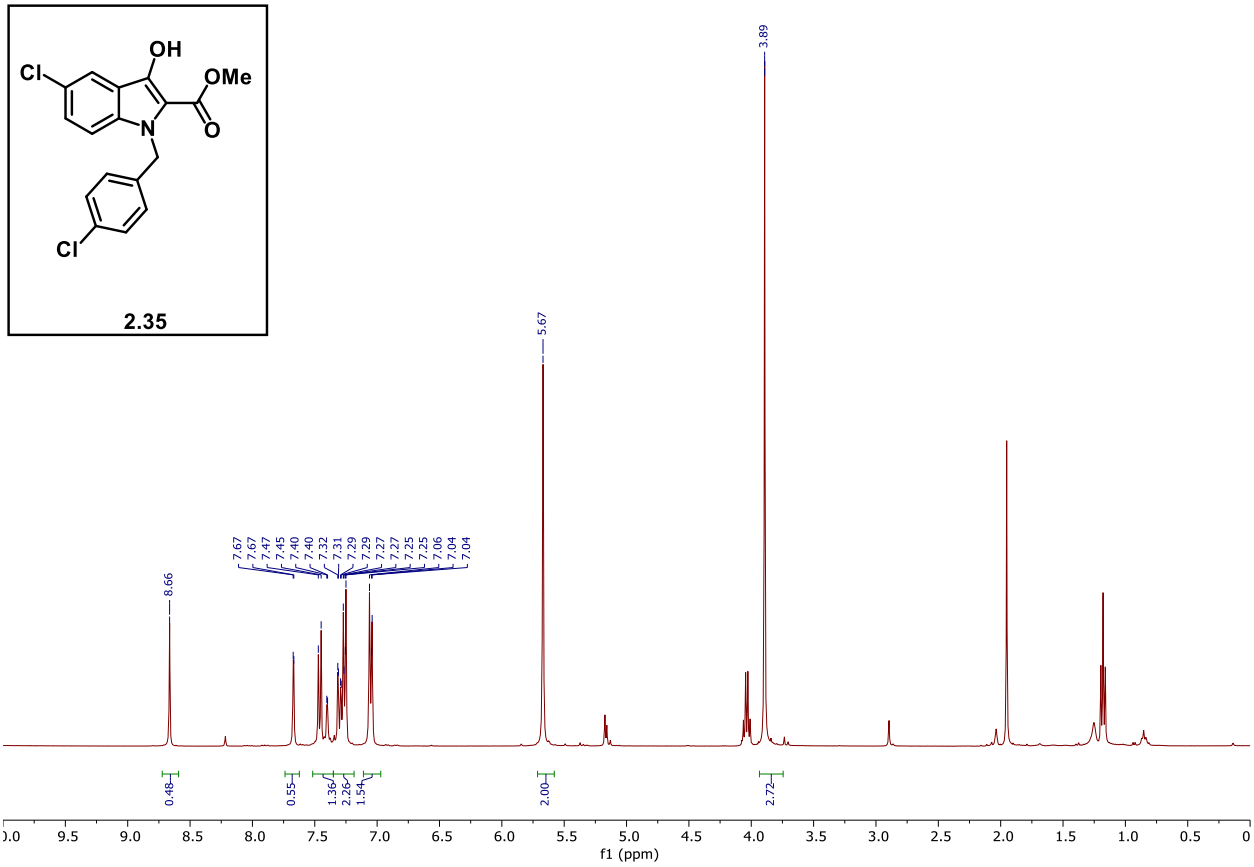
OH
Cl
OMe
N
O
Cl
2.35
3.89
5.67
8.66
7.67
7.67
7.47
7.45
7.40
7.40
7.32
7.31
7.29
7.29
7.27
7.27
7.25
7.25
7.06
7.04
7.04
0.48
0.55
1.36
2.26
1.54
2.00
2.72
f1 (ppm)

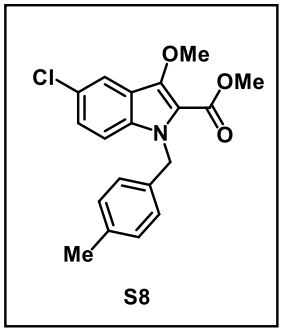
OMe
Cl
OMe
N
O
Me

S8

4.01
3.86
5.74
7.75
7.74
7.74
7.74
7.74
7.74
7.54
7.53
7.53
7.51
7.51
7.51
7.51
7.29
7.29
7.28
7.28
7.26
7.26
7.26
7.26
7.26
7.06
7.05
7.05
7.05
7.05
7.05
7.04
7.03
6.95
6.94
6.93
6.93
0.74
0.94
0.86
3.60
2.00
2.71
2.87
9.5
9.0
8.5
8.0
7.5
7.0
6.5
6.0
5.5
5.0
4.5
4.0
3.5
3.0
2.5
2.0
1.5
1.0
0.5
0
f1 (ppm)

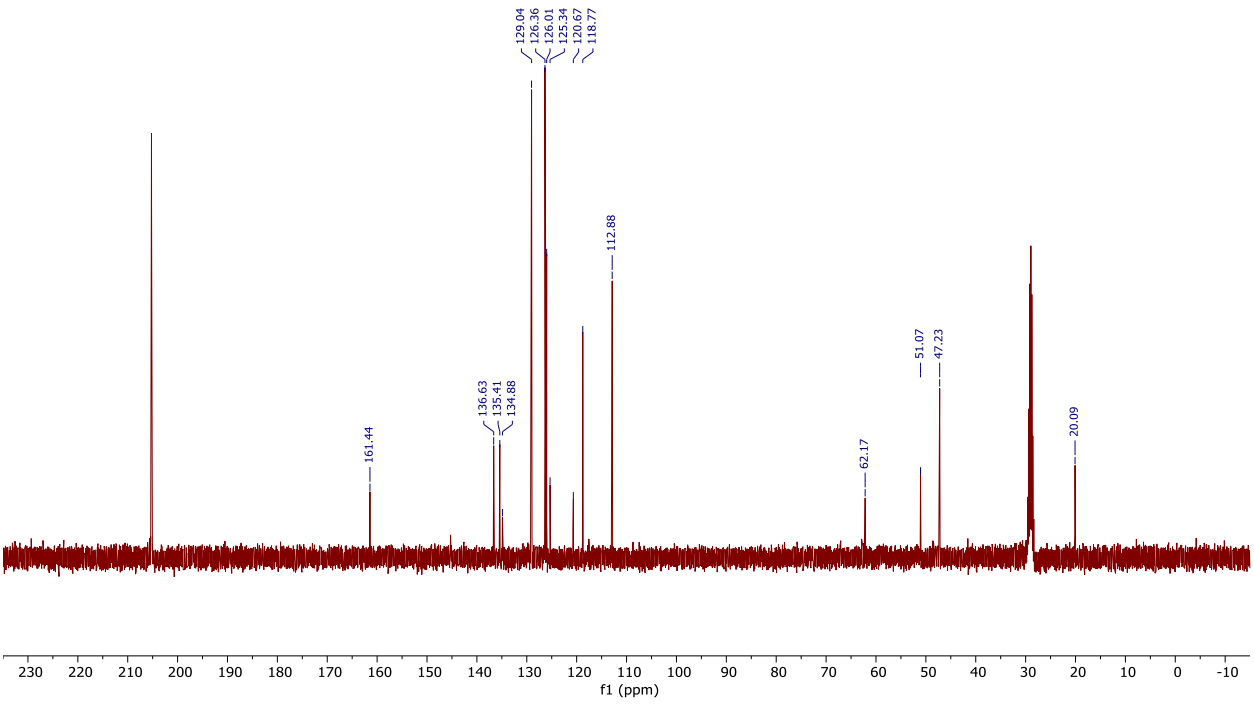
129.04
126.36
126.01
125.34
120.67
118.77
112.88
136.62
135.41
134.88
161.44
62.17
51.07
47.23
20.09
230
220
210
200
190
180
170
160
150
140
130
120
110
100
90
80
70
60
50
40
30
20
10
0
-10
f1 (ppm)

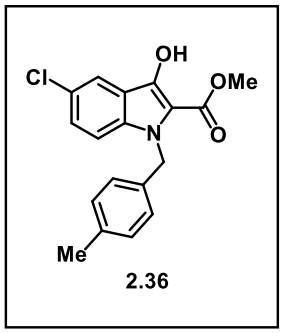
OH
Cl
OMe
N
O
Me

2.36

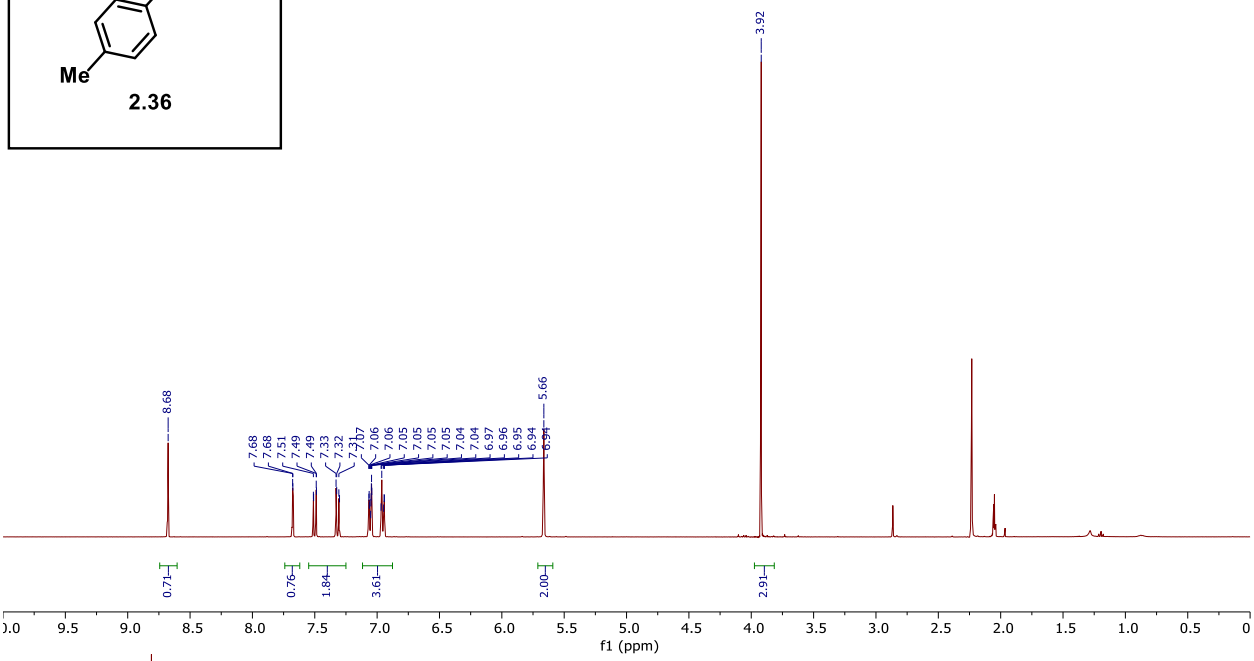
3.92
8.68
7.68
7.68
7.51
7.49
7.49
7.33
7.32
7.31
7.07
7.06
7.06
7.05
7.05
7.05
7.04
7.04
6.97
6.96
6.95
6.94
6.91
5.66
0.71
0.76
1.84
3.61
2.00
2.91
f1 (ppm)

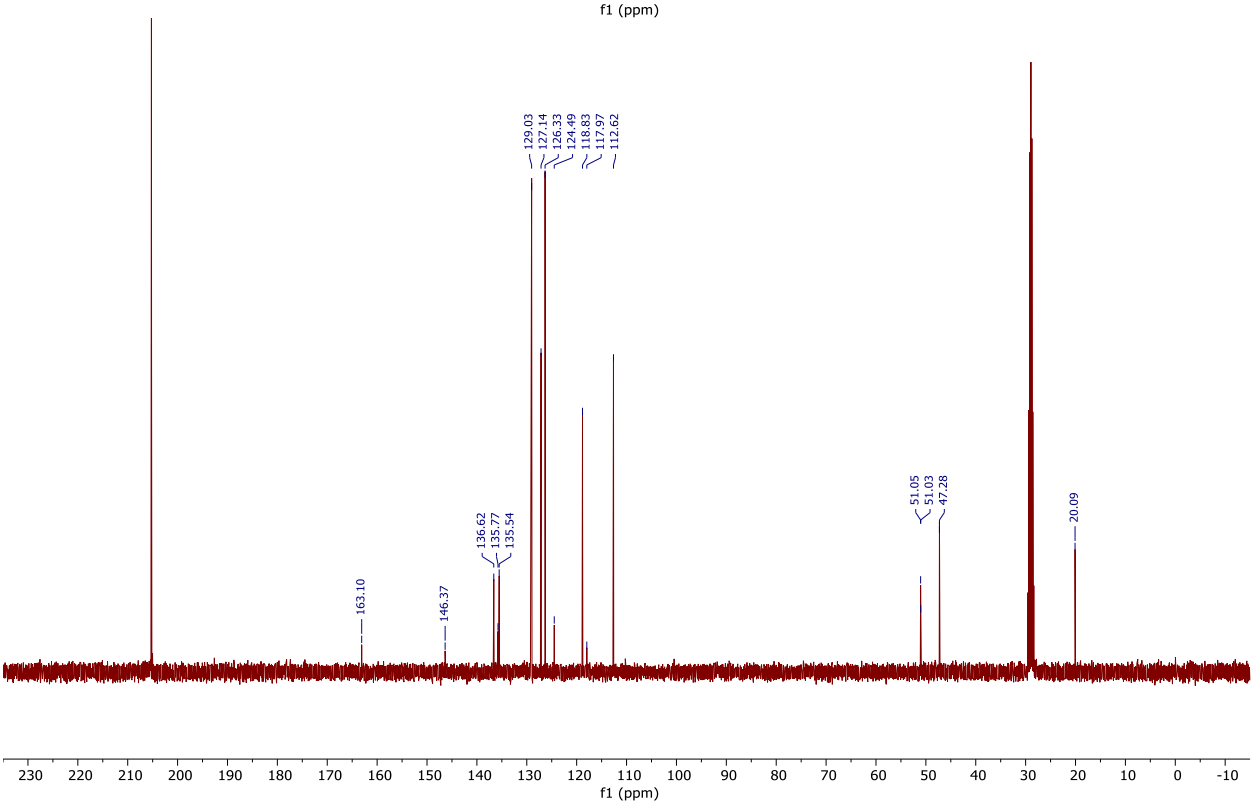
129.03
127.14
126.33
124.49
118.83
117.97
112.62
163.10
146.37
136.62
135.77
135.54
51.05
51.03
47.28
20.09
f1 (ppm)

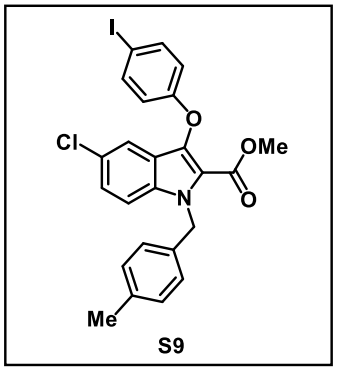
I
O
Cl
OMe
N
O
Me

S9

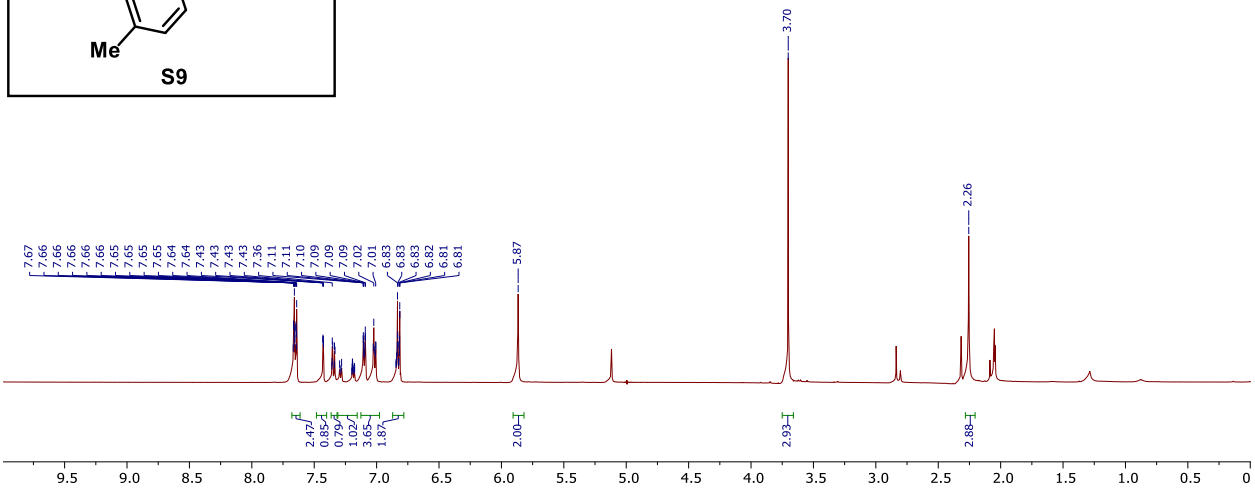
7.67
7.66
7.66
7.66
7.66
7.66
7.65
7.65
7.65
7.65
7.64
7.64
7.43
7.43
7.43
7.43
7.36
7.11
7.11
7.10
7.09
7.09
7.09
7.09
7.02
7.01
6.83
6.83
6.83
6.82
6.81
6.81
5.87
3.70
2.26
2.47
0.85
0.79
1.02
3.65
1.87
2.00
2.93
2.88
9.5
9.0
8.5
8.0
7.5
7.0
6.5
6.0
5.5
5.0
4.5
4.0
3.5
3.0
2.5
2.0
1.5
1.0
0.5
0

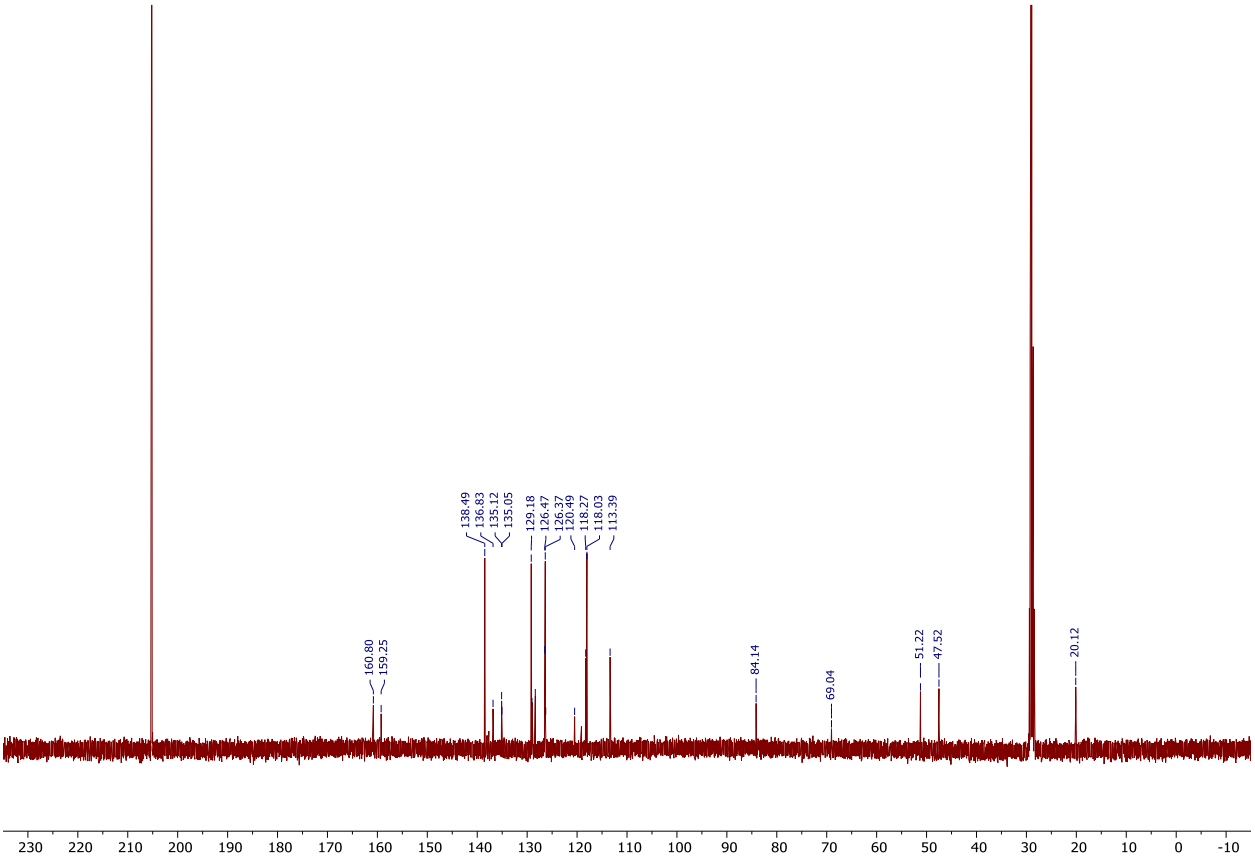
138.49
136.83
135.12
135.05
129.18
126.47
126.37
120.49
118.27
118.03
113.39
160.80
159.25
84.14
69.04
51.22
47.52
20.12
230
220
210
200
190
180
170
160
150
140
130
120
110
100
90
80
70
60
50
40
30
20
10
0
-10

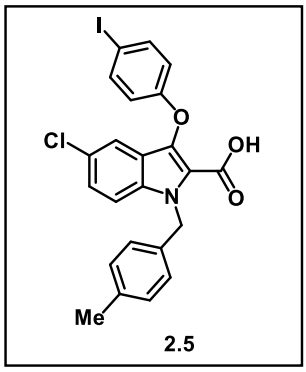
I
O
Cl
OH
N
O
Me

2.5

7.67
7.67
7.66
7.65
7.65
7.65
7.65
7.64
7.64
7.64
7.64
7.63
7.42
7.42
7.41
7.41
7.41
7.35
7.35
7.33
7.11
7.09
7.04
7.04
7.02
6.84
6.84
6.84
6.84
6.82
6.82
5.90
2.26
2.95
0.89
0.92
3.92
1.95
2.00
2.91
9.5
9.0
8.5
8.0
7.5
7.0
6.5
6.0
5.5
5.0
4.5
4.0
3.5
3.0
2.5
2.0
1.5
1.0
0.5
0
f1 (ppm)

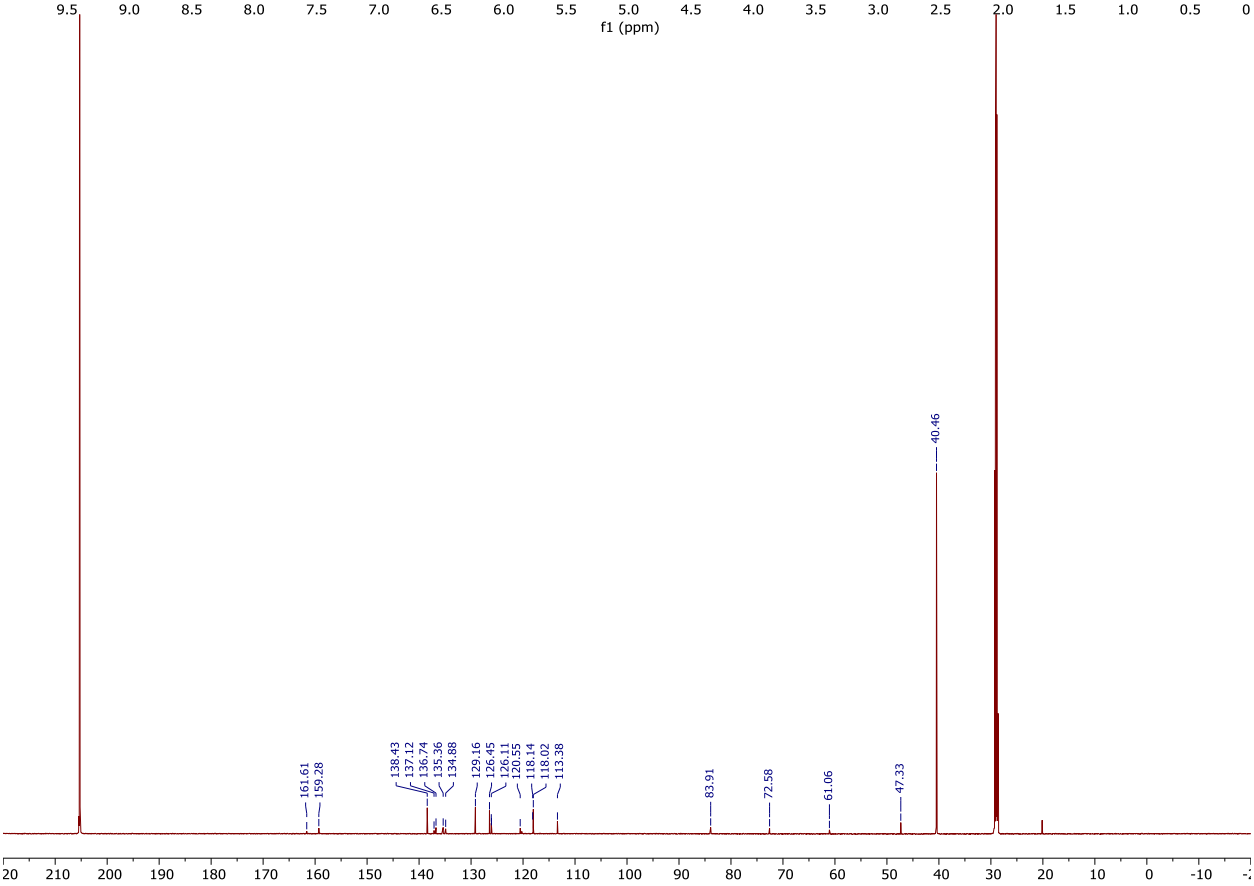
161.61
159.28
138.43
137.12
136.74
135.36
134.88
129.16
126.45
126.11
120.55
118.14
118.02
113.38
83.91
72.58
61.06
47.33
40.46
20
210
200
190
180
170
160
150
140
130
120
110
100
90
80
70
60
50
40
30
20
10
0
-10

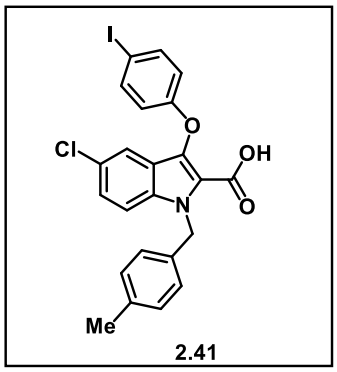
I
O
Cl
OH
O
N
Me

2.41

1.08
0.71
0.81
1.66
2.72
1.79
2.78
2.09
9.00
9.5
9.0
8.5
8.0
7.5
7.0
6.5
6.0
5.5
5.0
4.5
4.0
3.5
3.0
2.5
2.0
1.5
1.0
0.5
0

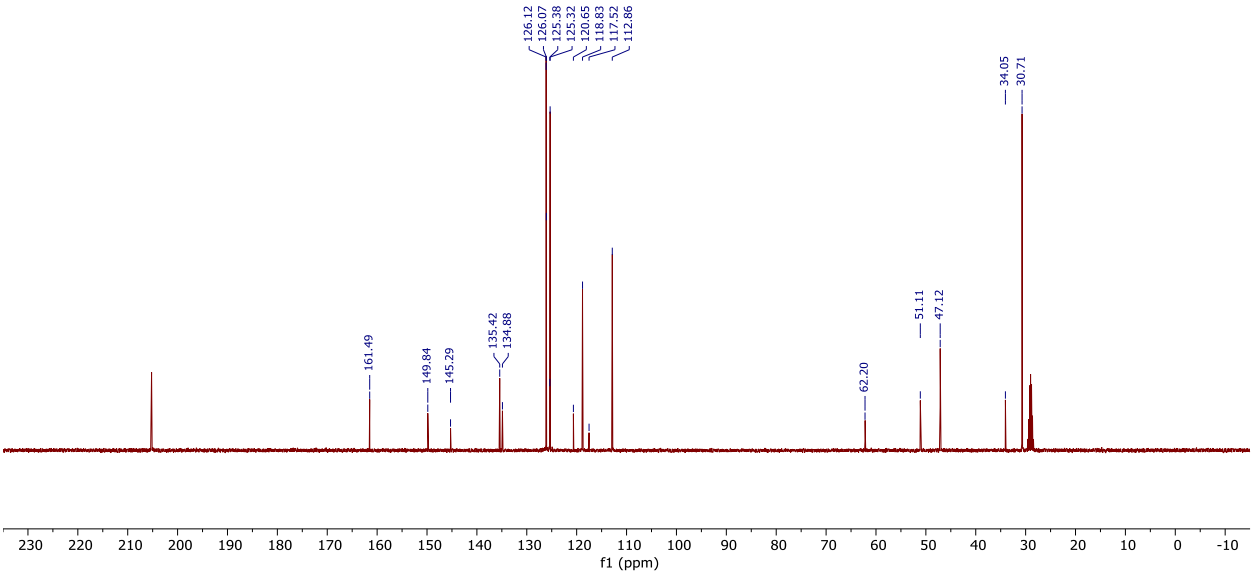
126.12
126.07
125.38
125.32
120.65
118.83
117.52
112.86
34.05
30.71
161.49
149.84
145.29
135.42
134.88
62.20
51.11
47.12
230
220
210
200
190
180
170
160
150
140
130
120
110
100
90
80
70
60
50
40
30
20
10
0
-10
f1 (ppm)

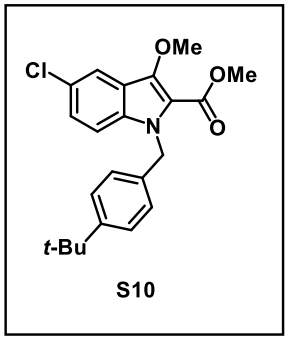
OMe
Cl
OMe
O
N
t-Bu

S10

8.66
8.66
7.66
7.66
7.48
7.46
7.46
7.30
7.28
7.27
6.99
6.99
6.99
6.97
6.97
5.66
3.91
1.22
0.55
0.51
0.86
2.31
1.53
2.00
2.62
9.21
f1 (ppm)

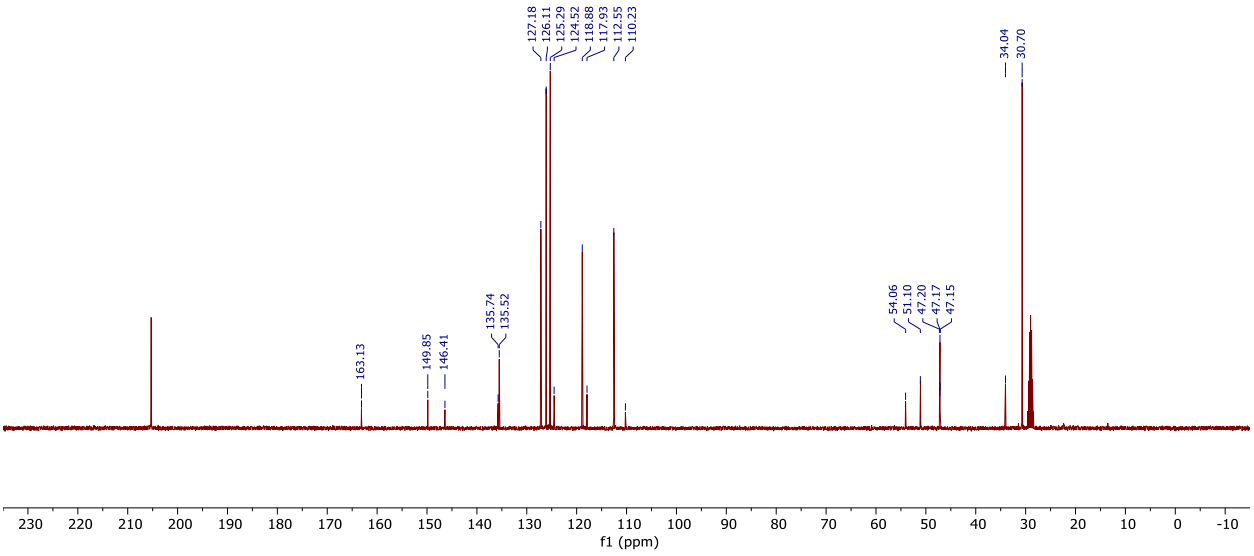
127.18
126.11
125.29
124.52
118.88
117.93
112.55
110.23
163.13
149.85
146.41
135.74
135.52
54.06
51.10
47.20
47.17
47.15
34.04
30.70
f1 (ppm)

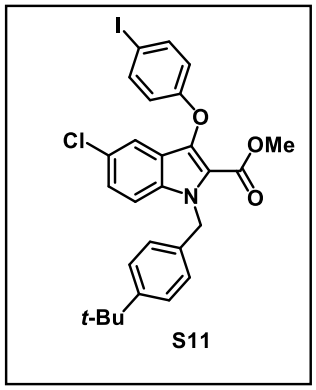
I
O
Cl
OMe
O
N
t-Bu

S11

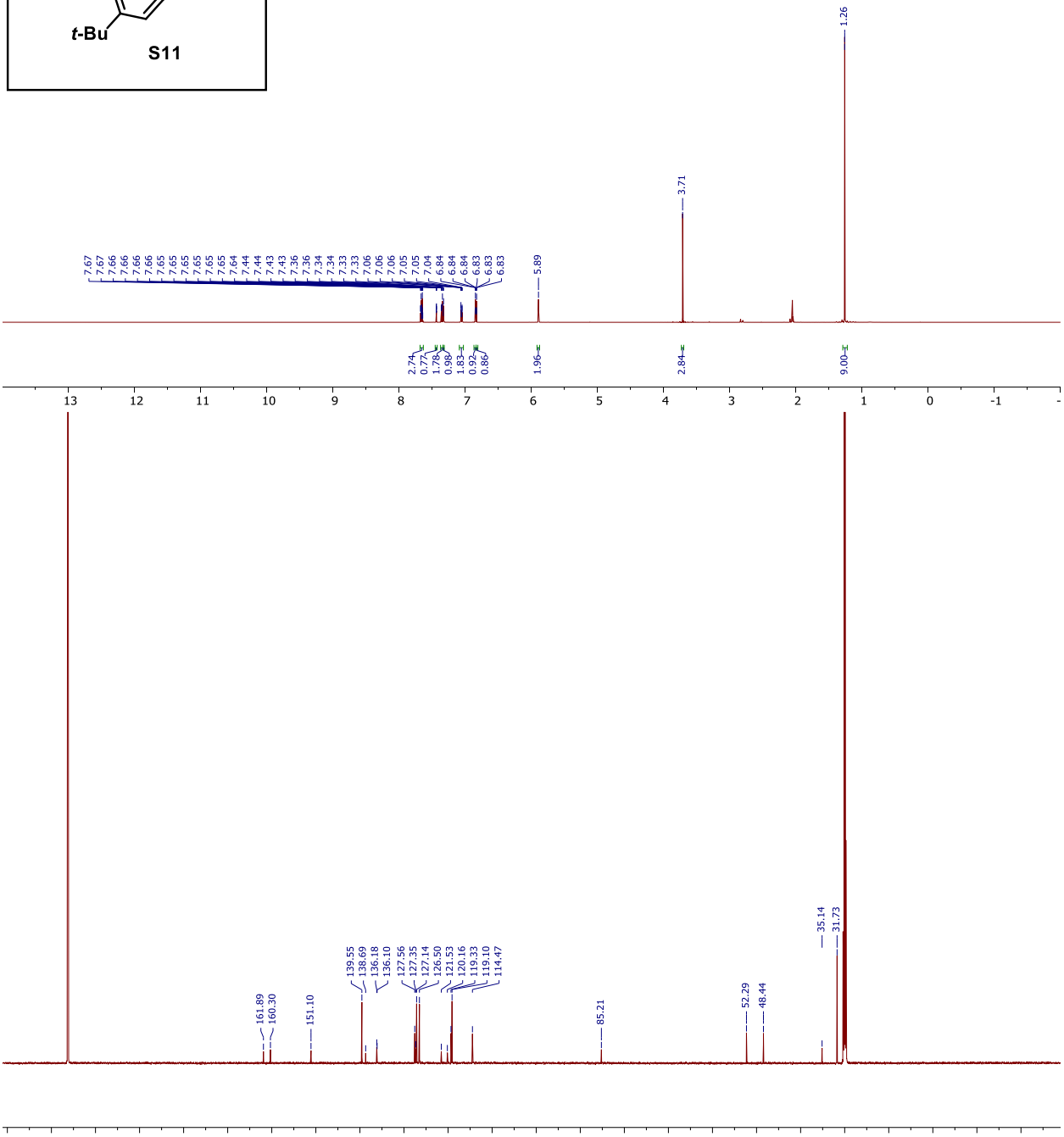
7.67
7.67
7.66
7.66
7.66
7.66
7.65
7.65
7.65
7.65
7.65
7.64
7.44
7.44
7.43
7.43
7.36
7.36
7.34
7.34
7.33
7.33
7.06
7.06
7.06
7.05
7.05
7.04
6.84
6.84
6.84
6.83
6.83
6.83
5.89
3.71
1.26
2.74
0.77
1.78
0.98
1.83
0.92
0.86
1.96
2.84
9.00
13
12
11
10
9
8
7
6
5
4
3
2
1
0
-1
161.89
160.30
151.10
139.55
138.69
136.18
136.10
127.56
127.35
127.14
126.50
121.53
120.16
119.33
119.10
114.47
85.21
52.29
48.44
35.14
31.73

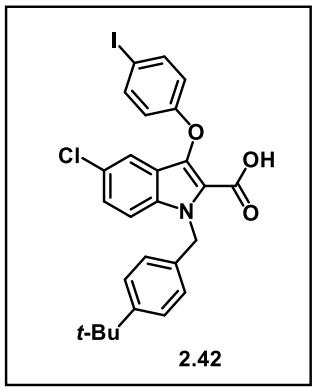
I
O
Cl
OH
O
N
t-Bu

2.42

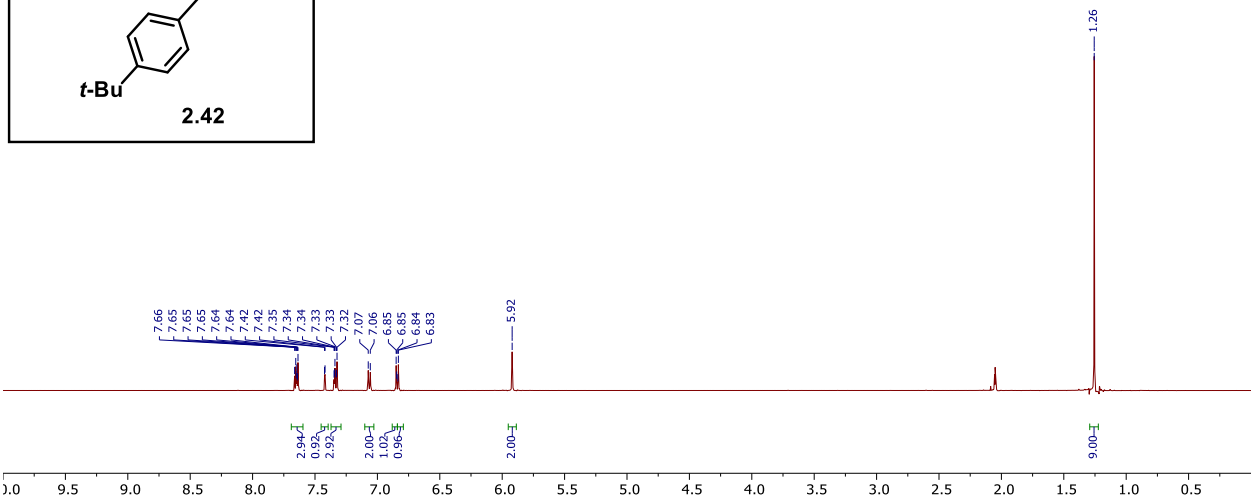
7.66
7.65
7.65
7.65
7.64
7.64
7.42
7.42
7.35
7.34
7.34
7.33
7.33
7.32
7.07
7.06
6.85
6.85
6.84
6.83
5.92
1.26
2.94
0.92
2.92
2.00
1.02
0.96
2.00
9.00

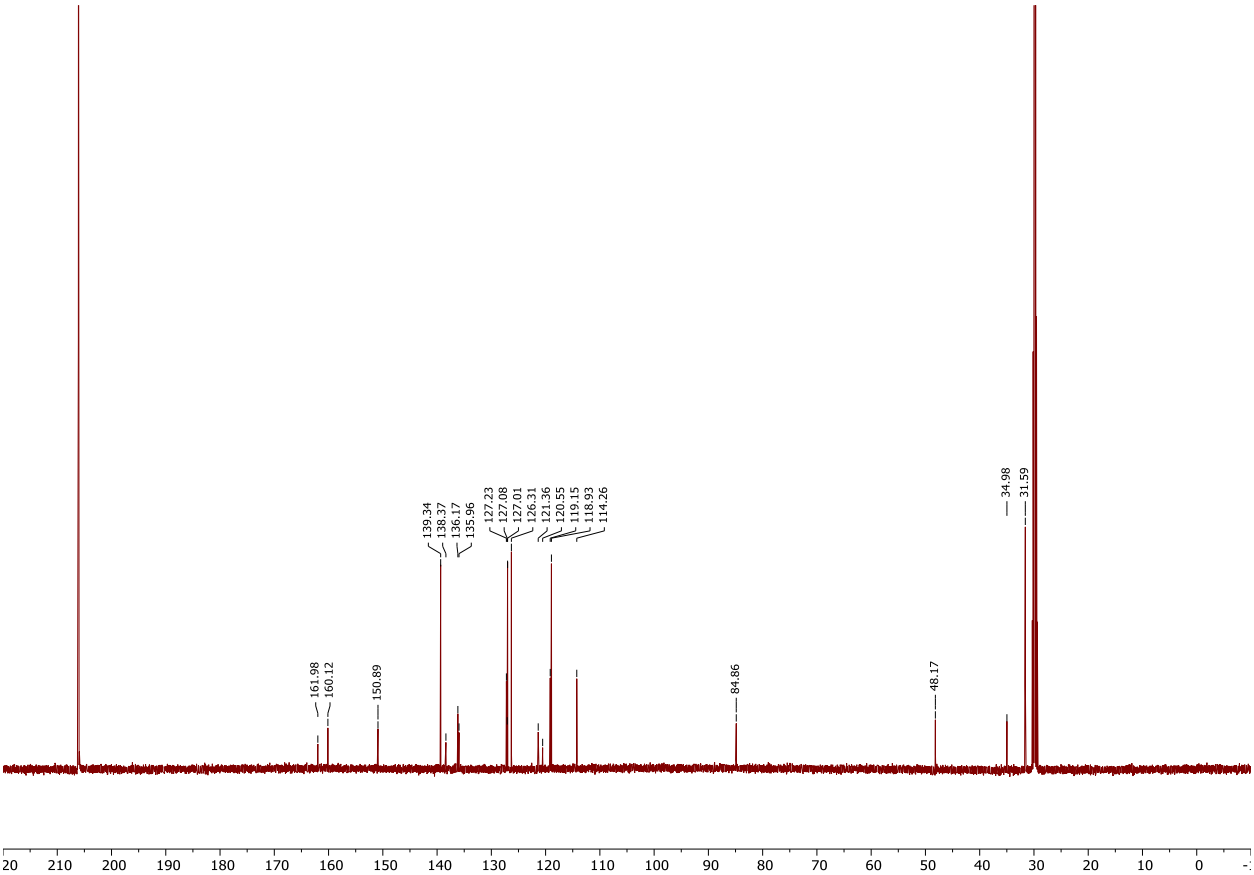
161.98
160.12
150.89
139.34
138.37
136.17
135.96
127.23
127.08
127.01
126.31
121.36
120.55
119.15
118.93
114.26
84.86
48.17
34.98
31.59

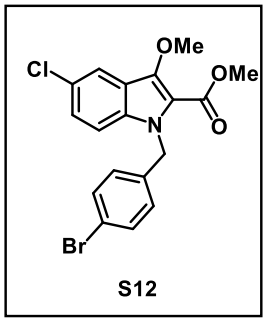
OMe
Cl
OMe
O
N
Br

S12

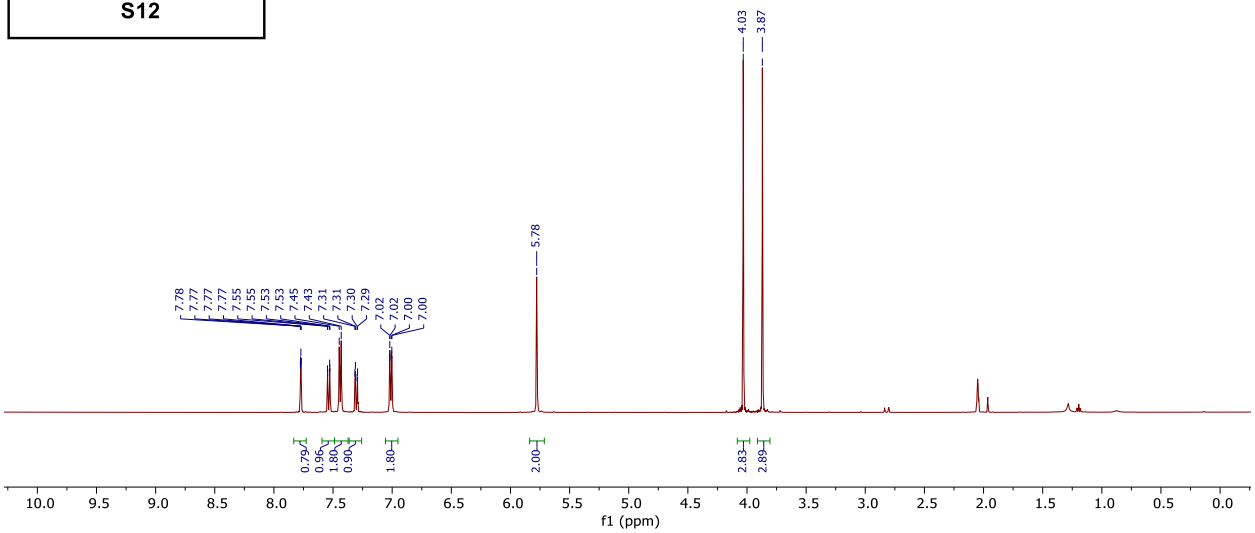
7.78
7.77
7.77
7.77
7.77
7.55
7.55
7.53
7.53
7.45
7.43
7.31
7.31
7.30
7.29
7.02
7.02
7.00
7.00
5.78
4.03
3.87
0.79
0.96
1.80
0.90
1.80
2.00
2.83
2.89
10.0
9.5
9.0
8.5
8.0
7.5
7.0
6.5
6.0
5.5
5.0
4.5
4.0
3.5
3.0
2.5
2.0
1.5
1.0
0.5
0.0
f1 (ppm)

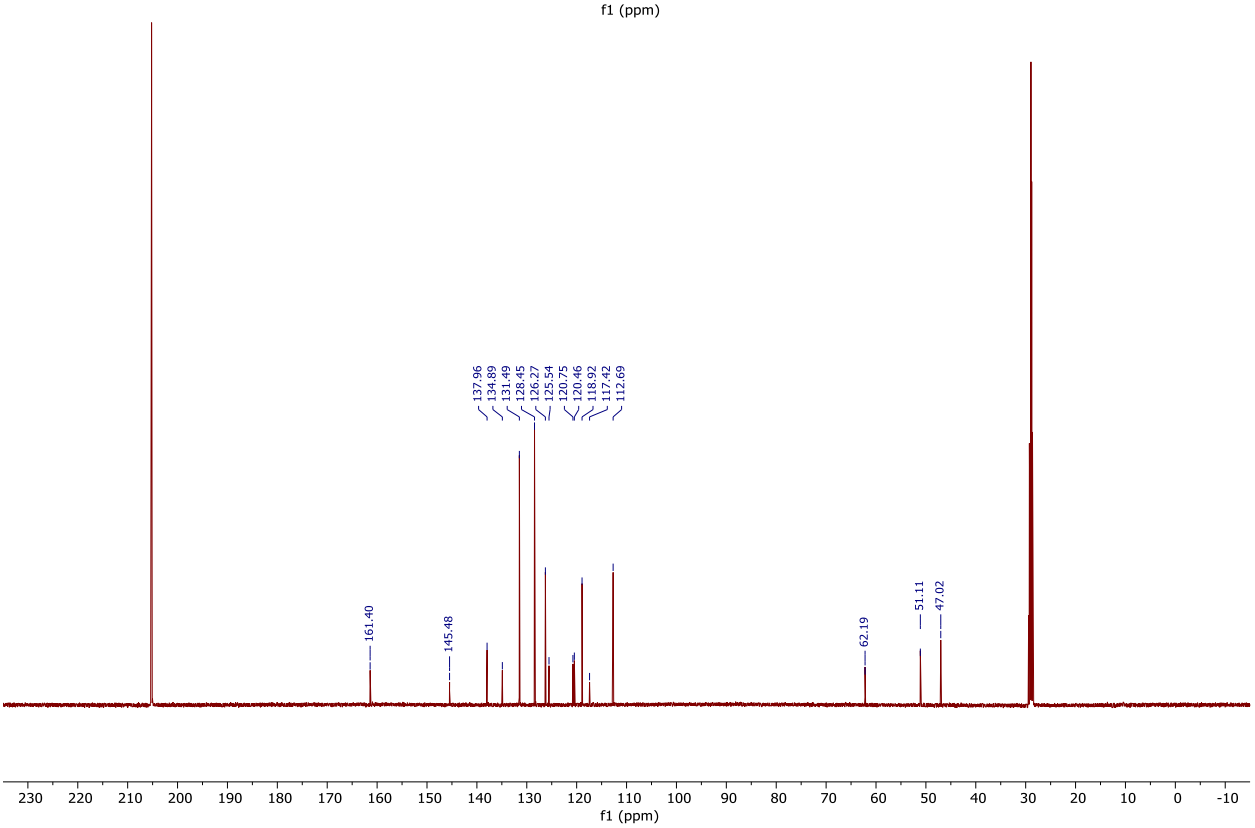
137.96
134.89
131.49
128.45
126.27
125.54
120.75
120.46
118.92
117.42
112.69
161.40
145.48
62.19
51.11
47.02
230
220
210
200
190
180
170
160
150
140
130
120
110
100
90
80
70
60
50
40
30
20
10
0
-10
f1 (ppm)

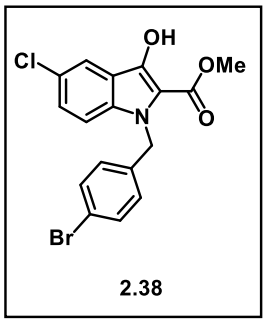
OH
Cl
OMe
N
O
Br

2.38

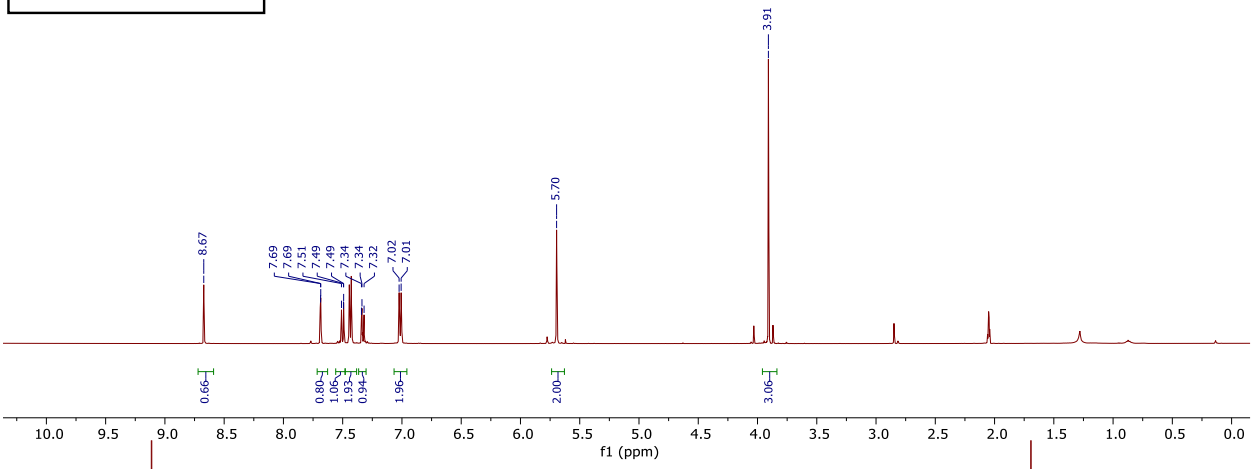
8.67
7.69
7.69
7.51
7.49
7.49
7.34
7.34
7.32
7.02
7.01
5.70
3.91
0.66
0.80
1.06
1.93
0.94
1.96
2.00
3.06
10.0 9.5 9.0 8.5 8.0 7.5 7.0 6.5 6.0 5.5 5.0 4.5 4.0 3.5 3.0 2.5 2.0 1.5 1.0 0.5 0.0
f1 (ppm)

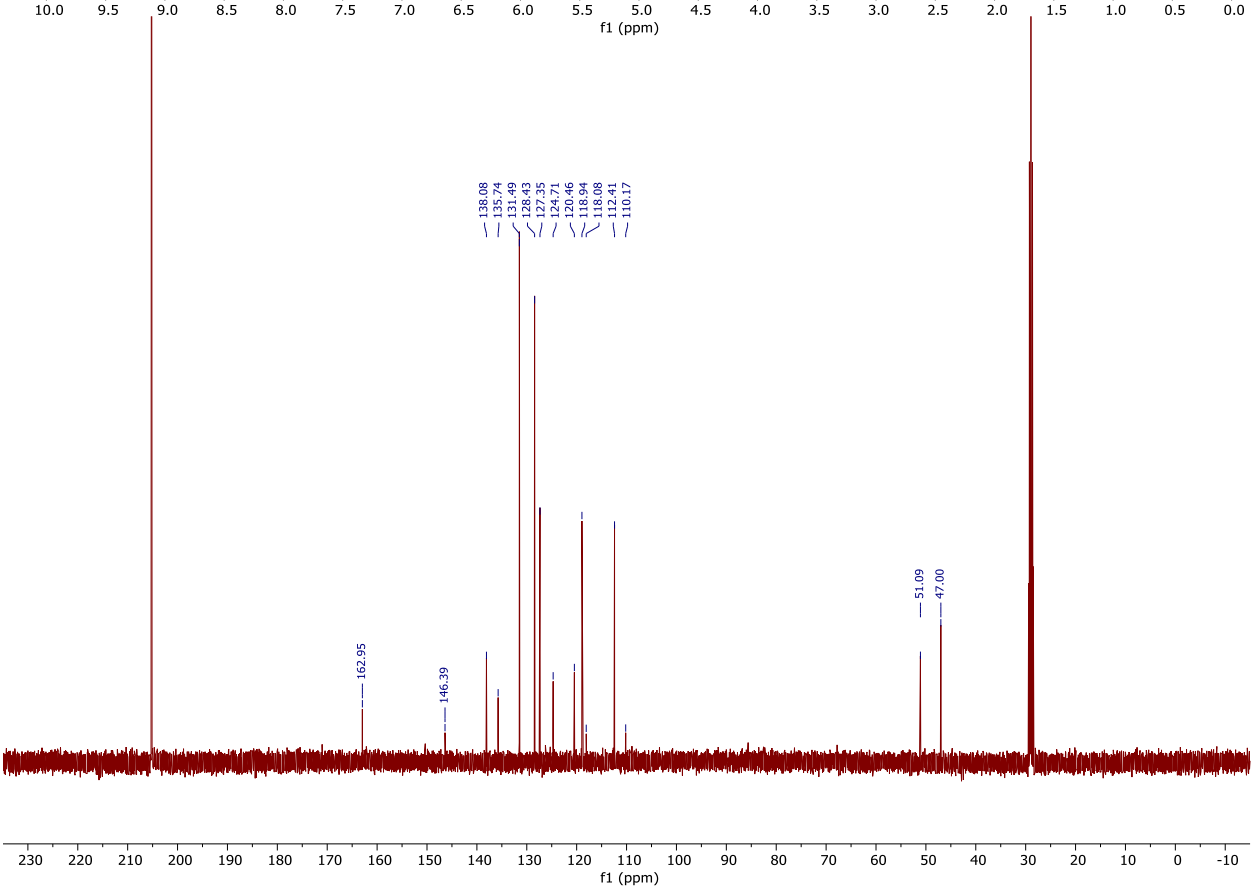
138.08
135.74
131.49
128.43
127.35
124.71
120.46
118.94
118.08
112.41
110.17
162.95
146.39
51.09
47.00
230 220 210 200 190 180 170 160 150 140 130 120 110 100 90 80 70 60 50 40 30 20 10 0 -10
f1 (ppm)

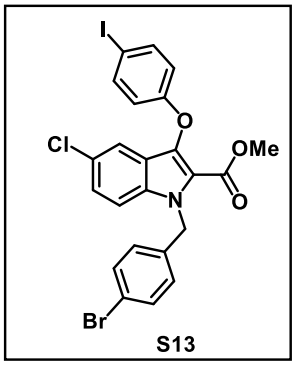
I
O
Cl
OMe
O
N
Br

S13

7.77
7.75
7.67
7.67
7.66
7.66
7.66
7.66
7.66
7.65
7.65
7.64
7.49
7.47
7.44
7.38
7.37
7.36
7.35
7.10
7.09
7.08
6.98
6.96
6.85
6.83
5.90
3.70
4.44
3.87
1.98
1.27
1.82
2.00
3.05
f1 (ppm)

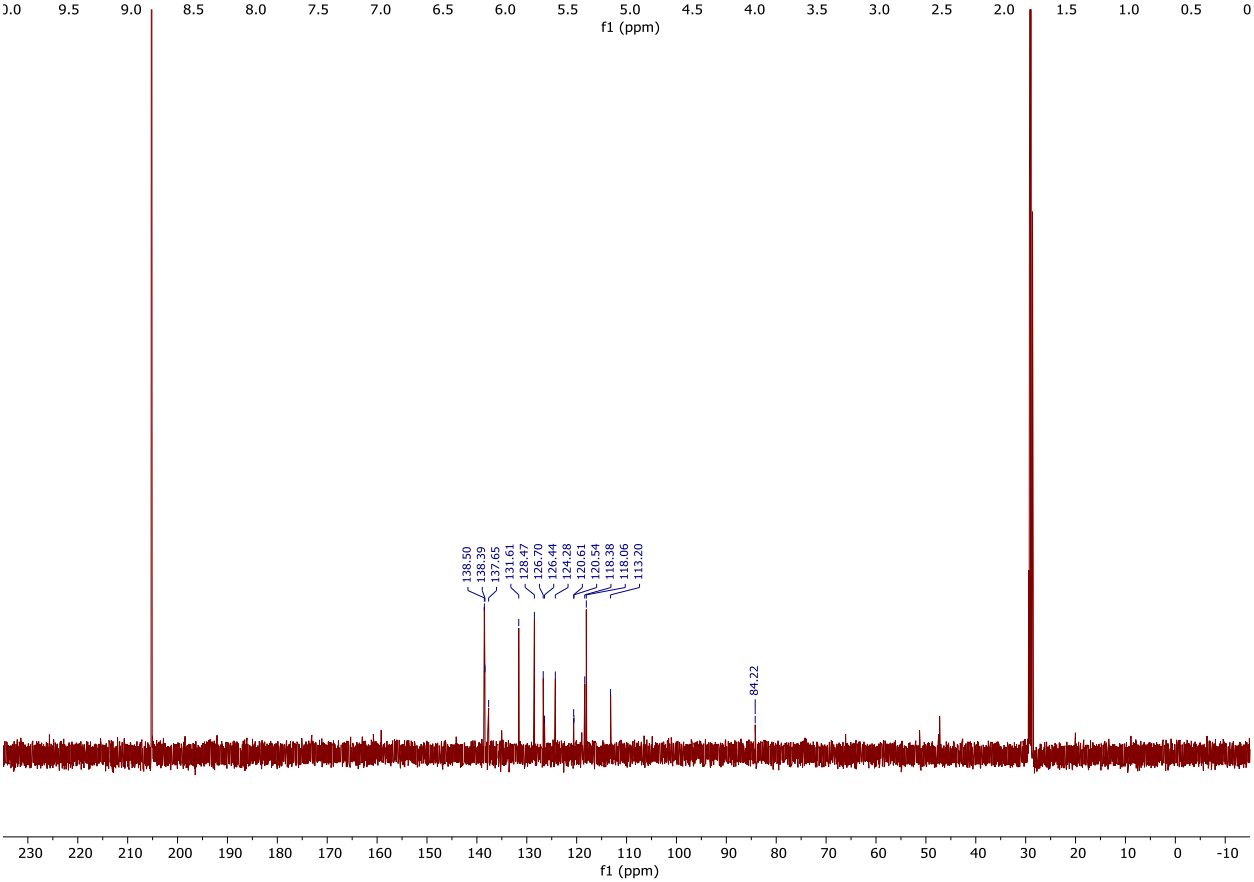
138.50
138.39
137.65
131.61
128.47
126.70
126.44
124.28
120.61
120.54
118.38
118.06
113.20
84.22
f1 (ppm)

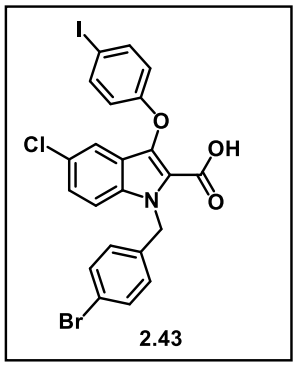
I
O
Cl
OH
O
N
Br

2.43

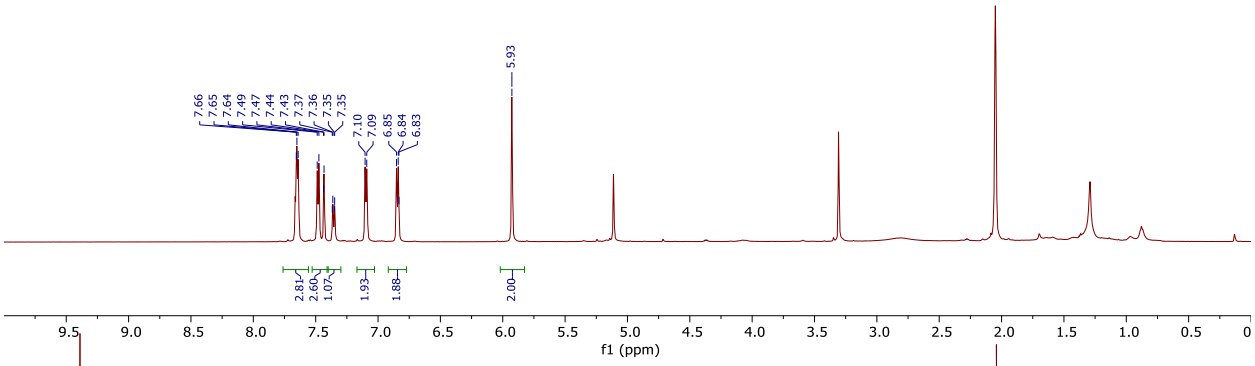
7.66
7.65
7.64
7.49
7.47
7.44
7.43
7.37
7.36
7.35
7.35
7.10
7.09
6.85
6.84
6.83
5.93
2.81
2.60
1.07
1.93
1.88
2.00
f1 (ppm)

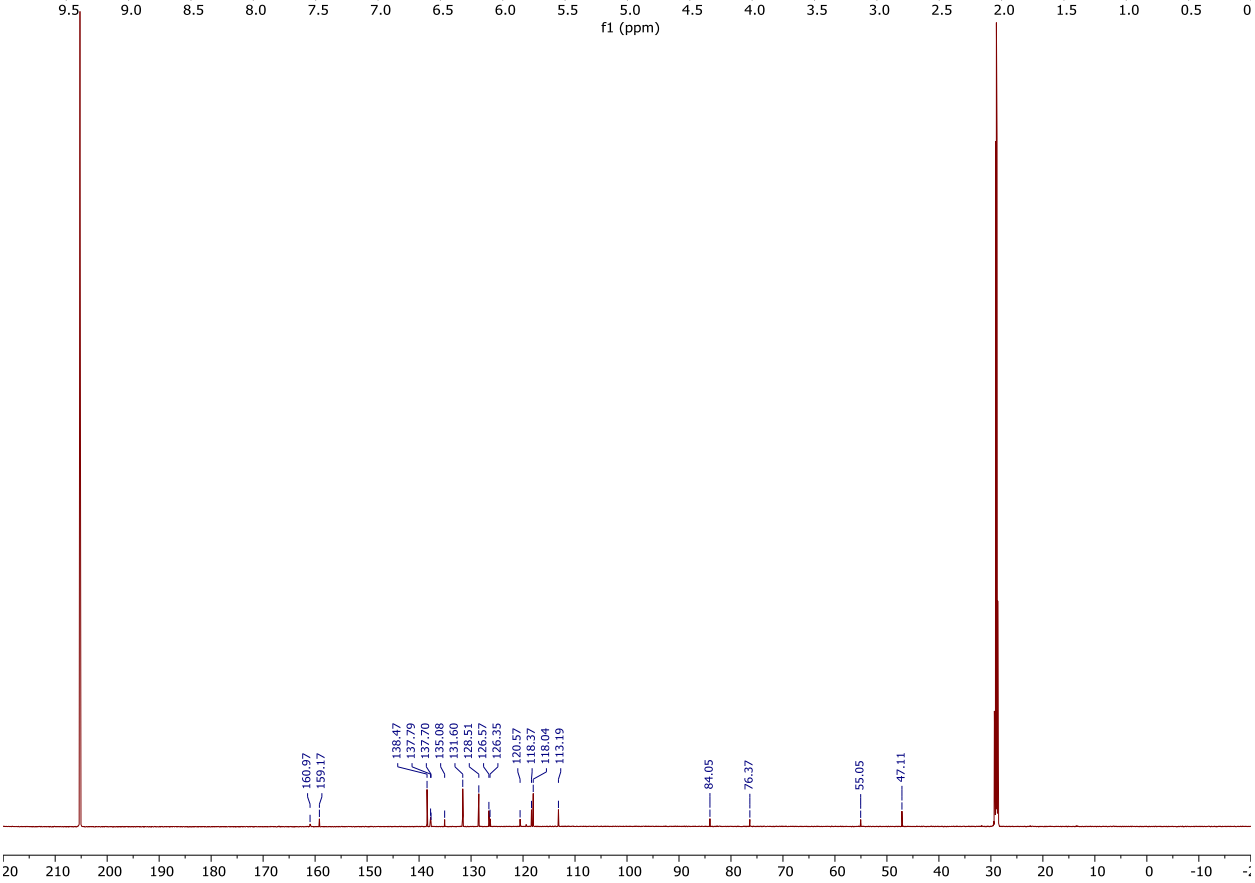
160.97
159.17
138.47
137.79
137.70
135.08
131.60
128.51
126.57
126.35
120.57
118.37
118.04
113.19
84.05
76.37
55.05
47.11

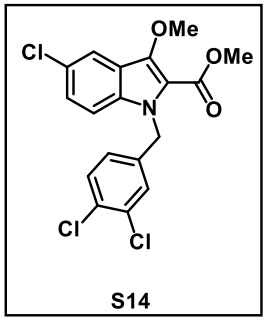
OMe
Cl
OMe
N
O
Cl
Cl

S14

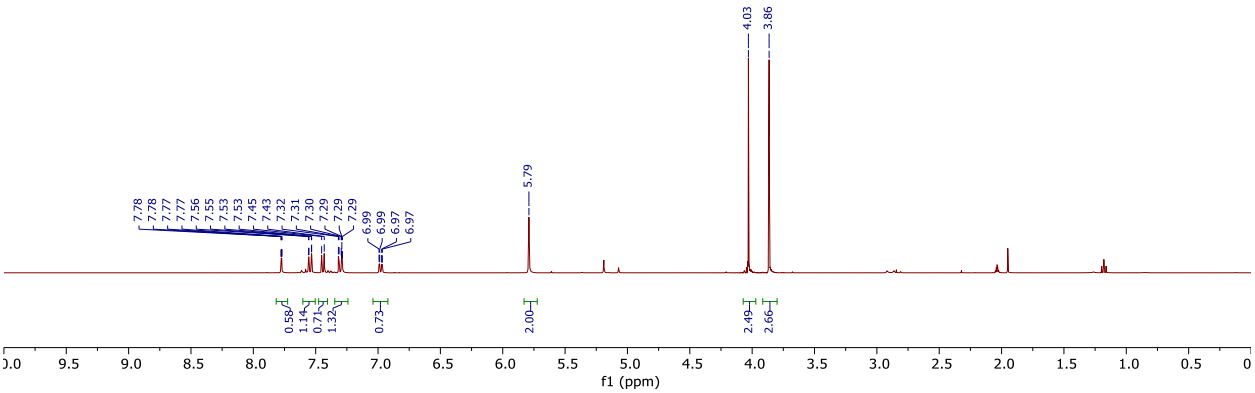
7.78
7.78
7.77
7.77
7.77
7.56
7.55
7.53
7.53
7.45
7.43
7.32
7.31
7.30
7.29
7.29
7.29
7.29
6.99
6.99
6.97
6.97
5.79
4.03
3.86
0.58
1.14
0.71
1.32
0.73
2.00
2.49
2.66
f1 (ppm)

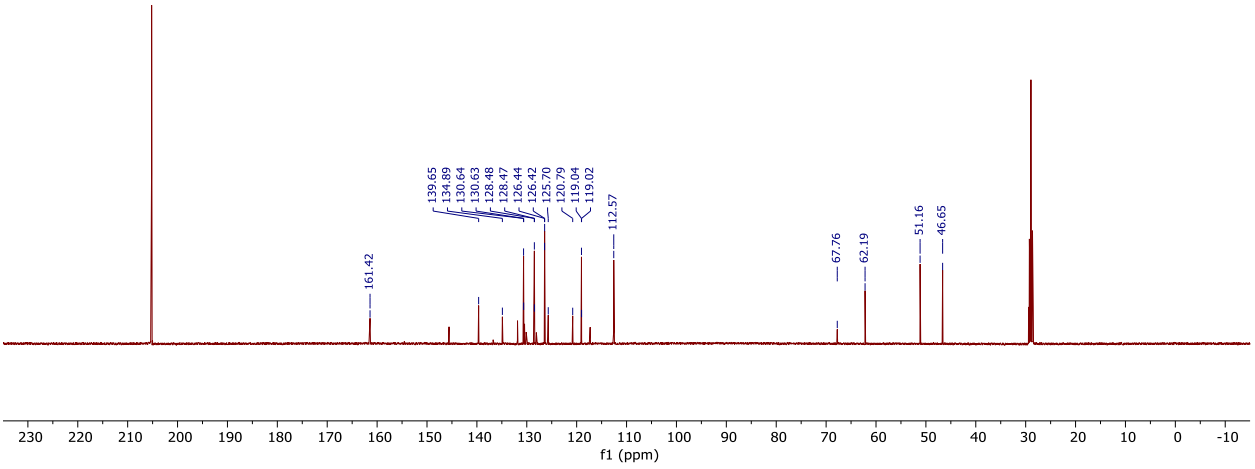
139.65
134.89
130.64
130.63
128.48
128.47
126.44
126.42
125.70
120.79
119.04
119.02
112.57
161.42
67.76
62.19
51.16
46.65
f1 (ppm)

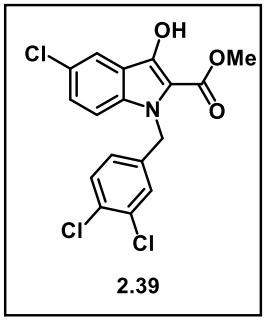
OH
Cl
OMe
N
O
Cl
Cl

2.39

8.67
7.70
7.70
7.70
7.69
7.53
7.52
7.51
7.46
7.45
7.36
7.35
7.34
7.33
7.30
7.30
7.01
7.01
7.00
6.99
6.99
6.99
6.99
5.73
3.91
0.58
0.71
1.82
0.88
0.99
0.94
2.00
2.89
f1 (ppm)

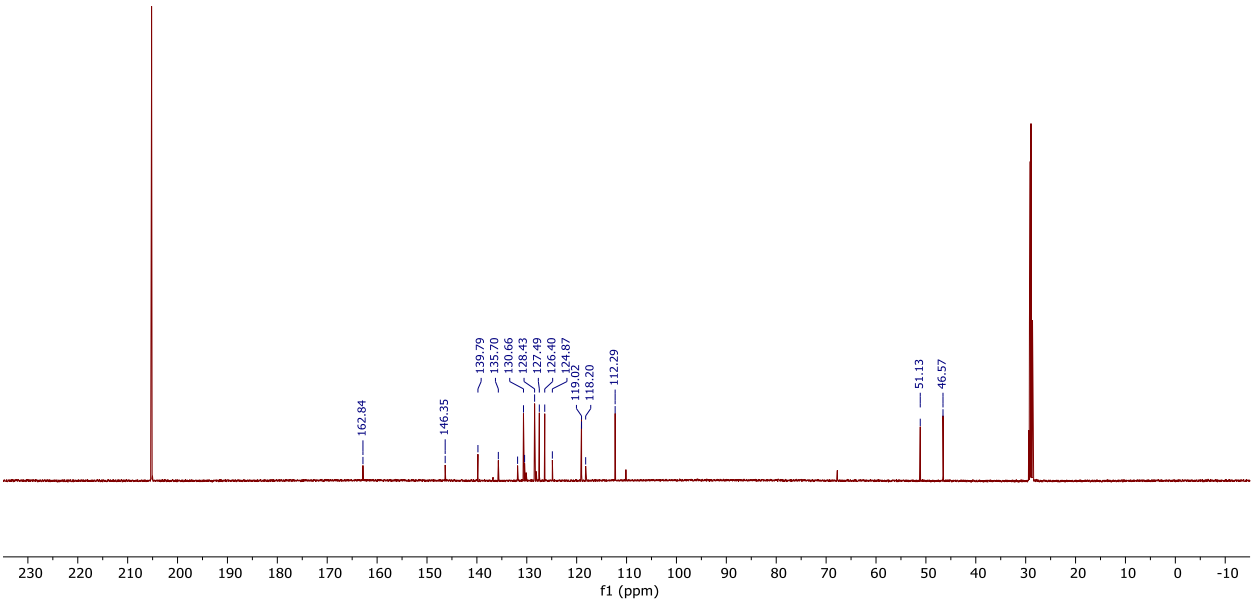
162.84
146.35
139.79
135.70
130.66
128.43
127.49
126.40
124.87
119.02
118.20
112.29
51.13
46.57
f1 (ppm)

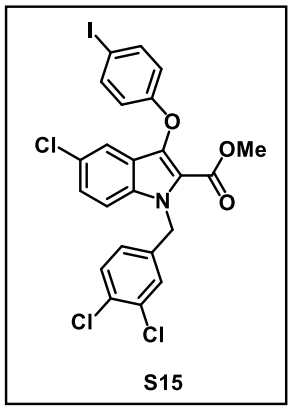
I
O
Cl
OMe
N
O
Cl
Cl

S15

7.69
7.69
7.67
7.67
7.66
7.66
7.64
7.50
7.48
7.45
7.45
7.45
7.45
7.39
7.38
7.08
7.07
7.06
7.05
6.86
6.84
5.92
3.70
3.26
3.59
0.98
1.87
2.09
3.00
f1 (ppm)

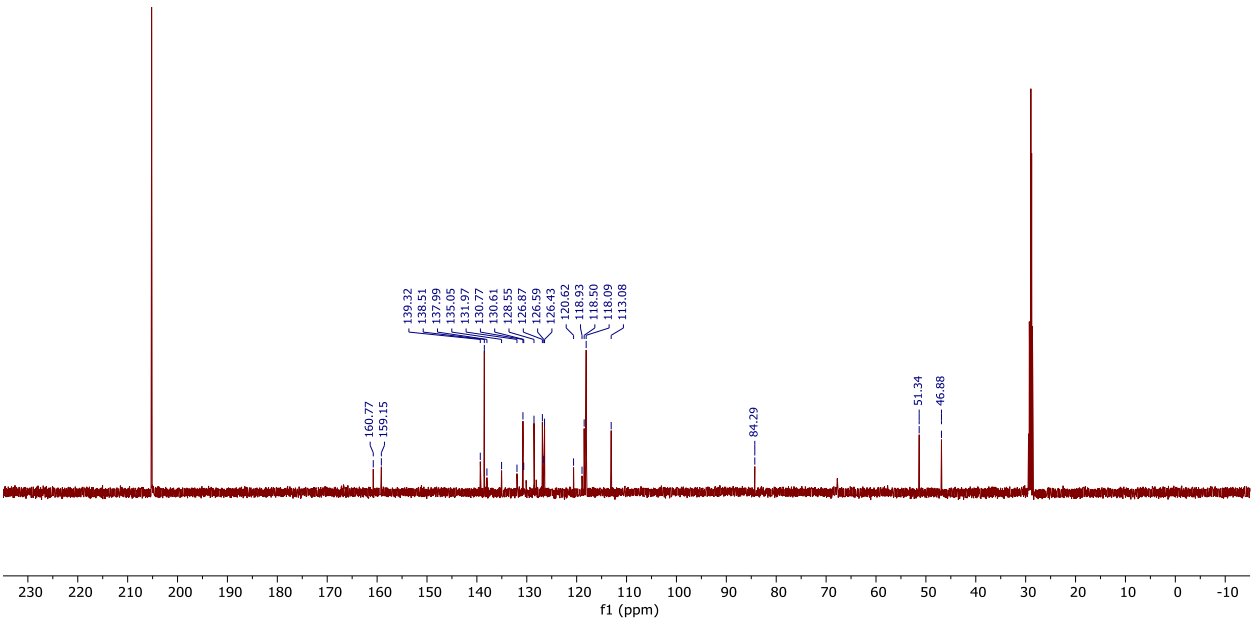
139.32
138.51
137.99
135.05
131.97
130.77
130.61
128.55
126.87
126.59
126.43
120.62
118.93
118.50
118.09
113.08
160.77
159.15
84.29
51.34
46.88
f1 (ppm)

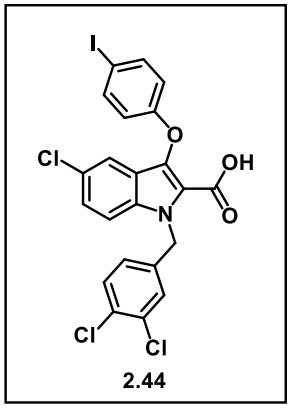
I
O
Cl
OH
O
N
Cl
Cl

2.44

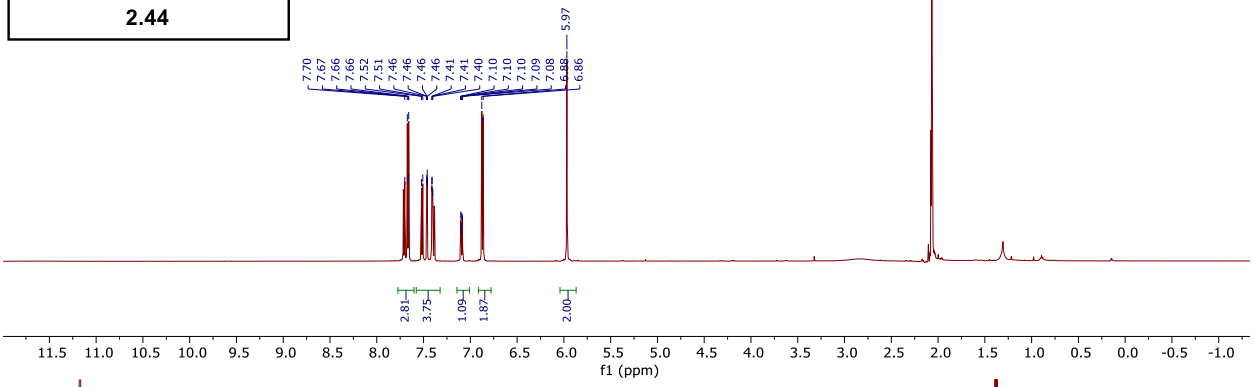
7.70
7.67
7.66
7.66
7.52
7.51
7.46
7.46
7.46
7.46
7.41
7.41
7.40
7.10
7.10
7.10
7.09
7.08
6.88
6.86
5.97
2.81
3.75
1.09
1.87
2.00
11.5 11.0 10.5 10.0 9.5 9.0 8.5 8.0 7.5 7.0 6.5 6.0 5.5 5.0 4.5 4.0 3.5 3.0 2.5 2.0 1.5 1.0 0.5 0.0 -0.5 -1.0
f1 (ppm)

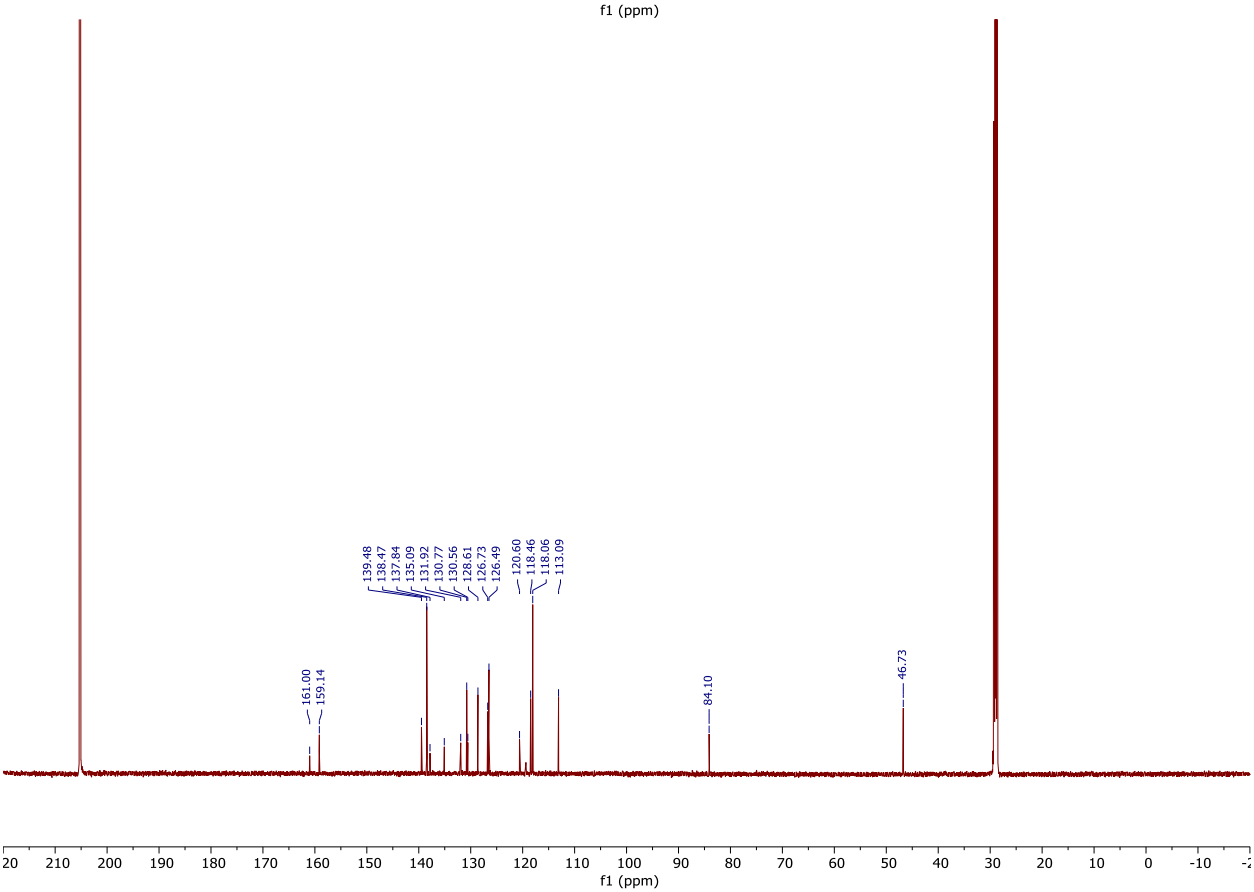
139.48
138.47
137.84
135.09
131.92
130.77
130.56
128.61
126.73
126.49
120.60
118.46
118.06
113.09
161.00
159.14
84.10
46.73
220 210 200 190 180 170 160 150 140 130 120 110 100 90 80 70 60 50 40 30 20 10 0 -10
f1 (ppm)

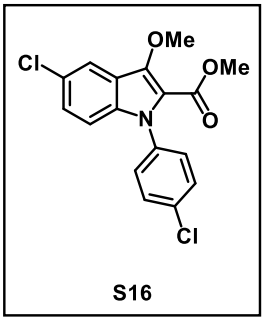
OMe
Cl
OMe
O
N
Cl

S16

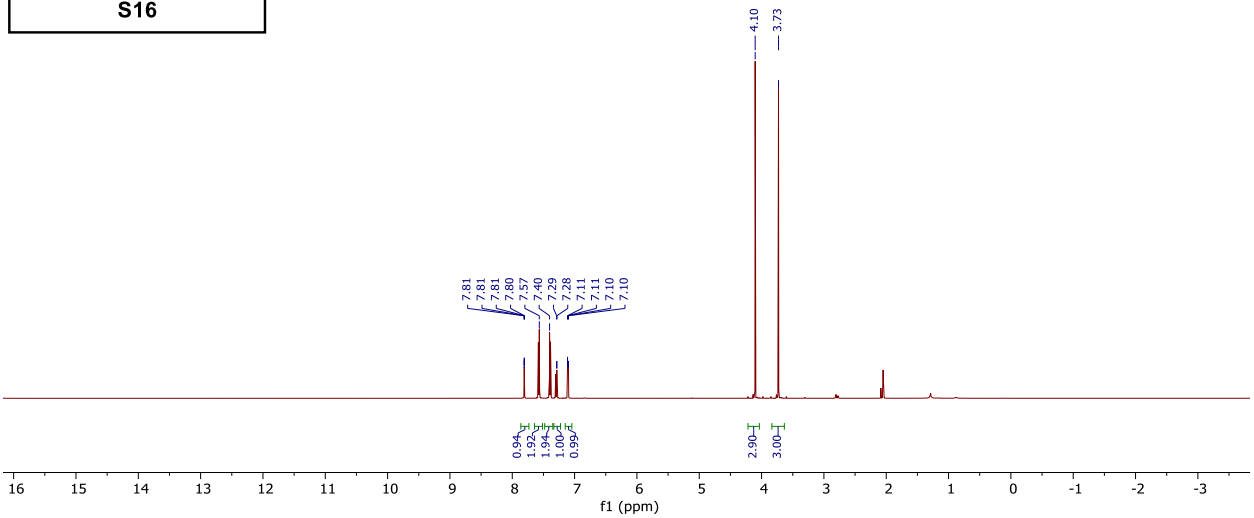
7.81
7.81
7.81
7.80
7.57
7.40
7.29
7.28
7.11
7.11
7.10
7.10
4.10
3.73
0.94
1.92
1.94
1.00
0.99
2.90
3.00
f1 (ppm)

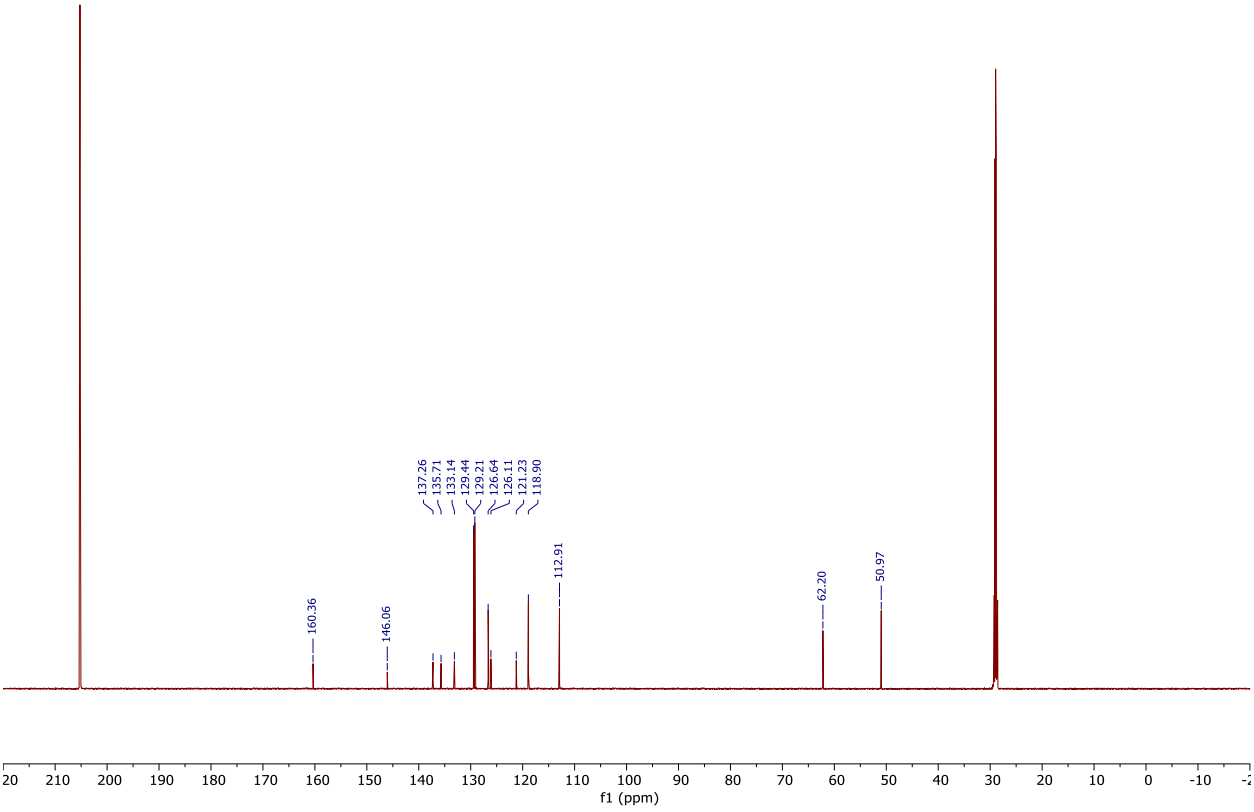
137.26
135.71
133.14
129.44
129.21
126.64
126.11
121.23
118.90
160.36
146.06
112.91
62.20
50.97
f1 (ppm)

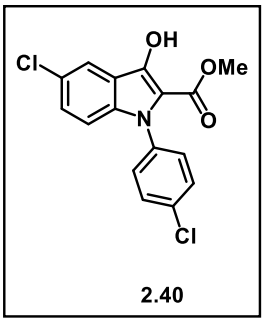
OH
Cl
OMe
N
O
Cl

2.40

3.73
7.72
7.71
7.57
7.54
7.42
7.40
7.33
7.32
7.30
7.30
7.10
7.08
8.86
0.45
0.64
1.61
1.63
0.85
0.88
3.00
10.0 9.5 9.0 8.5 8.0 7.5 7.0 6.5 6.0 5.5 5.0 4.5 4.0 3.5 3.0 2.5 2.0 1.5 1.0 0.5 0.0
f1 (ppm)

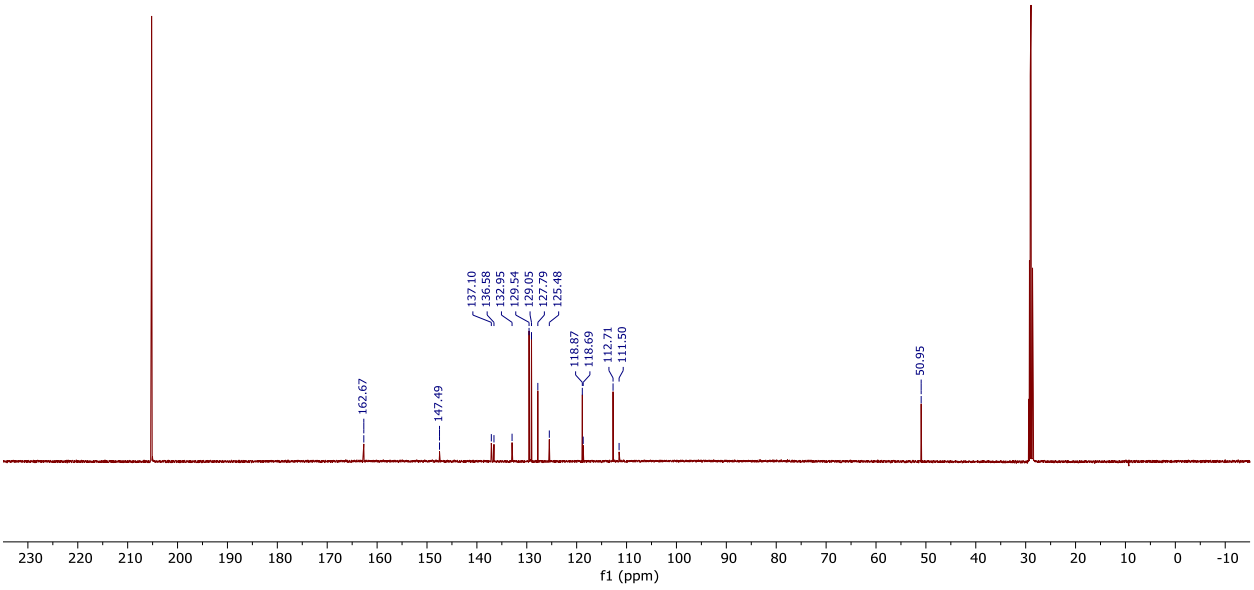
137.10
136.58
132.95
129.54
129.05
127.79
125.48
118.87
118.69
112.71
111.50
162.67
147.49
50.95
230 220 210 200 190 180 170 160 150 140 130 120 110 100 90 80 70 60 50 40 30 20 10 0 -10
f1 (ppm)

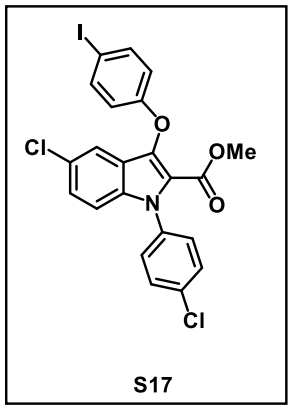
I
O
Cl
OMe
O
N
Cl

S17

7.69
7.66
7.63
7.61
7.53
7.51
7.47
7.47
7.47
7.47
7.37
7.36
7.21
7.21
7.19
7.19
6.95
6.93
3.60
2.26
1.18
0.47
0.58
0.62
1.18
2.05
f1 (ppm)

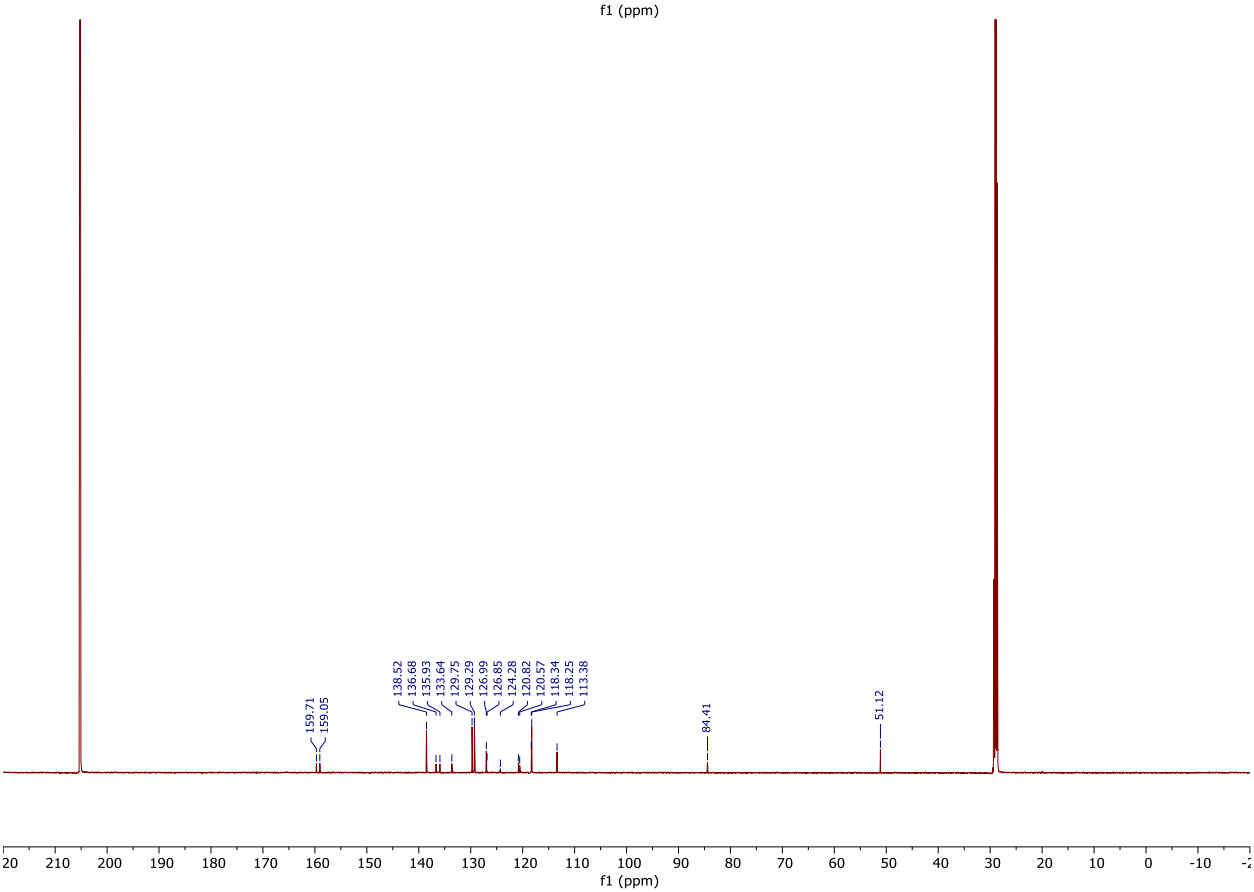
159.71
159.05
138.52
136.68
135.93
133.64
129.75
129.29
126.99
126.85
124.28
120.82
120.57
118.34
118.25
113.38
84.41
51.12
f1 (ppm)

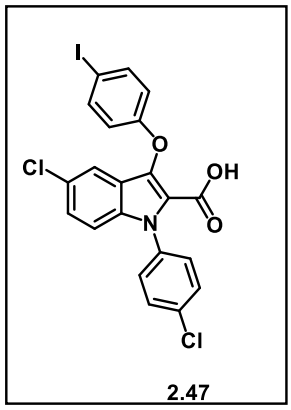
I
O
Cl
OH
O
N
Cl

2.47

7.67
7.67
7.66
7.65
7.61
7.59
7.53
7.53
7.51
7.51
7.46
7.46
7.45
7.45
7.36
7.35
7.33
7.33
7.21
7.21
7.19
7.18
6.95
6.95
6.94
6.93
6.93
6.93
1.67
3.73
0.82
0.89
1.00
1.98
10.0
9.5
9.0
8.5
8.0
7.5
7.0
6.5
6.0
5.5
5.0
4.5
4.0
3.5
3.0
2.5
2.0
1.5
1.0
0.5
f1 (ppm)

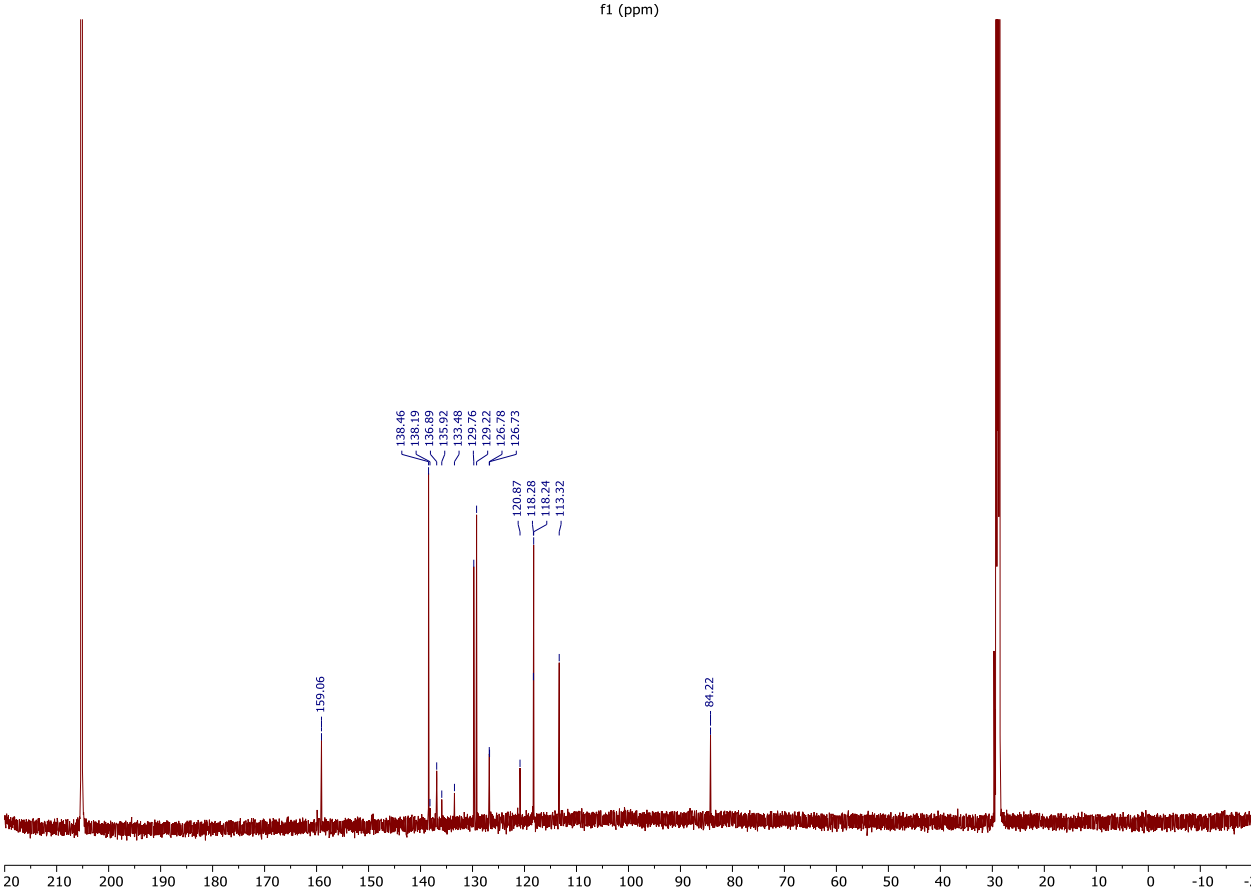
138.46
138.19
136.89
135.92
133.48
129.76
129.22
126.78
126.73
120.87
118.28
118.24
113.32
159.06
84.22
20
210
200
190
180
170
160
150
140
130
120
110
100
90
80
70
60
50
40
30
20
10
0
-10

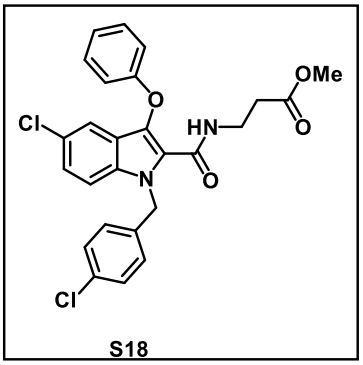
OMe
O
Cl
HN
O
N
O
Cl

S18

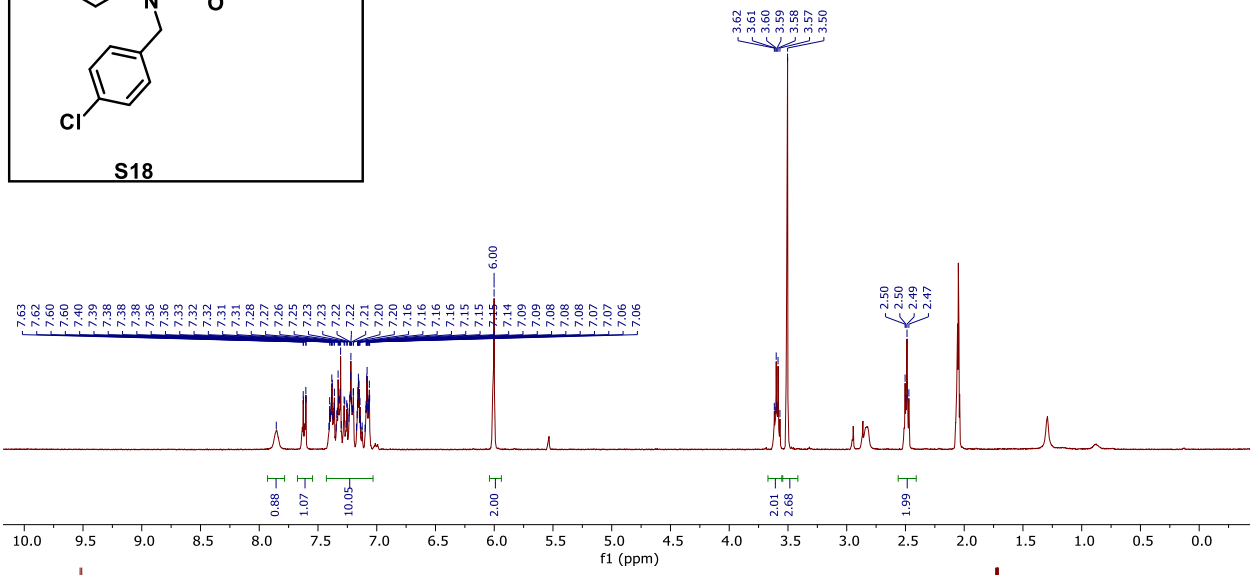
3.62
3.61
3.60
3.59
3.58
3.57
3.50
2.50
2.50
2.49
2.47
6.00
0.88
1.07
10.05
2.00
2.01
2.68
1.99
f1 (ppm)

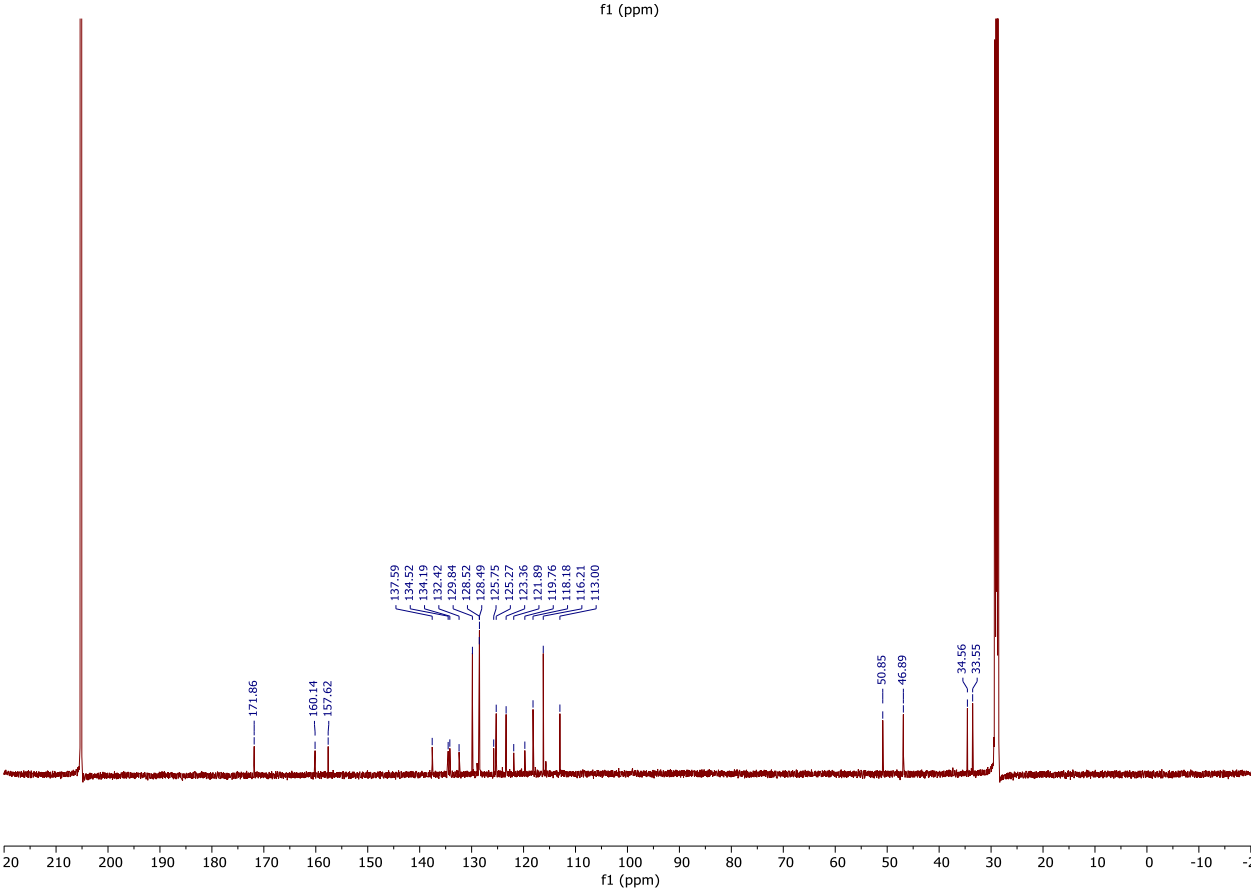
137.59
134.52
134.19
132.42
129.84
128.52
128.49
125.75
125.27
123.36
121.89
119.76
118.18
116.21
113.00
171.86
160.14
157.62
50.85
46.89
34.56
33.55
f1 (ppm)

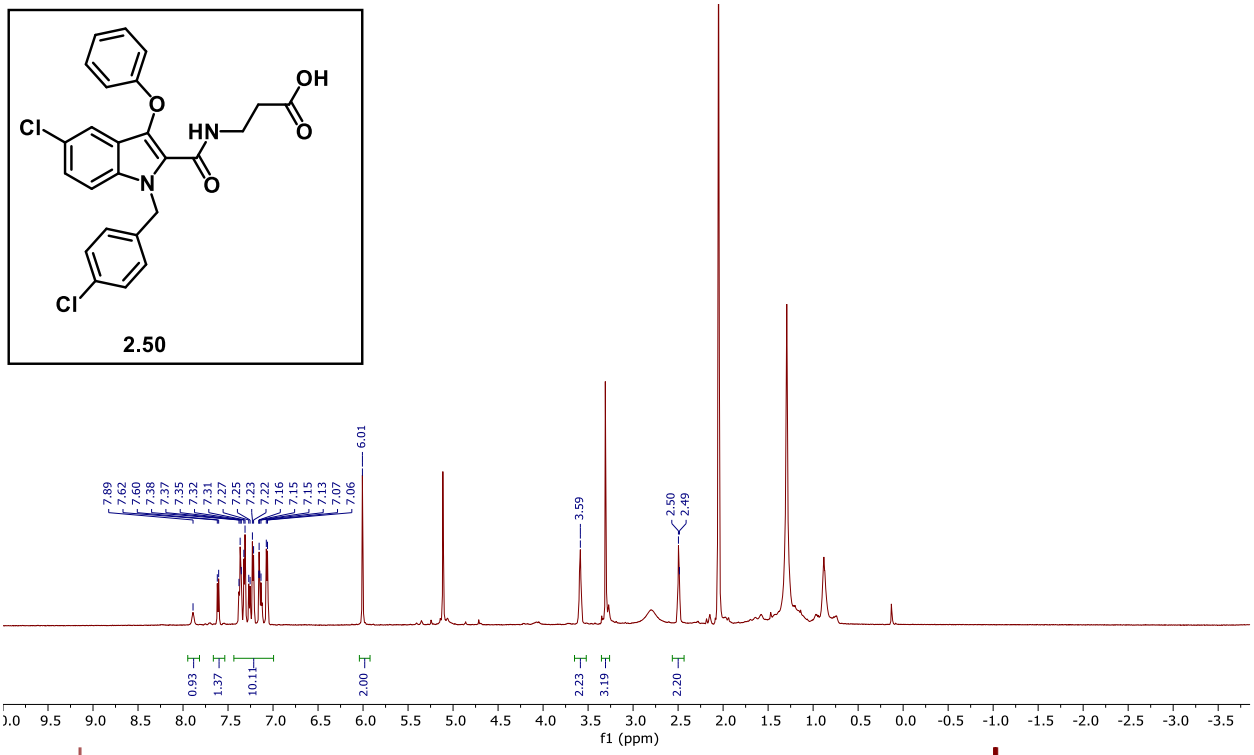
Cl
O
HN
OH
O
N
O
Cl
2.50
7.89
7.62
7.60
7.38
7.37
7.35
7.32
7.31
7.27
7.25
7.23
7.22
7.16
7.15
7.15
7.13
7.07
7.06
6.01
3.59
2.50
2.49
0.93
1.37
10.11
2.00
2.23
3.19
2.20
f1 (ppm)

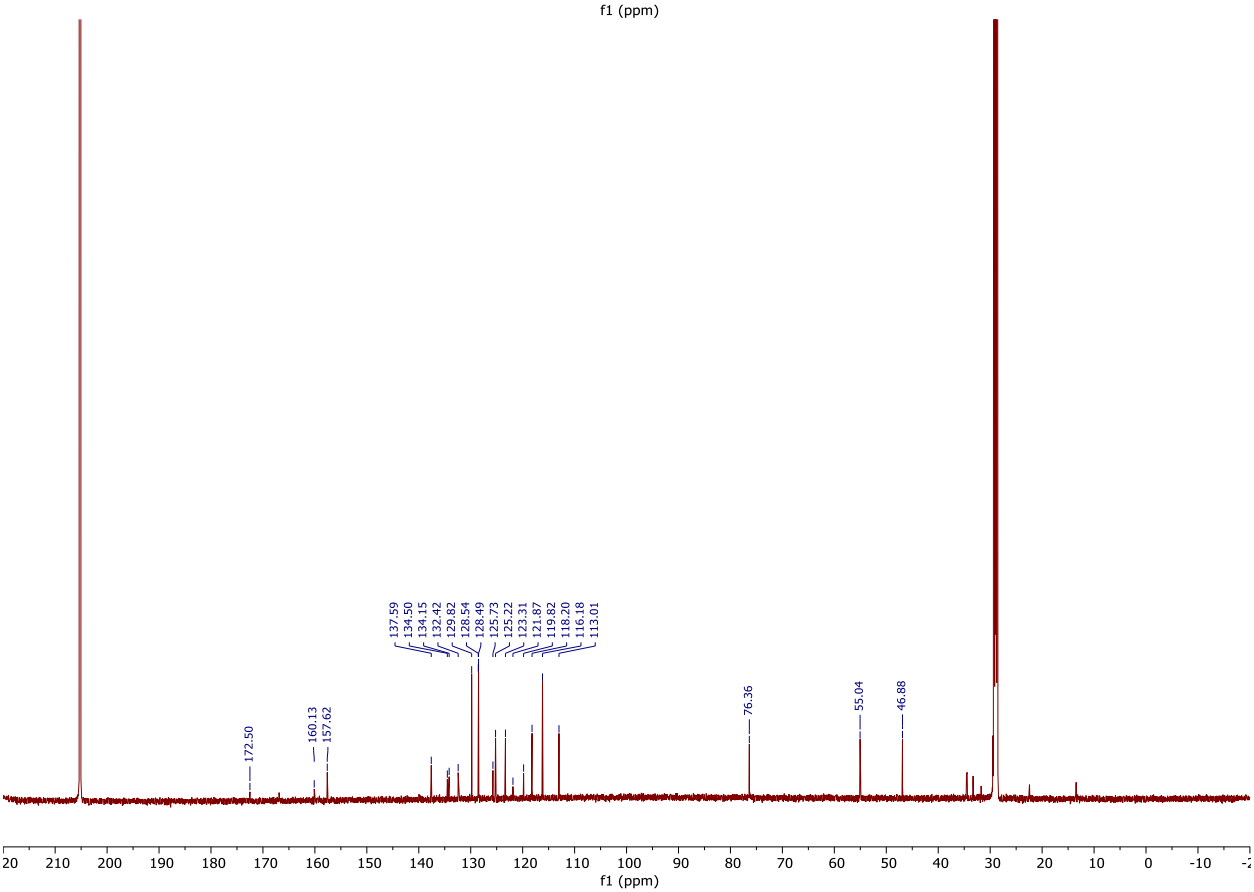
137.59
134.50
134.15
132.42
129.82
128.54
128.49
125.73
125.22
123.31
121.87
119.82
118.20
116.18
113.01
172.50
160.13
157.62
76.36
55.04
46.88
f1 (ppm)

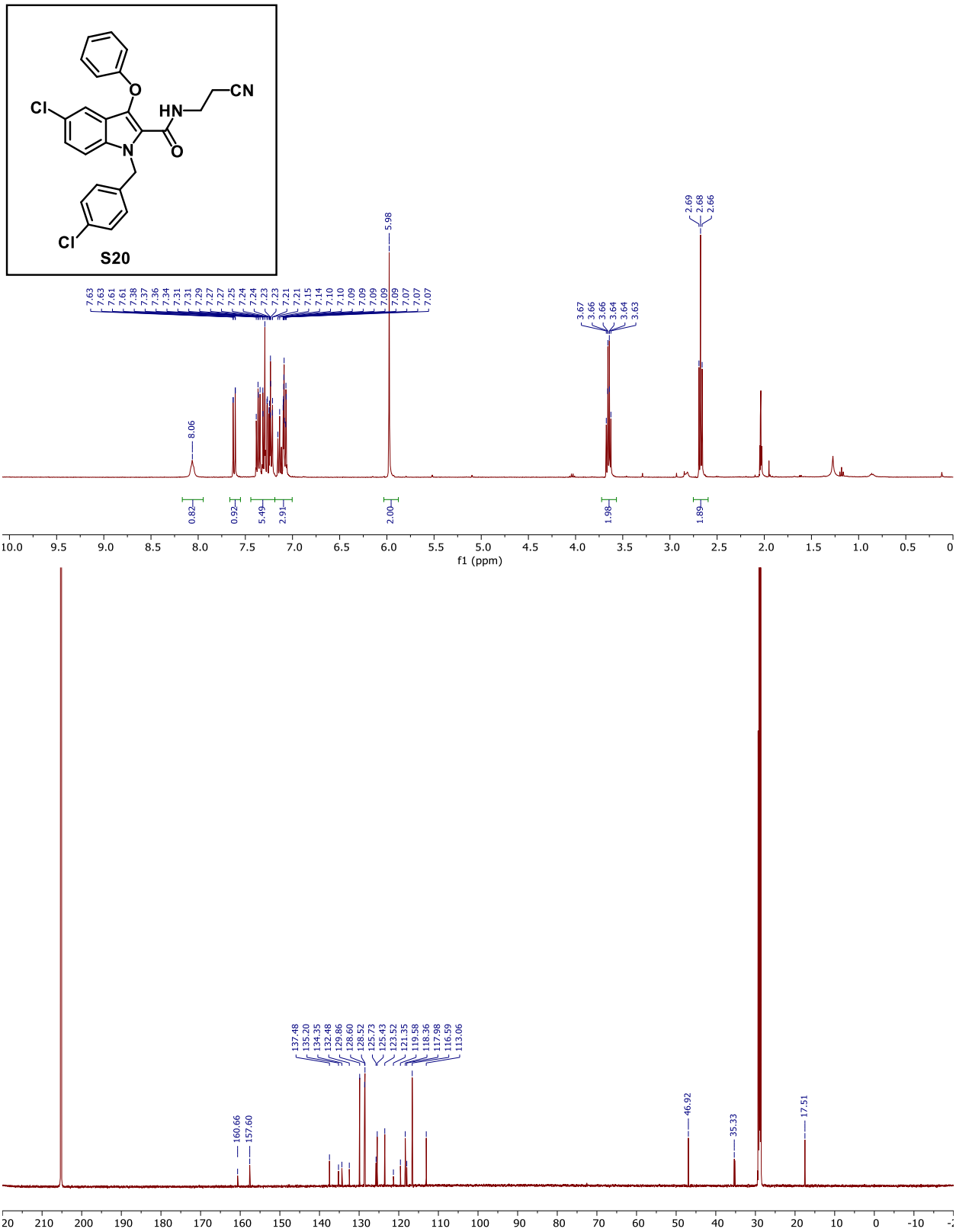
Cl
O
HN
CN
O
N
Cl
S20
7.63
7.63
7.61
7.61
7.38
7.37
7.36
7.34
7.31
7.31
7.29
7.27
7.27
7.25
7.24
7.24
7.23
7.23
7.21
7.21
7.15
7.14
7.10
7.10
7.09
7.09
7.09
7.09
7.09
7.07
7.07
7.07
5.98
3.67
3.66
3.66
3.64
3.64
3.64
3.63
2.69
2.68
2.66
8.06
0.82
0.92
5.49
2.91
2.00
1.98
1.89
f1 (ppm)
137.48
135.20
134.35
132.48
129.86
128.60
128.52
125.73
125.43
123.52
121.35
119.58
118.36
117.98
116.59
113.06
160.66
157.60
46.92
35.33
17.51

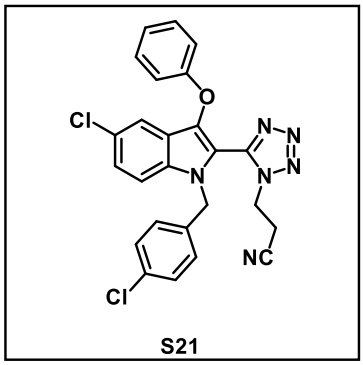
Cl
O
N
N
N
N
N
NC
Cl

S21

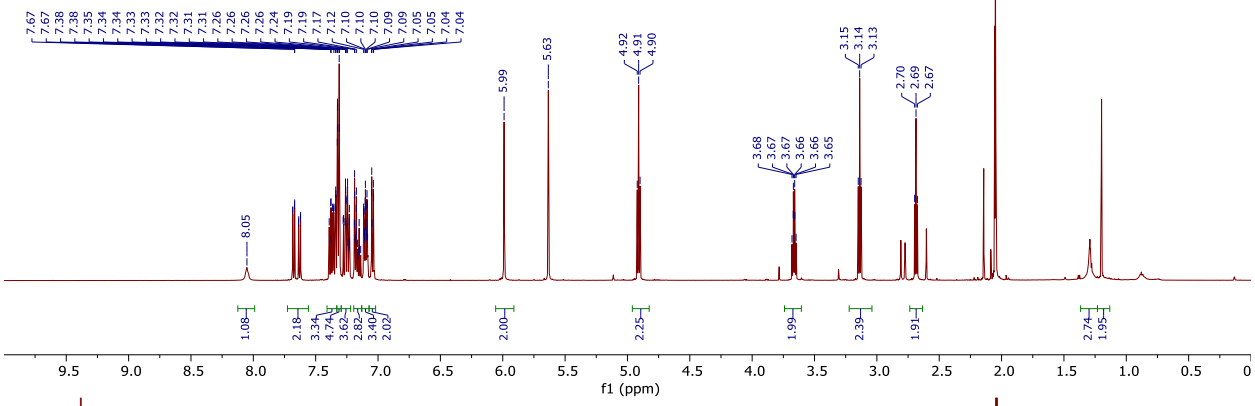
7.67
7.67
7.38
7.38
7.35
7.34
7.34
7.33
7.33
7.32
7.32
7.31
7.31
7.26
7.26
7.26
7.24
7.19
7.19
7.17
7.12
7.10
7.10
7.09
7.09
7.05
7.05
7.04
7.04
8.05
5.99
5.63
4.92
4.91
4.90
3.68
3.67
3.67
3.66
3.66
3.65
3.15
3.14
3.13
2.70
2.69
2.67
1.08
2.18
3.34
4.74
3.62
2.82
3.40
2.02
2.00
2.25
1.99
2.39
1.91
2.74
1.95
f1 (ppm)

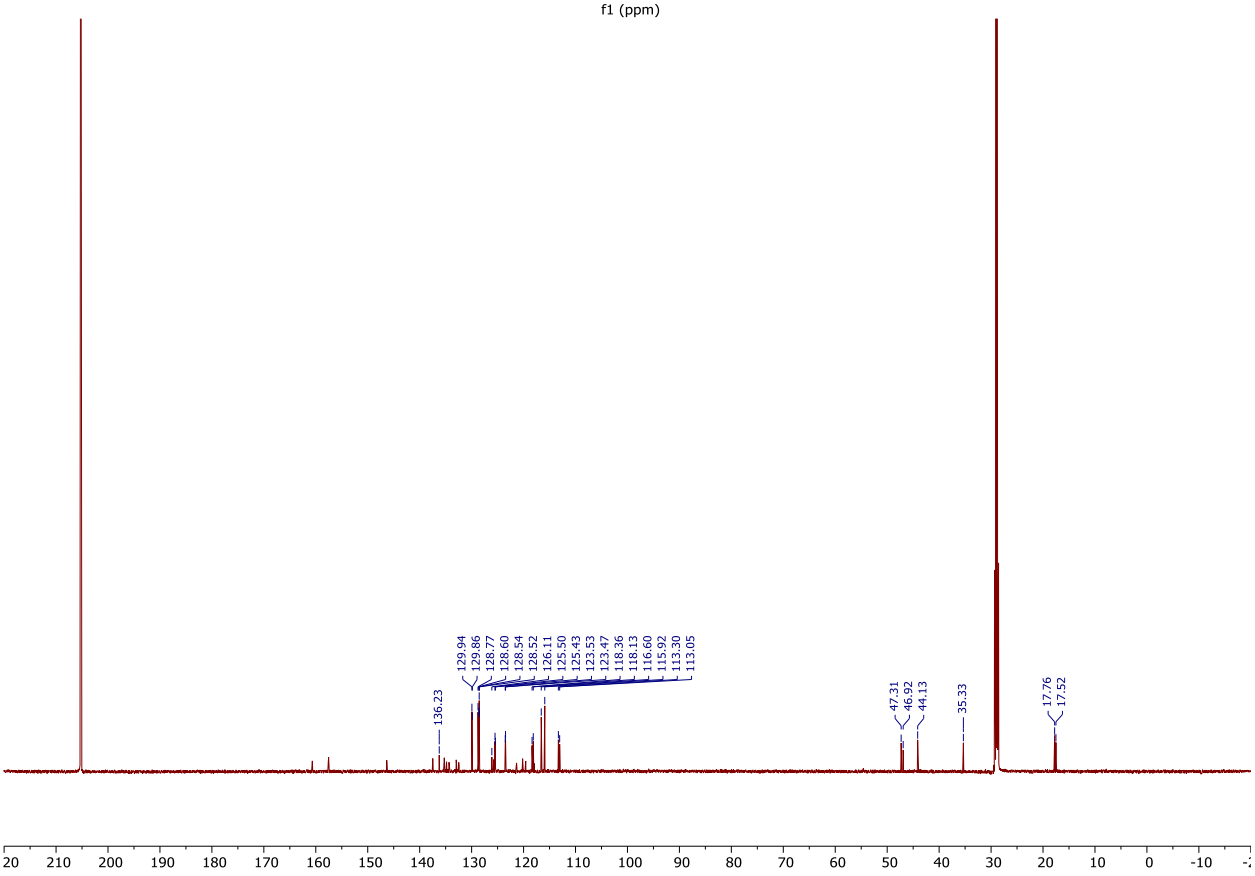
136.23
129.94
129.86
128.77
128.60
128.54
128.52
126.11
125.50
125.43
123.53
123.47
118.36
118.13
116.60
115.92
113.30
113.05
47.31
46.92
44.13
35.33
17.76
17.52

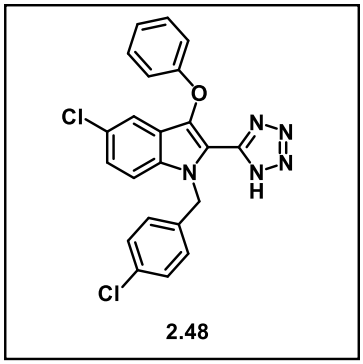
Cl
O
N
N
N
N
H
N
Cl

2.48

0.96
3.79
1.54
3.30
2.00
10.0
9.5
9.0
8.5
8.0
7.5
7.0
6.5
6.0
5.5
5.0
4.5
4.0
3.5
3.0
2.5
2.0
1.5
1.0
0.5

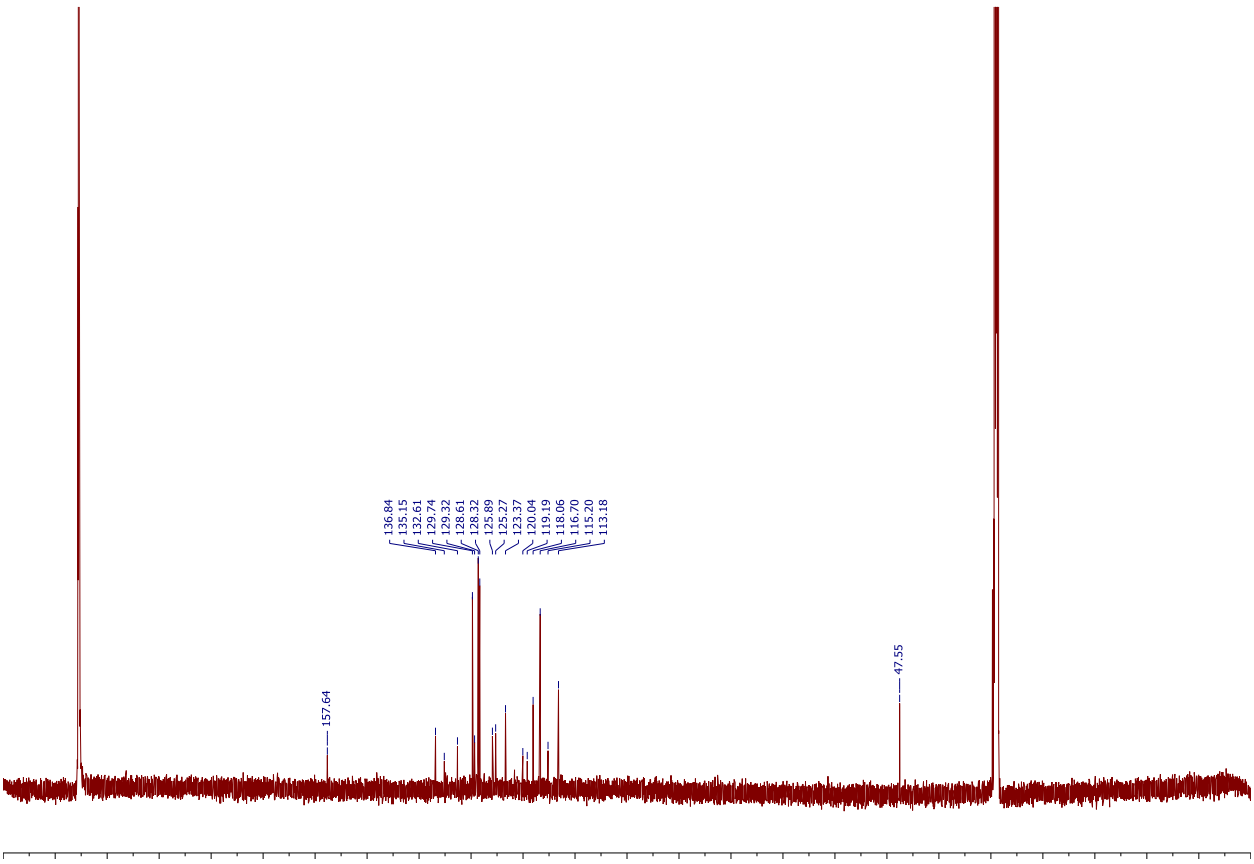
136.84
135.15
132.61
129.74
129.32
128.61
128.32
125.89
125.27
123.37
120.04
119.19
118.06
116.70
115.20
113.18
157.64
47.55

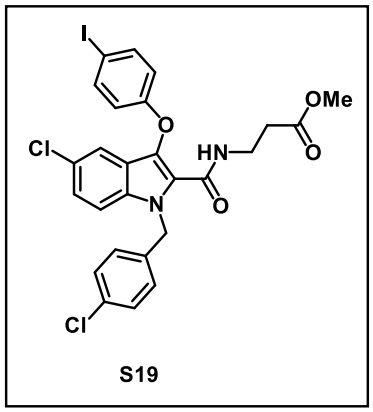
I
O
OMe
Cl
HN
O
N
O
Cl

S19

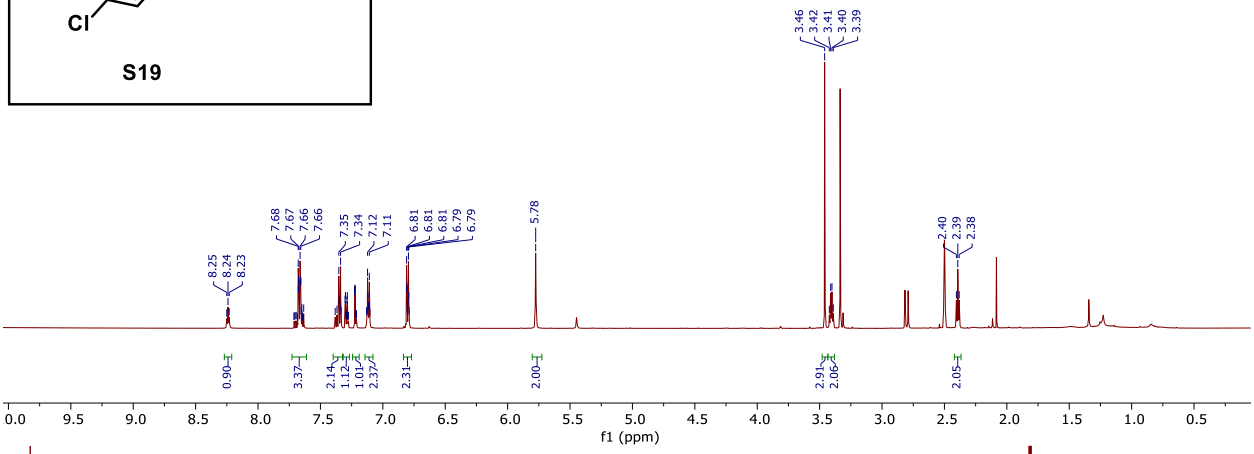
3.46
3.42
3.41
3.40
3.39
7.68
7.67
7.66
7.66
7.35
7.34
7.12
7.11
6.81
6.81
6.81
6.79
6.79
5.78
8.25
8.24
8.23
2.40
2.39
2.38
0.90
3.37
2.14
1.12
1.01
2.37
2.31
2.00
2.91
2.06
2.05
f1 (ppm)

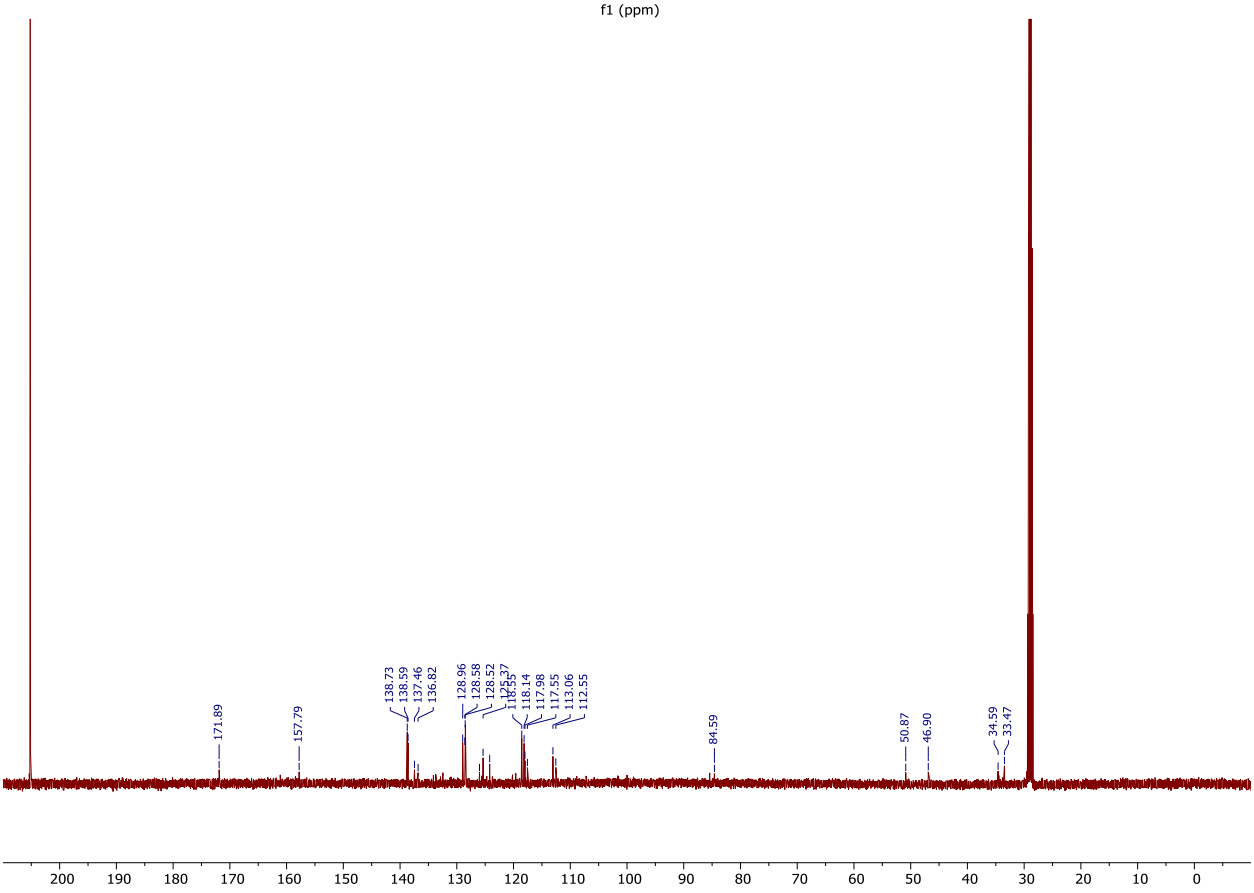
171.89
157.79
138.73
138.59
137.46
136.82
128.96
128.58
128.52
125.37
118.55
118.14
117.98
117.55
113.06
112.55
84.59
50.87
46.90
34.59
33.47

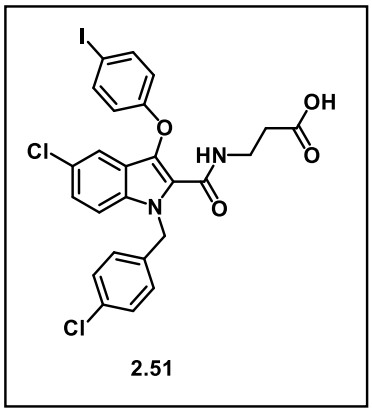
I
O
Cl
HN
OH
O
N
O
Cl

2.51

7.85
7.70
7.68
7.63
7.63
7.61
7.61
7.32
7.32
7.31
7.30
7.29
7.28
7.27
7.27
7.23
7.23
7.23
7.22
7.22
7.21
7.21
7.21
5.99
3.60
3.59
3.59
3.58
3.58
3.57
3.57
2.51
2.50
2.49
0.32
0.77
1.58
0.93
1.52
0.90
2.17
2.13
2.00
2.03
1.91
f1 (ppm)

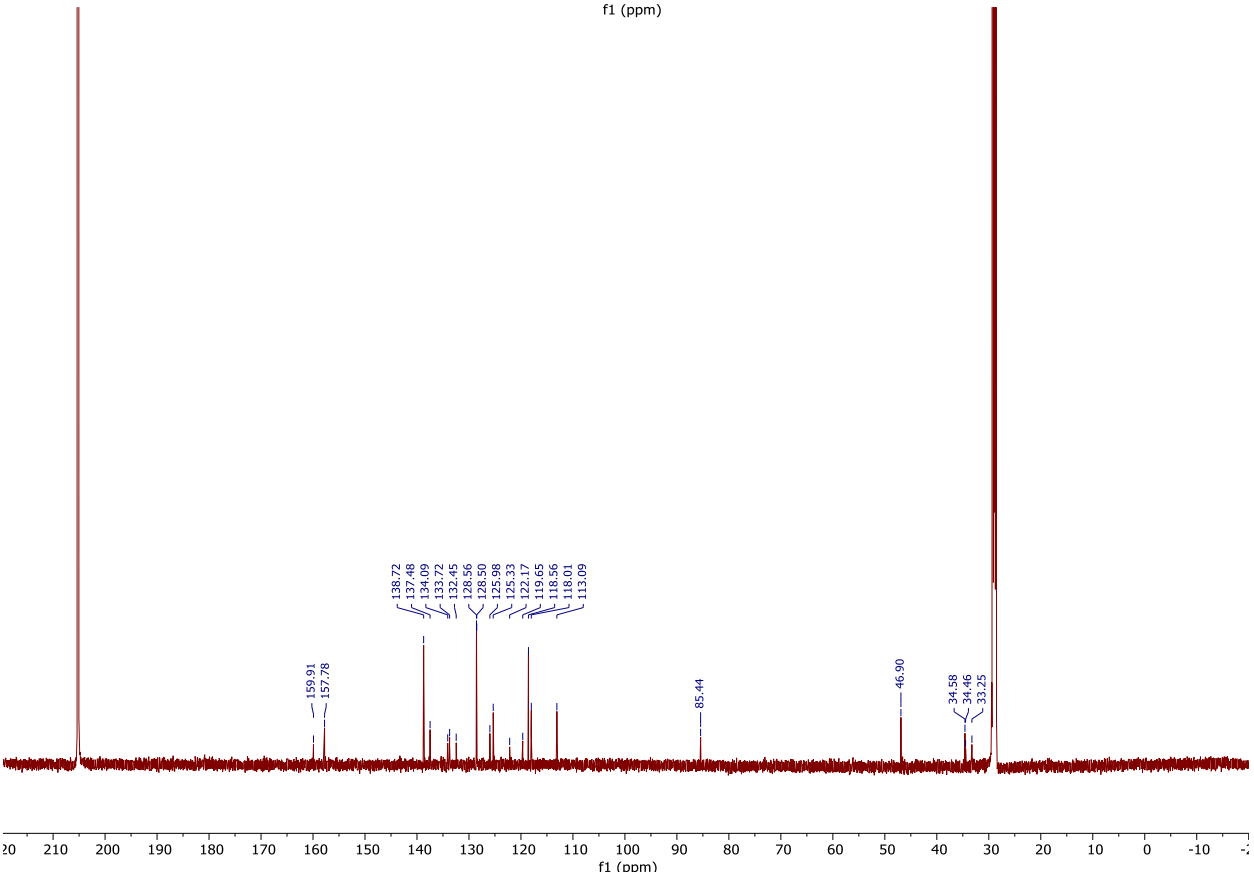
138.72
137.48
134.09
133.72
132.45
128.56
128.50
125.98
125.33
122.17
119.65
118.56
118.01
113.09
159.91
157.78
85.44
46.90
34.58
34.46
33.25
f1 (ppm)

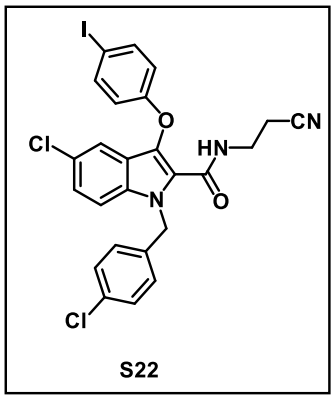
I
O
Cl
HN
CN
N
O
Cl

S22

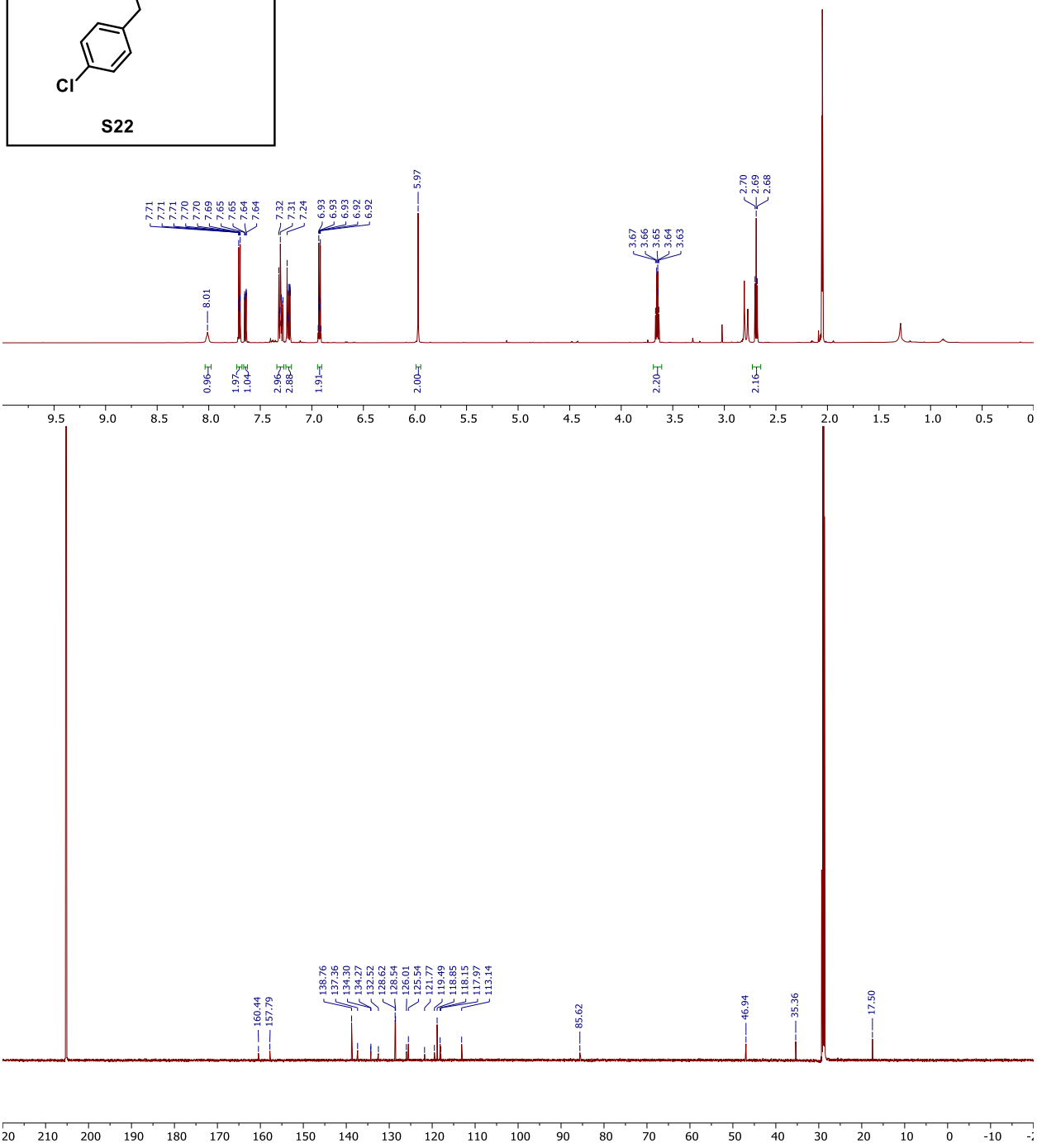
7.71
7.71
7.71
7.70
7.70
7.69
7.65
7.65
7.64
7.64
7.32
7.31
7.24
6.93
6.93
6.93
6.92
6.92
5.97
3.67
3.66
3.65
3.64
3.63
2.70
2.69
2.68
8.01
0.96
1.97
1.04
2.96
2.88
1.91
2.00
2.20
2.16
160.44
157.79
138.76
137.36
134.30
134.27
132.52
128.62
128.54
126.01
125.54
121.77
119.49
118.85
118.15
117.97
113.14
85.62
46.94
35.36
17.50

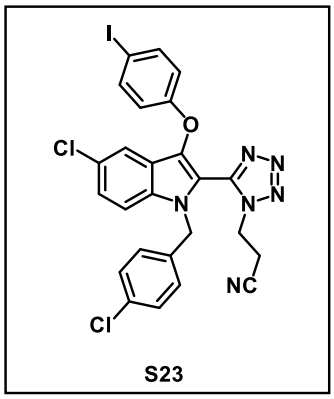
I
O
Cl
N
N
N
N
N
NC
Cl

S23

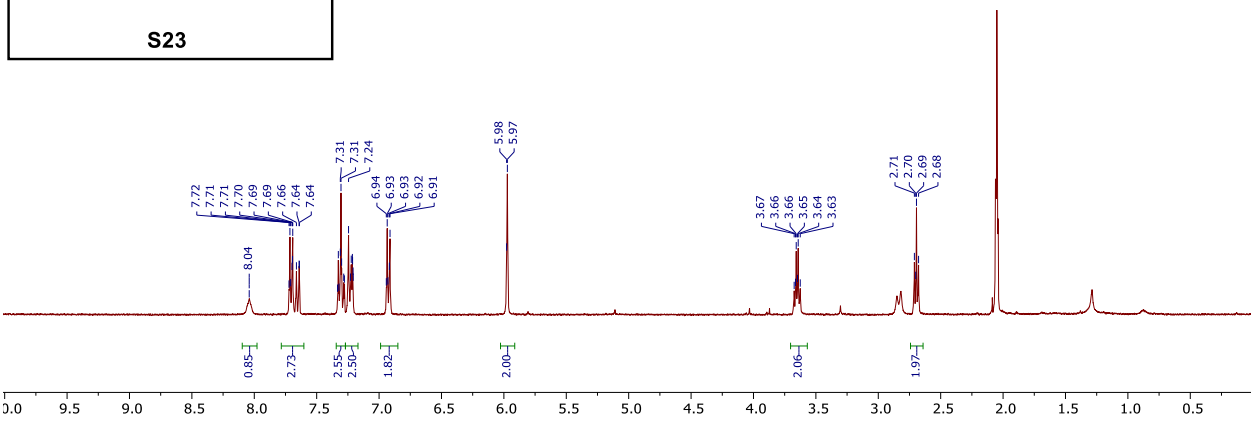
7.72
7.71
7.71
7.70
7.69
7.69
7.66
7.64
7.64
8.04
7.31
7.31
7.24
6.94
6.93
6.93
6.92
6.91
5.98
5.97
3.67
3.66
3.66
3.65
3.64
3.63
2.71
2.70
2.69
2.68
0.85
2.73
2.55
2.50
1.82
2.00
2.06
1.97

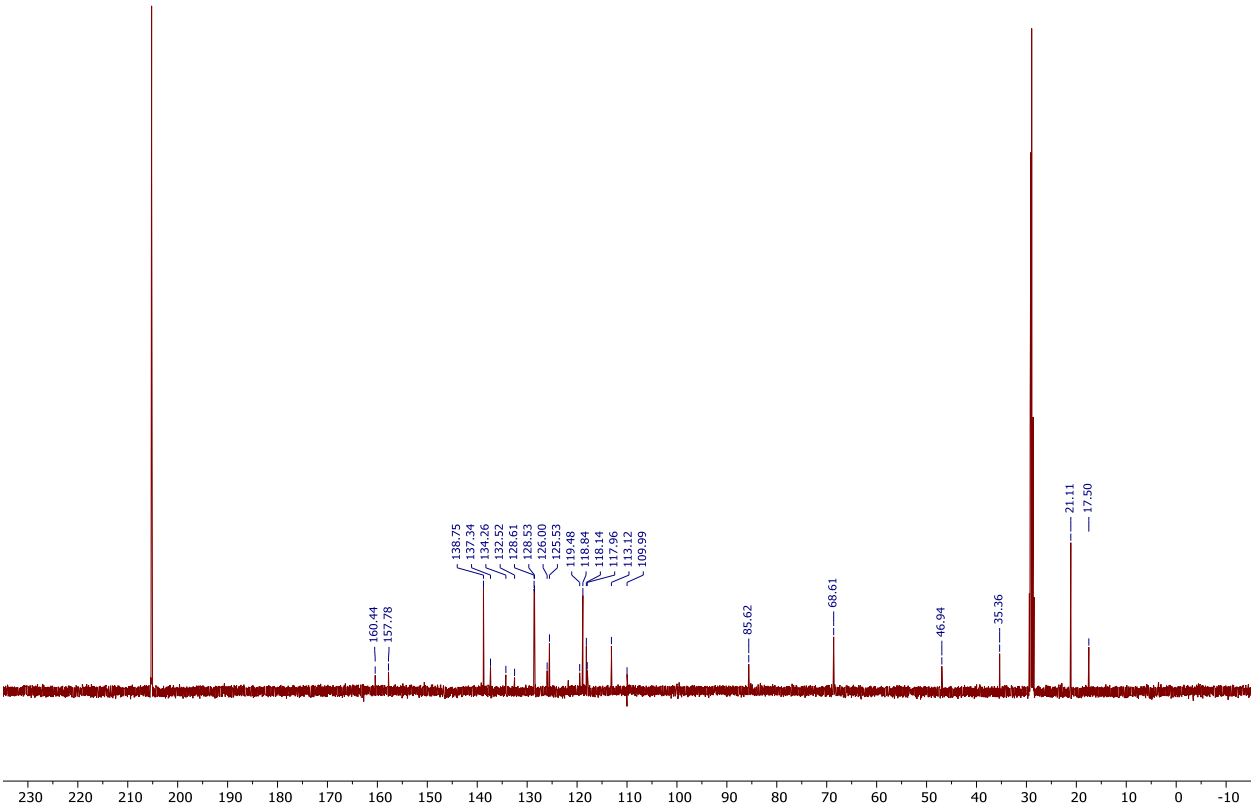
138.75
137.34
134.26
132.52
128.61
128.53
126.00
125.53
119.48
118.84
118.14
117.96
113.12
109.99
160.44
157.78
85.62
68.61
46.94
35.36
21.11
17.50

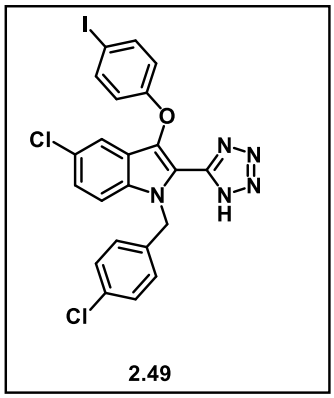
I
O
Cl
N
N
N
N
H
N
Cl

2.49

1.48
1.62
1.23
2.30
2.01
3.77
2.00
161.42
137.49
134.90
132.40
129.06
128.50
128.13
126.26
125.59
125.54
120.76
118.91
117.44
112.73
62.19
61.86
51.11
46.96

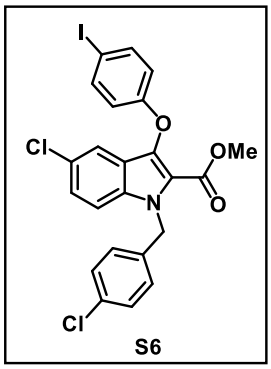
I
O
Cl
OMe
N
O
Cl

S6

3.66
3.66
7.65
7.64
7.63
7.63
7.63
7.62
7.62
7.61
7.61
7.41
7.41
7.34
7.34
7.13
7.12
7.12
7.10
7.10
6.81
6.79
6.79
5.88
5.88
5.88
2.83
0.72
2.65
1.84
1.78
2.20
3.06
f1 (ppm)

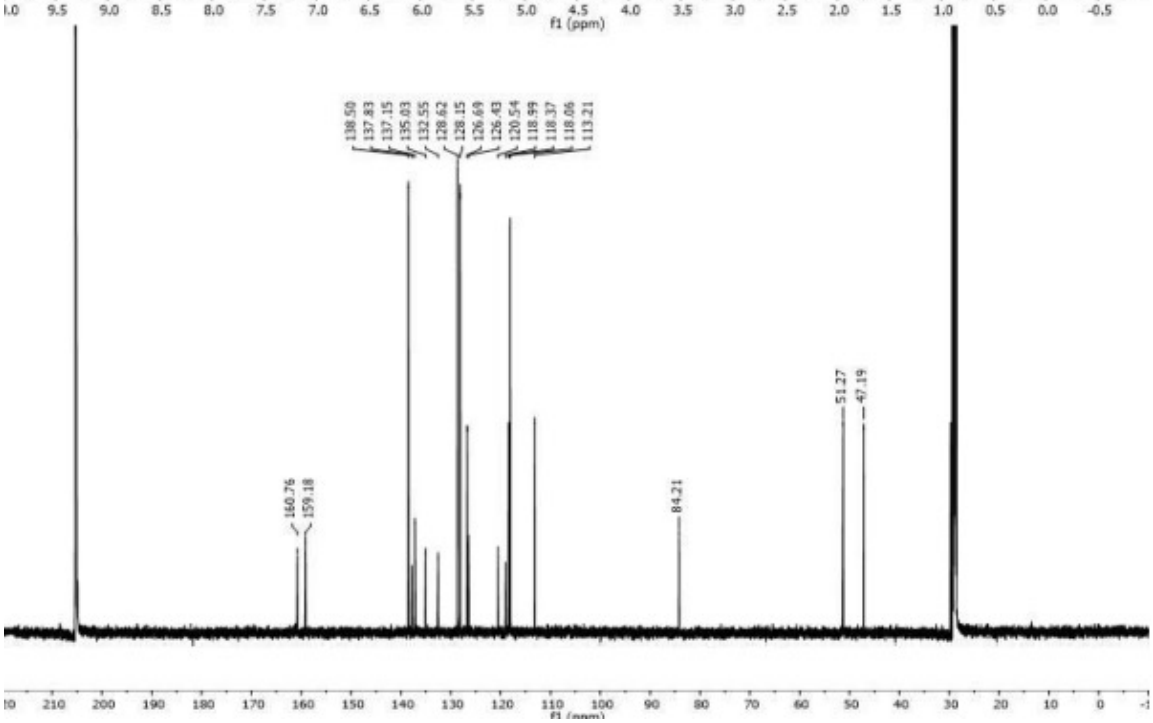
138.50
137.83
137.15
135.03
132.55
128.62
128.15
126.69
126.43
120.54
118.99
118.37
118.06
113.21
160.76
159.18
84.21
51.27
47.19

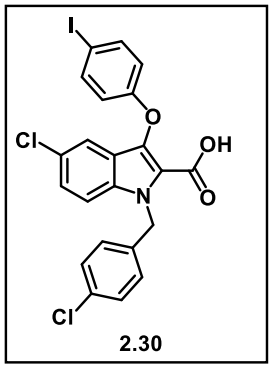
I
O
Cl
OH
O
N
Cl

2.30

7.68
7.67
7.66
7.65
7.65
7.45
7.44
7.38
7.36
7.36
7.35
7.34
7.34
7.18
7.17
7.17
6.86
6.86
6.85
6.85
5.96
2.81
0.94
2.72
1.75
1.86
2.20
f1 (ppm)

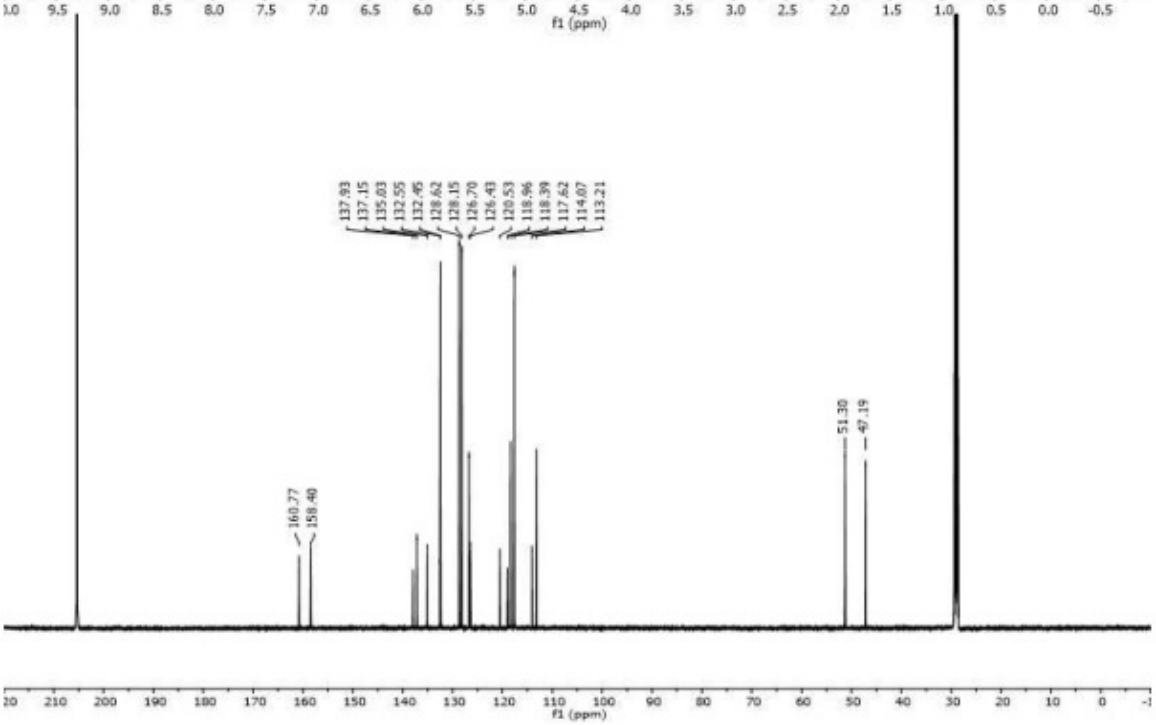
137.93
137.15
135.03
132.55
132.46
128.62
128.15
126.70
126.43
120.53
118.96
118.39
117.62
114.07
113.21
160.77
158.40
51.30
47.19
f1 (ppm)

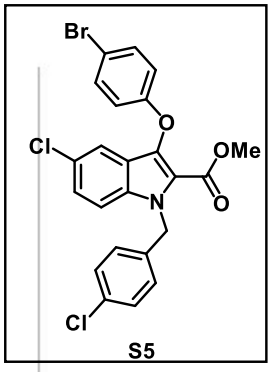
Br
O
Cl
OMe
N
O
Cl

S5

7.69
7.69
7.67
7.66
7.49
7.49
7.47
7.47
7.44
7.44
7.38
7.35
7.32
7.16
7.14
7.14
6.97
6.95
6.95
5.92
3.70
1.11
2.71
2.83
1.94
1.87
2.00
3.32
f1 (ppm)

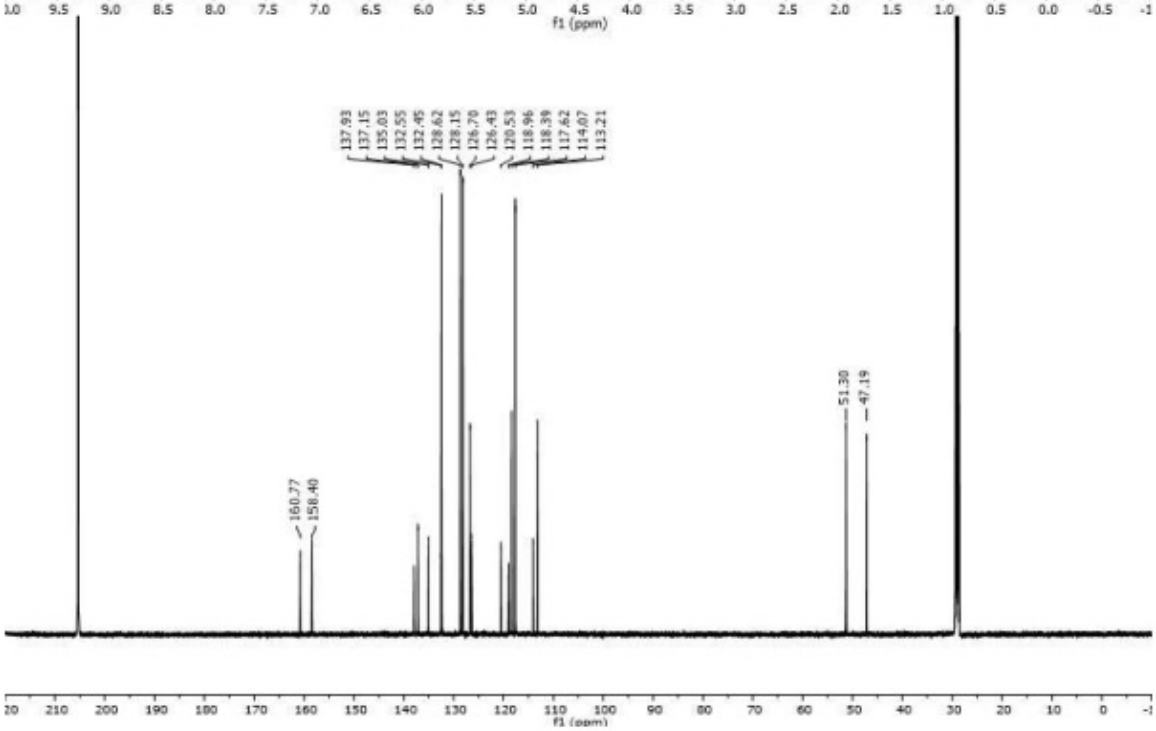
137.93
137.15
135.03
132.55
132.45
128.62
128.15
126.70
126.43
120.53
118.96
118.39
117.62
114.07
113.21
160.77
158.40
51.30
47.19
f1 (ppm)

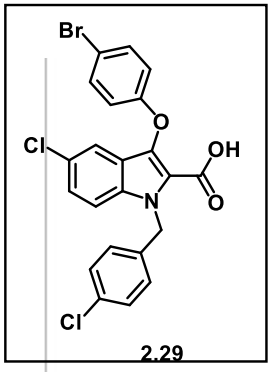
Br
O
Cl
OH
N
O
Cl

2.29

7.64
7.63
7.61
7.61
7.44
7.42
7.39
7.39
7.39
7.39
7.33
7.32
7.31
7.30
7.28
7.14
7.11
6.93
6.93
6.91
5.91
1.07
2.72
2.81
2.10
2.08
2.00
f1 (ppm)

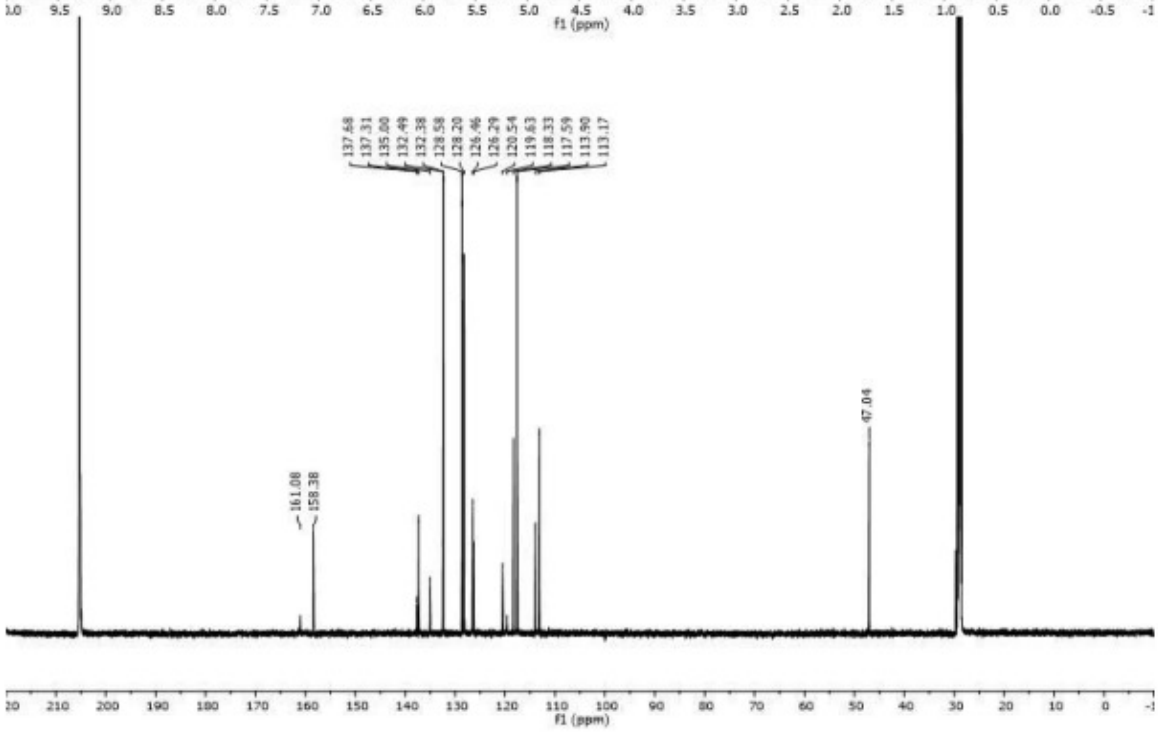
137.68
137.31
135.00
132.49
132.38
128.58
128.20
126.46
126.29
120.54
119.63
118.33
117.59
113.90
113.17
161.08
158.38
47.04
f1 (ppm)

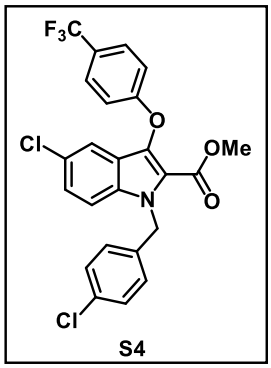
F3C
O
Cl
OMe
N
O
Cl

S4

3.68
5.94
7.71
7.71
7.70
7.70
7.69
7.69
7.68
7.50
7.49
7.40
7.35
7.35
7.33
7.33
7.18
7.18
7.16
7.16
7.16
2.98
0.83
2.81
3.75
2.00
2.99
f1 (ppm)
127.24
127.17
127.15
127.12
127.10
126.44
124.13
123.91
123.70
123.65
123.48
121.86
f1 (ppm)
137.34
137.10
135.03
132.59
128.64
128.16
126.82
126.62
120.50
119.02
118.27
115.88
113.26
161.78
160.64
51.32
47.25
f1 (ppm)

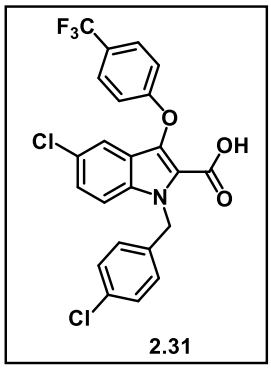
F3C
O
Cl
OH
N
O
Cl

2.31

7.68
7.67
7.66
7.65
7.65
7.45
7.44
7.38
7.36
7.36
7.35
7.34
7.34
7.18
7.17
7.17
6.86
6.86
6.85
6.85
5.96
2.81
0.94
2.77
1.75
1.86
2.20
f1 (ppm)
137.24
137.18
135.04
132.53
128.61
128.19
126.64
126.51
125.59
120.51
118.22
115.83
113.24
161.79
160.91
47.10
f1 (ppm)

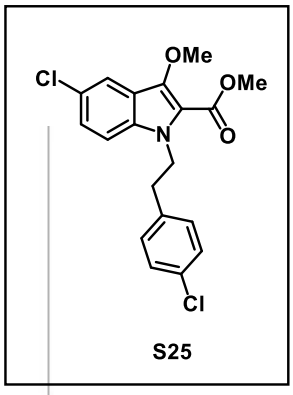
OMe
Cl
OMe
N
O
Cl

S25

4.00
3.93
7.71
7.71
7.71
7.71
7.23
7.22
7.22
7.22
7.20
7.16
7.04
7.04
7.02
4.65
4.63
4.63
4.63
4.61
2.99
2.97
2.95
0.92
1.85
1.06
1.11
2.05
2.27
3.00
3.37
2.33
f1 (ppm)
136.74
134.19
132.42
130.25
128.56
126.30
125.66
120.35
119.26
116.97
111.39
161.82
62.80
51.78
51.76
46.09
36.19
f1 (ppm)

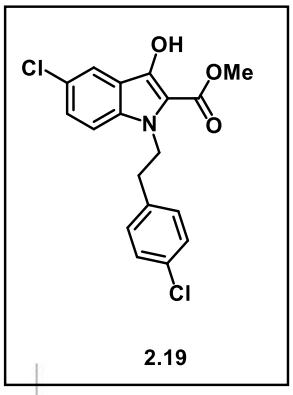
OH
Cl
OMe
N
O
Cl

2.19

7.24
7.23
7.23
7.21
7.21
7.20
7.20
7.19
7.19
7.18
7.17
7.01
7.01
6.99
6.99
6.98
6.98
6.97
6.96
6.96
6.95
8.37
7.70
7.69
7.69
7.69
4.50
4.48
4.47
4.46
3.95
2.92
2.91
2.89
0.50
0.67
0.64
1.29
0.99
2.98
2.21
3.00
2.23
f1 (ppm)

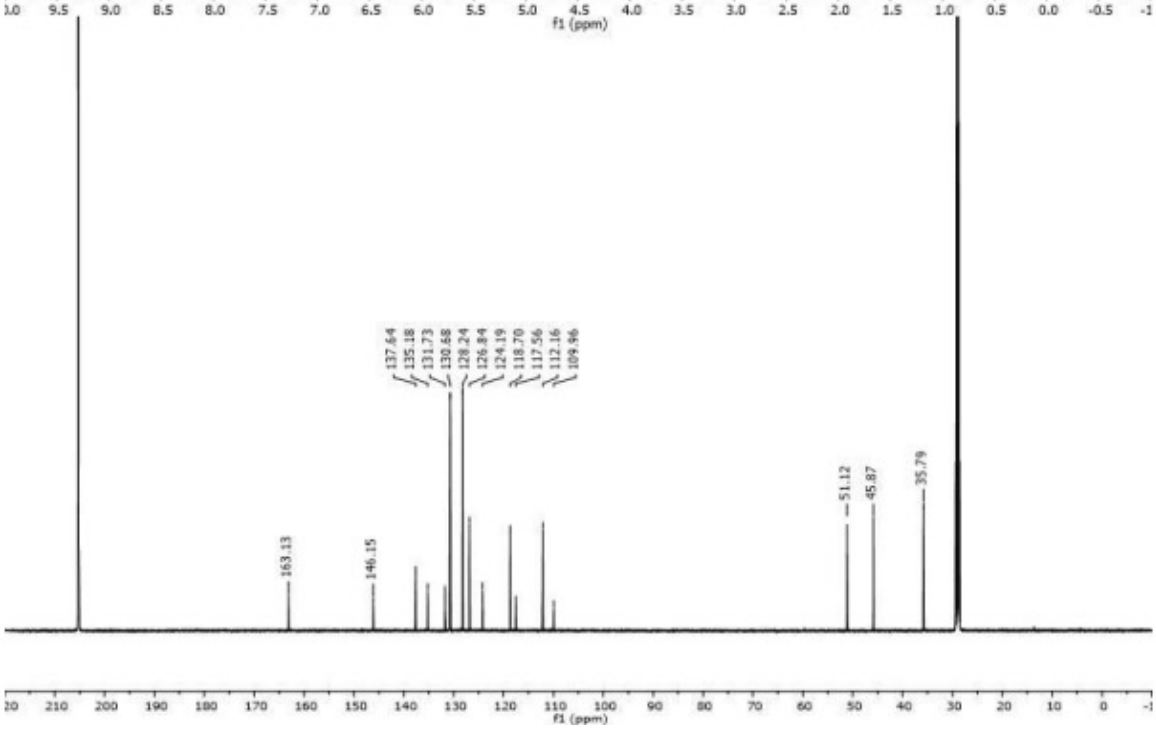
137.64
135.18
131.73
130.68
128.24
126.84
124.19
118.70
117.56
112.16
109.86
163.13
146.15
51.12
45.87
35.79
f1 (ppm)

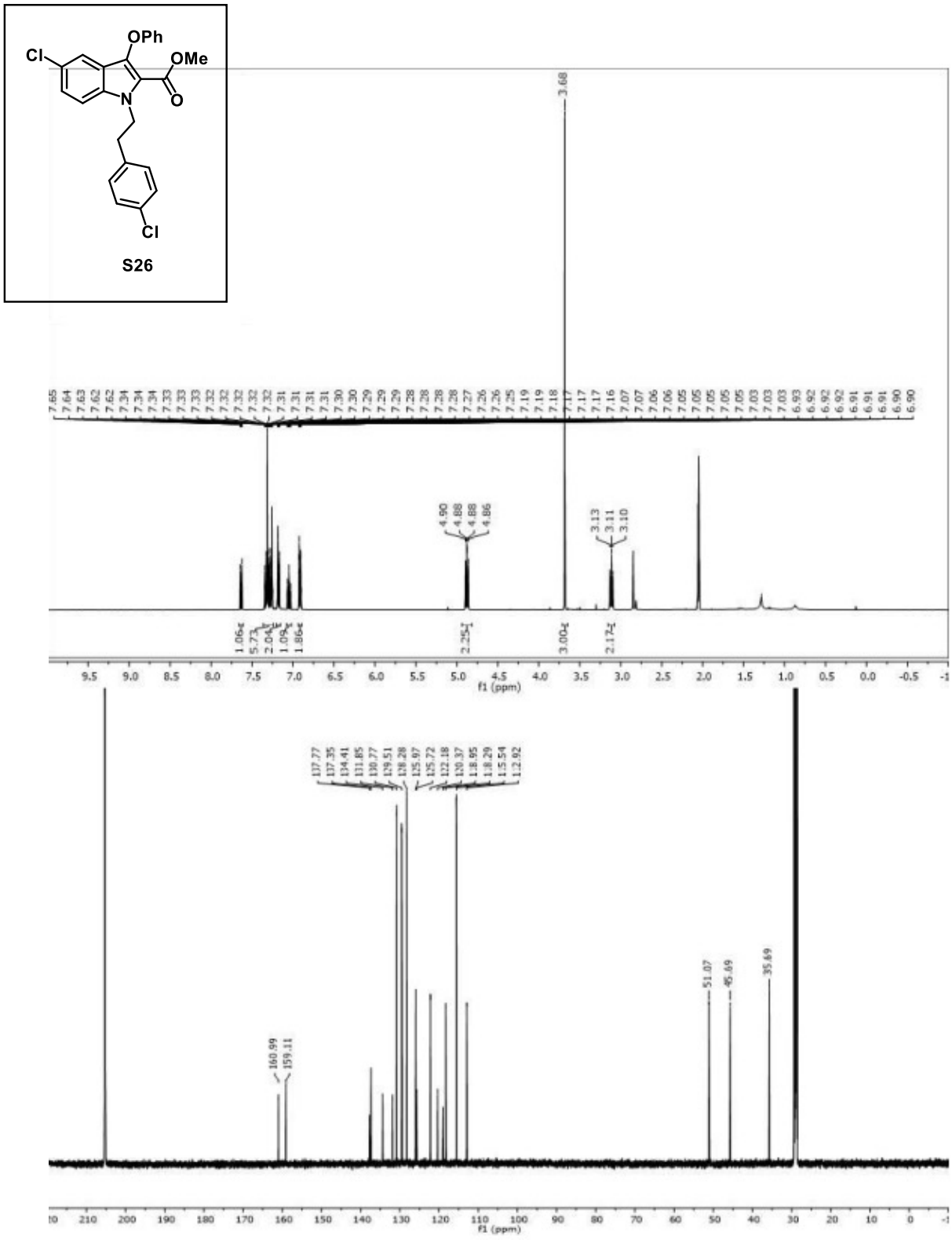
OPh
Cl
OMe
N
O
Cl
S26
f1 (ppm)

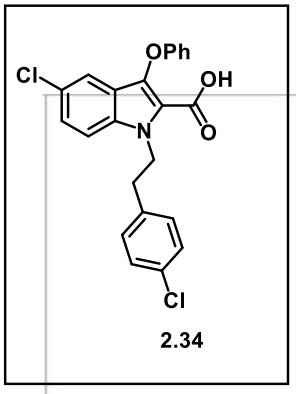
OPh
Cl
OH
N
O
Cl

2.34

7.62
7.61
7.60
7.59
7.32
7.31
7.30
7.30
7.28
7.28
7.26
7.26
7.25
7.24
7.24
7.23
7.21
7.20
7.20
7.19
7.18
7.04
7.04
7.04
7.02
7.02
7.02
7.00
7.00
7.00
6.93
6.93
6.92
6.92
6.91
6.91
6.91
6.90
4.90
4.88
4.86
3.14
3.12
3.10
1.06
7.79
0.99
2.00
2.26
2.37
f1 (ppm)

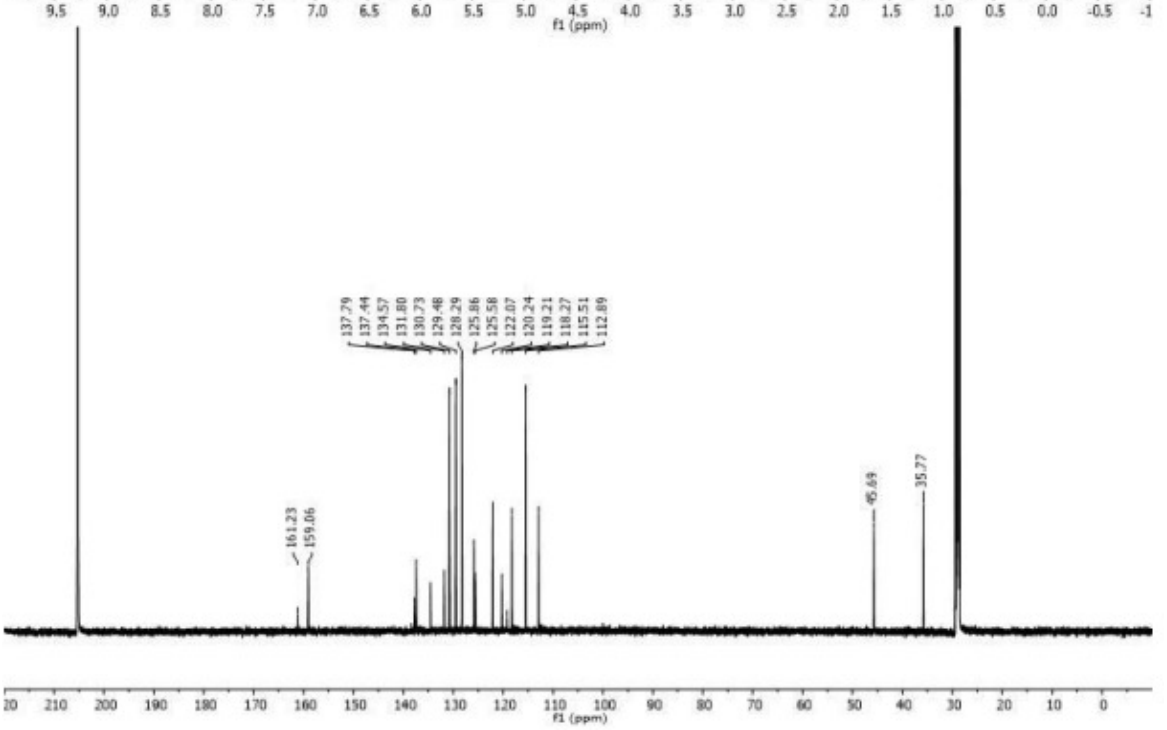
137.79
137.44
134.57
131.80
130.73
129.48
128.29
125.86
125.58
122.07
120.24
119.21
118.27
115.51
112.89
161.23
159.06
65.69
35.77
f1 (ppm)

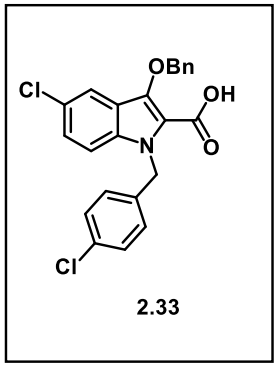
OBn
Cl
OH
O
N
Cl

2.33

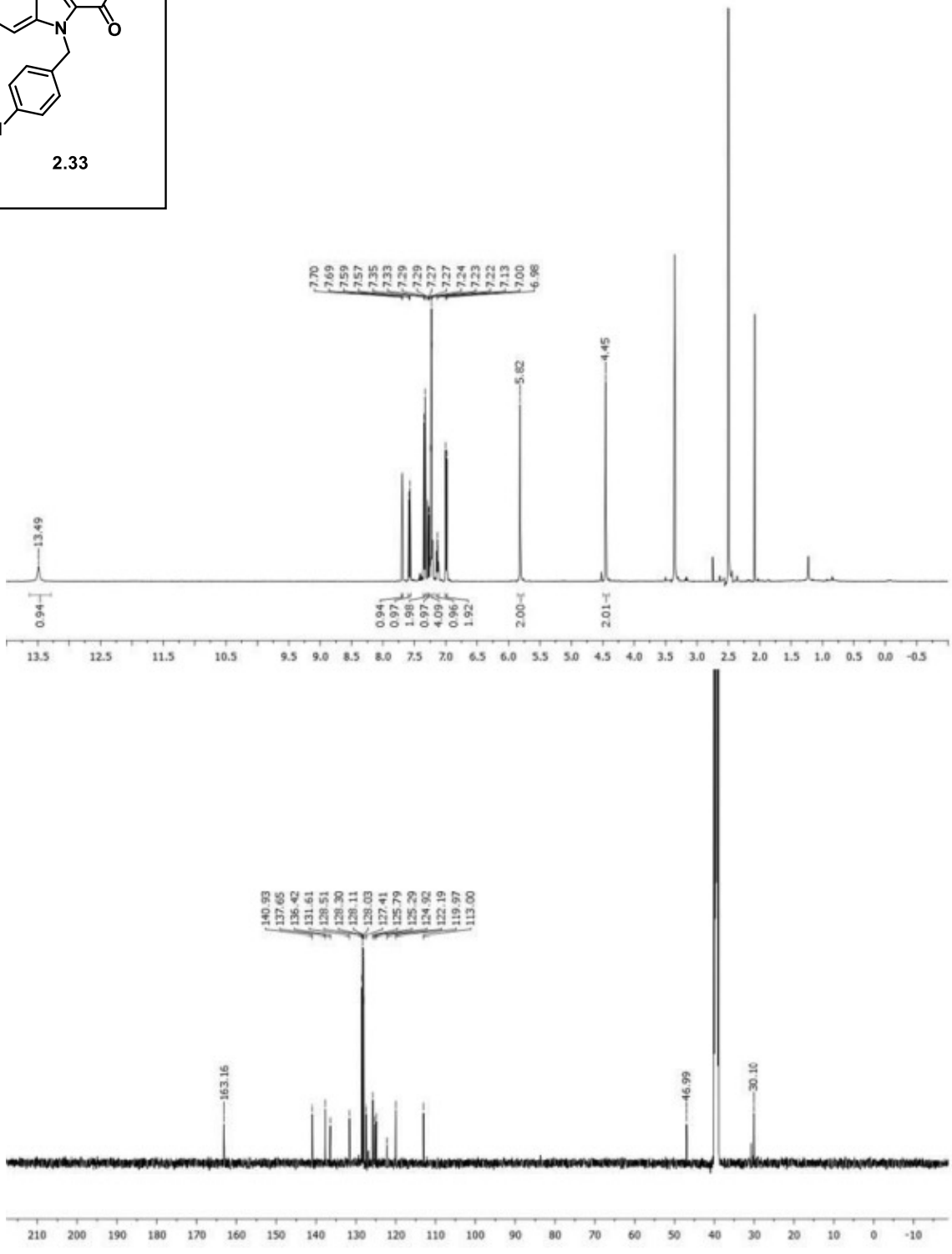
7.70
7.69
7.59
7.57
7.35
7.33
7.29
7.29
7.27
7.27
7.24
7.23
7.22
7.13
7.00
6.98
5.82
4.45
13.49
0.94
0.94
0.97
1.98
0.97
4.09
0.96
1.92
2.00
2.01
13.5 12.5 11.5 10.5 9.5 9.0 8.5 8.0 7.5 7.0 6.5 6.0 5.5 5.0 4.5 4.0 3.5 3.0 2.5 2.0 1.5 1.0 0.5 0.0 -0.5
140.93
137.65
136.42
131.61
128.51
128.30
128.11
128.03
127.41
125.79
125.29
124.92
122.19
119.97
113.00
163.16
46.99
30.10
210 200 190 180 170 160 150 140 130 120 110 100 90 80 70 60 50 40 30 20 10 0 -10

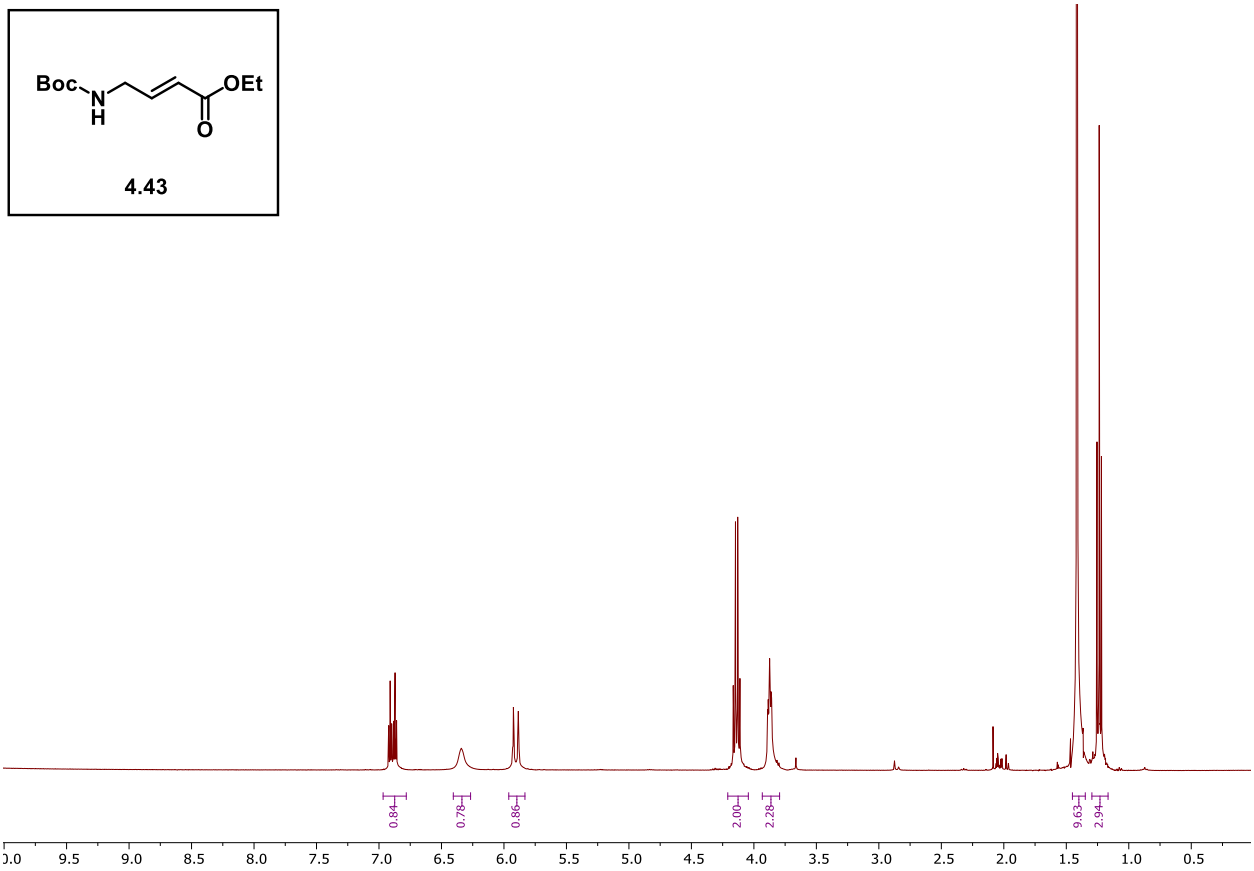
Boc
N
H
OEt
O
4.43
0.84
0.78
0.86
2.00
2.28
9.63
2.94
9.5
9.0
8.5
8.0
7.5
7.0
6.5
6.0
5.5
5.0
4.5
4.0
3.5
3.0
2.5
2.0
1.5
1.0
0.5

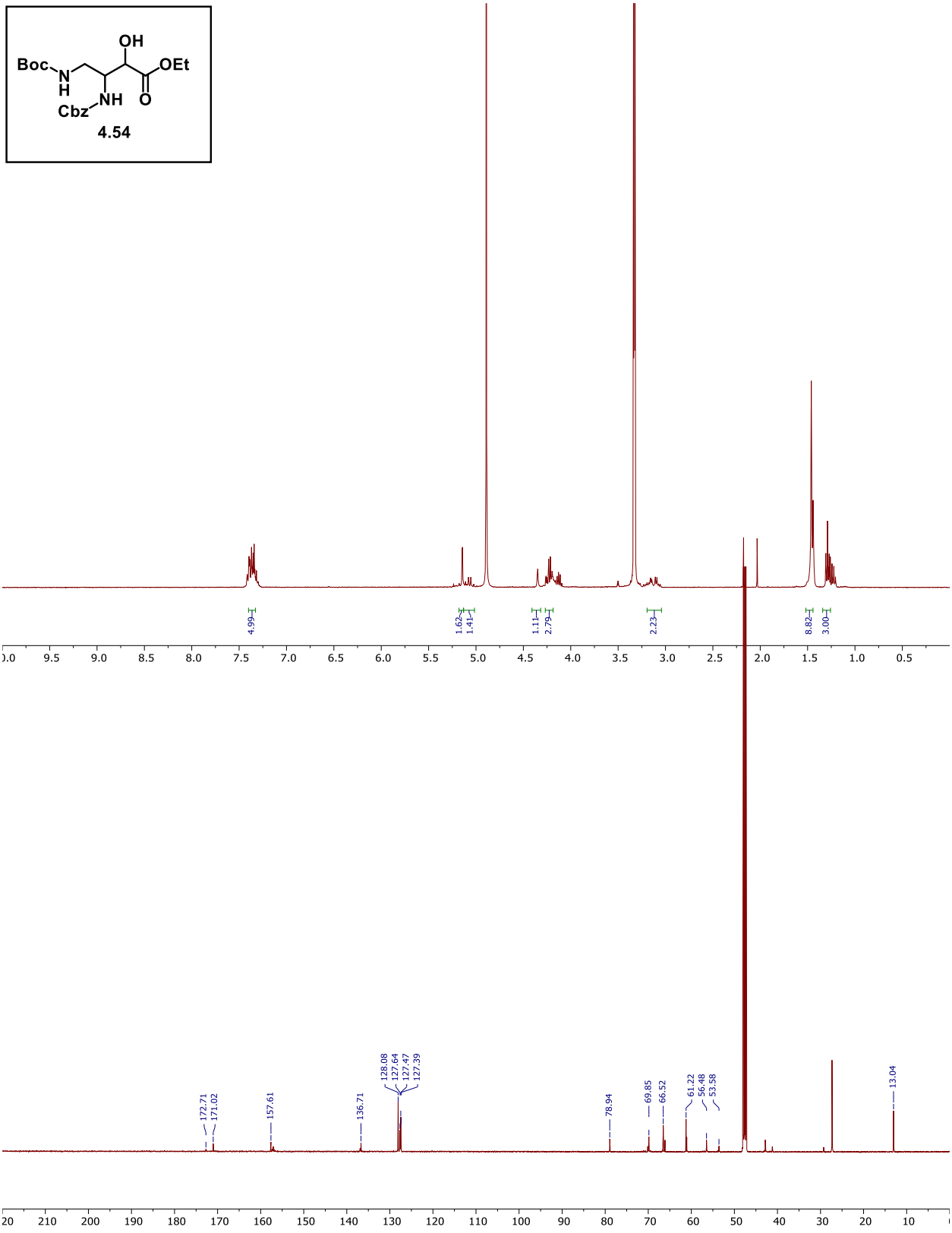
OH
Boc
N
H
OEt
NH
O
Cbz
4.54
4.99
1.62
1.41
1.11
2.79
2.23
8.82
3.00
172.71
171.02
157.61
136.71
128.08
127.64
127.47
127.39
78.94
69.85
66.52
61.22
56.48
53.58
13.04

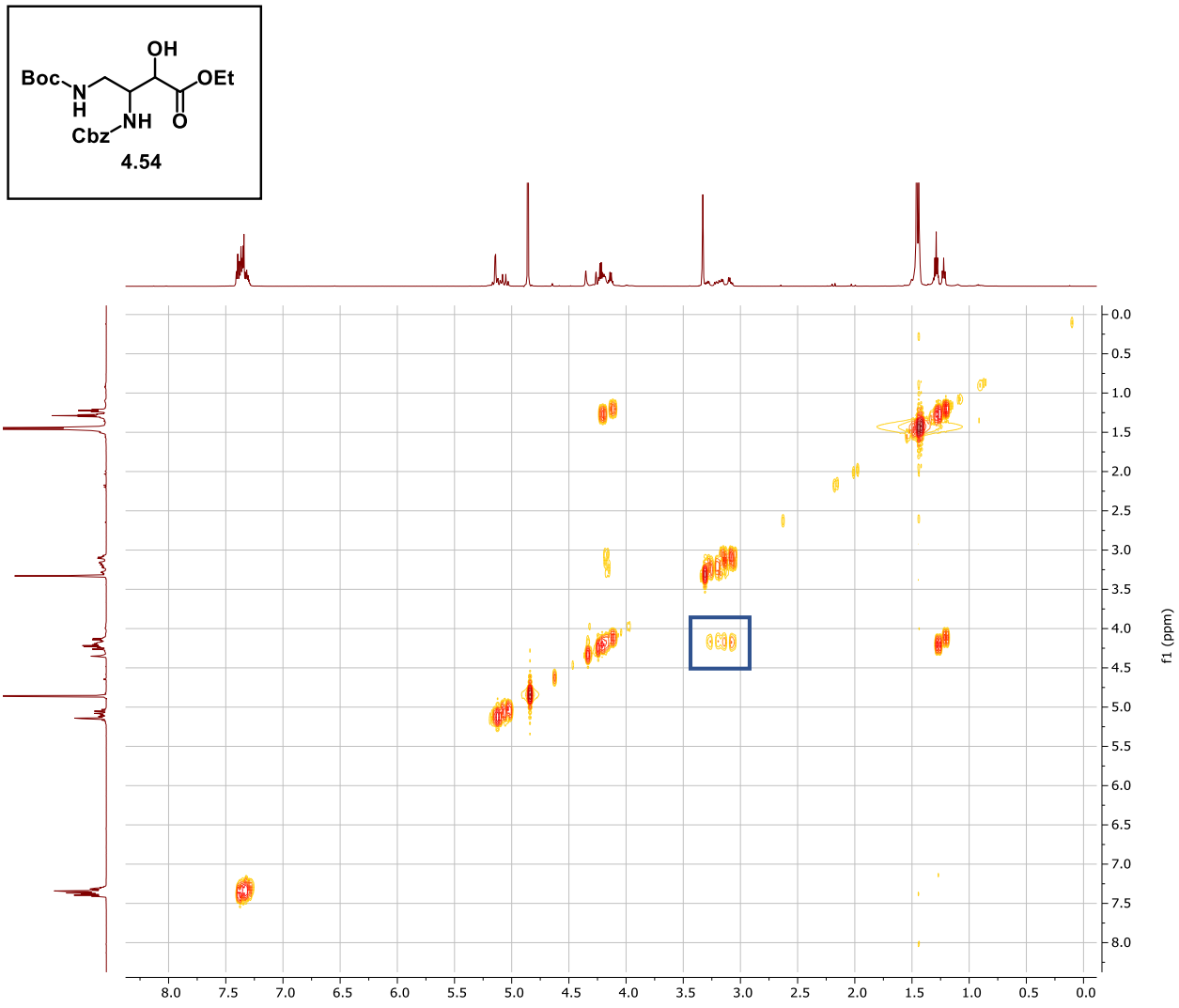
OH
Boc
N
H
OEt
NH
O
Cbz
4.54
f1 (ppm)
8.0
7.5
7.0
6.5
6.0
5.5
5.0
4.5
4.0
3.5
3.0
2.5
2.0
1.5
1.0
0.5
0.0

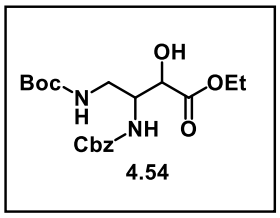

4.54

Previous spectrum but zoomed in

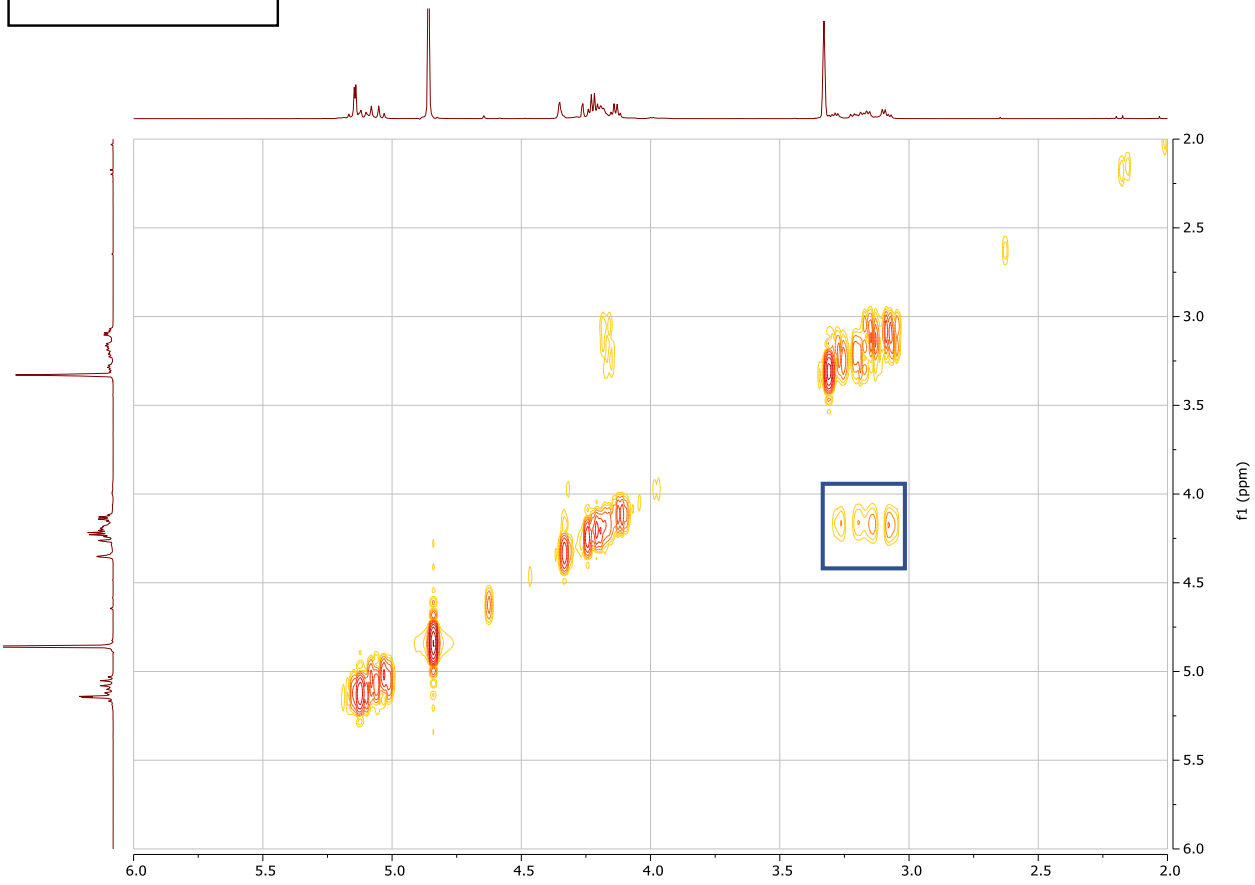

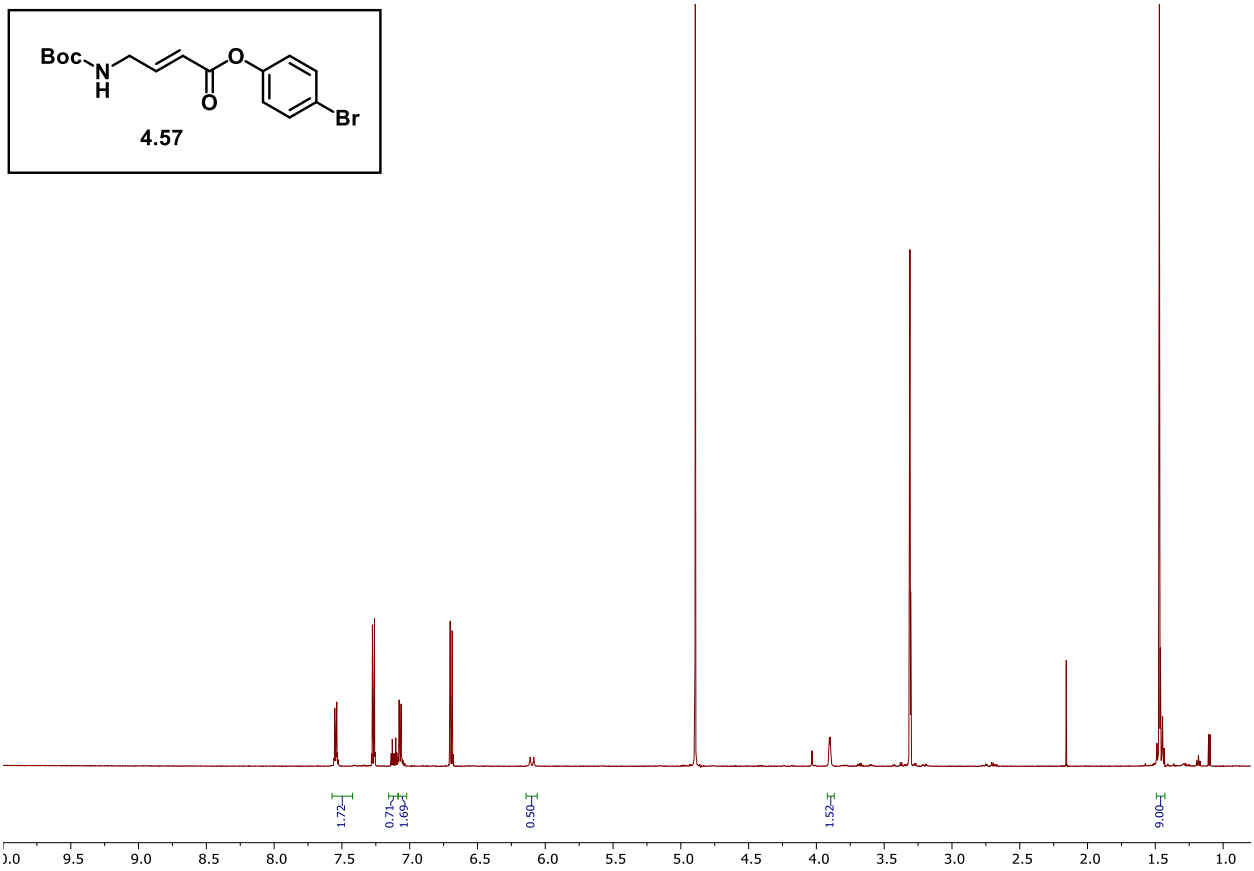
Boc
N
H
O
O
Br
4.57
1.72
0.71
1.69
0.50
1.52
9.00
9.5
9.0
8.5
8.0
7.5
7.0
6.5
6.0
5.5
5.0
4.5
4.0
3.5
3.0
2.5
2.0
1.5
1.0

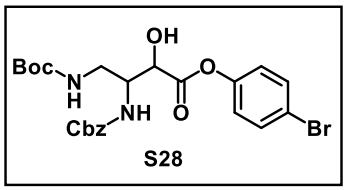
OH
Boc
N
H
NH
O
O
Cbz
Br

S28

1.47
6.41
1.34
0.61
1.59
0.65
1.00
0.85
1.44
9.00
9.5
9.0
8.5
8.0
7.5
7.0
6.5
6.0
5.5
5.0
4.5
4.0
3.5
3.0
2.5
2.0
1.5
1.0
0.5

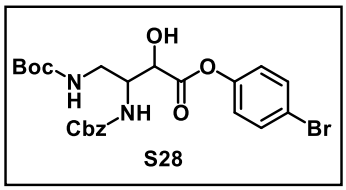
OH
Boc
N
H
O
O
NH
O
Cbz
Br

S28

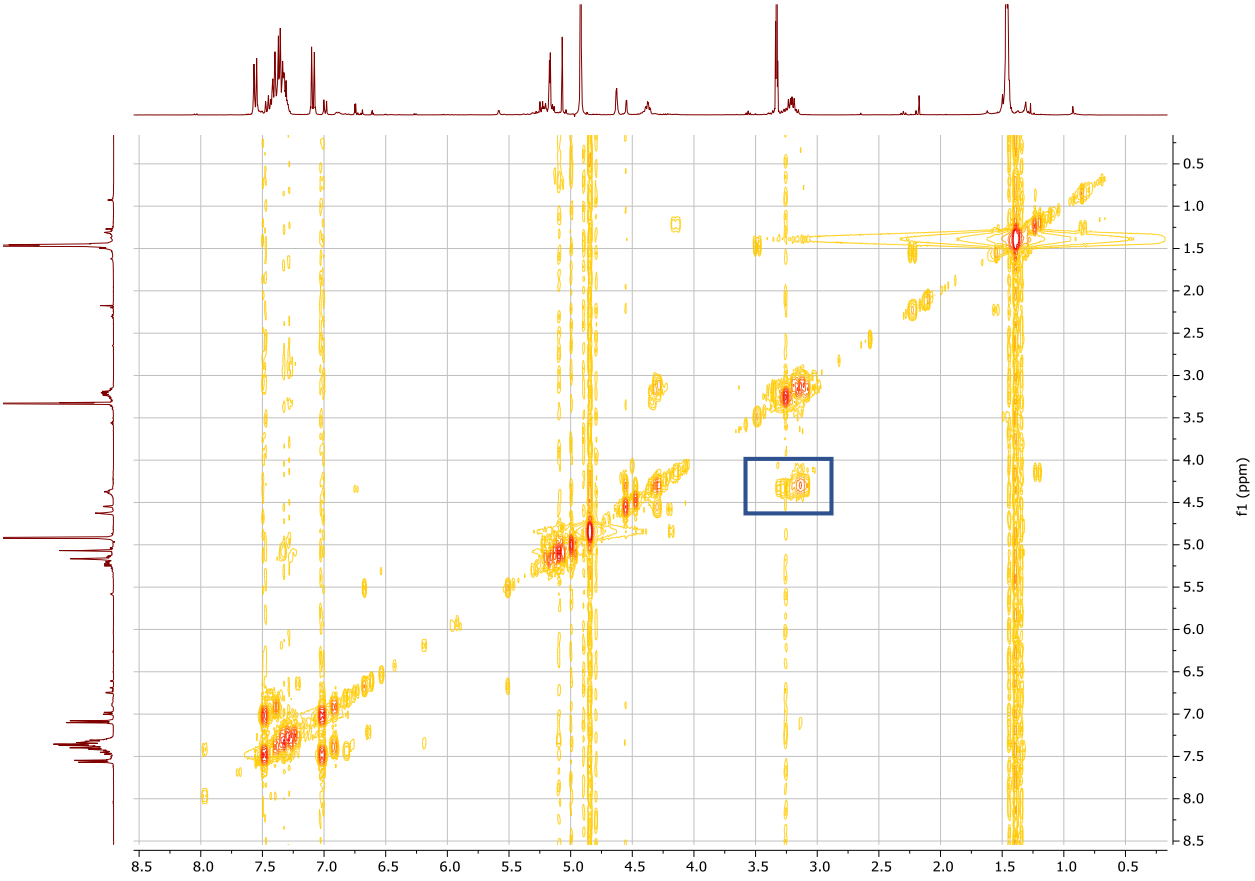
f1 (ppm)
8.5
8.0
7.5
7.0
6.5
6.0
5.5
5.0
4.5
4.0
3.5
3.0
2.5
2.0
1.5
1.0
0.5

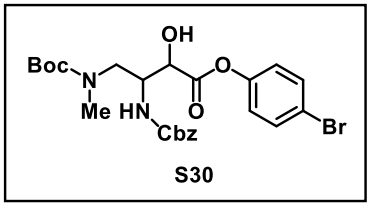
OH
Boc
N
Me
HN
Cbz
O
O
O
Br

S30


f1 (ppm)
0.5
1.0
1.5
2.0
2.5
3.0
3.5
4.0
4.5
5.0
5.5
6.0
6.5
7.0
7.5

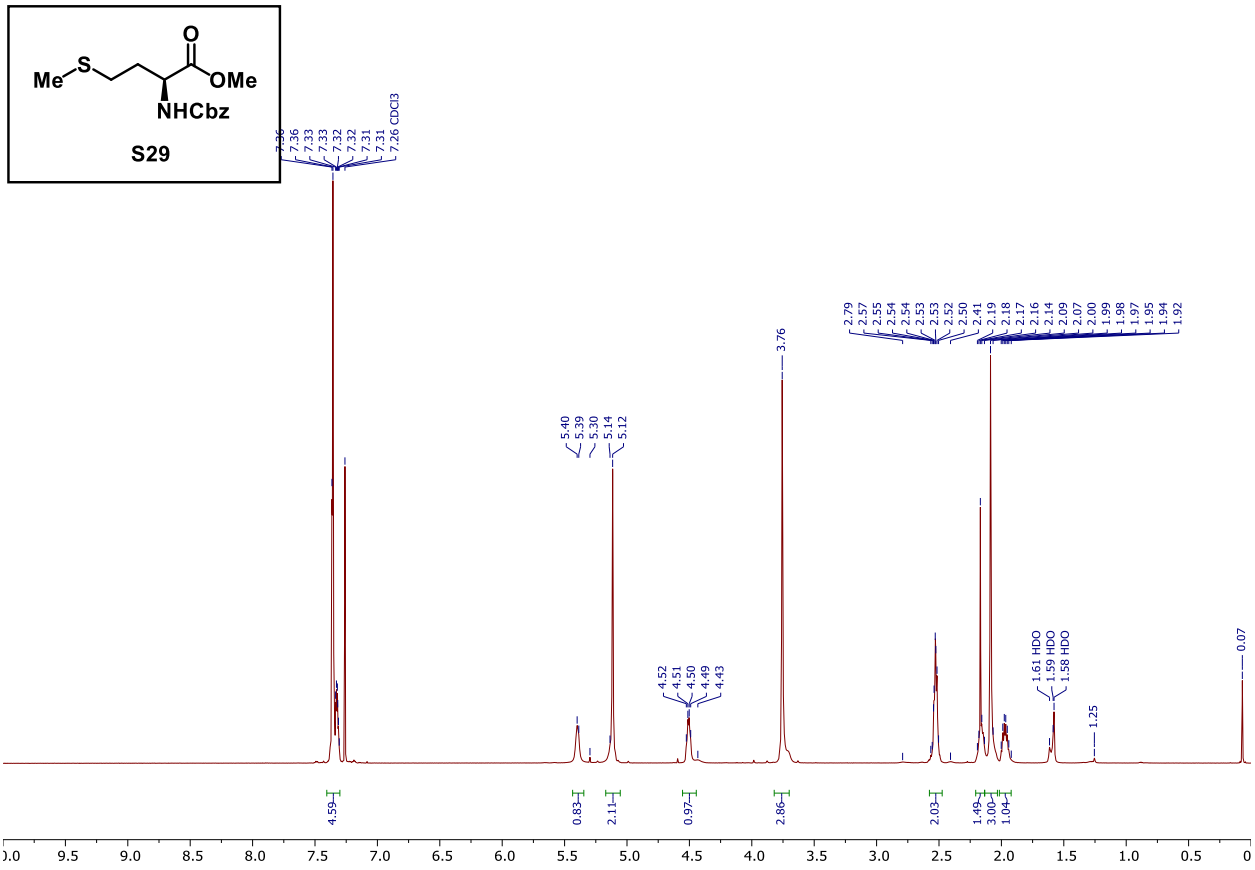
Me
S
O
OMe
NHCbz
S29
7.36
7.33
7.32
7.31
7.26 CDCl3
5.40
5.39
5.30
5.14
5.12
4.52
4.51
4.50
4.49
4.43
3.76
2.79
2.57
2.55
2.54
2.53
2.52
2.50
2.41
2.19
2.18
2.17
2.16
2.14
2.09
2.07
2.00
1.99
1.98
1.97
1.95
1.94
1.92
1.61 HDO
1.59 HDO
1.58 HDO
1.25
0.07
4.59
0.83
2.11
0.97
2.86
2.03
1.49
3.00
1.04

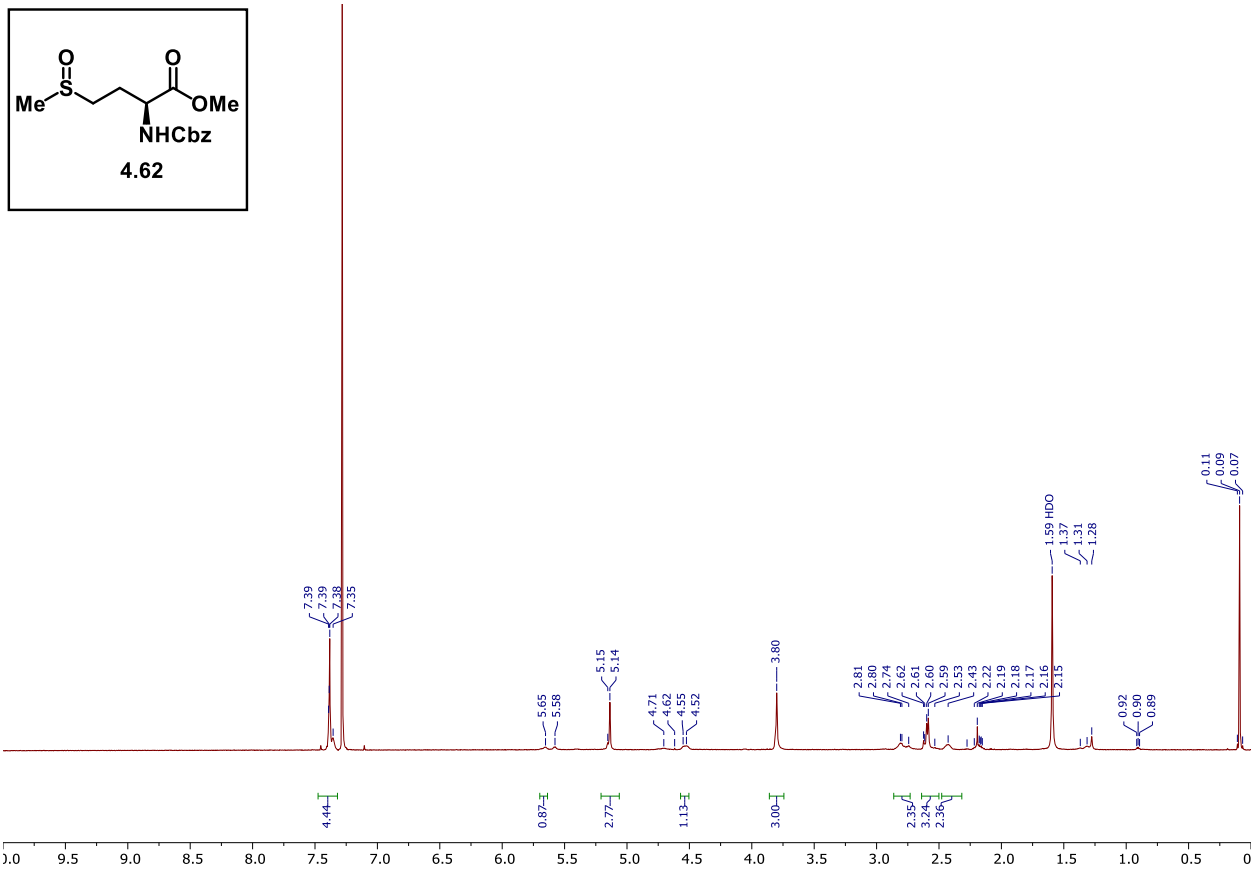
Me
S
O
O
OMe
NHCbz
4.62
7.39
7.39
7.38
7.35
5.65
5.58
5.15
5.14
4.71
4.62
4.55
4.52
3.80
2.81
2.80
2.74
2.62
2.61
2.60
2.59
2.53
2.43
2.22
2.19
2.18
2.17
2.16
2.15
1.59 HDO
1.37
1.31
1.28
0.92
0.90
0.89
0.11
0.09
0.07
4.44
0.87
2.77
1.13
3.00
2.35
3.24
2.36

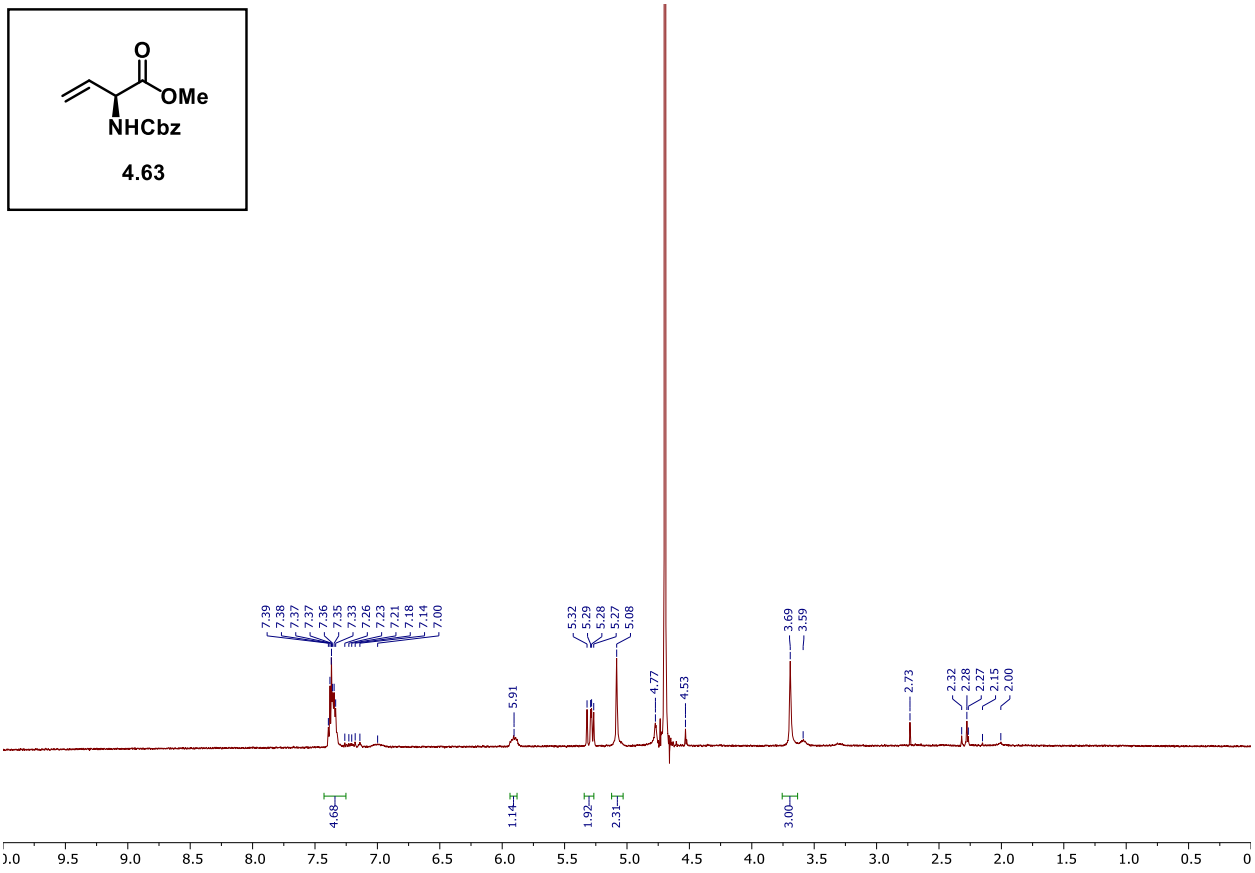
O
OMe
NHCbz
4.63
7.39
7.38
7.37
7.37
7.36
7.35
7.33
7.26
7.23
7.21
7.18
7.14
7.00
5.32
5.29
5.28
5.27
5.08
5.91
4.77
4.53
3.69
3.59
2.73
2.32
2.28
2.27
2.15
2.00
4.68
1.14
1.92
2.31
3.00
9.5
9.0
8.5
8.0
7.5
7.0
6.5
6.0
5.5
5.0
4.5
4.0
3.5
3.0
2.5
2.0
1.5
1.0
0.5
0

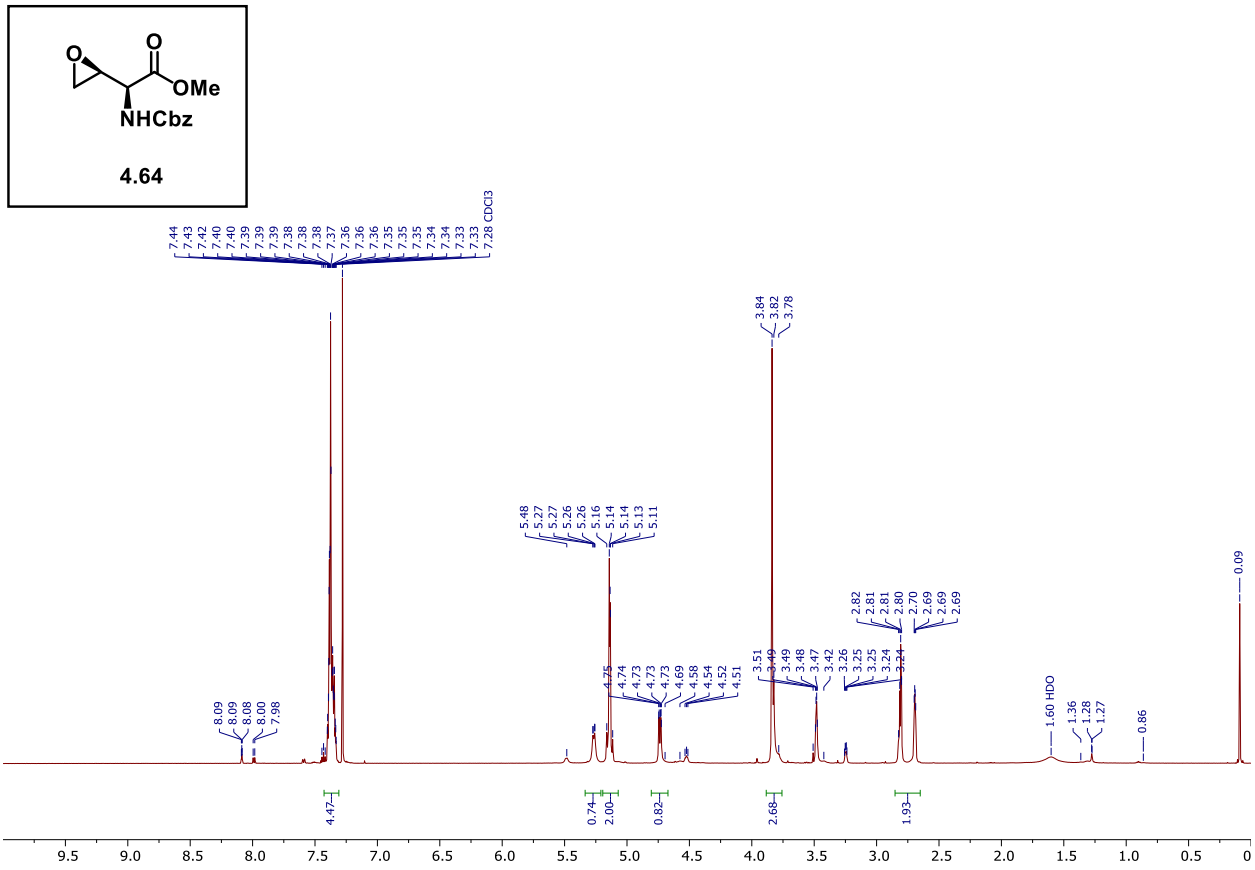
O
O
OMe
NHCbz
4.64
7.44 7.43 7.42 7.40 7.40 7.39 7.39 7.39 7.38 7.38 7.38 7.37 7.36 7.36 7.36 7.35 7.35 7.35 7.34 7.34 7.33 7.33 7.28 CDCl3
5.48 5.27 5.27 5.26 5.26 5.16 5.14 5.14 5.13 5.11
3.84 3.82 3.78
8.09 8.09 8.08 8.00 7.98
4.75 4.74 4.73 4.73 4.69 4.58 4.54 4.52 4.51
3.51 3.49 3.49 3.48 3.47 3.42 3.26 3.25 3.25 3.24 3.24
2.82 2.81 2.81 2.80 2.70 2.69 2.69 2.69
1.60 HDO 1.36 1.28 1.27 0.86
0.09
4.47 0.74 2.00 0.82 2.68 1.93
9.5 9.0 8.5 8.0 7.5 7.0 6.5 6.0 5.5 5.0 4.5 4.0 3.5 3.0 2.5 2.0 1.5 1.0 0.5 0

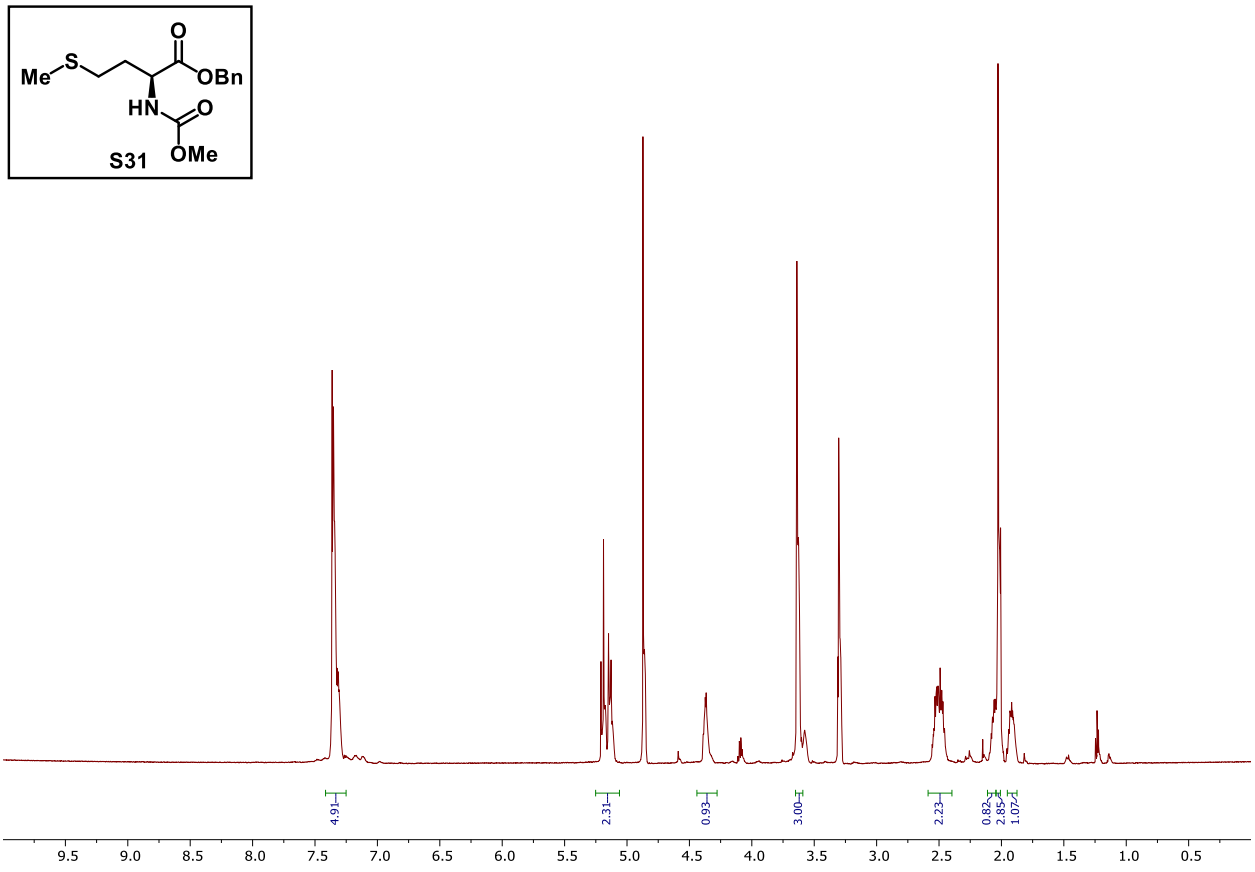
Me
S
O
OBn
HN
O
OMe
S31
4.91
2.31
0.93
3.00
2.23
0.82
2.85
1.07
9.5
9.0
8.5
8.0
7.5
7.0
6.5
6.0
5.5
5.0
4.5
4.0
3.5
3.0
2.5
2.0
1.5
1.0
0.5

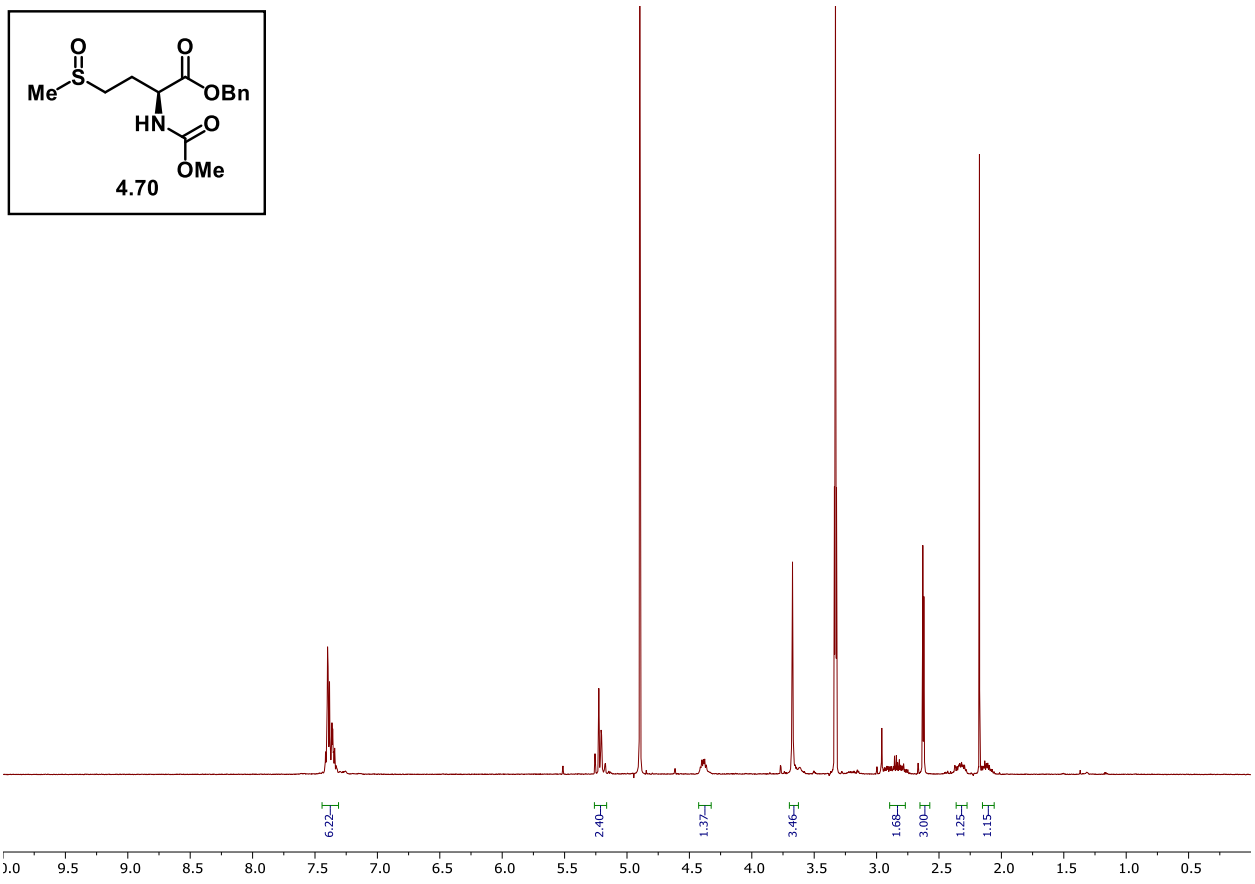
Me
S
O
O
OBn
HN
O
OMe
4.70
6.22
2.40
1.37
3.46
1.68
3.00
1.25
1.15
9.5
9.0
8.5
8.0
7.5
7.0
6.5
6.0
5.5
5.0
4.5
4.0
3.5
3.0
2.5
2.0
1.5
1.0
0.5

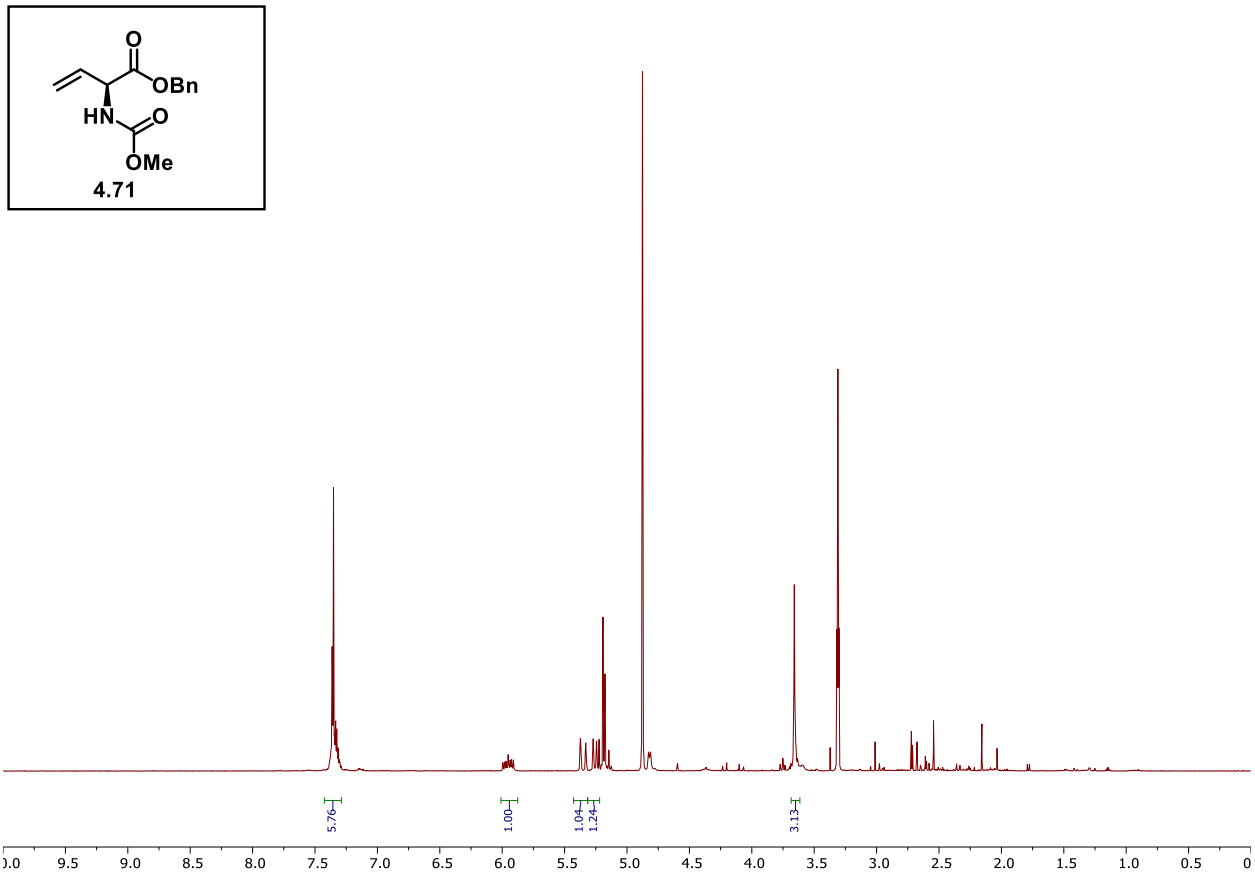
O
OBn
HN
O
OMe
4.71
5.76
1.00
1.04
1.24
3.13
9.5
9.0
8.5
8.0
7.5
7.0
6.5
6.0
5.5
5.0
4.5
4.0
3.5
3.0
2.5
2.0
1.5
1.0
0.5
0

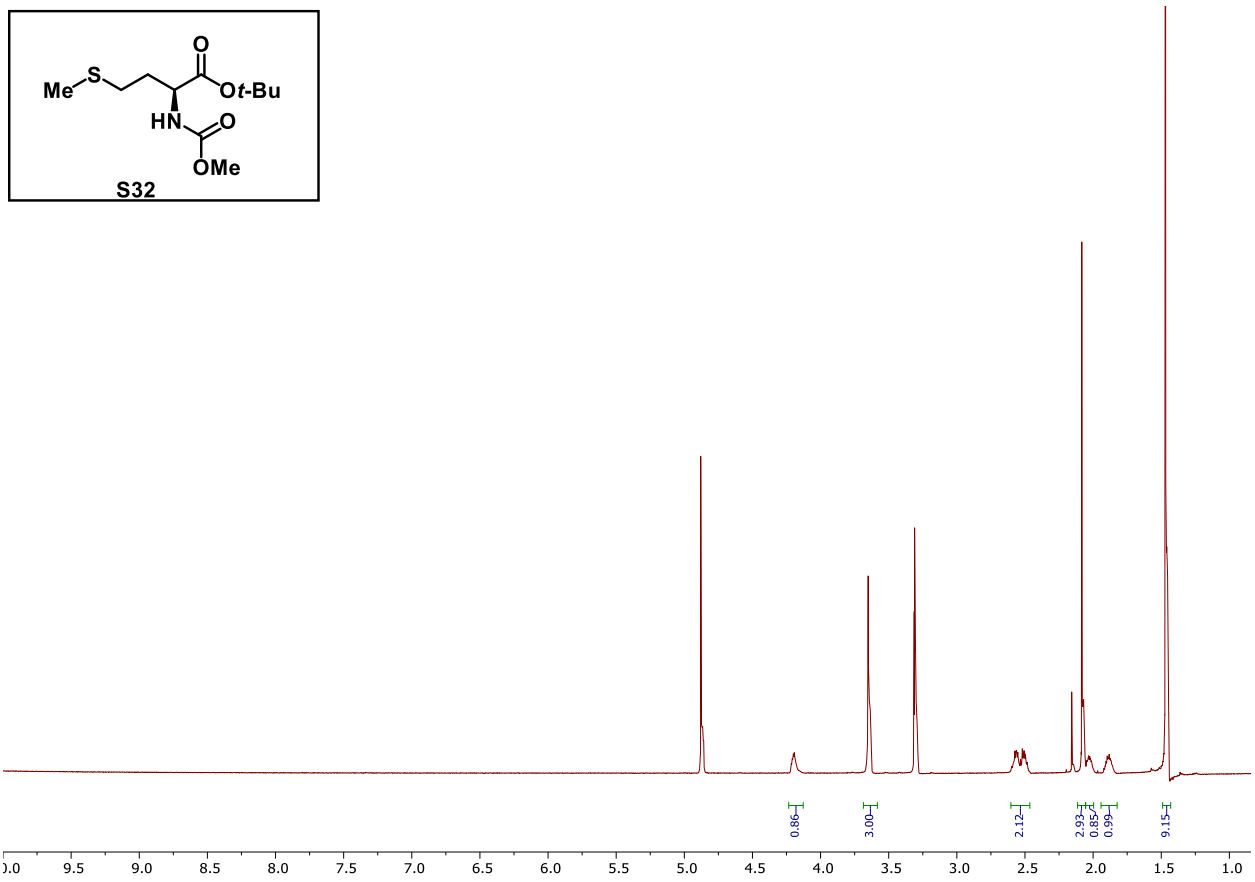
Me
S
O
Ot-Bu
HN
O
OMe
S32
0.86
3.00
2.12
2.93
0.85
0.99
9.15
9.5
9.0
8.5
8.0
7.5
7.0
6.5
6.0
5.5
5.0
4.5
4.0
3.5
3.0
2.5
2.0
1.5
1.0

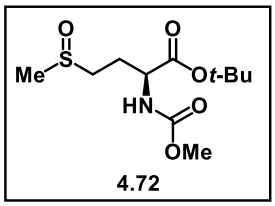
Me
S
O
O
Ot-Bu
HN
O
OMe

4.72

1.95
0.84
3.00
1.47
2.42
1.09
0.70
11.5
11.0
10.5
10.0
9.5
9.0
8.5
8.0
7.5
7.0
6.5
6.0
5.5
5.0
4.5
4.0
3.5
3.0
2.5
2.0
1.5
1.0
0.5

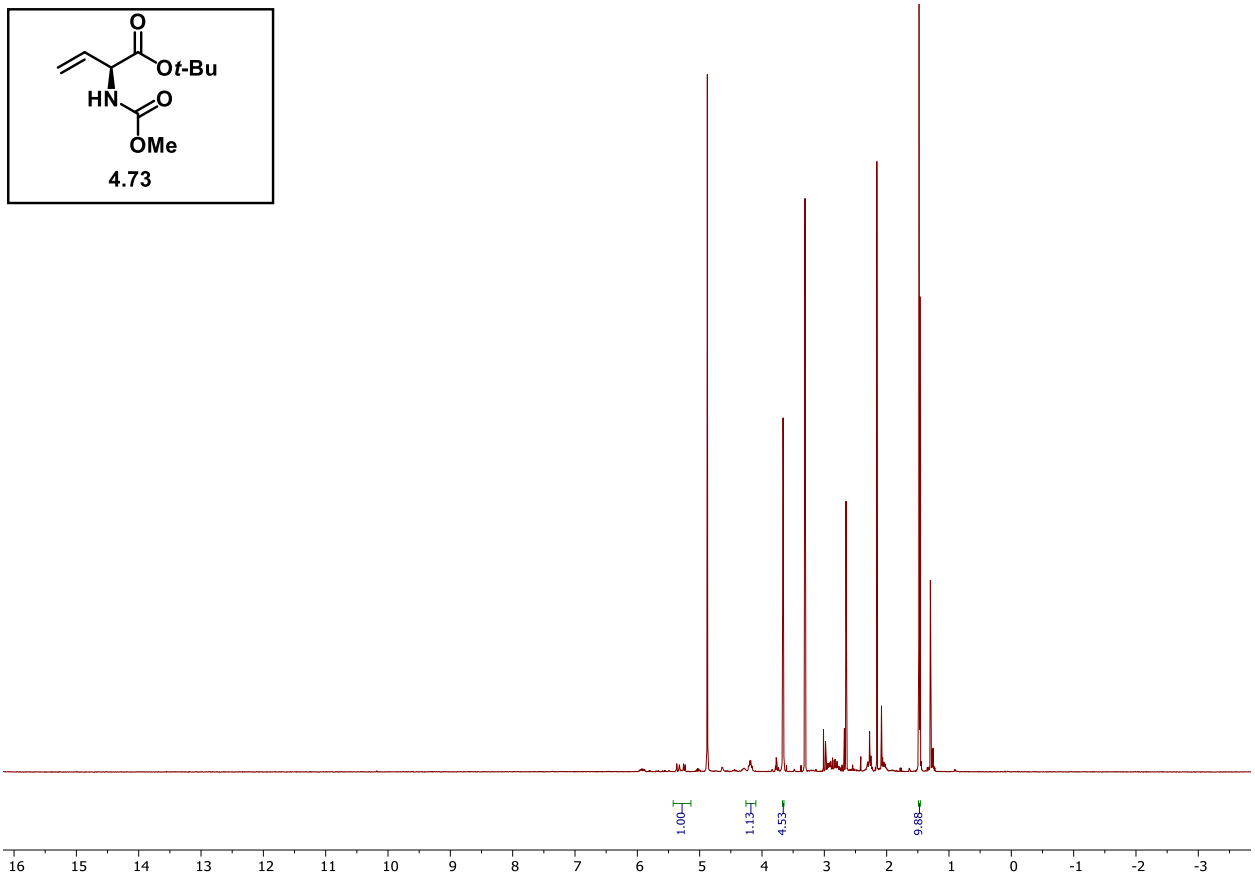
O
Ot-Bu
HN
O
OMe
4.73
1.00
1.13
4.53
9.88
16
15
14
13
12
11
10
9
8
7
6
5
4
3
2
1
0
-1
-2
-3

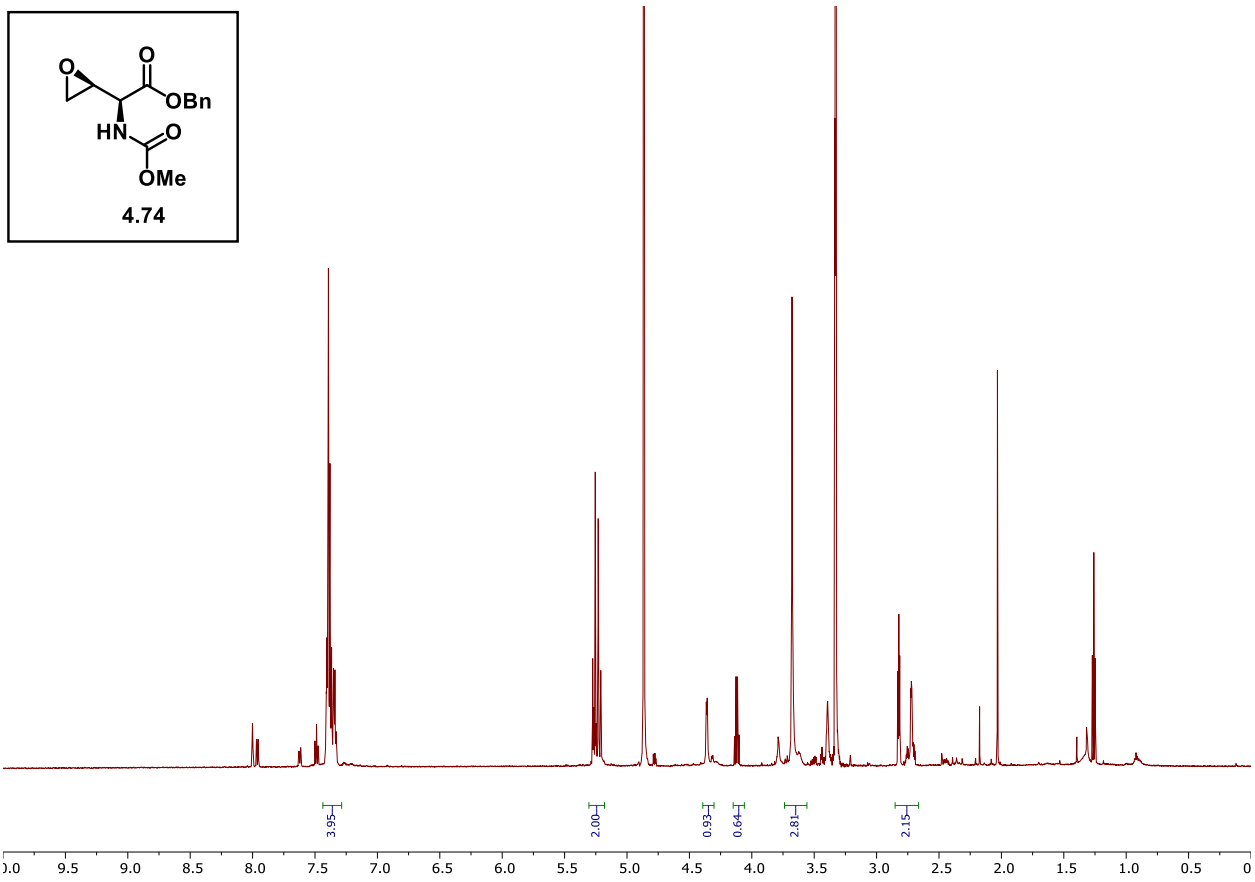
O
O
OBn
HN
O
OMe
4.74
3.95
2.00
0.93
0.64
2.81
2.15
9.5
9.0
8.5
8.0
7.5
7.0
6.5
6.0
5.5
5.0
4.5
4.0
3.5
3.0
2.5
2.0
1.5
1.0
0.5

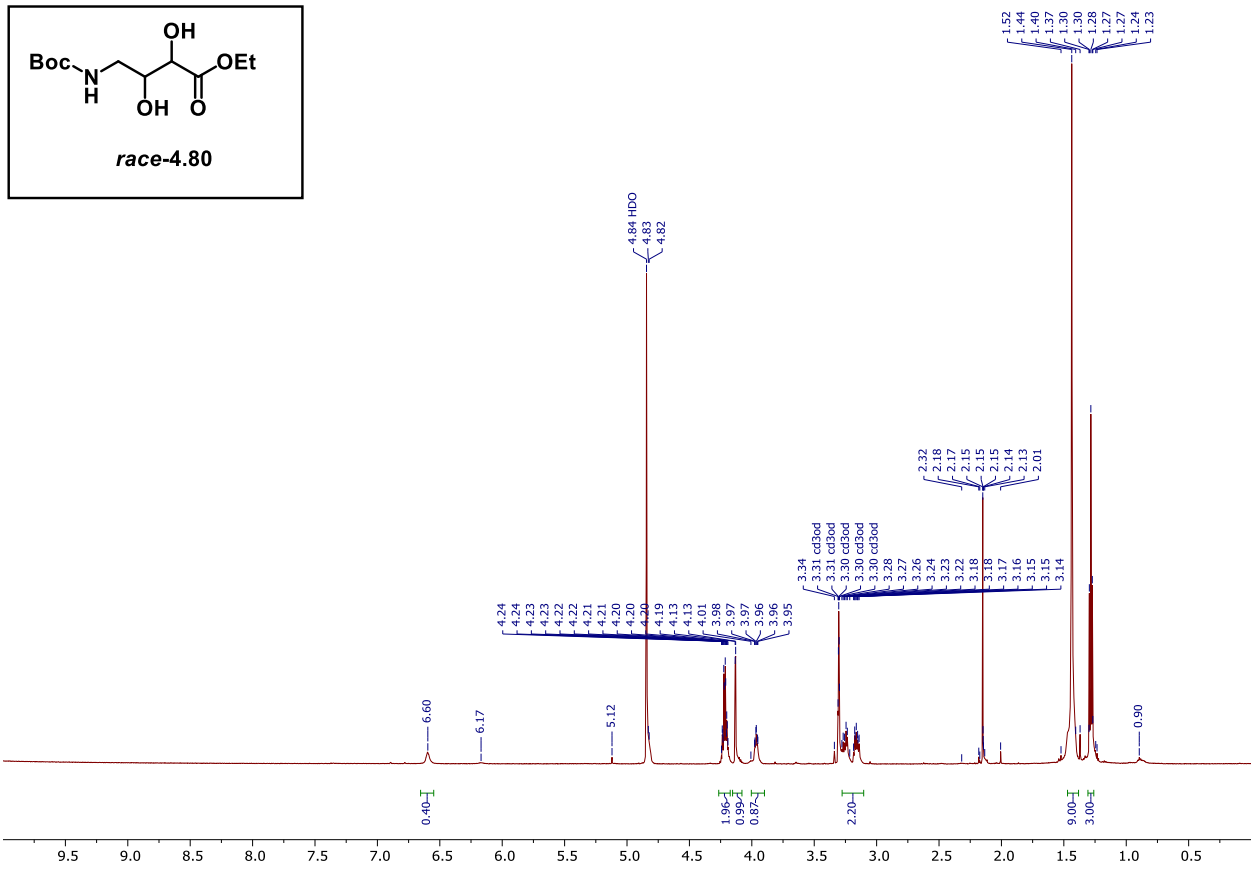
OH
Boc
N
H
OEt
OH
O
rac-4.80
4.84 HDO
4.83
4.82
6.60
6.17
5.12
0.90
0.40
1.96
0.99
0.87
2.20
9.00
3.00

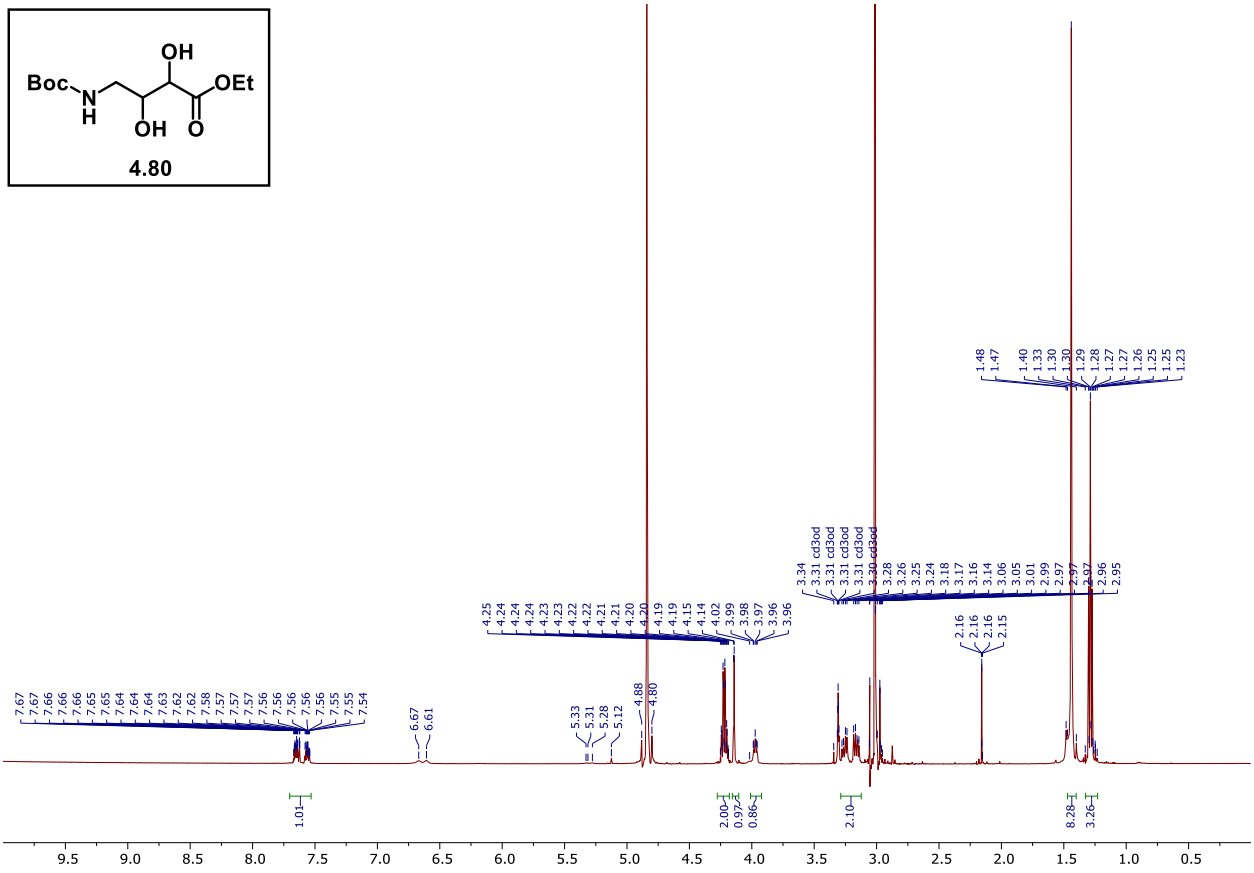
OH
Boc
N
H
OEt
OH
O
4.80

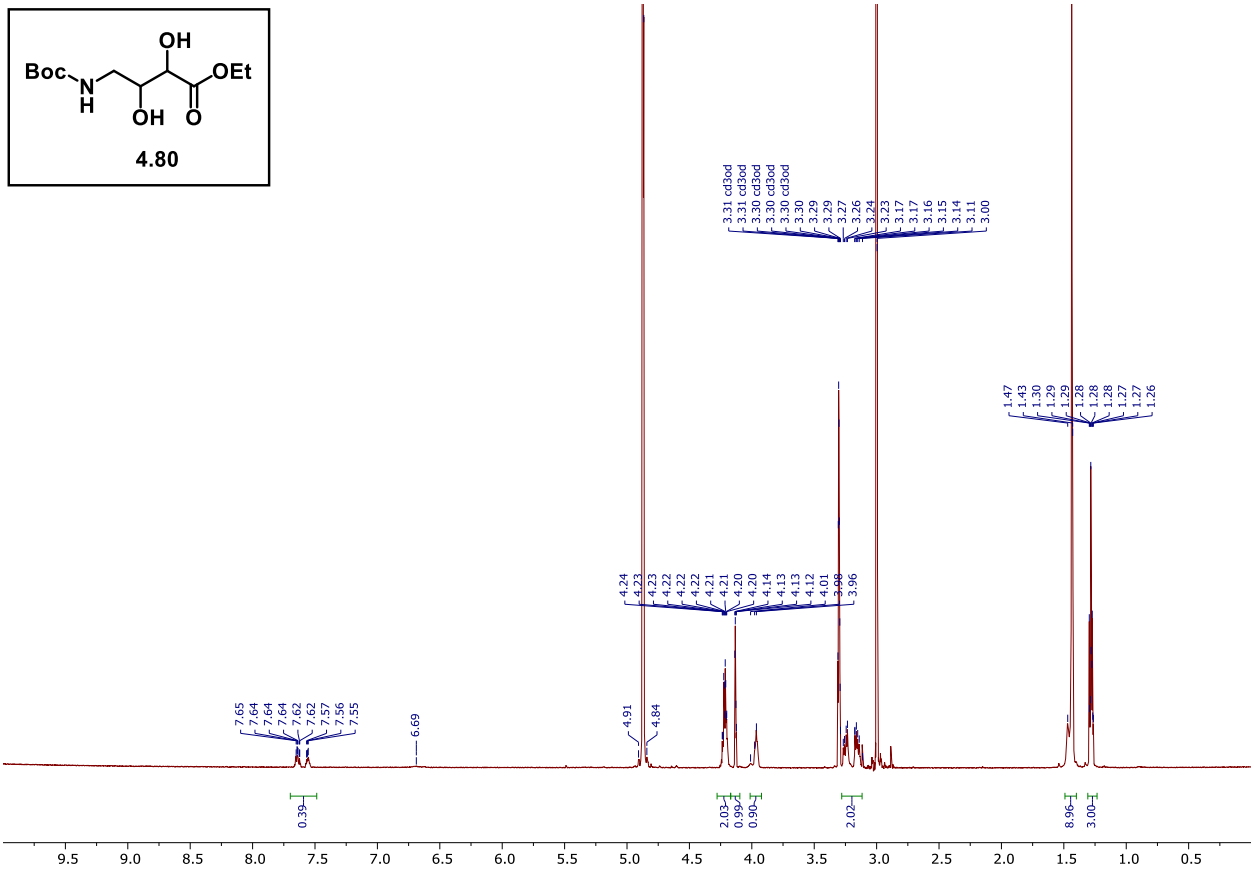
OH
Boc
N
H
OEt
OH
O
4.80
3.31 cd3od
3.31 cd3od
3.30 cd3od
3.30 cd3od
3.30 cd3od
3.30
3.29
3.29
3.27
3.26
3.24
3.23
3.17
3.17
3.16
3.15
3.14
3.11
3.00
1.47
1.43
1.30
1.29
1.29
1.28
1.28
1.28
1.27
1.27
1.26
4.24
4.23
4.23
4.22
4.22
4.22
4.21
4.21
4.20
4.20
4.14
4.13
4.13
4.12
4.01
3.98
3.96
7.65
7.64
7.64
7.64
7.62
7.62
7.57
7.56
7.55
6.69
4.91
4.84
0.39
2.03
0.99
0.90
2.02
8.96
3.00
9.5
9.0
8.5
8.0
7.5
7.0
6.5
6.0
5.5
5.0
4.5
4.0
3.5
3.0
2.5
2.0
1.5
1.0
0.5

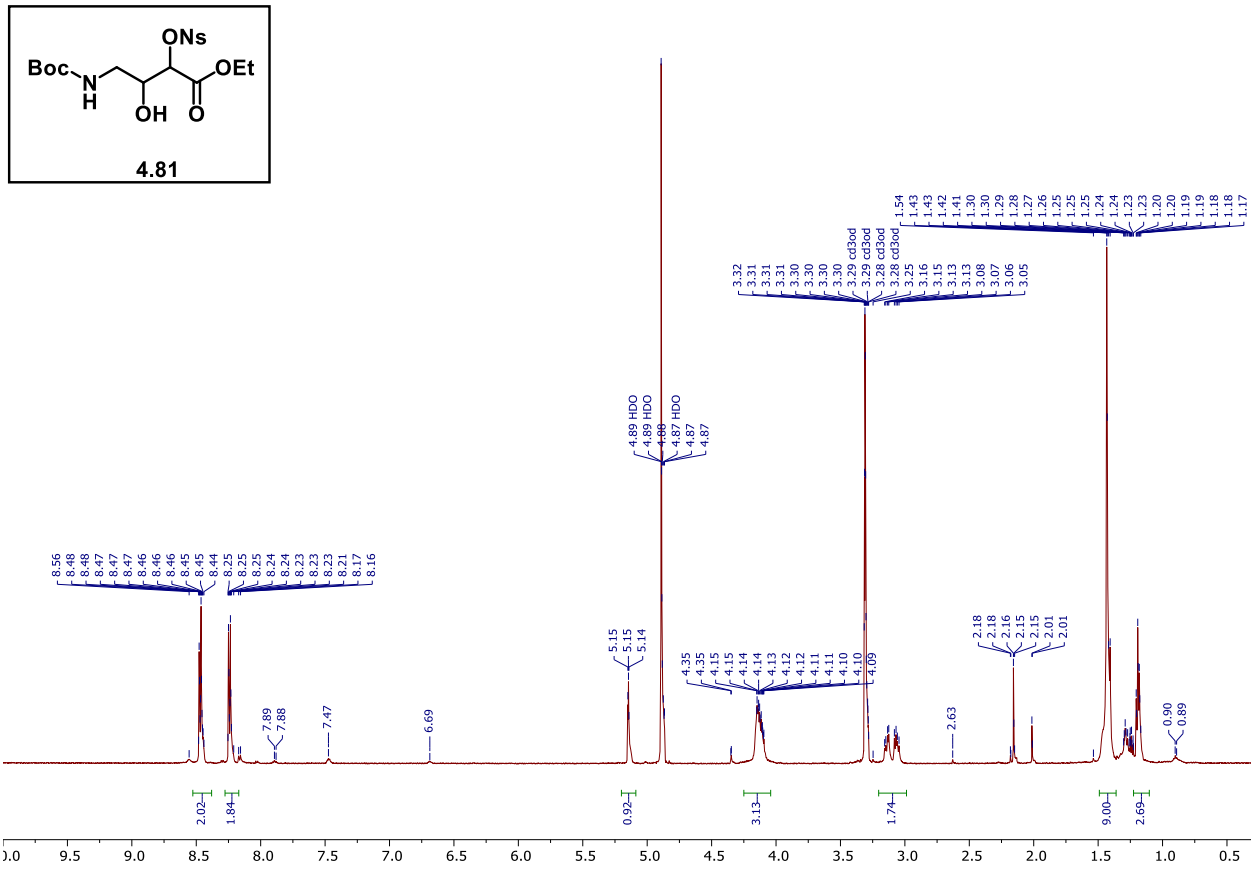
ONs
Boc
N
H
OEt
OH
O
4.81

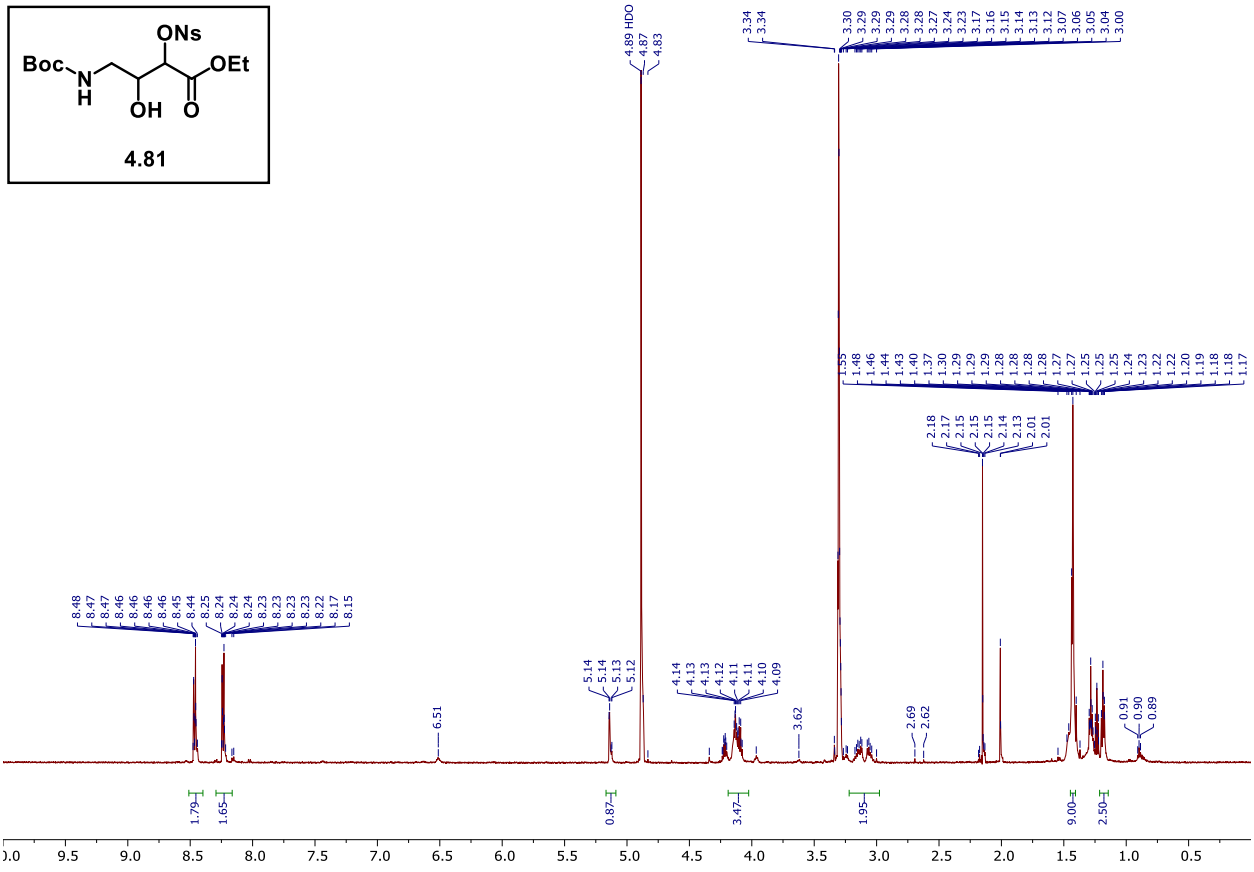
ONs
Boc
N
H
OEt
OH
O
4.81